Low Resolution Spectral Atlas for Amateur Astronomers

Demystifying spectroscopy for beginners

Anthony S. Harding Jr. and Scott P. Donnell

Low Resolution Spectral Atlas for Amateur Astronomers

Anthony S. Harding, Jr.

Scott P. Donnell

© Copyright 2025 Anthony S. Harding Jr. and Scott P. Donnell (Some Rights Reserved)

Front Matter

How do we know what chemical elements are present in the atmospheres of stars? After all, even the closest stars (other than the Sun) are many light years away. Professional astronomers found the answer to this question in the very light the stars emit, buried within like encoded fingerprints. Of course, at first, they could see these fingerprints but had no idea what they meant. Once it was realized that these fingerprints reflected the composition of the atmospheres of stars, they were able to identify their components, like hydrogen, helium, calcium, iron, and so on.

For a long time, this process involved very expensive equipment—and immense amounts of time to capture photographs of the light from those stars to analyze. This made it impractical for amateurs. Recently, however, newer, lower-cost equipment and digital cameras have brought it within reach of most amateur astronomers. Relatively simple equipment can now be used to capture spectra from stars in a short time and enable virtually anyone to see these chemical fingerprints hidden in starlight.

This Atlas has been compiled for the amateur just getting started in spectroscopy. Some theoretical background is provided, as are the details of the acquisition, processing, and analysis of spectra in order to determine what elements are present. With this, we hope to provide a starting point—a collection of basic theory and examples against which the beginner can compare and contrast his own results.

About the Authors



Anthony S. Harding Jr. has held a deep interest in astronomy since his first unexpected spotting of a meteor streaking across the sky when he was 8 years old. After that single fleeting experience, anything related to the mysteries of the sky has fascinated him. With a voracious appetite for reading, he absorbed all the texts on astronomy he could locate from the 1970s up to the present day.

Anthony is a member of the ALPO (Association of Lunar and Planetary Observers), and an occasional contributor to The

Lunar Observer, the organization's monthly magazine dedicated to lunar observation and detailed analysis.

Only recently, he discovered that amateur spectroscopy is within reach. After obtaining the additional low-cost equipment and software needed, he began a survey of bright stars from his mid-northern-latitude home. Since July 2023, this catalog has been slowly but steadily growing, and is now available for free from the RSpec website (at https://rspec-astro.com/sample-

projects/#:~:text=Spectra%20Library%20of%20Constellations.

Anthony lives in northeast Indiana, where he works in IT. Keen-eared passersby can often hear him cursing the bad weather and light pollution.



Scott Donnell is an active member of the American Association of Variable Star Observers (AAVSO.org) and assumed leadership of its Spectroscopy Special Interest Group in January 2024. In this role Scott works to develop educational and instructional materials for the group's members. He also organizes and conducts monthly information exchange meetings for anyone who wishes to pursue amateur astronomical spectroscopy and develop a strong foundational knowledge base and skill set. He is also

passionate about promoting amateur astronomical spectroscopy as an important tool in understanding the underlying physics of the observed behaviors of variable stars.

Scott is a semi-retired Senior Space Systems Engineer residing with his wife in Peyton, Colorado. He is an active member of the Colorado Springs Astronomical Society (CSASTRO.org), having served over the past decade as President, Vice President, Treasurer, Trustee, and Co-Director for the Rocky Mountain Star Stare (RMSS.org) conducted annually by CSASTRO in southern Colorado.

Scott holds a B.S. with a double major in physics and mathematics from the University of Wisconsin and an M.S. in Astronomy from the Pennsylvania State University. He continues to expand his knowledge of astronomical spectroscopy and other astronomical topics through independent research, programs of observation, and his volunteer work at the US Air Force Academy Observatory.

Version History

Version	Date	Changed By	Reason
1.0	Sep 2025	Harding, Donnell	Initial release

Copyright © 2025 Anthony S. Harding and Scott P. Donnell. Some rights reserved. You may download and distribute this work in its entirety for your personal use. You may not revise or extract portions of this work for republication or distribution, but you may use limited portions of this work for purposes covered under fair use. Unless otherwise noted, all text and graphics within this document are the product of the authors. No artificial intelligence was used in the generation of any part of this atlas.

Contents

1. Introduction	5
1.1 Purpose of this Atlas	5
1.2 Intended Audience	5
1.3 Limitations	5
2. Terms and Definitions	6
3. Background on Stellar Spectra	11
3.1 Fraunhofer Lines	11
3.2 Characteristics of the Spectrum	11
3.3 The Continuum	12
3.3.1 Sources of the Continuum	13
3.3.2 The Shape of the Continuum	15
3.4 Absorption Lines	17
3.4.1 The Presence of Elements in Stellar Spectra - Abundances	18
3.4.2 The Presence of Elements in Stellar Spectra - Temperature	20
3.4.3 Effect of Excitation and Ionization on the Spectral Lines	23
3.4.4 Ionization Stages of an Element and the Spectral Lines	27
3.4.5 The Appearance of Molecules in Stellar Spectra	30
3.4.6 Telluric Absorption Bands	30
3.4.7 The General Spectral Sequence	31
3.5 Emission Lines	32
3.5.1 Shells from Stellar Winds	33
3.5.2 Shells from Nova	35
3.5.3 Spectral Features from Circumstellar Disks	36

3.5.4 Other Sources for Emission Lines in Stellar Spectra	38
4. Generation of the Profiles	39
4.1 Equipment Used and Observing Location	39
4.2 Data Ranges for Acquiring the Spectra	41
4.3 Selection and Presentation of the Spectra	41
4.3.1 Classification of Spectra	41
4.4 Data Collection and Processing Details	44
4.4.1 Capture Process	44
4.4.2 Image Stacking	46
4.4.3 RSpec—Creating Instrument Response Curve (Relative Flux Calibration Curve)	47
4.4.4 RSpec–Analyzing Captures	51
5. Atlas of Spectra	54
5.1 Spectral Type O Stars	55
5.2 Spectral Type O/B Stars (Very Late O and Very Early B)	64
5.3 Spectral Type B Stars	72
5.4 Spectral Type B/A Stars (Very Late B and Very Early A)	97
5.5 Spectral Type A Stars	103
5.6 Spectral Type A/F Stars (Very Late A and Very Early F)	125
5.7 Spectral Type F Stars	133
5.8 Spectral Type F/G Stars (Very Late F and Very Early G)	155
5.9 Spectral Type G Stars	163
5.10 Spectral Type G/K Stars (Very Late G and Very Early K)	185
5.11 Spectral Type K Stars	193
5.12 Spectral Type K/M Stars (Very Late K and Very Early M)	209
5.13 Spectral Type M Stars	217
6. Acknowledgements	237
7. References	237
8. Appendices	240
Appendix 1 - Physical Constants	240
Appendix 2 - Representative Temperatures of Main Sequence Stars	240
Appendix 3 - Temperatures of Peak Line Intensities of the 20 Most Abundant Elements i Solar Spectrum	n the 241
Appendix 4 - Elements and Ions by Spectral Type	242
Appendix 5 - Element Profiles and Spectral Lines	245

1. Introduction

1.1 Purpose of this Atlas

This atlas provides amateur astronomers engaged in low resolution spectroscopy a reference for the identification of spectral lines in stars. It is intended to be a guide for the amateur getting started in astronomical spectroscopy using a spectroscopic grating filter in the imaging system rather than a traditional slit spectrograph. Slitless spectroscopy is the least expensive way into astronomical spectroscopy and is often the first step many amateurs take into astronomical spectroscopy. Slitless spectroscopy serves to introduce the practitioner to the foundational skills and knowledge needed to perform spectroscopy with higher resolution slit spectrographs, and to develop the basic skill of identifying the major spectral lines in an observed stellar spectrum.

While there are spectroscopic atlases available to the amateur spectroscopist, such as Richard Walker's "Spectral Atlas for Amateur Astronomers", these may not fully address the needs of those engaged in low resolution spectroscopy. These atlases may include a few subtypes within each spectral type and with selected spectral features identified at a higher resolution that, for slitless spectra, can make identification of low-resolution spectral features more difficult and uncertain. This atlas includes annotated spectra for the range of spectral types from O to M and particularly notes those spectral lines which may appear blended due to the inherent low resolution of slitless spectrographs.

1.2 Intended Audience

Those new to spectroscopy as well as those more advanced will find within this document useful background information on stellar spectra as well as a comprehensive atlas of stellar spectra spanning the range of spectral types. Low resolution spectroscopy is a low-cost way to engage in the science of astronomical spectroscopy, and this volume intends to provide information, tools, and examples to help those getting started in astronomical spectroscopy to understand the basics of stellar spectra.

1.3 Limitations

This atlas is intended to serve those engaged in astronomical spectroscopy of stars and does not include spectra of non-stellar objects, such as emission nebula, nor does it include spectral features of special classes of star such as those with surrounding emitting shells such as the Wolf-Rayet stars.

This atlas provides a set of spectra for the range of stellar spectral types typically encountered by the amateur astronomer and does not distinguish between luminosity classes, so the spectrum presented for a spectral type A star in this low resolution atlas

serves to identify the main spectral features not only for the main sequence stars, but the sub giants and giants as well.

The spectra presented in this atlas are low resolution, meaning typical of that obtained using a spectral grating filter, such as the Star Analyzer 100 or 200. These filters are inexpensive compared to typical amateur slit spectrographs and provide a lower resolution than that of more expensive spectrographs. Being low resolution, these spectra will show spectral features that are more often than not a blend of two or more individual spectral lines. Still, if sufficient care is taken in obtaining and processing your spectra, it is possible to identify a number of spectral features and, in so doing, develop the knowledge and skill in identifying spectral lines that will provide a solid foundation for engaging in the identification of spectral lines in higher resolution spectra.

2. Terms and Definitions

1D Spectral Profile	A graphical representation of a 2D spectrum in which the horizontal axis represents wavelength and the vertical axis represents relative intensity, typically in arbitrary units. Also referred to as a 1D spectrum or 1D profile to distinguish it from the 2D spectrum. Wavelength is typically in units of either Angstroms or nanometers.
2D Spectrum	A spectrum obtained by a spectrograph in which the horizontal component is produced by the dispersion of the instrument and has a width corresponding to either the angular size of the observed object (in the case of a slitless spectrograph) or the width of the slit (in the case of a slit spectrograph).
Absorption Lines	Wavelength-specific reductions in the intensity of the continuum due to absorption of radiation by neutral and ionized atoms.
Angstrom (Å)	A unit of wavelength equal to 1E-10 meters. Although still widely used in astronomy, the Angstrom is not officially a part of the International System of Units (SI).
Atomic Energy Levels	Energy corresponding to the allowed orbital state of an electron in an atom. Multiple allowed orbital states, as allowed by quantum mechanics, results in multiple energy levels of the electron within the atom.

	_
Balmer Jump	The apparent drop in intensity of the continuum at the blue end of the spectrum due to closely spaced hydrogen Balmer absorption lines that are absorbing flux from the continuum.
Be Stars	Stars of spectral class B showing emission lines in their spectrum due to a gaseous disk that is formed of material ejected from the star.
Boltzmann Constant	Symbolized as k or k_b , the Boltzmann constant is the proportionality factor that relates the average relative thermal energy of particles in a gas with the thermodynamic temperature of the gas. The Boltzmann constant is defined to be 1.380649×10^{-23} joules/ Kelvin.
Collisional De-excitation	De-excitation of an atom that occurs as a result of an interaction with another particle in which the passing particle absorbs energy from the atom.
Collisional Excitation	Excitation of an atom that occurs as a result of an interaction with another particle in which the passing particle adds energy to the atom.
Contact Binaries	Stars in a close binary system in which the outer atmospheres of either or both stars are passing material to the other.
Continuum	The general shape of the 1D spectral profile that is related to a star's temperature.
Deexcitation	The process in which one or more of an atom's electrons return to the lowest available energy level, or ground state for that electron.
Detached Binaries	Stars in a binary system in which no transfer of material from their atmospheres is occurring.
Dispersion	The separation of light into its component colors by a prism or diffraction grating.
Emission Lines	Wavelength-specific emissions above the level of the continuum due to emission of radiation by neutral and ionized atoms.

Excitation	The process in which one or more of an atom's electrons move to an energy level of the atom greater than the lowest available energy level, or ground state for that electron. An atom with one or more electrons in these higher energy levels is said to be excited.
Fraunhofer Lines	Prominent lines in the solar spectrum observed by Joseph von Fraunhofer in the early 19th century and annotated by upper case letters of the alphabet starting at the red end of the spectrum and proceeding toward the blue end. Less prominent lines were labeled with lower case letters. Notable spectral lines still referred to by their Fraunhofer designation include the H and K lines due to singly ionized calcium and the G line due to the CH molecule as well as lines of neutral calcium and iron.
Giant Star	Generally referring to those stars that have transitioned from fusing hydrogen in its core to fusing helium in its core with a surrounding hydrogen fusing shell. This dual fuel source results in the star swelling in size and often becoming variable.
HR Diagram	A plot developed in the early part of the 20th century that places stars on the diagram according to their temperature and luminosity. The HR diagram proved to be instrumental in the development of understanding of stellar evolution.
Instrument Response	More properly termed "Relative Flux Calibration", is the process for correcting a spectrum for the effects of wavelength-dependent flux loss using the spectrum of a standard reference star to assess the effects of the atmosphere and instrument.
Luminosity Class	A Roman numeral roughly indicating the position of a star on the HR diagram. Ranging from I to V, the luminosity class indicates whether a star is a normal main sequence star (luminosity class V), a giant star (luminosity class III), or a supergiant star (luminosity class I), for example.
Main Sequence	A reference to stars that fall along a curve on the HR diagram that runs from the lower right to the upper left of the diagram. Stars along the main sequence are those in the stable hydrogen fusing phase of their lifetime.

Mean Free Path	The distance a photon, electron, or other particle travels in a medium before an encounter with another particle that changes its energy and/or direction.
Nanometer (nm)	An SI unit of wavelength equal to 1E-9 meters. One nanometer equals 10 Angstroms.
Opacity	The degree to which a layer of material or gas is transparent to incident radiation. Higher opacity means less of the incident radiation passes through the material unhindered while low opacity means more passes through. Scattering and absorption are the primary effects on radiation that determine opacity.
Optical Depth	A measure of the opacity of a medium and is the distance in which the intensity of a light beam is reduced by a factor of 1/e due to absorption and scattering. An optical depth of 1 corresponds to 1 photon mean free path, so that at an optical depth of less than one nearly all photons are emitted without appreciable absorption or scattering. As optical depth increases above 1, so does the number of photons that are scattered and absorbed by the medium.
Optically Thick/Thin	Referring to the opacity of the medium. An optically thick medium is one with high opacity and small mean free path of photons, while optically thin is one with low opacity and large mean free path of photons.
Planck Constant	Symbolized as h, the Planck constant is a fundamental constant that defines the quantum nature of energy relating the energy of a photon to its frequency. In the International System of Units (SI), the constant value is 6.62607015×10 ⁻³⁴ joule-hertz ⁻¹ (or Joule-seconds).
Radiative De-excitation	De-excitation of an atom that occurs as a result of an interaction with a photon in which the photon absorbs energy from the atom.
Radiative Excitation	Excitation of an atom that occurs as a result of an interaction with a photon in which the photon adds energy to the atom.

Rectified Spectrum	A 1D spectral profile with the continuum removed. Useful for discerning finer detail in the extreme ends of the spectrum.
Semi-detached binaries	A binary system in which one star is passing material from its outer atmosphere to the other star.
Spectral Class	A number generally between 0 and 9 subdividing spectral types into smaller temperature ranges, with the smaller number at the higher end of the temperature range for a spectral type and the smaller number at the lower end. A spectral type A star, for example, contains spectral subtypes A0 through A9 in order of decreasing temperature.
Spectral Type	An uppercase letter related to the temperature of a star. The primary spectral types are O, B, A, F, G, K, and M in order of temperature from highest to lowest with each spectral type representing a range of temperatures.
Spectrum	An image of an object in which the light is dispersed into its component colors. A spectrum is typically shown with the short wavelength (blue) end of the spectrum to the left and the long wavelength (red) to the right.
Statistical Mean Energy	The average energy of a system of particles used to define the temperature of the system.
T Tauri type stars	A class of pre-main sequence variable stars that are less than about ten million years old and in the process of contracting to the main sequence.

3. Background on Stellar Spectra

3.1 Fraunhofer Lines

English physician William Wollaston was the first person to note the presence of dark lines in the solar spectrum. In 1802, Wollaston directed sunlight through a narrow slit and observed within the spectrum a series of narrow dark lines which he thought were the natural divisions in the primary colors of light in a spectrum.

Twelve years later in 1814, German optician Joseph von Fraunhofer performed the same observation, but now incorporating a small telescope to magnify the dispersed spectrum. He observed a large number of dark lines within the solar spectrum and denoted the most prominent features with uppercase letters A, B, C, D, etc. starting at the red end of the visible spectrum and proceeding through to the blue end. Interspersed with these are lines of lesser prominence which he labeled with lowercase letters. Fraunhofer's nomenclature continues into modern times as a reference for certain lines in the Sun's spectrum, such as the H and K lines (393.4 nm and 396.8 nm) due to singly ionized calcium, the D doublet line (589.0 nm and 589.6 nm) due to neutral sodium, and the A and B lines (759.4 nm and 686.7 nm) due to absorption by oxygen in the earth's atmosphere.

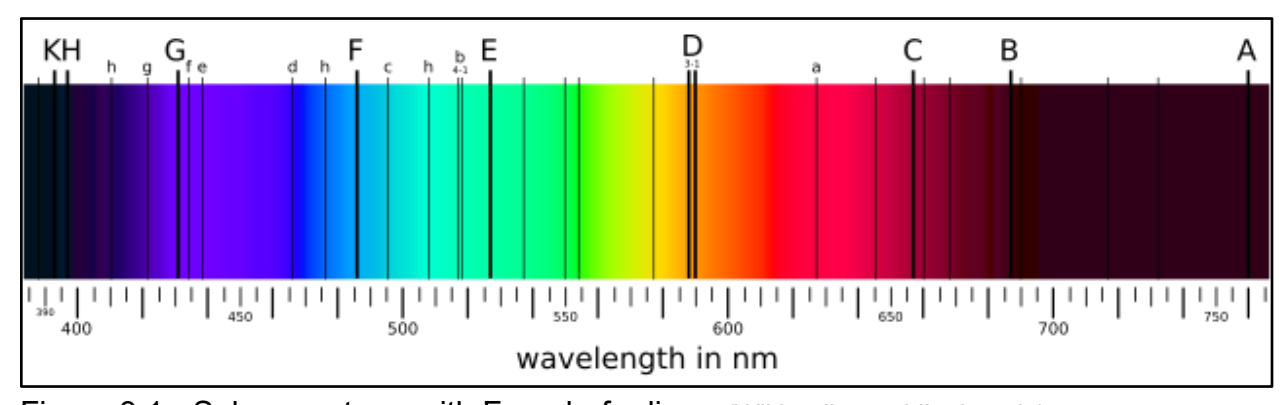


Figure 3.1 - Solar spectrum with Fraunhofer lines (Wikipedia - public domain)

3.2 Characteristics of the Spectrum

A typical stellar spectrum consists of two components: the continuum and absorption or emission lines. The continuum represents the general shape of the spectral profile and results from radiation processes in deeper, optically thick, layers of the stellar photosphere below where the absorption or emission lines originate. Absorption lines represent a reduction in intensity of the continuum at specific wavelengths due to

absorptions of photons in higher, optically thin, layers of the photosphere. Emission lines represent an increase in intensity at specific wavelengths superimposed on the continuum.

Figure 3.2 shows the spectral profile of Altair - a spectral type A star. The continuum is represented by the general shape of the spectrum curving upward from right to left (red to blue) and then sharply decreasing at the blue end of the spectrum. Absorption lines due to hydrogen are prominent and have the effect of decreasing the intensity of the continuum at those specific wavelengths.

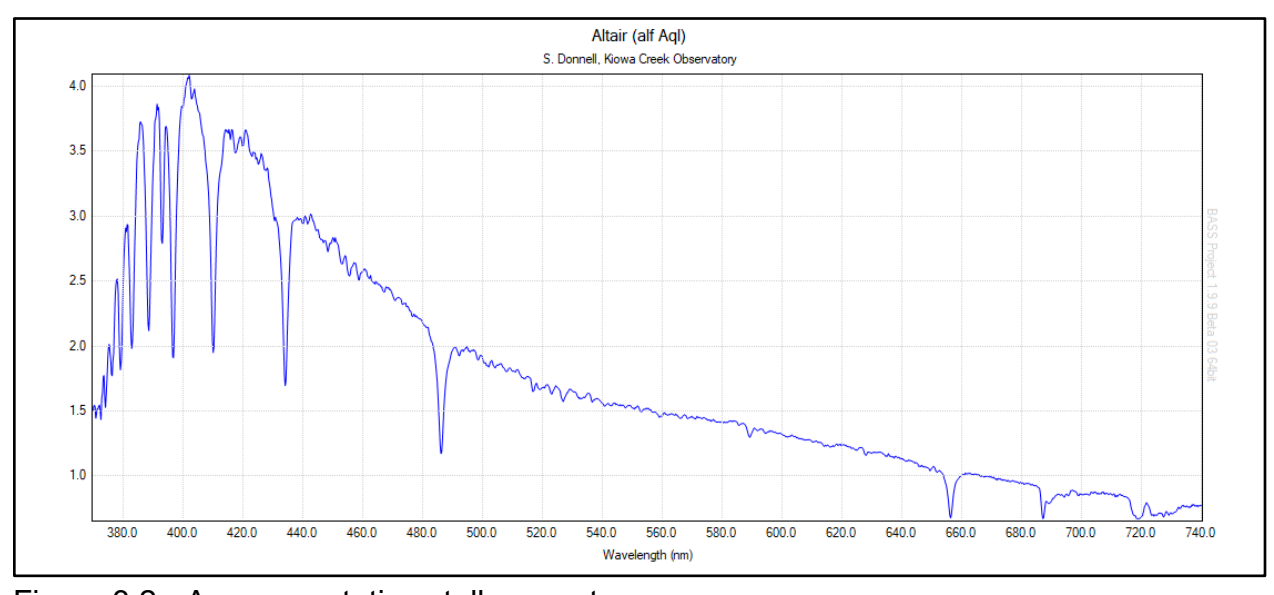


Figure 3.2 - A representative stellar spectrum

3.3 The Continuum

The continuum is the result of interactions between photons and atoms that occur in the lower layers of a star's photosphere where the density of matter is large enough for a photon to have an interaction with a particle of matter within very short distances. The result is that a photon emanating from deeper layers in the stellar photosphere will experience many interactions with particles of matter, each interaction changing its energy and direction of propagation, so that by the time it emerges from the star and propagates through free space, the information of its original energy and direction has been lost. When we consider the multitudes of photons emanating from a star each second, each having their energies and directions modified as described above, it becomes clear that the result is a uniform "glow" of radiation emanating from the star's photosphere.

An analogy to this is a dense daylight fog on Earth. If the fog is dense enough and extends high enough above the observer, then what is seen is not the bright Sun in a specific direction, as we would see on a clear day, but instead a uniform illumination coming from all directions and without any indication of the direction of the Sun at all. This is the situation in the deeper layers of the photosphere giving rise to the continuum.



Figure 3.3 - A dense fog simulating the conditions giving rise to the continuum (Wikipedia)

3.3.1 Sources of the Continuum

There are four possible types of interactions between photons and particles of matter contributing to the continuum:

1. <u>Transitions of an electron in an atom from one energy level to another</u>. Commonly called "bound-bound" transitions, as the electron remains bound to the atom in these transitions. When an electron receives energy, either from an interaction with another particle (collisional excitation), or by absorption of a passing photon (radiative excitation), the electron will transition to a higher energy state. It will typically remain in this excited state for only a very short amount of time, after which it transitions to the lowest available level either

directly or by cascading down through intermediate energy levels. One or more photons are emitted in the process (depending on the path down to the lower level), each emitted in a random direction. If the electron was radiatively excited, then the net effect is that the incident photon is changed in direction, and possibly energy - effectively scattering the photon from its original direction.

- 2. <u>lonizations</u>. Commonly called "bound-free" transitions, any incident photons with energy greater than the amount needed to bind an electron to the atom results in the photon being absorbed and the electron ejected from the atom. Any energy carried by the photon in excess of that needed to ionize the atom is carried away by the electron in the form of kinetic energy of motion increasing the temperature of the gas.
- 3. <u>Interactions between free electrons and ions</u>. This is a free-free interaction in which a photon is created through the interaction between a free electron and an electrically charged ion. The ion's electric field causes the moving electron to decrease its speed to decelerate. As with any charged particle experiencing a deceleration, a photon is emitted with energy corresponding to the kinetic energy lost by the electron. This process has the effect of adding to the radiation field while cooling the gas.
- 4. <u>Interactions between free electrons and photons</u>. Also a free-free interaction. In this process, the electric field of the photon interacts with a free electron causing the electron to accelerate. This acceleration results in the emission of a photon of the same energy, but in a random direction. This changes the direction of the photon without change to the temperature of the gas and is essentially a pure photon scattering process.

Each of these processes contributes to the continuum to a greater or lesser extent depending on conditions within the photosphere such as temperature, density, and degree of ionizations of the elements present. The net effect of these processes is to redirect, or scatter, photons in random directions and, in the case of the lower photosphere where the distance a photon travels between interactions (the mean free path) is very short, to "smooth out" the individual photon energies and directions into a smooth continuum across wavelengths.

Returning to our analogy of a very dense fog on an otherwise sunny day, light from the Sun is scattered as it travels through the fog with the result that the intensity of the Sun is distributed throughout the fog - we see the brightness the Sun adds, but in all directions and without any indication of the direction of the Sun. Near to us we can

discern objects such as trees and utility poles, but as we peer deeper into the fog we see objects become less distinct until we eventually see only the fog itself - appearing as a uniform glow of light in every direction we look. This is the same for the continuum in the deeper layers of the stellar photosphere - look deep enough, a few hundred kilometers or so, and all that is seen is a uniform radiation with no distinct features.

3.3.2 The Shape of the Continuum

A distinctive characteristic of the continuum in a spectral profile is its shape and the behavior of that shape as the temperature of the photosphere increases. First, the number of photons emitted at any given energy is greater for stars of higher photospheric temperature than stars of lower temperature. This seems reasonable as you would expect the number of interactions between photons and particles of matter (atoms, ions, and electrons) in hotter stars to be greater than for stars of lower temperature since higher temperature means higher particle velocities and less time between interactions, resulting in more photons being created per unit time.

Second, the energy at which the highest number of photons is produced is greater for stars of higher temperature than stars of lower temperature. Higher energy means shorter wavelength, so the wavelength at which the maximum number of photons is produced shifts toward shorter wavelengths as temperature increases. This also seems reasonable since higher temperatures means more energy involved in the interactions between photons and particles, and so the statistical mean energy increases as well.

The shape of the continuum in a spectral profile is closely approximated by a theoretical construct called a blackbody - describing a body that is both a perfect absorber and emitter of radiation. The general shape of the emission by a blackbody is given by Planck's law:

$$B_{\lambda,T} = \frac{2hc^2}{\lambda^5} \frac{1}{e^{hc/k_b T} - 1}$$

Where $B_{\lambda T}$ is the intensity at wavelength λ , h is the Planck constant, c is the speed of light, k_b is the Boltzmann constant, and T is temperature in Kelvins. The shape of the continuum for a photosphere at three temperatures is depicted in Figure 3.4.

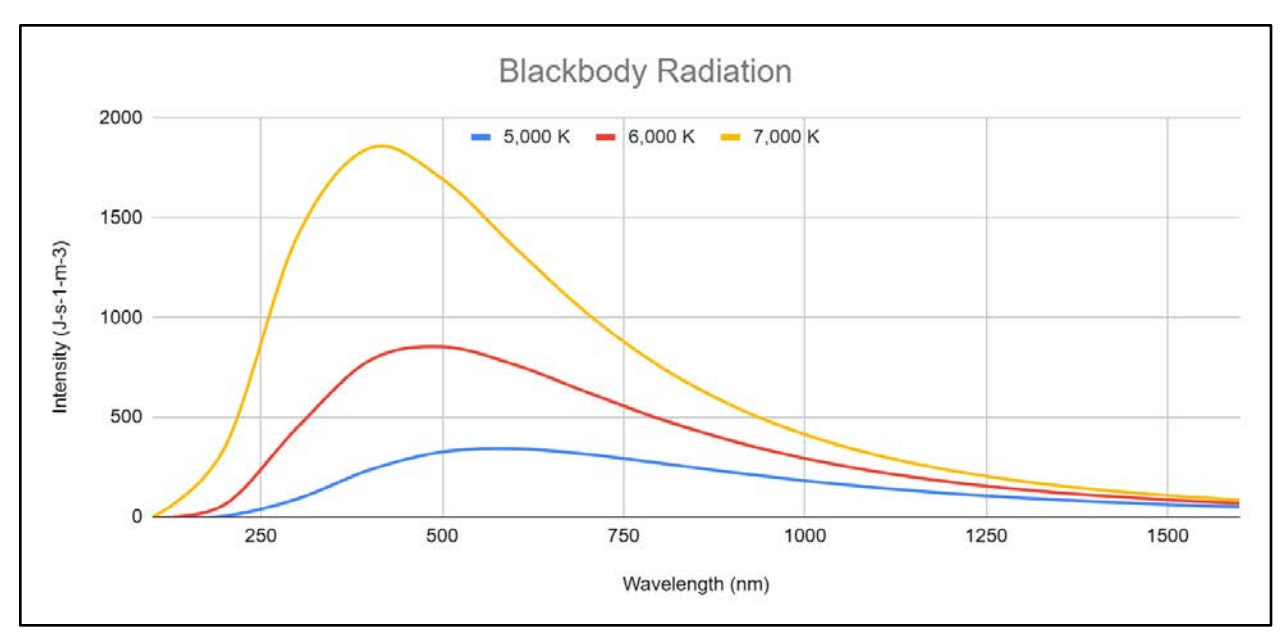


Figure 3.4 - Planck curves for a perfect blackbody radiator

A few things to note here. The first is that the curves never cross one another. This is interpreted to mean that as temperature increases, so does the intensity of radiation emitted at all wavelengths. The second is that as temperature increases, the wavelength of maximum intensity shifts to shorter wavelengths. The wavelength of maximum intensity for a given temperature is given by Wien's Displacement Law, after German physicist Wilhelm Wien.

$$\lambda_{max} = \frac{b}{T}$$

Where λ_{max} is the wavelength of peak intensity, T is the temperature in Kelvin, and b is Wien's displacement constant.

From both of these an estimate of stellar temperature can theoretically be made - fitting a Planck curve to the continuum and using Wien's law to estimate temperature from the peak wavelength. In practice one can only obtain a very rough estimate of temperature since the actual stellar continuum is modified by effects altering the shape of the continuum. Even for a well-defined continuum, the peak wavelength is difficult to determine with any certainty as the peak is often not sharp but rather a shallow curve in which only a range of wavelengths for the peak can be estimated with any certainty. Additionally, the peak may fall outside the range of the visible spectrum - making the use of Wien's law to determine temperature impossible. Other methods for determining

a star's temperature, and therefore spectral type, are employed, such as measurements of relative absorption depths, to obtain a better estimate of temperature.

Table 3.1 - Temperatures and peak radiation wavelengths for the spectral types (main sequence)

Spectral Type	Temperature (K)	Wien Peak Wavelength (nm)
O5	47,828	60.6
В0	23,422	123.6
A0	11,470	252.5
F0	7,554	383.4
G0	5,617	515.6
K0	4,464	648.7
MO	3,699	782.9

Ref: University of Northern Iowa

https://sites.uni.edu/morgans/astro/course/Notes/section2/spectraltemps.html

In summary, the continuum represents the general shape of the spectral profile and is a result of numerous interactions between photons and particles of matter in the deeper layers of the stellar photosphere. The result is a uniform field of radiation closely approximating that of a theoretical blackbody and with characteristics, such as its general shape and wavelength of maximum energy, described by the Planck equation and Wien's Law.

3.4 Absorption Lines

Absorption lines represent a reduction from the continuum at specific wavelengths due to absorptions of photons at higher, optically thin, layers of the stellar photosphere. In the previous section we used the analogy of a dense fog in describing the origin of the continuum. As you look deeper into the fog you see only the uniformly scattered light from the Sun. This is because as you look deeper into the fog, you are looking through progressively more layers of atmosphere in which light is being scattered. But closer to you, you can make out a few trees. A bit further into the fog the trees begin to disappear, and then farther in yet are lost to sight altogether. For the trees closest to you, the depth of the fog you're looking through is small and increases for the trees farther from you. So, although you know there are plenty of trees along your line of sight, the fog allows you to see only those closest to you. And you see them only

because these nearby trees are blocking (absorbing) some of the light from the fog behind them.

A similar mechanism is in play in the appearance of spectral absorption lines. Interactions between photons and atoms result in electrons being excited to higher energy states within the atom. As the electron cascades down to its original state, one or more photons are emitted at various energies and in random directions. The net effect of these types of transitions within the atom is to diminish the intensity of radiation along the line of sight to the observer. This reduction is a subtraction from the continuum. Although the electron transitions leading to the formation of absorption features in the spectrum occur at various layers, it is only those in the upper photosphere that produce the absorption lines we observe. To the analogy of the fog, the reduction in the intensity of the fog (the continuum) along our line of sight is primarily due to the trees closest to us (i.e., the upper layers of the photosphere). Similarly, the absorption features we observe in a stellar spectrum originate in the upper layers of the photosphere.

Absorption lines due to hydrogen are generally the most prominent and also the simplest of the atomic spectra. These lines are present to some degree in nearly all spectral types but are strongest in the type A stars. Other lines include those from neutral and singly ionized elements in cooler stars, multiply ionized elements in hotter stars, and broad absorption bands due to molecules in very cool stars.

3.4.1 The Presence of Elements in Stellar Spectra - Abundances

Whether an element or any of its ions is present as an absorption line in a stellar spectrum depends on the abundance of that element as well as the temperature of the stellar photosphere. Knowing what elements are present and the abundances of those elements is the first step in determining what elements we can expect in a stellar spectrum. For this we will focus on the 20 most abundant elements by number in the Sun's spectrum.

Table 3.2 - Abundance of elements by number in the solar photosphere

Element	Symbol	Atomic Weight	Percent Abundance	Element	Symbol	Atomic Weight	Percent Abundance
Hydrogen	Н	1.01	92.05	Argon	Ar	39.95	0.00058
Helium	He	4.00	7.83	Aluminum	Al	26.98	0.00023
Oxygen	0	16.00	0.061	Calcium	Ca	40.08	0.00018
Carbon	С	12.01	0.030	Nickel	Ni	58.69	0.00018
Nitrogen	N	14.01	0.0084	Sodium	Na	22.99	0.00016
Neon	Ne	20.18	0.0077	Chromium	Cr	52.00	0.00007
Iron	Fe	55.85	0.0037	Chlorine	CI	35.45	0.00004
Silicon	Si	28.09	0.0030	Phosphorus	Р	30.97	0.00003
Magnesium	Mg	24.31	0.0024	Manganese	Mn	54.94	0.00002
Sulfur	S	32.06	0.0015	Titanium	Ti	47.90	0.00001

Allen, C. W. (1981)

Table 3.2 presents the 20 most abundant elements by number present in the Sun's photosphere in order of abundance. Generally, but not always, the elements of lower atomic weight are more abundant than those of higher atomic weight. There are a few exceptions, such as oxygen being twice as abundant as carbon, even though it has a higher atomic weight than carbon. Another is iron with atomic weight 55.85 being the 7th most abundant element in the solar photosphere even though, based on its atomic weight, it should be near the end of the list. There are more exceptions, but the general trend of abundance decreasing with atomic weight remains mostly intact.

Another notable feature of this list is the absence of the light elements lithium, beryllium, and boron. These are elements that, once manufactured in the interior of a star like our Sun, are quickly transmuted into other elements, and therefore do not survive in any appreciable number in a typical stellar photosphere.

Hydrogen and helium together constitute 99.98 percent of the total number of atoms in the Sun's photosphere with the remaining 0.02 percent consisting of the 18 other elements in this list. Based on this, one could expect that lines of hydrogen and helium would dominate the solar spectrum, but that is not entirely the case. Lines from elements other than hydrogen and helium can show strong lines in the solar spectrum - stronger than those of hydrogen, with the Fraunhofer H and K lines due to ionized calcium being a notable example. It turns out that temperature plays a significant role in the appearance and strength of spectral lines - with abundance taking on a secondary

role, and this is the reason why the H and K lines from calcium can appear stronger than the lines from hydrogen in the solar spectrum.

3.4.2 The Presence of Elements in Stellar Spectra - Temperature

As a first step in understanding how temperature plays its part in determining the presence and strength of absorption lines in a spectrum we will consider the excitation energies of the neutral form of the elements in our list of 20 most abundant elements. A neutral element is one which has its full complement of electrons, as opposed to an ion in which one or more electrons has been removed. In astronomical nomenclature, a neutral element is designated by its atomic symbol followed by the Roman numeral I. Neutral hydrogen is designated H I and neutral iron is designated Fe I, for example. The Roman numeral increments with each stage of ionization, so singly ionized Iron is designated as Fe II and doubly ionized Iron as Fe III.

The excitation energy is the energy required to excite an electron to a higher bound level. Subsequent deexcitations result in absorption lines in the spectrum as the photons emitted in the transition of the electron to lower levels of the atom are emitted in random directions, effectively reducing the photon flux in the direction of the observer. Since lower energy corresponds to lower temperature and higher excitations to higher temperatures, we can use this as a rough indication of which elements will produce spectral lines in a stellar spectrum for stars of different temperatures. The excitation energy listed for each element is the average excitation energies for all spectral lines produced by that element within the range of the visible spectrum (380 nm to 780 nm).

Table 3.3 - Average excitation energies of the neutral elements (20 most abundant)

Element	Excitation Energy (eV)	Percent Number Abundance	Element	Excitation Energy (eV)	Percent Number Abundance
Til	4.51	0.00001	SI	9.96	0.0015
Ca I	4.81	0.00018	СІ	10.74	0.0305
Ni I	5.21	0.00018	CII	11.64	0.00004
Al I	5.74	0.00023	НΙ	12.70	92.05
Mn I	5.79	0.00002	NΙ	13.47	0.0084
Fe I	6.03	0.0037	01	13.64	0.0608
Cr I	6.14	0.00007	Ar I	14.77	0.00058
Mg I	7.18	0.0024	Na I	20.51	0.00016
Si I	7.22	0.0030	Ne I	21.04	0.0077
PΙ	9.56	0.00003	He I	23.71	7.83

(From calculations by S. Donnell and NIST spectral line data)

Table 3.3 shows the 20 most abundant neutral elements by number in the solar photosphere ordered by their average excitation energy. Since excitation energy increases with temperature, this serves as a rough guide for what neutral elements to expect in stellar spectra for stars of different temperatures. Titanium, calcium, nickel, etc. would first appear in the cooler stars, hydrogen, nitrogen, and oxygen in hotter stars, and neon and helium in stars hotter yet, with the strengths of these lines being influenced in part by abundance.

A graphical representation of this table in which the abundance is plotted against the average excitation energy allows us to get a better idea of which elements we can expect to appear most prominently in the spectrum as a function of temperature and abundance.

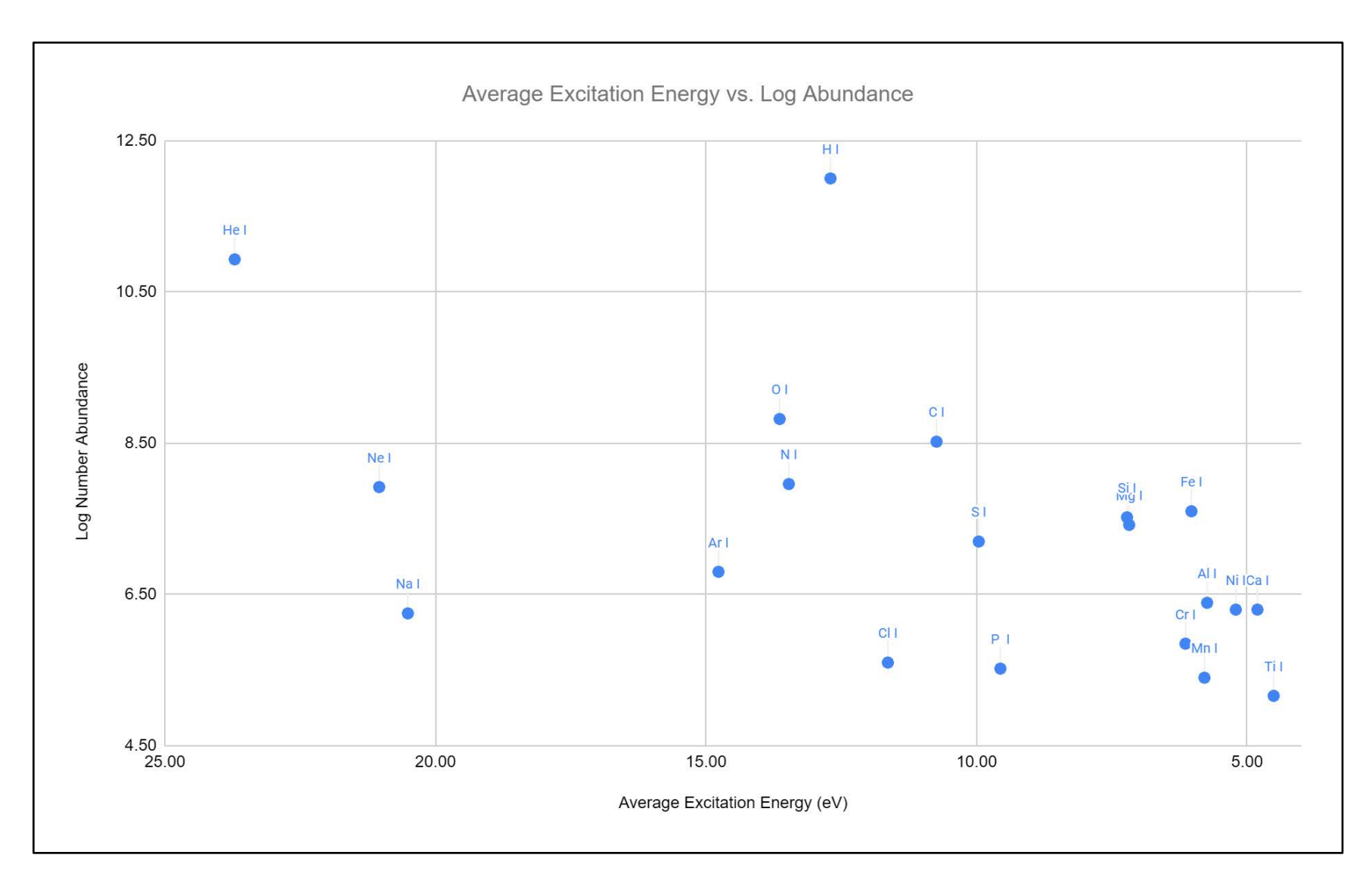


Figure 3.5 - Average excitation energies of the neutral elements by abundance

In this plot the horizontal axis is shown in order of lower to higher excitation energy from right to left. This is consistent with plots of spectral types in which the temperature scale is in order of higher to lower temperature as you move from left to right. The vertical axis is the number abundance of the element in the solar photosphere. Here we can see, for example, that neutral iron (Fe I) has a relatively low excitation energy but is present in larger numbers than other neutral elements of similar excitation energies. It is not surprising, then, that iron is predominant in many stellar spectra over that of other elements of similar excitation energy.

3.4.3 Effect of Excitation and Ionization on the Spectral Lines

The number of photons capable of exciting an atom is determined by temperature - first small numbers of photons with the required energy and then progressively more as temperature increases. As such, one would expect the strength of a spectral line to increase as temperature increases. This is true, but only up to a point. Although as the temperature increases and the number of photons of the required excitation energy increases, some of the photons produced will be sufficiently energetic to remove the electron from the atom entirely - ionizing it via a bound-free interaction. The effect of this ionization is to reduce the number of neutral atoms capable of being excited. At first, the level of ionization is very small, but as temperature increases, more and more atoms become ionized, to a point finally where nearly all of the atoms are ionized and there are none left to become excited and produce the spectral lines. The result is that, for a given element in a given ionization stage (i.e. neutral, singly ionized, etc.), the spectral lines due to excitations begin to appear at some temperature, increase in strength as temperature increases, reaching a maximum at yet higher temperature, and then decline in strength with further increasing temperature as ionizations become dominant.

The principal atomic energy levels are designated as "N =" with a numerical value indicating the level. The ground state of the hydrogen atom is labeled as N = 1 and the next higher as N = 2. These states are also referred to as the 1st and 2nd energy levels in the atom. For hydrogen, higher energy levels are progressively closer spaced until the point where the energy associated with the highest energy levels approaches that required for the electron to become unbound from the atom, or ionized. Figure 3.6 depicts these energy levels and the corresponding wavelengths of photons absorbed or emitted for electrons transitioning between these levels.

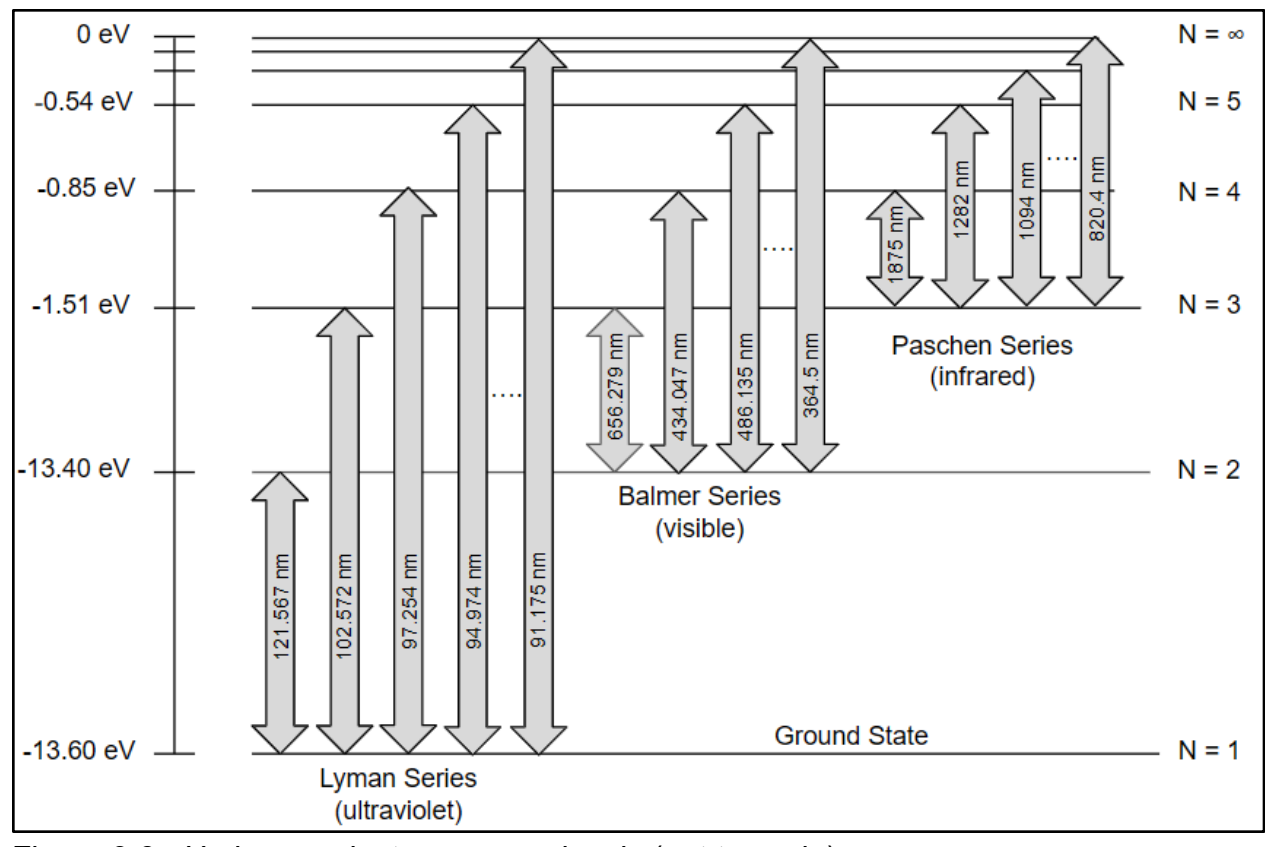


Figure 3.6 - Hydrogen electron energy levels (not to scale)

Transitions to and from the ground state are called the Lyman series and the wavelengths corresponding to transitions to and from the ground state are in the ultraviolet portion of the spectrum. The Balmer series of transitions are those for which an electron transitions to or from the 2nd energy level, producing lines in the visible portion of the spectrum. The Paschen series are those in the infrared and involve electron transitions to and from the 3rd energy level of the hydrogen atom. There are additional series corresponding to transitions to the N=4 and higher levels, but these produce lines in the far infrared and longer wavelength regions of the electromagnetic spectrum.

Figure 3.7 shows the effect of temperature on excitations of the hydrogen atom. At temperatures below 3,000 K nearly all of the hydrogen atoms have their electrons populating the lowest energy level, or ground state. At this low temperature there is insufficient energy to excite electrons to higher energy levels. We refer to these atoms as "unexcited". As temperature increases, the number of hydrogen atoms with electrons in energy levels above the ground state begins to increase as the energy required for these transitions begins to increase. These atoms are beginning to become "excited".

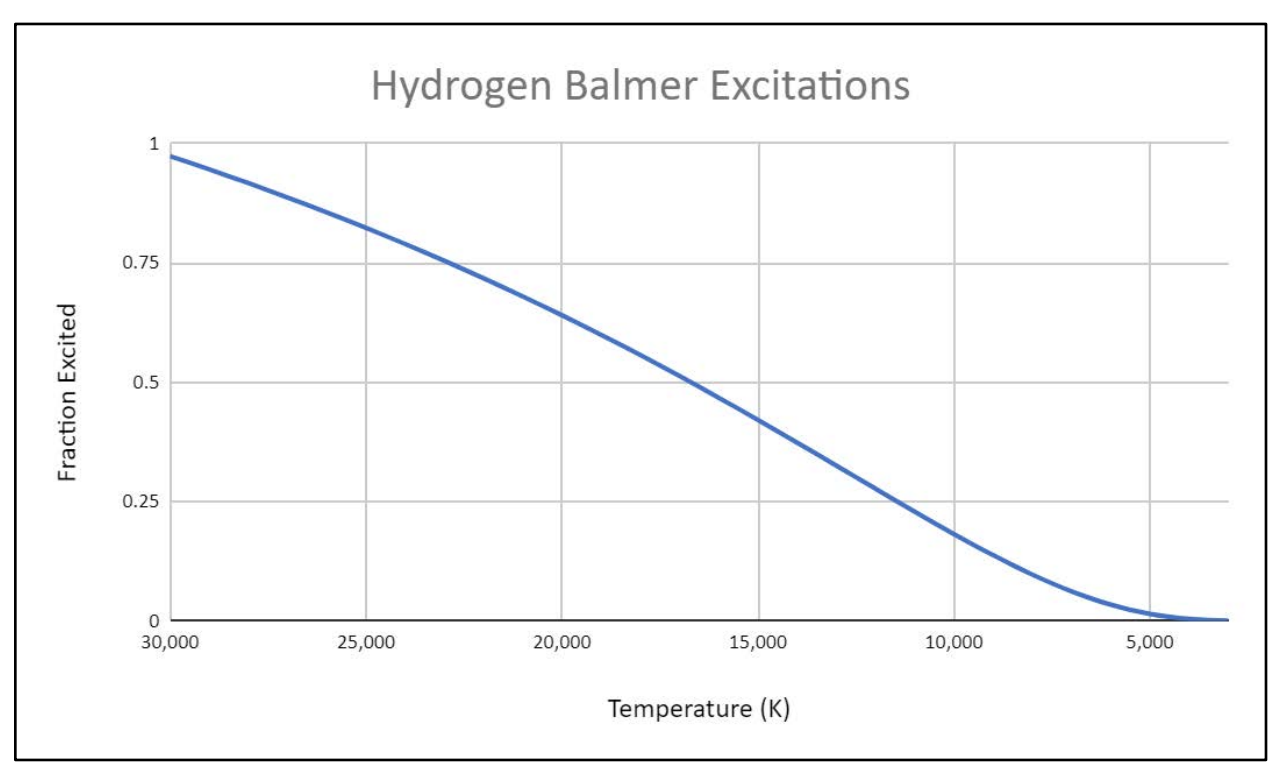


Figure 3.7 - Hydrogen Balmer excitations with increasing temperature

With increasing temperature, the hydrogen atoms begin to become excited with more electrons populating higher energy levels. The electrons remain in these higher levels only for very short periods of time (on the order of nanoseconds) and spontaneously cascade down through lower energy levels until they reach the ground state, with each transition between levels producing a spectral line. For hydrogen, transitions to and from the ground state (N=1) result in spectral lines in the ultraviolet part of the spectrum. Transitions to and from the N=2 level result in spectral lines within the visible portion of the spectrum and transitions to and from the N=3 level result in lines in the infrared portion of the spectrum. In the discussion following, we are concerned only with transitions into or out of the N=2 level, i.e., the Balmer series.

As stated previously, at temperatures below 3000 K nearly all of the electrons in the hydrogen atoms are in the N = 1 level (the ground state). As temperature increases, the number of electrons in higher levels, that is, in energy levels N = 2 and higher, begins to increase. This continues until, at about 30,000 K, nearly all of the hydrogen electrons have been excited to higher levels. As the temperature increases there are more electrons transitioning from these higher levels into the N = 2 state and producing spectral lines, and so the strength of the hydrogen Balmer lines increases in strength as temperature increases.

Now we discuss the effect of ionizations. At temperatures less than about 9,000 K almost none of the hydrogen atoms are ionized. Between about 9,000 K and 17,000 K the number of ionized hydrogen atoms increases rapidly (and the corresponding number of neutral atoms decreases) such that at temperatures greater than about 17,000 K, nearly all of the hydrogen atoms are ionized. With an increasing number of ionizations there are fewer neutral hydrogen atoms with bound electrons remaining capable of producing spectral lines, and so the strength of the hydrogen Balmer lines decrease in strength to disappear entirely as the hydrogen atoms become fully ionized. Figure 3.8 shows the effect of temperature on ionizations.

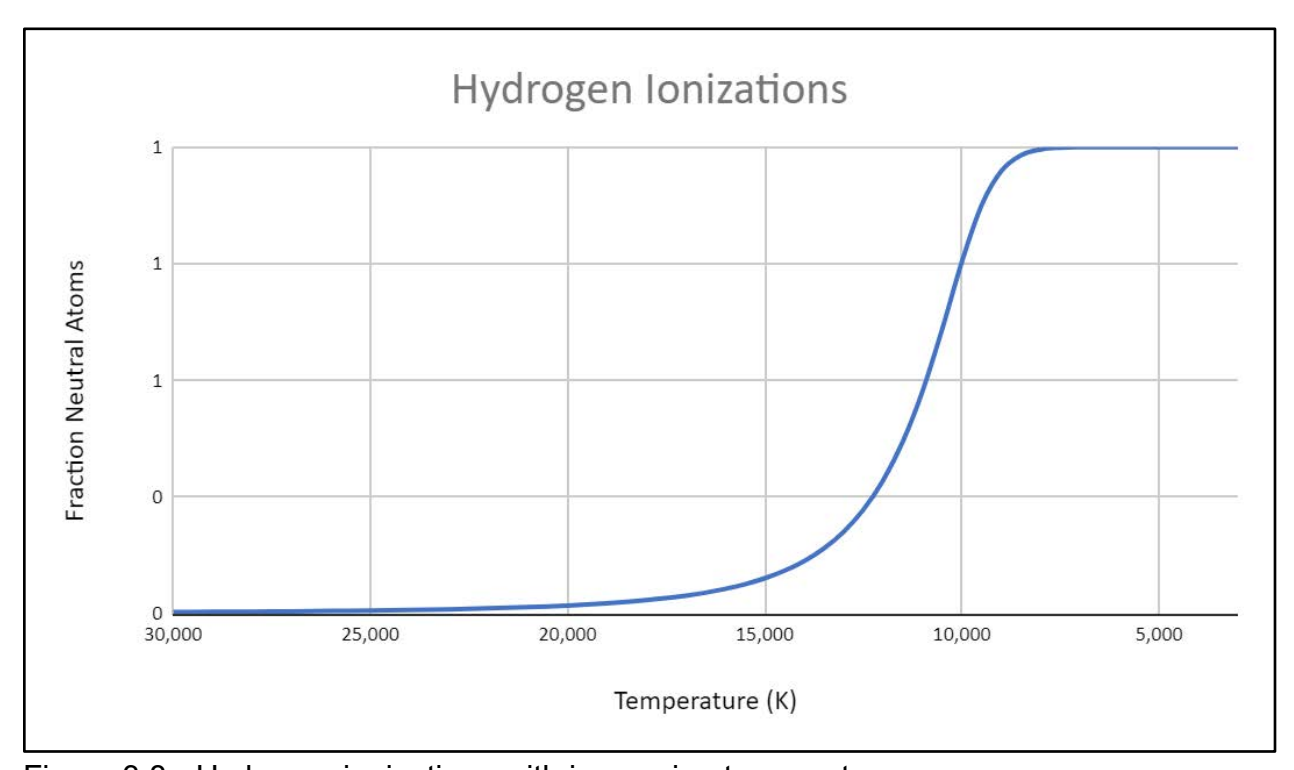


Figure 3.8 - Hydrogen ionizations with increasing temperature

Figure 3.9 shows the combined effect of excitations and ionizations for the hydrogen Balmer lines for temperatures between 3,000 K and 30,000K. From 3,000 K to 10,000 K the number of excited hydrogen atoms increases as expected and the strength of the Balmer lines increases in the spectrum. At about 9,500 K this trend reverses as ionizations act to reduce the number of neutral hydrogen atoms capable of producing spectral lines. The strength of the Balmer lines decreases as temperature continues to increase.

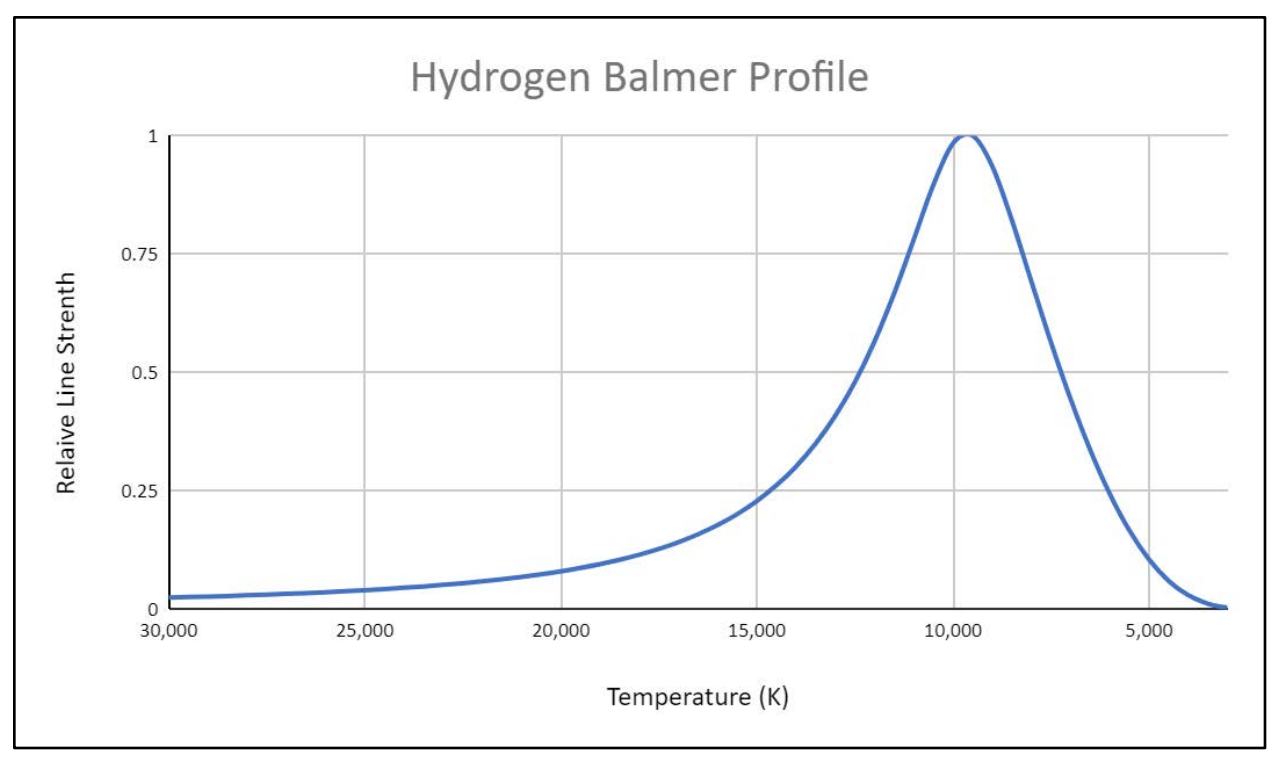


Figure 3.9 - Hydrogen combined excitation and ionization

Similar graphs can be constructed for other elements in their neutral and various ionization stages and each will display a similar curve in which the strength of their spectral lines will increase with temperature, reach a peak, and then decrease with further temperature increase as shown in Appendix 5.

3.4.4 Ionization Stages of an Element and the Spectral Lines

Figure 3.10 below shows profiles of combined excitation and ionization for Fe I through Fe III. As expected, the profiles for the higher ionization stages are displaced toward higher temperatures as higher temperatures are required to produce photons with the required excitation and ionization energies. Also note that these curves overlap each other to some extent - meaning that we can expect multiple stages of ionization for an element to appear in a stellar spectrum at a given temperature. For example, we can expect to see absorption lines due to Fe I and Fe II in stars of temperature between about 4000 K and 8000 K. In hotter stars, between temperatures of about 15,000 K and 25,000 K we can expect to see absorption lines due to Fe II and Fe III. Also note that the vertical scale for the three profiles shown in Figure 3.10 is normalized to highlight the differences in shape and temperature of peak line strength for these three profiles.

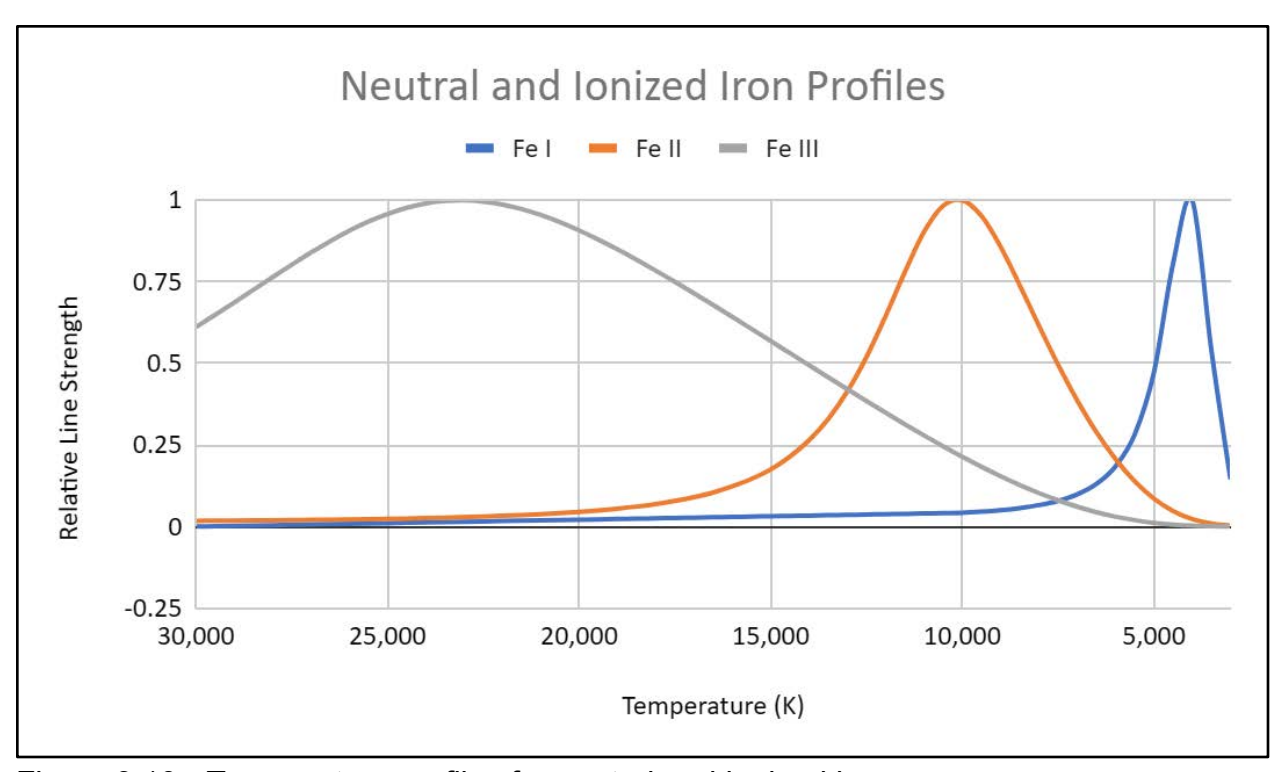


Figure 3.10 - Temperature profiles for neutral and ionized iron

Figure 3.11 shows the ionization energies for the 20 most abundant elements for successive ionization stages. What is seen in this view is that for any given element, the energy of ionization increases with each ionization stage. This reflects the physical principle that as more electrons are removed from the atom, the remaining electrons are more tightly bound to the nucleus and therefore require more energy to ionize. Because of this, we expect to find elements of higher ionization stages, such as Na III and N IV present in the spectra of only the hottest stars. This means that each element will show a similar temperature profile for its neutral and ionized states as shown for iron in Figure 3.10. From this we can expect that the neutral elements will generally be found in cooler stars, such as spectral types K and M as shown in Figure 3.5, and with higher stages of ionization appearing as temperature increases, such as in spectral types B and A. This is the general progression we can expect for the appearance of elements and their ions in a stellar spectrum.

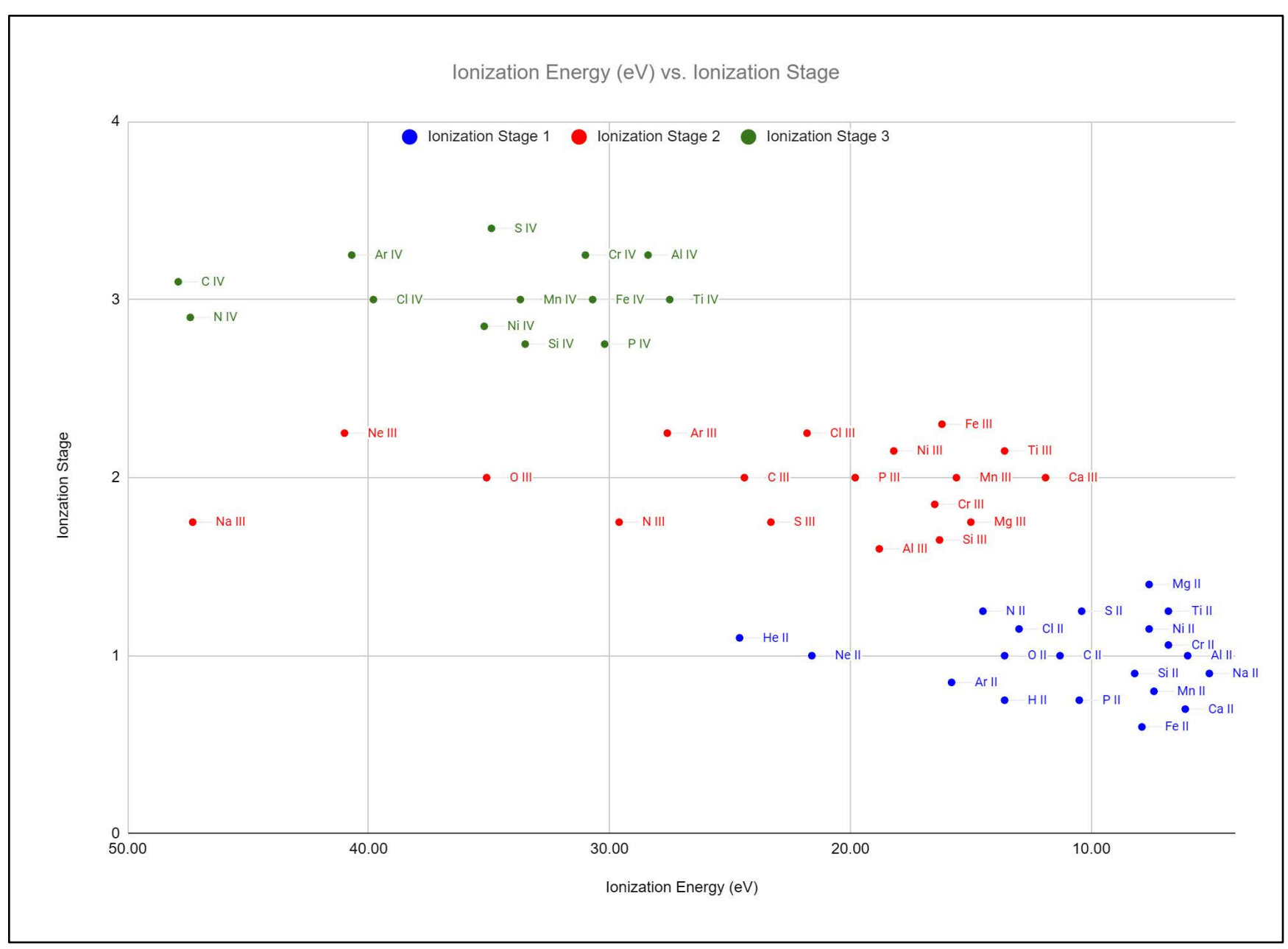


Figure 3.11 - Ionization energies increase for successive ionization stages

3.4.5 The Appearance of Molecules in Stellar Spectra

In cool stars of spectral types K and M we find numerous closely spaced lines, or bands, due to molecules such as titanium oxide (TiO), vanadium oxide (VO), calcium hydride (CaH), and magnesium hydride (MgH). The temperatures in these stars are low enough that the energy of the bonds between atoms forming these molecules is larger than the photon energy or the kinetic gas energy, and so these molecules experience a low number of dissociations.

Unlike atoms with distinct absorption lines due to transitions of an electron between energy levels, molecules introduce the possibility of photons stimulating transitions between vibrational and rotational states of the molecule. These vibrations and rotations, like the electron energy levels in an atom, are discrete, and the transitions between rotational and vibration states involve small energy differences. These small energy differences between molecular rotation and vibration states, combined with the large number of states possible, results in a series of closely spaced lines that typically converge at the short wavelength (i.e. higher energy) end. This set of closely spaced lines are called "molecular bands" with the wavelength where the lines converge called the "band head".

Table 3.4 - Prominent molecules in cooler stars

Spectral Type	Molecular Species
	Titanium Oxide (TIO), Vanadium Oxide (VO), Magnesium Hydride
М	(MgH), Calcium Hydride (CaH)
K	Cyanogen (CN), Methylidyne (CH)
G	Cyanogen (CN), Methylidyne (CH)

Walker, Richard (2017)

3.4.6 Telluric Absorption Bands

In the early 1800's, Joseph von Fraunhofer observed and measured prominent absorption features in the solar spectrum, denoting the most prominent features with capital letters and less prominent ones with lower-case letters, starting at the red end of visible spectrum and proceeding through to the blue end. Of these, Fraunhofer's A and B lines at 759.4 nm and 686.7 nm respectively are not produced by the Sun, but rather by the earth's atmosphere through which we observe it. Both the A and B lines are caused by absorption by molecular oxygen, O2, in the earth's atmosphere. The less prominent Fraunhofer a and y lines are also attributable to molecular oxygen in the

earth's atmosphere at 627.7 and 898.8 nm. An additional line due to molecular atmospheric oxygen is the Fraunhofer Z line at 822.7 nm.

The earth's atmosphere is relatively transparent to the absorption of water vapor over the visible spectrum, however localized areas of increased absorption can be seen in an astronomical spectrum, with absorptions discernable near 720 nm and 820 nm.

Like the molecular bands found predominantly in the spectra of cool stars, the atmospheric molecular oxygen and water vapor features are also bands, since these molecules have many vibrational modes resulting in closely-spaced lines with a somewhat sharp band head on the blue side of the band. And because the telluric lines exhibit no redshift, they can be used as wavelength references for calibration of high-resolution spectra.

3.4.7 The General Spectral Sequence

We can now assemble the above into a coherent picture of the characteristics of the spectral types.

Stars of spectral type O are hot enough that most of its hydrogen is ionized and helium is singly ionized. Elements such as nitrogen, and oxygen are doubly ionized, meaning that two electrons have been stripped away from these atoms.

In type B we see lines due to ionized and neutral helium becoming prominent along with lines due to a large mix of doubly ionized and singly ionized elements, including Si III, and O II. In the type B stars we see the hydrogen Balmer lines increase in strength.

In the type A stars we see the hydrogen Balmer lines at their strongest. Lines due to singly ionized magnesium, chromium, and titanium are at their strongest along with lines from neutral oxygen, nitrogen, and neutral and ionized iron.

In somewhat cooler stars of type F and G we find the strength of the hydrogen Balmer lines weaken. The strengths of the singly ionized atoms diminish and those of the neutral atoms become more prominent, including carbon, silicon, and phosphorus. In type G we see some molecular absorption bands due to CN and OH. The Fraunhofer H and K lines due to singly ionized Calcium are prominent. In the G type stars appear more blends of absorptions.

Finally, cool stars of type K and M show lines of neutral elements such as calcium, sodium, iron, and titanium, as well as increasing numbers of molecular absorption

bands. In type M stars in particular, these molecular absorption bands are so abundant as to mask the elemental absorption lines and the underlying continuum.

Table 3.5 - Characteristics of the spectral types

Spectral Type	Temperature Range	Hydrogen Balmer Lines	Other Elements and Ions
0	> 30,000 K	Weak	C III, Si IV, N III, He II, O III
В	10,000 K - 30,000 K	Strong	Fe II, Al II, Si II, Ne I, He I, Cl II, C II, Ti III, Al III, N II, Si III, Fe III, O II, S III, Ne II, Cl III, Na II
А	7,500 K - 10,000 K	Strongest	O I, N I, Ti II, H I, Mg II, Mn II, Cr II, Ca I
F	6,000 K - 7,500 K	Strong	Ca II, C I, Mg I, Mg II, Fe I, Fe II, Ni I
G	5,200 K - 6,000 K	Weak	Fe I, Fe II Mg I, Mg II, Mn I, Mn II, Ca I, Cr I. Weak molecular absorption due to CN and strong molecular absorption due to CH.
К	3,700K - 5,200 K	Very weak	Fe I, Ti I, Ca I, Co I, V I, Cr I, Mg I, Mn I, Ni I CN molecular band is detectable with the CH molecular band is more notable.
M	2,400 K - 3,700 K	Very weak	Ca I, Na I, Mg I, Fe I. Molecular TiO bands dominate and some VO bands are present. Na I and Mg I are often blended with TIO. A Ca II triplet may be visible in the near infrared from 849.8 to 866.2 nm.

Walker, Richard (2017)

3.5 Emission Lines

Although not common, there are some stars that show some of their spectral lines in emission rather than absorption. These emission lines are produced in an optically thin shell or disk of gas surrounding the star in which energetic photons from the star excite the atoms of the gas into higher energy levels and then emit photons of various energies and in various directions. Highly energetic photons can ionize the gas, stripping away an electron in the process. Subsequent capture of a free electron by an ion in the gas results in a downward cascade of the electron into the various energy levels and releasing photons in the process.

In these types of spectra, we still see the absorption lines as we would expect from the star's photosphere, but now with emission lines from the surrounding shell or disk of gas superimposed on the spectrum. In the case of the hydrogen Balmer lines, for example, the intensity of the emission lines from the shell or disk may be much larger than the

absorption lines from the star with the result that the emission lines mask the absorption lines and what we see is a normal stellar absorption spectrum but with some hydrogen emission lines instead of hydrogen absorption lines.

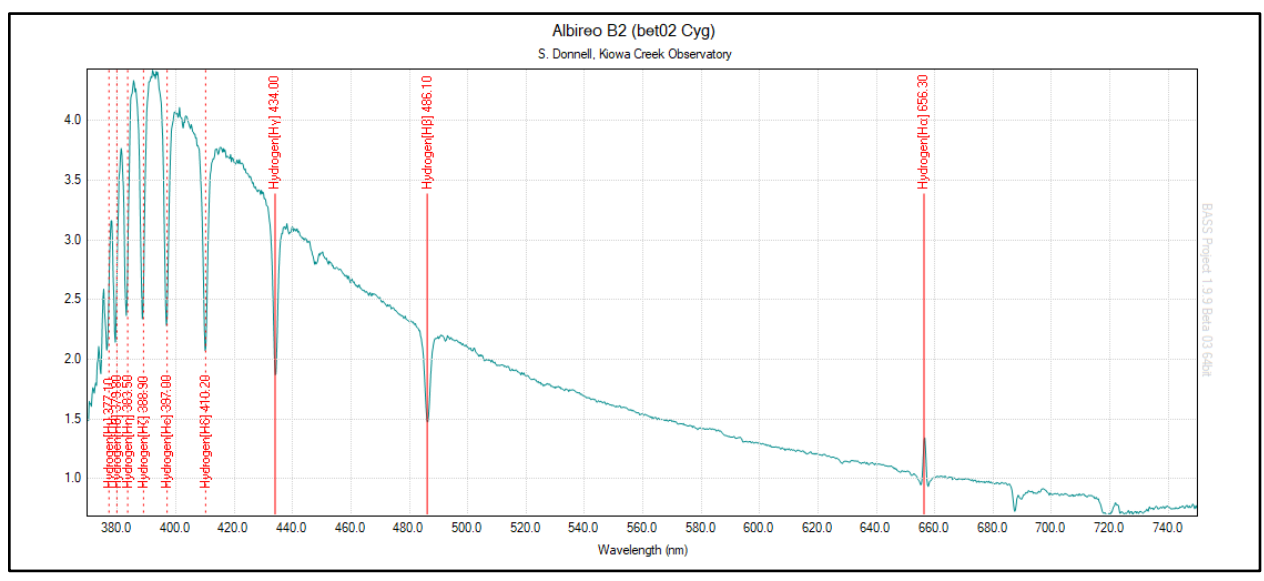


Figure 3.12 - Spectral profile of Albireo B2 showing Ha emission

In the case where the emission from the shell or disk is less than the absorption from the photosphere, we see shallower hydrogen absorption lines, or normal hydrogen absorption lines but with a smaller emission component somewhat displaced from the main absorption line due to motion of the gas. Some of these stars may also show weak emission lines from other elements such as singly ionized iron.

3.5.1 Shells from Stellar Winds

A shell is an envelope of gas surrounding the star that results from a strong outflow or wind from the star. The stars producing such strong winds are typically high mass, hot stars, such as spectral type O and B stars, post main sequence giant and supergiant stars of spectral types A and F, and young T Tauri type stars just evolving onto the main sequence. These shells typically expand at a rate measured in the hundreds of kilometers per second - much faster than the expansion rate of a typical planetary nova shell.

Spectra of stars with a surrounding expanding shell typically show a small absorption feature on the blue side of the emission lines. While the presence of emission lines indicates the presence of the shell, the blue-shifted absorption indicates an expansion of the shell. A careful measurement of the difference in wavelength between the emission peak and the center of the smaller absorption component tells us how fast the shell of gas is expanding. The peak of the emission line results from those parts of the

gas shell expanding away from our line of sight while the smaller blue shifted component is from that part of the shell directly in front of the star and expanding toward us.

This spectral feature of a broad emission line with a smaller absorption line just to the blue side is called a P Cygni profile, after the star in which it was first observed and understood. Figure 3.13 below shows the geometry of an expanding shell due to a strong stellar wind. The hot gas of the expanding shell produces emission lines, and those lines produced in the part of the shell expanding toward us are blue shifted while those produced in the part of the shell expanding away from us are red shifted. There is a region directly between the shell and the observer where the cooler gas of the outer shell is projected against the inner, hotter gas or the stellar photosphere itself. Photons from the hotter inner shell are absorbed in the outer cooler shell producing absorption lines. These absorption lines will be blue shifted as we are viewing that part of the shell which is expanding directly toward us.

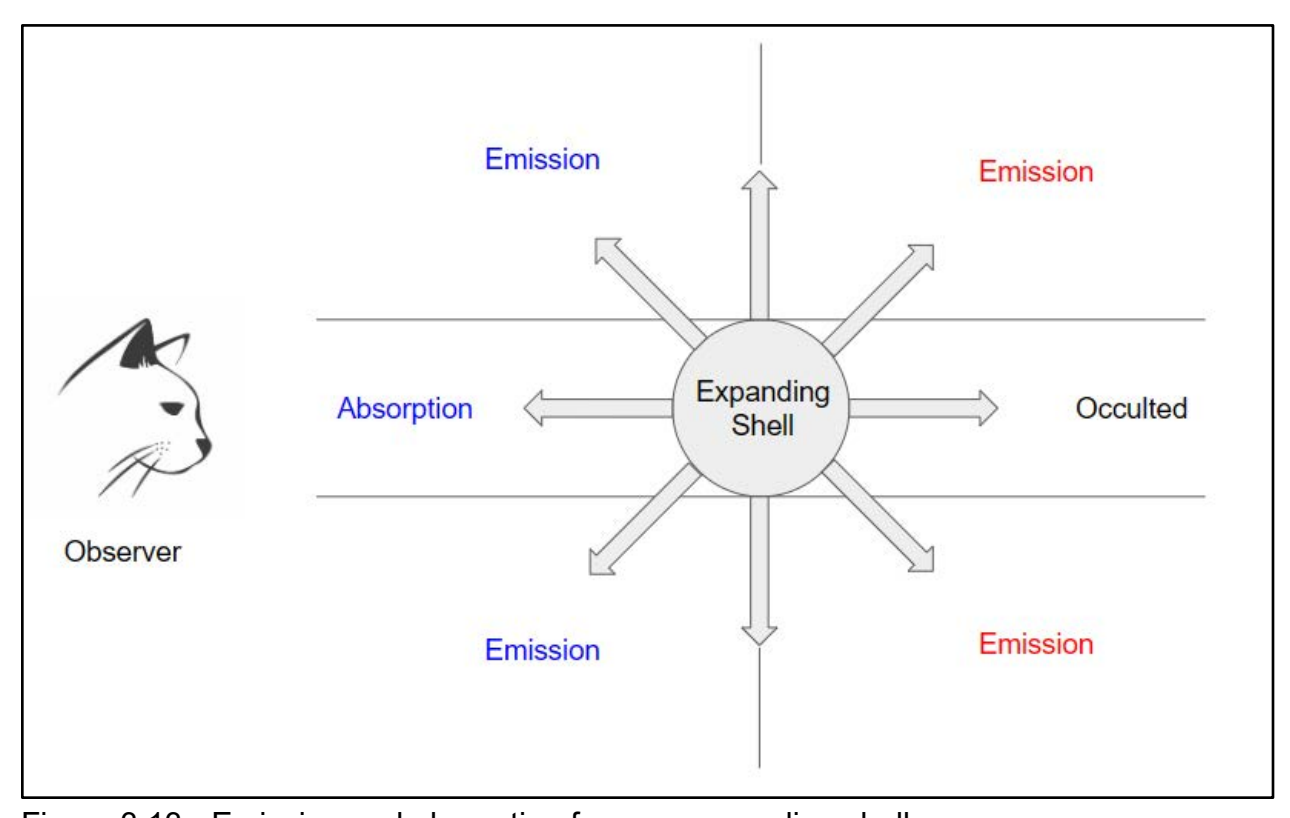


Figure 3.13 - Emission and absorption from an expanding shell

The left side of Figure 3.14 below shows the red and blue shifted emission lines and the blue shifted absorption lines. The right side of Figure 3.14 shows the superposition of these two spectral features that results in the P Cygni profile. A doppler broadened emission line is accompanied by a blue shifted absorption component. This is a general

characterization, as the density of the gas and its opacity will vary from shell to shell and therefore affects the shape of the resulting profile, but the general feature of the blue shifted absorption next to a broad emission component is common to all shell stars.

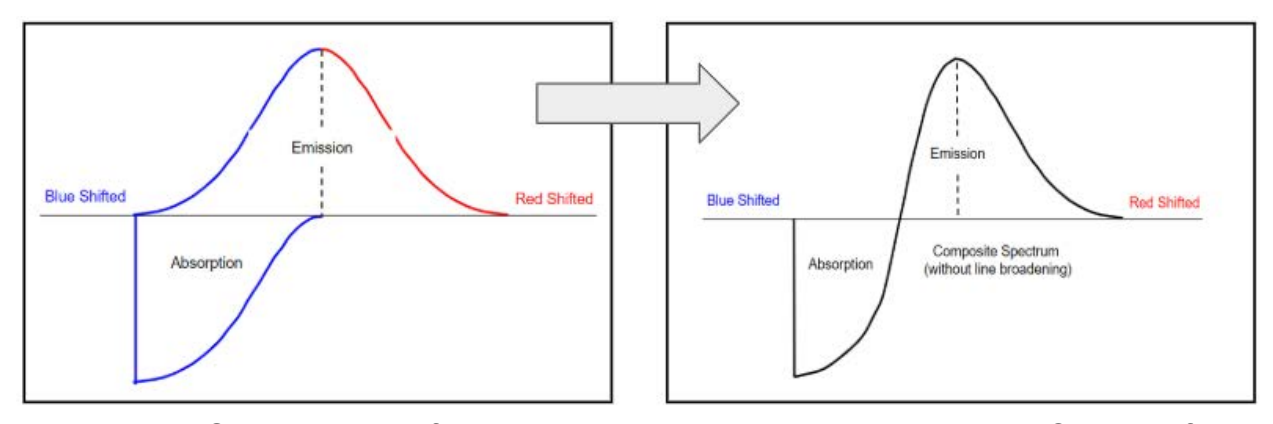


Figure 3.14 - Superposition of emission and absorption to produce the P Cygni profile

Some examples of stars whose spectra show emission features indicative of an expanding shell of gas include P Cygni, Achernar (alpha Eridani), gamma Cassiopeiae, and Albireo's blue component (beta Cygni B).

3.5.2 Shells from Nova

Expanding shells with emission lines are also observed in the post-eruption phase of a nova. These shells are similar to those described in section 3.5.1 but may include emission lines of other elements and in higher ionization stages due to the higher energy photons released in the outburst. While the nova eruption results in a new shell, it is also possible that the energy released from the eruption makes shells generated in previous outbursts visible again, if only briefly.

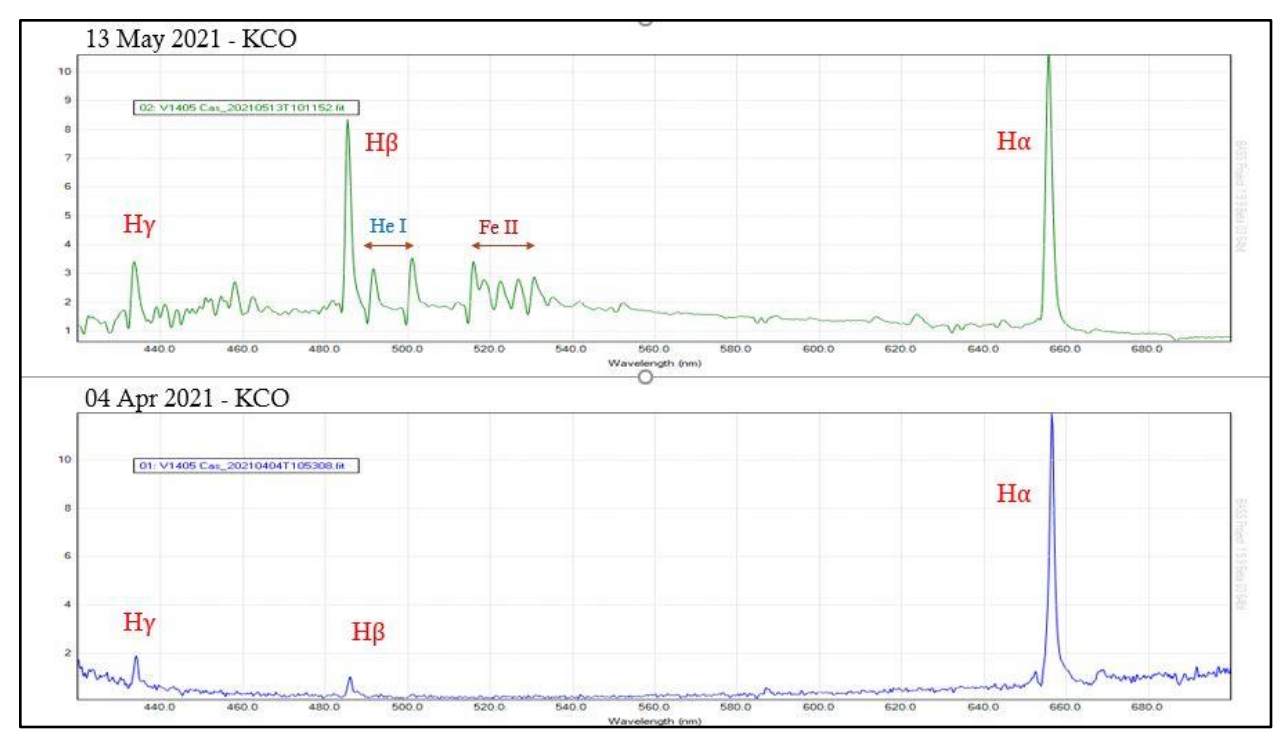


Figure 3.15 - Spectral profiles obtained by S. Donnell at Kiowa Creek Observatory of Nova Cassiopeia showing changes to emission lines over a five-week period

As the shell of the nova expands it can show significant changes in the observed spectrum. In the case of Nova Cassiopeiae that erupted in March 2021, the spectrum obtained by the author on April 4 shows a prominent H alpha emission and smaller emission lines of H beta and H gamma. Another spectrum obtained on May 13 shows the same H alpha emission line, but now with much stronger H beta and H gamma emission lines. Also observed in this spectrum are emission lines of neutral helium and singly ionized iron.

3.5.3 Spectral Features from Circumstellar Disks

Disks are, in a sense, a special case of a shell in which the mass of the shell is constrained to a flattened ring around the star. This is the case for the cataclysmic variables in which a donor star passes matter to a companion in a binary system, conserving angular momentum in the process of creating a rotating disk of matter. It also is the case for the Be stars in which the disk is formed from matter ejected from a rapidly rotating star. Unlike the P Cygni profile seen in an expanding shell, the rotating disk produces a "double hump" profile in the emission lines, where that portion of the disk rotating toward the observer displaces the line toward the blue end of the spectrum and that portion rotating away from the observer displaces the line toward the red. The central dip between the two peaks is the emission from that part of the disk in which the motion is tangential to our line of sight and no red or blue shifting occurs. The

difference in wavelengths between the red and blue peaks defines a lower limit to the rate of rotation of the disk as the inclination of the plane of the disk to our line of sight determines the extent to which we observe the rotation in the spectrum.

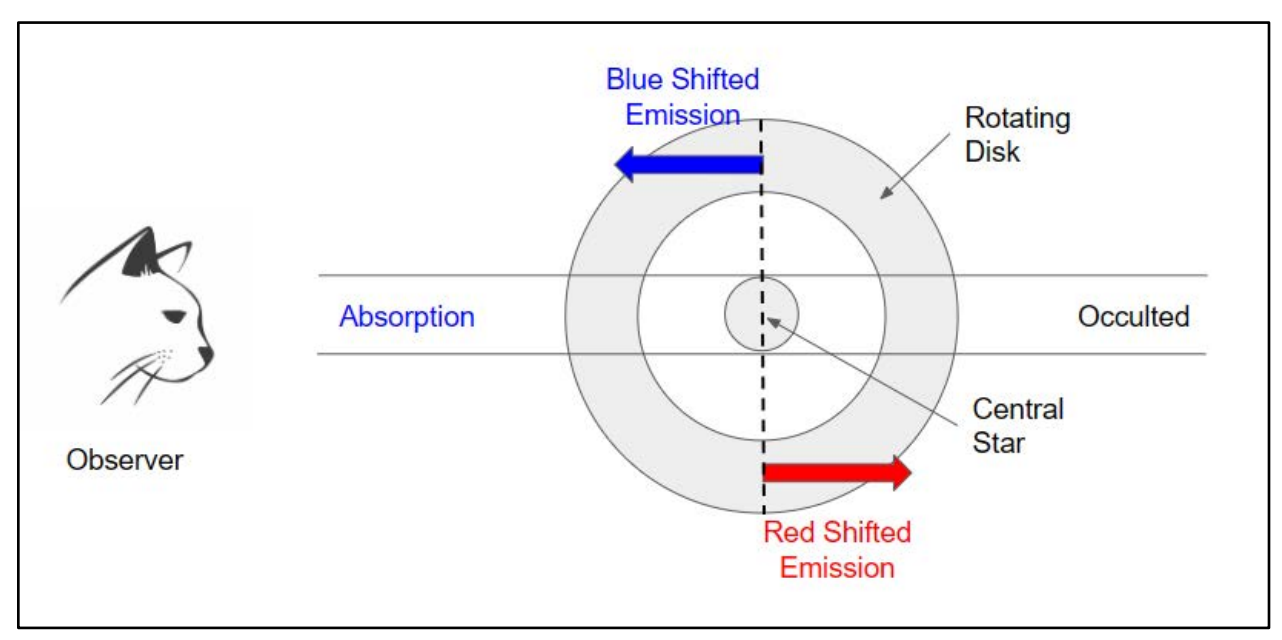


Figure 3.16 - Emission and absorption from a rotating circumstellar disk

Figure 3.16 depicts the geometry of a rotating circumstellar disk. From the observer's perspective, the emissions from the portion of the disk rotation toward the observer produce a blue shifted emission line while the portion of the disk rotating away from the observer produces a red shifted emission line. Between the two is the portion of the disk that is rotating tangentially to the line of sight, and these emissions are not doppler shifted at all.

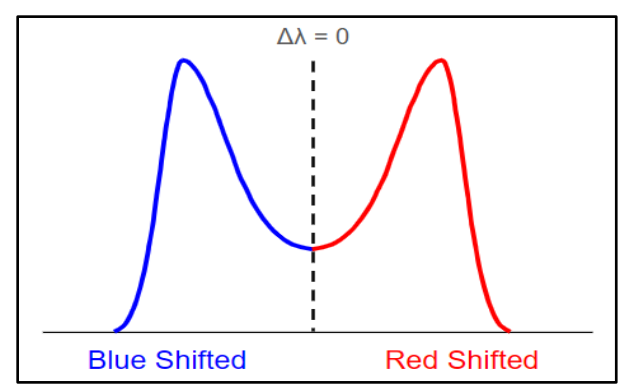


Figure 3.17 - Line profile for a rotating circumstellar disk

A combination of absorptions in the line of sight to the star along with a lower volume of gas in the viewed column (geometric effect) contributing to emission results in a decrease in overall emissions in this region. The result of all this is a "double hump"

profile in which the blue and red shifted emission lines show a dip in intensity between them as depicted in Figure 3.17.

3.5.4 Other Sources for Emission Lines in Stellar Spectra

Other types of stars showing emission lines include chromospherically active stars such as Chi Draconis, Epsilon Eridani, UV Ceti, and Barnard's Star. Semi-detached systems such as the dwarf novae and nova-like cataclysmic variables exhibit emission lines in their spectra in addition to being variable and are interesting objects to monitor for behavior variations.

4. Generation of the Profiles

4.1 Equipment Used and Observing Location

The equipment used in the acquisition of the spectra contained herein is fairly basic. Any amateur who has performed even the most rudimentary lunar or planetary astrophotography is certain to already possess most of what is needed. The complete list of equipment used is presented here:

- Celestron C6-N Newtonian Reflector Telescope (152mm aperture, 750mm focal length, f/5.0)
- Meade LX85 German Equatorial Go-To Mount with Tracking Drive
- ZWO ASI290MM Monochrome CMOS Camera
- Star Analyzer 100 Diffraction Grating (with 100 lines/mm)
- HP 17-inch Laptop with ASI Studio Software (for capture of raw data and image stacking)
- Stellarium planetarium software (for identification of targets and obtaining SAO or other catalog numbers)
- Rspec Software (for analysis and presentation of spectra)



Figure 4.1 - Observer's Scope, Mount, and Camera Used for Atlas

The optical tube of the telescope has not been modified in any way. The stock focuser, though sometimes a bit sloppy, is still usable. The mount has also not been modified, nor has any guiding system been incorporated into it. The camera used was chosen for its sensor array size, but other monochrome cameras are certainly suitable. (The use of color cameras is not generally recommended for serious work, as these tend to cause significant difficulties in generating frequency response curves. Despite this, color cameras can produce very aesthetically appealing spectrographs, and so are often used in outreach and demonstrations.) The Star Analyzer 100 is a filter-type grating that simply screws onto the nosepiece of the camera. The ASI Studio software employed is available for ZWO cameras, and includes modules for capturing data and image stacking. Stellarium is planetarium software, and is free for Windows, Mac, and Linux systems. The software can be found at https://stellarium.org/. The RSpec software is

available from https://rspec-astro.com/. The software is not free, but is modestly priced and extremely useful in the analysis and presentation of data. (A free thirty-day trial of the software is also available.) The location used was the backyard deck of one of the authors (A. Harding). No structure was used to shelter the equipment (or the observer!) from the weather. Each session was conducted by setting up the equipment, aligning the mount, and collecting data. Teardown was done after each session.

4.2 Data Ranges for Acquiring the Spectra

The wavelength range of the data presented is generally 3800-8000 Angstroms. For very dim specimens, the data range may begin at 4000 Angstroms due to practical limitations of the equipment used (camera exposures, tracking accuracy, etc.). However, the camera used does collect data into the near-infrared. M-type stars, whose radiation mostly falls in the higher wavelength region, may have ranges extending to 9000 Angstroms or more.

Each spectrum presented will have its horizontal axis labeled in Angstroms so that the wavelength range used for any particular specimen may be quickly determined at a glance.

4.3 Selection and Presentation of the Spectra

The selection of stars used for this Atlas were constrained by three factors. The first is the availability of the targets themselves. The observing location is at a mid-northern latitude, which places constraints on which stars would serve as viable candidates. As all amateur astronomers are aware, when a target is too near the horizon it becomes blurred by atmospheric dispersion. This is disastrous to spectroscopy.

The second criterion used was the star's luminosity class. Main sequence specimens were used when available to try and avoid changes in the spectra that can be induced by evolved giants or supergiants. Stars of different luminosity classes were used when necessary.

The final factor was the general quality of the resulting spectra. When multiple options were available, the one best demonstrating the general characteristics of the type of star involved was used

4.3.1 Classification of Spectra

The classification of spectra in this Atlas is done in a different manner from that which the reader may already be familiar. The standard manner of classification is referred to as the Morgan-Keenan classification scheme (also simply known as the MK system). In this scheme, the star's general type is listed as a letter sequence: O-B-A-F-G-K-M. O-type stars are the hottest, whereas M-type stars are the coolest. This sequence is easily remembered by using a simple mnemonic: "Oh Be A Fine Girl/Guy, Kiss Me".

Stars falling near the beginning part of this sequence are often referred to as "early-type" stars, whereas those nearer the end are "later-type" stars. This nomenclature is a relic of early theories of stellar evolution in which hotter stars were thought to be younger and would evolve into cooler, redder stars. As such, a blue star of spectral type O or B, for example, would have been referred to as "early" (younger), and a red star of spectral type K or M, for example, would have been referred to as "late" (older). Although we now know this not to be the case, the old terminology is still frequently encountered today.

Within each letter category, the MK system assigns a number from 0 to 9 to reflect a finer temperature gradient. An assignment of 0 is the hottest within that type, while 9 is the coolest. Using this assignment, a B2 star is hotter than a B9 star. These are the spectral subclasses.

Table 4.1 - Temperature progression within the spectral subclasses

Spectral Subclass									
0	1	2	3	4	5	6	7	8	9
<< Hotter (early)					Cooler	(late) >>	•		

Our own Sun, for example, is a G2 star. Vega, the brightest star in the constellation of Lyra, the Harp, is an A0 star. Again, the hotter stars within a given category are sometimes referred to as "early-type" stars, while those nearer the end are called "late-type."

Additionally, a Roman numeral is normally appended to the MK classification to reflect the star's luminosity class. This reflects the star's intrinsic brightness and evolutionary stage. This can range from 0 (for a hypergiant) to VII (for a white dwarf).

Table 4.2 - Luminosity classes

0	Hypergiant	
I	Supergiant	
-	Giant	
IV	Subgiant	
V	Main Sequence	
VI	Subdwarf	
VII	White Dwarf	

Harrison, Ken M, (2011)

Again, our own Sun is given the classification G2V (read as "G-two-five"). Betelgeuse is an M1I star ("M-one-one"). For amateur spectroscopy work, the VI and VII luminosity classes are not normally used.

Now, this is all very good for high-resolution work where the results are detailed enough to make fine distinctions, such as telling the difference between an F4 and an F5 star. However, for our purposes here it provides more detail than is needed. The low-resolution results presented here will not usually be detailed enough to make finer determinations with any confidence. We will therefore employ a modified and simplified custom classification scheme in this atlas that was originally presented in one of the authors' other works (A. Harding). We will still characterize stars by their general MK type (such as O, B, A, etc.). However, we will concern ourselves only with the following very general subtypes:

Table 4.3 - Specialized Classification Schema

able 1:0 openialized diadelineation continu			
Example (B-A-F)			
B9-A0			
A1-A3			
A4-A6			
A7-A8			
A9-F0			

The "very late-very early" types can be regarded as a sort of transitional type, where the very late subtypes of a given MK letter classification blend with the very early types of the next. Such stars may contain features in common with both types. For example, very early A-types often show some of the neutral helium absorptions more common in the later B-types. Often their low-resolution spectra show very little in differences, so it makes sense to group them together.

4.4 Data Collection and Processing Details

For those just getting started in amateur spectroscopy, the process of collecting and processing spectra can seem confusing, even daunting. This section will explain the processes used in the preparation of the Atlas in great detail. This should allow readers to grasp the methods used and get started collecting their own spectra in the shortest time possible. These processes are intentionally kept to a minimum, and so the results are not precise enough to be used for professional-level work. Of course, the addition of a few simple additional steps are enough to bring them in line with such precise work if desired. These will be mentioned where they apply.

The results presented here are therefore not intended to represent "the best" that an amateur can expect. Quite to the contrary, they can more accurately be regarded as "the worst" results that one can expect and still have a useful outcome—even if only on a personal level. The premise here is to provide an Atlas of spectra that a beginner can use for comparison. The procedures used can then later be refined if more detailed results are desired.

The equipment and software used were listed in Section 4.1. Differences in equipment and software will introduce deviations from what is presented here, but such deviations should be easy to accommodate.

4.4.1 Capture Process

The capture process used is detailed here:

1. Set up the equipment: The observer (A. Harding) normally uses his back deck, which is attached to the east side of his home. The location is in northeastern Indiana, which is not known for incredibly dark skies or necessarily cloudless skies. The nearest estimated Bortle rating is somewhere between 4 and 5. (The Bortle rating is a comparative measure of the darkness of an observing location. The scale goes from 1 (the darkest skies available on earth) to 9 (inner-city bright skies.) The site used does have a clear view of the eastern sky up to well past zenith. However, as targets pass the zenith, the telescope has to be aimed over the top of a house. During the winter months, this can cause significant seeing issues from the heat rising from the home. So, normally targets are captured as they are ascending in the sky, at altitudes high enough to avoid most atmospheric distortions. A small card table is set up next to the scope with the laptop used for the session.

- 2. <u>Align the scope</u>: Normally, a three-star alignment is used for the Go-To system of the LX85 mount, which seems to usually get the best results. A 40mm Plossl eyepiece is used for rough target acquisition, then a 25mm double-crosshair eyepiece is used to center each target.
- 3. Prepare Camera: The SA100 grating is screwed into the filter threads of the nosepiece of the camera, just as any commonly used filter would be. The tricky part can be making sure the grating is aligned properly with the camera. The SA100 grating has an alignment mark, which should be at the right-most position of the nosepiece. (You can imagine this as the three o'clock position when holding the camera with the nosepiece pointed directly away from you toward the telescope drawtube, with the camera markings on the rear of the camera being upright, readable, and level. You can also think of this as the +90-degree mark if 0-degrees is defined as being straight up and proceeding clockwise from there.) Even between sessions, it can be necessary to adjust the retaining ring to get the camera in the right position when screwing it in. This can be due to temperature and humidity differences between sessions. Alternatively, a small piece of tape can be used to secure the outer mounting of the SA100 grating to the nosepiece while it is in the proper position. (Just be **extremely** careful not to let any part of the sticky tape make contact with the glass of the grating!) The camera, with the SA100 attached and oriented correctly, is then connected to the computer with a USB cable.
- 4. <u>Select target</u>: Choosing a target from Stellarium, its SAO catalog number (or other listed catalog number) is entered into the mount's Go-To system, which then slews the scope to the proper location. The 40mm and 25mm eyepieces are then used to center the target, refocusing as needed.
- 5. <u>Capture footage</u>: The camera is inserted into the telescope drawtube and the ASI Studio software is used to preview the capture, fine-tune the target's location on the camera sensor, and perform the final focus on the target. The planetary imaging option is used, with short exposures (10 seconds or less, typically), using RAW16 format for SER files. When the focused spectrum line and the star are in the preview, adjustments are made to the focus, exposure, and gain to obtain the best overall result. Care must be taken not to overexpose the images. Remember, you are aiming for the clearest image on the spectrum, not the star! The author (A. Harding) prefers to keep the gain under 100 but has gone as high as 200(-ish) for dimmer targets. Higher gain levels introduce more noise into the resulting image, so keep it as low as possible. (The lower the gain, the better the dynamic range of the image.) After these adjustments, video footage is captured.

At least two minutes of exposures are desired so that there are a good number of frames to stack later.

6. Repeat steps 4 and 5 for additional targets.

This may seem unnecessarily verbose, especially to those who are already familiar with basic astrophotography, but this is the setup and capture process used in this Atlas. It may help those just getting started, especially those without a lot of astrophotography experience.

An alternative to video capture is to capture individual frames. These frames can then be used for stacking (in the following step). This alternative procedure is common for deep-sky photography, but was not used in the generation of profiles used in the Atlas.

Before jumping into the next step of the processes used in the reports included herein, it is important to note that if you will be submitting your work for use in scientific or professional circles, then the subtraction of the camera bias frames and dark frames must be done *before* proceeding with the steps below! These steps were skipped in generating the spectra presented in this Atlas. The goal, as mentioned previously, was to keep the procedures as minimal as possible in order to assist newcomers in gathering and processing data in the shortest time possible. The refinements of subtracting bias and dark frames will enable results of a more accurate nature, and therefore suitable for use in professional applications.

4.4.2 Image Stacking

After collecting the raw data, the next major step is stacking the acquired video or images. Though an upcoming release of the RSpec software will reportedly be capable of performing this stacking, the procedure listed here was used in this Atlas:

- 1. <u>Open ASI Studio and launch ASIVideoStack</u>. Locate the .SER file for the target and drag and drop it into the program window to open it. A preview of the first frame is presented.
- 2. <u>Estimate percentage of video to stack</u>. This is one of the tricky bits. The ASIVideoStack software will play the entire video. Carefully watch the playback and visually estimate the percentage of frames to use. This is an entirely subjective appraisal, and it is not uncommon that a return to this step and restack of the video is needed in order to obtain better results. Make a note of the total number of frames and the percentage of them that are used.

- 3. After the stack is done, the program presents a set of controls to enhance the image. Slide the Sharpen control to its lowest level (1) and click Save. This saves a JPG preview into the target folder location that matches the created FITS image.
- 4. <u>Using ASI Studio, launch ASIFitsView</u>. Open the created FITS file in the program. Note that the image will look TERRIBLE! This is a preview issue in the software, not a problem with the created file! Save the file as a TIF file. (Alternatively, a PNG file may be created instead.)
- 5. Repeat steps 1 through 4 for each target.

Alternate stacking software may be used. If you are more proficient with another program, then feel free to use it. Just save the stacked image in a completely lossless format to be imported into RSpec later (such as a FITS, TIF, or PNG file).

4.4.3 RSpec—Creating Instrument Response Curve (Relative Flux Calibration Curve)

RSpec is a powerful and easy-to-use tool for analyzing spectra. A large number of tutorial videos are available from the vendor's site (https://rspec-astro.com), so make sure to review these to become familiar with using it.

In generating profiles that will be used only for identifying absorption features, and which will not be compared to any work performed by others, this step can be skipped. The author of the RSpec software (Tom Field) now recommends this for absolute beginners in order to allow them to obtain some results in the shortest time possible. However, such a shortcut produces spectra with limited potential. For example, without instrument/atmospheric corrections, the results cannot be used for temperature estimations using Wien's Law. Since the spectra presented in this Atlas are meant to be compared and contrasted with work produced by others, this step was not skipped.

So, the first important thing that must be done for serious work is the creation of an "instrument response curve," which may be more accurately called a "relative flux calibration curve." This is a curve that is generated to reflect the peculiarities of the telescope, the camera, and the atmospheric conditions at the observing site. Some of the tutorials on the site above are dedicated to this and outline the process in great detail. In the event that it may prove useful, the procedure used for this Atlas is detailed below. Some of the steps (like saving files after each change) are not strictly speaking necessary, but it pays to be thorough in case it is necessary to backtrack, and to be able to do so without having to start over completely.

The choice of star to be used in this step is very important. A fairly bright, main sequence star with very strong hydrogen Balmer lines is greatly preferred for this purpose. To that end, a specimen of the late or very late B-type or the very early or early A-type is the best bet. These stars show the strongest hydrogen Balmer absorptions, making it easier to perform the wavelength calibration detailed here. The target star should also be positioned well above the horizon to avoid the worst atmospheric dispersion effects. It is recommended that the star be at least 45 degrees above the horizon. The general atmospheric conditions are also important; don't try to generate a relative flux calibration on any star if the transparency and seeing are sub-average.

The choice of star should also not be a member of an unresolved binary pair, if possible. A close binary pair can be used, provided that the companion star is dim enough to not pollute the spectrum from the brighter primary. For example, if the companion star is too dim for the exposure and gain settings on the camera to be hypothetically able to pick up the companion star, then for the purposes of low-resolution spectroscopy it should be usable.

The most commonly used stars for this purpose (as suggested on the RSpec website) are Vega (Alpha Lyrae) and Sirius (Alpha Canis Majoris). Both are A-type stars (A0 and A1, respectively), and are easily located. From the author's (A. Harding) observing location, Vega was used when the star was near the zenith.

Many of the steps outlined below are covered in very fine detail in the videos presented on the RSpec website, so the steps used in this Atlas are listed very generally. Additional details can be easily found on the software vendor's website. The procedure here is given as if using an A0V star. If a different star is used for the generation of the relative flux calibration curve, then please substitute the target star's type as needed.

1. Open stacked spectrum image file (TIF) in RSpec. Adjust the brackets to contain the star image and spectrum of the target star. The data contained within these brackets is the primary concern. The image can also be rotated to make it as level as possible if it is slightly uneven. Move the upper and lower bracket lines as close as possible to the star and spectrum image without excluding or cutting off any of the data. Once the desired data is bracketed properly, the Subtract Background option can be checked to remove any detectable glow from the sky background. A number of pixel lines above and below the bracketed area will be measured, and the results subtracted from the light inside the brackets. This serves to "clean up" the light inside the brackets. This is especially important on nights when Moonlight is flooding the sky.

2. Perform 2-point calibration using the star itself (the zero-order) and the Hydrogen Beta absorption line (4861.3 Angstroms). If striving for more accurate results, a non-linear calibration may be performed using the various hydrogen Balmer lines that are visible. The SA100 grating does not produce a perfectly linear result, though it is close. The non-linear calibration compensates for the small curvature in the result. Refer to the RSpec tutorials for guidance on performing non-linear calibrations.

3. Save the wavelength-calibrated profile

- 4. <u>Use Reference, Edit Points Delete Range function to trim profile outside readable/usable range</u>. (ie- 3300-9500 Angstroms). You may have noticed that this range is wider than that used for the finished spectra. This allows the "wings" of the spectrum to be trimmed away later. Plus, the extension into longer wavelengths is important if your camera is capable of picking up signals in the near infrared range. For example, the author (A. Harding) often extends the wavelength range of M-type stars to about 9000 Angstroms. When determining what exact wavelength ranges to trim, you should usually trim away the spectrum where the y-axis values are consistently very close to 0.
- 5. Save your trimmed profile.
- 6. <u>Close your trimmed profile and open the Pickles library reference profile for your reference star</u>. This library is included in RSpec's library of reference profiles. The star used for this procedure was Vega, so the A0V reference profile was used. If a different star type was used, then substitute the appropriate type.
- 7. <u>Use the Reference, Edit Points, Delete Range function to trim profile outside usable range</u> (ie- 3300-9500 Angstroms). Again, you may note that this wavelength range is wider than what is typically used for the finished spectrum. This extra range will be trimmed later again later. When determining what exact wavelength ranges to trim, you should usually trim away the spectrum where the y-axis values are consistently very close to 0.
- 8. <u>Save the trimmed Pickles library profile</u>. Use a different file name than the original; **do not overwrite the Pickles library file!** In our case, the result is a trimmed Pickles library file for an A0V star. (The result will be different if another star, such as a late B-type star, is used.)

- 9. <u>Use the Reference, Edit Points, Draw Continuum Add Points function to define points along the curve</u> that are on the continuum level to create a smooth curve. Ignore any absorptions that are present. The goal here is to trace the continuum level of the curve smoothly.
- 10. <u>Save the smoothed reference profile</u>. Again, use a different file name; **do not overwrite the Pickles library file!**
- 11. Close the open profiles, then open your calibrated and trimmed profile from above (5).
- 12. Open reference series and load the saved, smoothed reference from above (10).
- 13. <u>Trim your main profile</u> so that no part of the curve touches the x-axis. This is necessary to avoid huge spikes in the results.
- 14. <u>Use the Math on 2 Series function to divide your main profile by the smoothed reference profile</u>, and move the resulting curve to the main profile.
- 15. Save your raw relative flux calibration curve.
- 16. <u>Use the Reference, Edit Points, Delete function to cut out the absorption bands</u> for the hydrogen Balmer series (and others, such as the Telluric O2, if desired). Your goal is to create a smooth curve, with no absorptions present.
- 17. <u>Use the Reference, Edit Points, Spline Smoothing function</u> on the result—but only very gently!
- 18. <u>Save the smoothed curve</u>; this is your relative flux calibration curve. Make a note of the number of Angstroms/pixel that the spectrum uses. This is the "dispersion" of your spectra, expressed as a number of Angstroms/pixel), and gives a good estimate to use in wavelength calibrating future work.

This procedure will give you the smoothed relative flux calibration curve that you will use to correct your data (unless you are collecting reference star data each session; see below). Remember, though, that if any part of your imaging train changes, such as changing cameras, gratings, or telescopes, a new curve **must** be generated to keep your results consistent. Even if a piece of equipment is replaced with an identical model, a new curve must be created. It is also recommended to create a new relative flux calibration curve annually to account for the aging of the equipment used.

Now, this entire procedure is acceptable for quick results that may be used for personal exploration. (This is what one of the authors, A. Harding, refers to as the "quick and dirty" method.) However, if you wish to submit your results to any professional databases, or if you wish for them to be directly comparable with results obtained by others, then a new relative flux calibration curve **must** be generated for each session, and for each region of sky that is being imaged. The same guidelines apply to the choice of star given previously, but the reference star chosen should also be close in the sky to the target being imaged—typically within a couple degrees. This can mandate capturing data for multiple reference stars if your targets for the evening are spread across the sky.

This difference between the "quick and dirty" results vs. more refined work must be made clear when discussing spectra. Many amateurs insist on taking the extra steps when capturing and processing any spectra. However, in order to demonstrate what is possible with the minimum of time and effort, the spectra presented in this Atlas are all of the "quick and dirty" type. Refinements to them are certainly possible if the extra steps are taken.

4.4.4 RSpec-Analyzing Captures

After you have created a relative flux calibration curve, you have what you need to analyze a stacked capture. The general procedure is outlined below. Again, some of these steps are not absolutely necessary (such as saving files for each step), but this can be useful in case you want to backtrack without starting completely over.

- 1. Open stacked spectrum image file (TIF) in RSpec. Adjust the brackets to contain the star image and spectrum of the target star. The data contained within these brackets is the primary concern. The image can also be rotated to make it as level as possible if it is slightly uneven. Move the upper and lower bracket lines as close as possible to the star and spectrum image without excluding or cutting off any of the data. Once the desired data is bracketed properly, the Subtract Background option can be checked to remove any detectable glow from the sky background. A number of pixel lines above and below the bracketed area will be measured, and the results subtracted from the light inside the brackets. This serves to "clean up" the light inside the brackets. This is especially important on nights when Moonlight is flooding the sky.
- 2. <u>Perform 1-point calibration using the zero image</u> of the star and the dispersion (Angstroms/pixel) determined earlier. (Typical values for the equipment used here are around 6.3 Å/pixel.) Minor tweaks may need to be applied to the dispersion value to get visible absorption features to line up better. If you prefer,

you may employ a non-linear calibration to compensate for the slight curvature that the SA100 grating creates. Make sure to do this if your relative flux calibration curve was created using a non-linear calibration!

- 3. Save the calibrated profile.
- 4. <u>Use Reference, Edit Points, Delete Range function to trim the profile outside the usable range</u> (ie- 3300-9500 Angstroms to match the range of the relative flux calibration curve.)
- 5. Save the trimmed profile.
- 6. Open reference profile for smoothed relative flux calibration curve created earlier.
- 7. <u>Use Math on 2 Series to divide the calibrated and trimmed spectrum by the relative flux calibration curve</u>, and move the result to the main profile.
- 8. Save the corrected spectral curve.
- 9. <u>Use the Reference, Edit Points, Delete Range function to re-trim the spectrum for final wavelength range</u>. (Here a reduced range of 3800-8000 Angstroms was typically used to avoid bleed over into the second order spectrum that the grating creates. This can be extended to up to about 9000 Angstroms if analyzing an M-type star, since there is virtually no detectable bleedover at that point.)
- 10. Save the re-trimmed profile.
- 11. If the result looks good, add labels, etc. and save the final version. In some instances, it can be necessary to tweak the calibration by re-calibrating the spectrum using a known absorption line. It is best **not** to do this, but if the initial calibration is off by a significant amount, throwing off the labels, then it will help realign the labels with their absorption lines. The recalibration introduces some error into the spectrum, but it is not usually significant with respect to these low-resolution results.
- 12. Repeat steps 1 through 11 for each target,

Step 11 above is typically the most time consuming, as you must identify and label each of the absorptions. This requires referencing the RSpec Elements library, or using another reference source. Try to be careful. If you label a feature and it doesn't look right, it probably isn't. Some elements or molecules have the same apparent lines

involved in their spectra, which can make identifying them tricky. Looking at the spectral type of the star (listed in Stellarium or on Wikipedia) can help. Cooler stars, for example, will not have helium absorptions in them—they aren't hot enough for that. Likewise, hotter stars won't have the TiO molecular absorptions that are seen in cooler stars. As you gain experience, you will get better at identifying absorption lines and having an idea of what to expect. But, even so, there is plenty of room for error (as the author, A. Harding, can attest!).

The recommended primary resources for identifying absorptions are the elements library built into RSpec, and the *Spectral Atlas for Amateur Astronomers* by Richard Walker. The SAO/NASA Astrophysics Data System (ADS), maintained by Harvard University, can also be useful for browsing papers relating to spectral analyses of specific types of stars (https://ui.adsabs.harvard.edu/). Regarding the RSpec elements library, it is important to note that the library provides little indication of what elements appear at what effective temperatures. Though it does have collections based on stellar type (O, B, A, etc.), it does not indicate at what temperatures specific features are appropriate. Therefore, some caution must be exercised when using it to identify absorptions. Time and practice will also provide guidance as more experience is gained.

5. Atlas of Spectra

This section presents the spectra of example stars, one from each of the custom classifications explained in Section 4.3. They are arranged in the Morgan-Keenan (MK) order of hottest stars to coolest and are arranged in the custom classifications explained in Section 4.3. Type-O stars are presented first, followed by type-O/B, type-B, type-B/A, type-A, and so on.

Relevant astrophysical data is presented for main sequence specimens of the general type being discussed, including the expected temperatures, luminosities, and lifespans of the type of star involved. Some general spectroscopic features are also mentioned. Afterward, a single spectrum of a star belonging to the custom classification is presented. Superimposed on this is a rectified spectrum shown in red. A rectified spectrum is one in which the continuum has been removed. This continuum removal can make identification of features clearer. Such a spectrum is ideally a flat line, with features providing clear dips and peaks along its length. Of course, when working with the basic equipment and low-resolution results used in the Atlas, the result is rarely a flat line. However, the result is often still useful for line identification.

After the spectrum is presented, specific spectroscopic features are explained. Each one is labeled with its wavelength, with a short note regarding its presence.

Following this, a continuum curve is shown for the spectrum, and Wien's Law is used to calculate the effective temperature of the star. This is compared with the temperature range given for the star's general classification. Differences between the calculated temperature and the expected temperature are discussed, with some explanation provided for the apparent difference. (This will help clarify the limitations of this method of temperature estimation when it comes to using amateur equipment.)

5.1 Spectral Type O Stars

The O-type stars occupy the extreme high end of the Morgan-Keenan (MK) stellar classification temperature sequence, and it is here that we begin our survey. These stars usually appear with a bluish-white light, often visible at the centers of the nebulous clouds from which they formed. They burn extremely brightly and are the shortest-lived stars. As of the date of this report, no very early O-type stars are known; they remain a hypothetical possibility, but none have been discovered. There are some early O-type stars known, but unfortunately the equipment used to compile this Atlas is not able to detect them from the observer's location. Therefore, we will provide only one example of this type, of the late variety. (Another example, of the very late O-type, can be found in Section 5.2, Spectral Type O/B Stars (Very Late O-Type and Very Early B-Type Stars.)

These O-type stars are extremely massive, and quite rare. A typical O-type star of the early-, middle-, and late-type will have a mass somewhere between 120 and roughly 23 times the mass of our Sun⁽⁹⁾. With such huge amounts of matter, the cores of these stars are immensely hot and so consume their fuel at a frantic pace. They shine with a brightness between 1,400,000 times down to about 170,000 times solar luminosity⁽⁹⁾. These frantically burning stars are usually only on the main sequence for 1-10 Myr⁽⁷⁾. When these stars run out of fuel and die, they create cataclysmic supernovae. These colossal explosions often leave behind either a black hole or a neutron star.

The effective temperature range of stars of the early, middle, and late O-types range from 45,000K or more down to about 35,000K⁽⁹⁾. Most of their radiation is emitted in the form of high-energy ultraviolet radiation. This often energizes any leftover clouds from the stars' formations and causes them to emit their own light as emission nebulae. Since these stars primarily emit such ultraviolet radiation, Wien's Law will be of little use. Since our camera is not able to register photons in that range, the results of the computations will fall incredibly short. Still, we will perform the calculation to demonstrate this.

The most characteristic spectroscopic features of these stars is typically both neutral and ionized helium (He i and He II), with some weaker metals, such as silicon, oxygen, nitrogen, and carbon in various states of ionization. The hydrogen Balmer lines tend to appear extremely weak, and the shape of the spectral curve appears to reach its peak in the very low wavelength region. (As mentioned previously, the peak is actually in the ultraviolet, but amateur equipment is not typically able to pick up data in this region.)

The stars chosen to represent the various custom subtypes are presented here:

Table 5.1 - Representative O-Type Stars

Subtype	Star	
Very Early	Not used	
Early	None available	
Middle	None available	
Late	Xi Persei (Menkib)	

Late O-Type Stars

The late O-type stars are extremely massive, extremely bright stars. They are characterized by weak hydrogen Balmer lines, as well as neutral and ionized helium lines. Carbon, oxygen, nitrogen, and some others are usually evident in various stages of ionization. These stars are quite rare, with only a small number known.

The late O-type stars are extremely hot, on the order of 37,000K down to about 35,000K⁽⁹⁾. These stellar furnaces burn through their fuel very rapidly, typically staying on the main sequence for only about 7 Myr⁽⁷⁾. They are much more massive than our Sun, weighing in at between 31 and 23 times solar mass⁽⁹⁾. They are extremely bright, with luminosities between 320,000 and 170,000 times solar luminosity⁽⁹⁾. As noted above, they are spectroscopically characterized by weak hydrogen Balmer lines, as well as neutral and ionized helium (He I and He II), with some weaker elements visible, including various species of silicon, carbon, oxygen, and nitrogen.

The star chosen as an example of the late O-types is Xi Persei, also called by the common name Menkib, in the constellation of Perseus, the Hero. This star is an evolved giant, which indicates that the absorptions may be somewhat muted, but no main sequence specimens were readily available. Still, it should serve as an adequate example of the late O-types.

The spectrum for Xi Persei (Menkib) follows, along with a rectified spectrum in red.

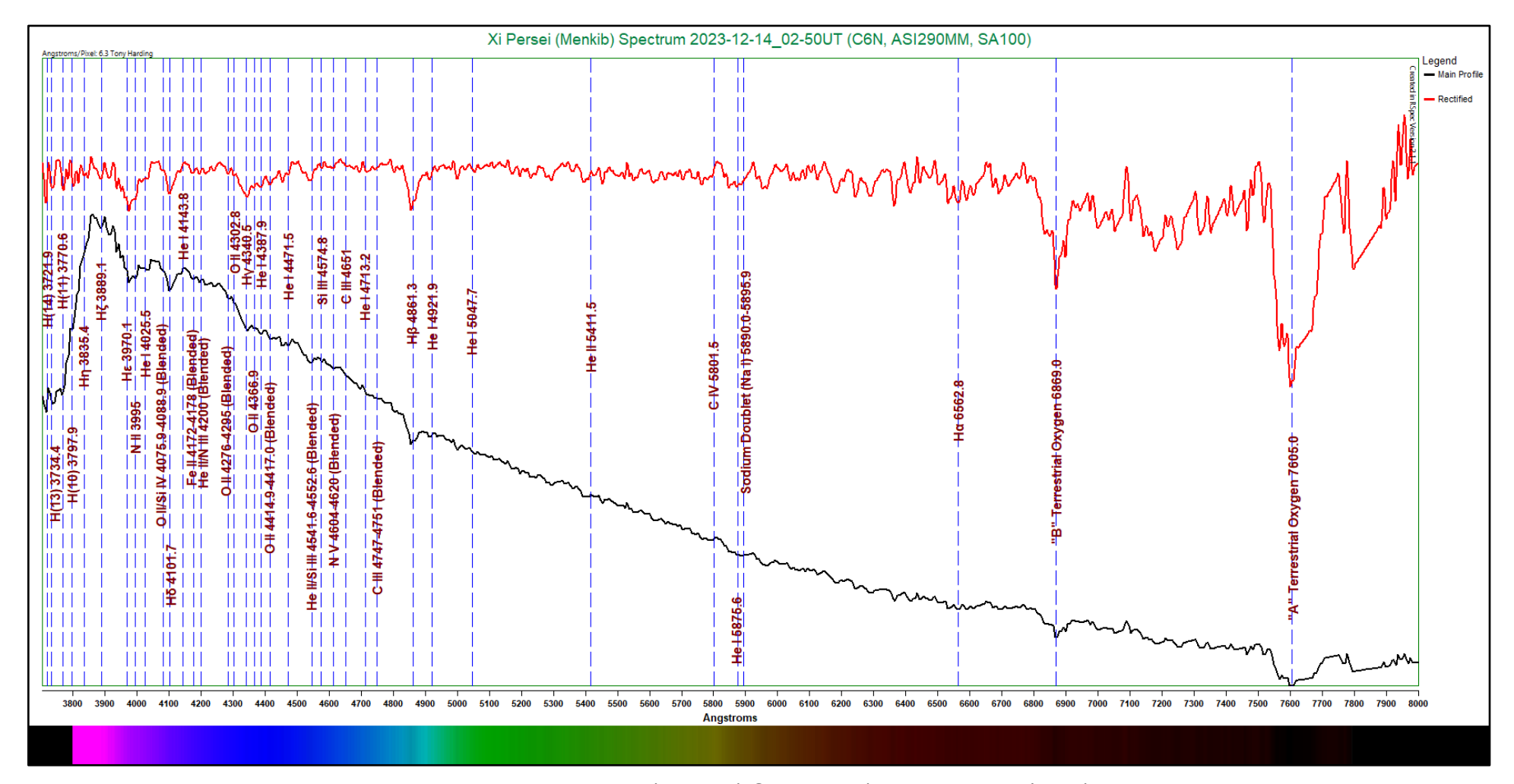


Figure 5.1: Xi Persei (Menkib) Spectrum (6.3 Angstroms/pixel) Capture Details: Exposure 398ms, Gain 154, 30% of 611 frames stacked, Integration Time 72s

The hydrogen Balmer lines here indeed appear quite weak, due not only to the extremely high temperature of the star but also by virtue of the evolved nature of the star, which often serves to make absorption features appear weaker. We can also see numerous helium lines, both in neutral and ionized states, at 3970.1, 4025.5, 4143.8, 4200 (blended with N III), 4387.9, 4471.5, 4541.6 (blended with Si III), 4713.2, 4921.9, 5047.7, 5411.5, and 5875.6 Angstroms. The sodium doublet at 5890.0-5885.9 Angstroms is visible here, but only weakly; this is probably interstellar in nature, but the adjacent He I absorption causes it to appear broad. Mixed in (and often blended with other absorptions) we see ionized species of nitrogen, oxygen, silicon, iron, and carbon. It is also noteworthy to see that the curve peaks very low in the apparent wavelength range, a reflection of the star's incredibly high effective temperature.

The following table shows the indicated absorption features of the Xi Persei (Menkib) spectrum.

Table 5.2 - Xi Persei (Menkib) Line Identification Details

Feature	Wavelength	Comments
	(Angstroms)	
H(14)	3721.9	Higher order neutral hydrogen line; common in hot stars
H(13)	3734.4	Higher order neutral hydrogen line; common in hot stars
H(11)	3770.6	Weaker hydrogen line; also common in hot stars
H(10)	3797.9	Extremely weak hydrogen line; not always visible
Ηη	3835.4	Hydrogen Balmer absorption; appears very weakly here
Ηζ	3889.1	Hydrogen Balmer absorption feature
Ηε	3970.1	Moderately strong hydrogen Balmer line; well defined blend
N II	3995	Weak ionized nitrogen line
He I	4025.5	Common neutral helium absorption; appears broadened here
O II/Si IV	4075.9-4088.9	Very weak blended absorption
Нδ	4101.7	Obvious hydrogen Balmer absorption
He I	4143.8	Very weak neutral helium line
Fe II	4172-4178	Weak ionized iron line; more common in B-type stars
He II/N III	4200	Weak helium/nitrogen blend
O II	4276-4295	Weak blend of ionized oxygen lines
O II	4302.8	Extremely weak ionized oxygen absorption
Нү	4340.5	Weak to moderate hydrogen Balmer absorption
OII	4366.9	Extremely weak ionized oxygen absorption
He I	4387.9	Weak neutral helium absorption
OII	4414.9-4417.0	Weak blend of ionized oxygen lines
He I	4471.5	Common but weak neutral helium absorption
He II/Si III	4541.6-4552.6	Moderately strong ionized helium/silicon blend
Si III	4574.8	Very weak doubly-ionized silicon line
N V	4604-4620	Blend of highly ionized nitrogen lines
C III	4651	Extremely weak doubly-ionized carbon absorption feature
He I	4713.2	Weak neutral helium line
Нβ	4861.3	Obvious hydrogen Balmer line
He I	4921.9	Weak neutral helium line
He I	5047.7	Extremely weak neutral helium line; dubious identification
He II	5411.5	Extremely weak ionized helium line; dubious identification
C IV	5801.5	Extremely weak triply-ionized carbon absorption; dubious identification
He I	5875.6	Very common neutral helium line; often indistinct from sodium doublet in low-resolution spectra

Feature	Wavelength	Comments	
	(Angstroms)		
Sodium Doublet (Na I)	5890.0-5895.9	Blended Fraunhofer "D1" and "D2" neutral sodium absorption; probably interstellar in origin here	
Ηα	6562.8	Extremely weak hydrogen Balmer line; dubious identification	
Telluric Oxygen	6869.0	Fraunhofer "B" absorption due to atmospheric oxygen	
Telluric Oxygen	7605.0	Fraunhofer "A" absorption due to atmospheric oxygen	

With these stars being so hot, their peak energy wavelength resides deep in the ultraviolet wavelength range. These wavelengths are mostly beyond the capabilities of the type of camera used. The Balmer jump, however, is causing an apparent false peak at the extreme lower wavelength area of our spectrum. (The Balmer jump is an area in the ultraviolet range where absorptions are positioned tightly together, causing it to appear that the peak energy wavelength lies elsewhere.) For demonstration purposes, we will use Wien's Law to calculate an effective temperature based on this apparent peak, then contrast this with the actual temperature.

The continuum curve for Xi Persei (Menkib) is plotted here, along with the main spectrum. The labels have been removed so that an easier comparison can be made between the two curves.

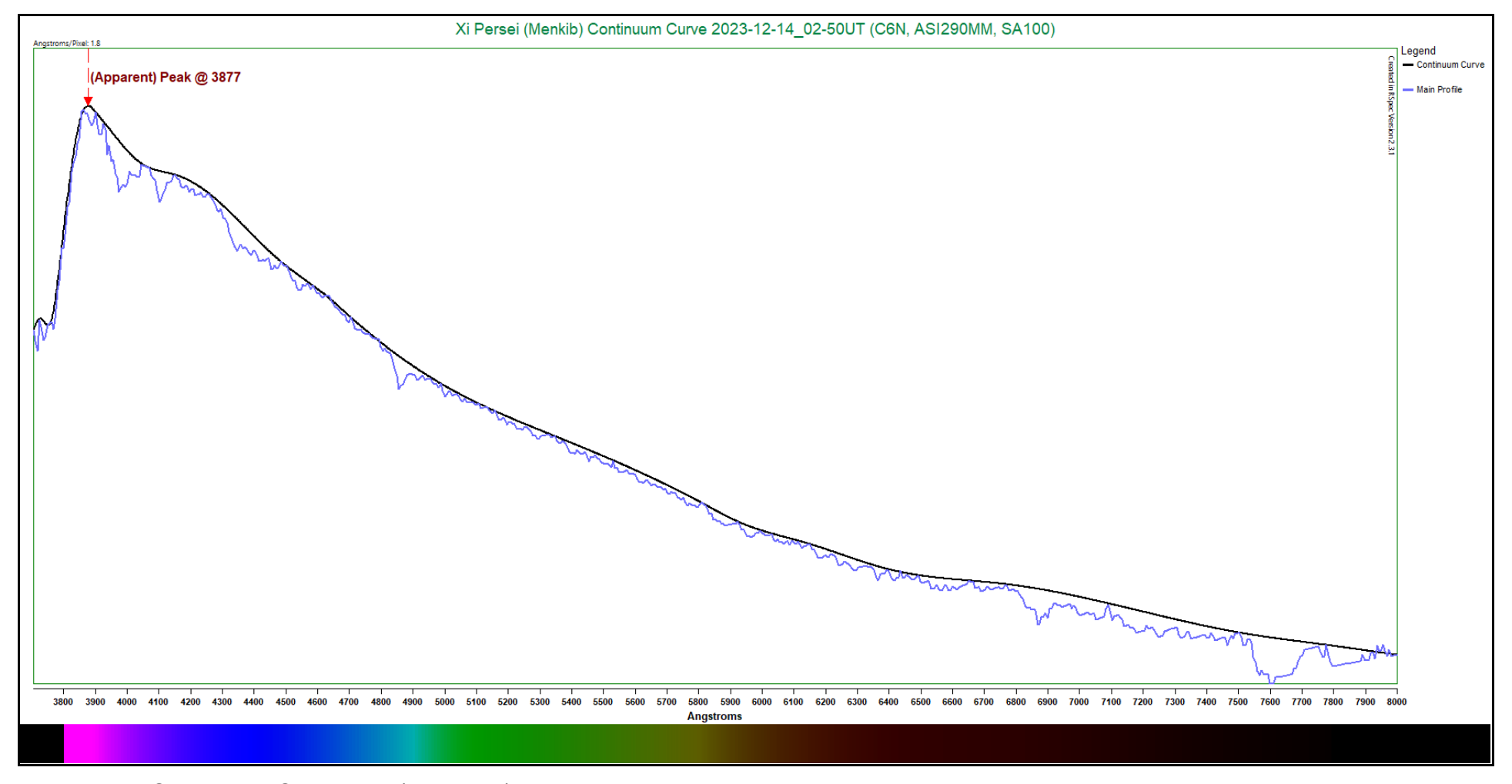


Figure 5.2 - Continuum Curve Plot (Xi Persei)

From our result above, the apparent peak energy wavelength lies at 3877 Angstroms. (As noted previously, this is an erroneous estimate due to the Balmer jump, where closely spaced higher-order hydrogen absorptions are removing the continuum.) Using this value of 3877 Angstroms, Wien's Law returns an estimated effective temperature of 7,474K. This result is indeed far short of the expected temperature range of 37,000K-35,000K. Our estimate falls short by a factor of approximately 4.82 times the median of the expected range (36,000K)! The star's professionally estimated temperature is listed as 35,000K⁽¹⁰⁾. Alternatively using this value for comparison, our effective temperature estimate is only off by a factor of 4.68. As you can see, Wien's Law is woefully inadequate for temperature estimations based on curves obtained using typical amateur astronomy cameras. We will, however, continue this practice throughout the Atlas to demonstrate when Wien's Law can be reasonably applied and when it cannot.

5.2 Spectral Type O/B Stars (Very Late O and Very Early B)

This custom category of stars consists of the very late O-types and the very early B-types. They are bluish white in appearance, and can be visible amidst the remnants of the nebulae from which they formed. Like the late O-types, they burn very brightly and are short-lived. They are uncommon, but not quite as rare as the O-types.

These stars are extremely massive. A typical O/B star will have a mass around 20 to 17 times the mass of our Sun^(11,12). They are also immensely hot, and so consume their fuel quickly. They shine with a brightness range between 90,000 times down to about 45,000 times solar luminosity^(11,12). These stars are usually only on the main sequence for approximately 10 Myr⁽⁷⁾. When these stars run out of fuel and die, they create cataclysmic supernovae, leaving behind either a black hole or a neutron star.

The temperatures of these stars is normally around 33,000K down to about 31,000K^(11,12). Most of their radiation is still emitted in the form of high-energy ultraviolet radiation. Like with the earlier O-type stars, this often energizes any clouds left over from the stars' formations and causes them to emit their own light as emission nebulae. Since these stars primarily emit such ultraviolet radiation, Wien's Law will again be wildly inaccurate. Since our camera is not able to register photons in that range, the results of the computations will fall incredibly short. Like with the O-type star in the previous section, we will perform the calculation anyway as a means of demonstration.

The most prominent spectroscopic feature of these stars is typically ionized and neutral helium. Some other elements can be visible, including silicon, oxygen, nitrogen, and carbon. The hydrogen Balmer lines again tend to appear extremely weak, and the shape of the spectral curve peaks in the very low wavelength region.

The star chosen to represent this customized type is presented here:

Table 5.3 - Representative O/B Star

Subtype	Star		
Very Late O/Very Early B	Zeta Orionis (Alnitak)		

O/B Stars (Very Late O and Very Early B)

The very late O-type and very early B-type stars can appear very similar to stars of the late O-type and early B-type. They remain extraordinarily massive and bright, with very weak hydrogen Balmer absorptions. The mixture of neutral and ionized helium lines is present, as are variously ionized species of silicon, nitrogen, carbon, and oxygen. Like the late O-types, these stars are rare or uncommon.

These stars remain extremely hot, being around 32,000K^(11,12). They have main sequence lifespans of only approximately 10 Myr⁽⁷⁾. The O/B stars are massive, being roughly 18.5 times the mass of our Sun, and shine brilliantly in a range of 90,000 times down to about 45,000 times solar luminosity^(11,12). They bear many of the same spectroscopic signatures of earlier O-types, showing very weak hydrogen Balmer lines and a mixture of neutral and ionized helium lines. They also show various species of silicon, carbon, oxygen, and nitrogen, though typically not as strongly as their hotter O-type cousins.

The star chosen as an example of this type is Zeta Orionis, commonly called Alnitak, in the constellation of Orion, the Hunter. This star is an evolved supergiant, which will serve to lessen the appearance of many of the absorptions. (No main sequence example was readily available at the time of data collection.) Still, it can serve as an example of the types of absorptions these stars produce.

The spectrum of Zeta Orionis (Alnitak) is presented here, along with a rectified spectrum in red.

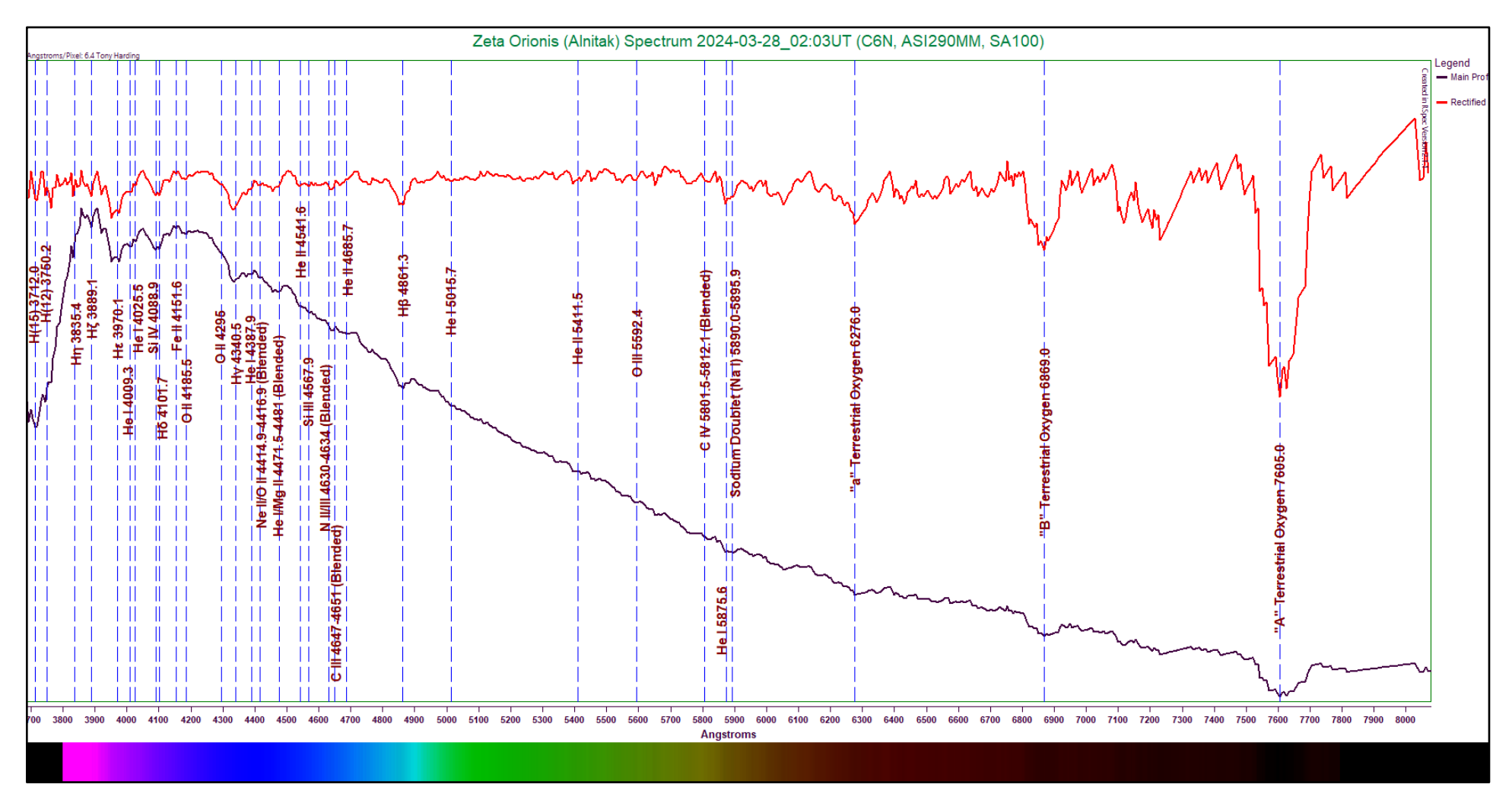


Figure 5.3: Zeta Orionis (Alnitak) Spectrum (6.3 Angstroms/pixel)
Capture Details: Exposure 198ms, Gain 59, 20% of 1236 frames stacked, Integration Time 48s

As expected, this spectrum shows very weak hydrogen Balmer absorptions. The Hα line appears to be missing entirely. We do see a number of neutral and ionized helium absorptions—at 4009.3, 4025.5, 4387.9, 4471.5 (blended with Mg II), 4541.6, 4685.7, 5015.7, 5411.5, and 5875.6 Angstroms. The neutral helium line at 5015.7 Angstroms is extremely weak and nebulous here, and should be regarded as a dubious identification. Additionally, we see variously ionized species of silicon, oxygen, iron, carbon, and nitrogen. The common ionized magnesium absorption at 4481.2 Angstroms appears fairly strong here. The neutral sodium doublet at 5890.0-5895.9 Angstroms is also visible, but is likely interstellar in nature. This appears broadened due to the presence of the neutral helium line just below it at 5875.6 Angstroms.

The following table shows the indicated absorption features of the Zeta Orionis (Alnitak) spectrum.

Table 5.4 - Zeta Orionis (Alnitak) Line Identification Details

Feature	Wavelength	Comments
, catalo	(Angstroms)	
H(15)	3712.0	Moderately strong higher order hydrogen absorption
H(12)	3750.2	Weak neutral hydrogen line
Hn	3835.4	Appears weak but distinct here
Ηζ	3889.1	Relatively weak hydrogen Balmer absorption
He I	4009.3	Weak neutral helium line
He I	4026.2	Extremely weak neutral helium line
Si IV	4088.9	Moderately strong triply-ionized silicon line; appears broadened due to adjacent hydrogen Balmer line
Fe II	4151.6	Extremely weak ionized iron line
O II	4185.5	Weak ionized oxygen line
OII	4295	Extremely weak ionized oxygen absorption; dubious identification
Нү	4340.5	Moderately strong hydrogen Balmer absorption
He I	4387.9	Very weak neutral helium line
OII	4414.9-4416.9	Very weak blend of ionized oxygen lines
He I/Mg II	4471.5-4481	Weak to moderate blend of neutral hydrogen and ionized magnesium
He II	4541.6	Weak ionized helium line
Si III	4567.9	Extremely weak doubly-ionized silicon line
N II/III	4630-4634	Weak blend of nitrogen lines; broadened by adjacent C III absorption
C III	4647-4651	Extremely weak blend of doubly-ionized carbon absorptions; broadened by adjacent nitrogen absorption
He II	4685.7	Extremely weak ionized helium line; dubious identification
Нβ	4861.3	Moderately strong hydrogen Balmer line
He I	5015.7	Common neutral helium line; extremely weak here; definitely a dubious identification
He II	5411.5	Very weak ionized helium line; possibly a dubious identification
O III	5592.4	Extremely weak doubly-ionized oxygen line; difficulty to distinguish from continuum noise
C IV	5801.5-5812.1	Very weak blend of triply-ionized carbon lines
He I	5875.6	Common but weak neutral helium line; appears broadened due to adjacent sodium doublet
Sodium Doublet (Na I)	5890.0-5895.9	Blended Fraunhofer "D1" and "D2" neutral sodium absorption; probably interstellar; broadened by He I line
Telluric Oxygen	6276.0	Fraunhofer "a" absorption due to atmospheric oxygen
Telluric Oxygen	6869.0	Fraunhofer "B" absorption due to atmospheric oxygen
Telluric Oxygen	7605.0	Fraunhofer "A" absorption due to atmospheric oxygen

Regarding temperature, these O/B type stars continue to generate most of their light in the ultraviolet wavelength range. Like with the O-types, the Balmer jump masks this area and causes an apparent false peak to appear. We will calculate a temperature based on this false peak using Wien's Law, and compare it to the actual temperature to demonstrate its inaccuracy.

The continuum curve for Zeta Orionis (Alnitak) is plotted here, along with the main spectrum. The labels have been removed so that an easier comparison can be made between the two curves.

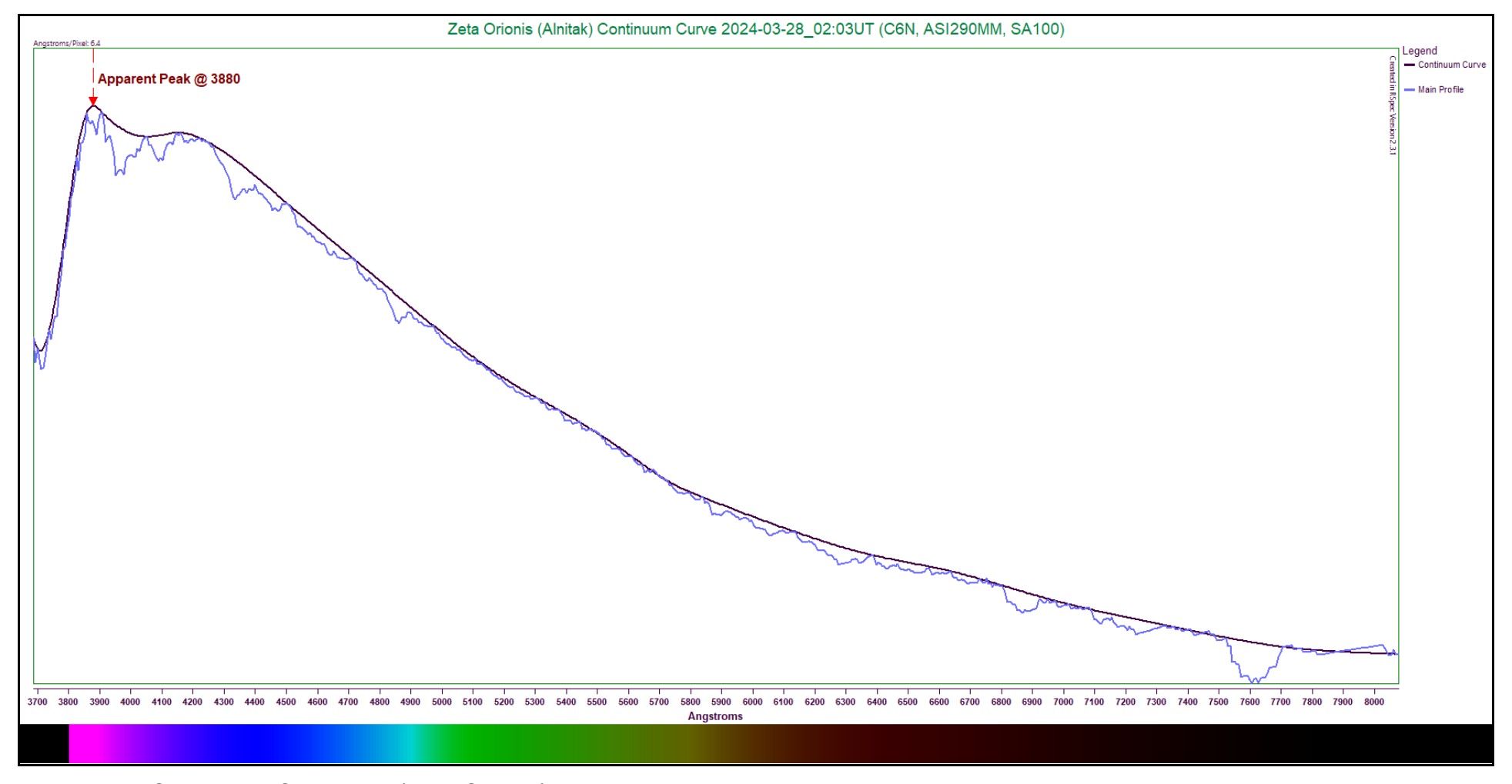


Figure 5.4 - Continuum Curve Plot (Zeta Orionis)

From this curve, the apparent peak energy wavelength appears to lie at 3880 Angstroms. Applying Wien's Law with this value, we receive an effective temperature estimate of only 7,468K. This is indeed far removed from the expected temperature of 32,000K; our estimate is short by a factor of 4.28. The professionally determined temperature of the star is listed as 29,500K⁽¹³⁾. Using this as the target temperature, our estimate is still extremely short—by a factor of 3.95.

5.3 Spectral Type B Stars

B-type stars are very hot. They sit between the scorchingly hot O-types and the hot A-types. They usually produce visible hydrogen Balmer absorptions in their spectra, which become stronger in the later sub-types. These stars shine with a bright white light, often tinged slightly blue in appearance.

These stars are massive, but not quite so much as the O-types. They typically range in mass between 11 and 3 times the mass of our Sun⁽¹²⁾. They are also bright, ranging from about 13,500 times solar luminosity down to approximately 150 times that of our Sun⁽¹²⁾. B-type stars are short-lived, existing on the main sequence for only 11-250 Myr⁽⁷⁾. When they exhaust their fuel and effectively die, they can produce either fantastic supernovae or leave behind higher mass white dwarfs.

The effective temperature range for these stars lies between approximately 25,000K for the earlier subtypes down to about 12,000K for the later ones⁽¹²⁾. Their peak energy wavelength lies in the ultraviolet range, so the use of Wien's Law to obtain temperature estimates using amateur equipment is certain to provide results that are much too low. Regardless, we will calculate these temperatures to demonstrate this point.

The earlier B-type stars show only moderately strong hydrogen Balmer absorptions in their spectra, while the later subtypes show them quite strongly. The earlier types can show absorption features from some of the same elements present in O-type stars, such as carbon and oxygen—though not as strongly. Neutral helium lines are normally visible, which is a hallmark of this stellar type. In the earlier subtypes, some ionized helium may be seen.

One special type of star included in this section is the Be, or B emission-type, star. These stars are normally very hot, rapidly rotating B-types with hydrogen emission lines in their spectra. This is caused by material ejected from the star due to its rapid rotation, which absorbs the intense ultraviolet radiation from the star and re-radiates it. This shows up as emission features in the spectra.

The stars chosen to represent the various subtypes are presented here:

Table 5.5 - Representative B-Type Stars

	· /
Subtype	Star
Early	Epsilon Cassiopeiae (Segin)
Middle	Nu Andromedae
Late	Zeta Pegasi (Homan)
Be Stars	Gamma Cassiopeia (Navi)

Early B-Type Stars

Early B-type stars are very massive, bright stars. They show some of the same characteristics as the O-type and custom O/B type presented prior, but with a somewhat lower temperature. It can be challenging to visually see much difference between the O/B types and early B-types in low-resolution spectra. The most notable difference lies in the apparent peak of the curve, which will appear shifted slightly toward longer wavelengths, reflecting the lower temperature. Amateur cameras do not normally reach far into the ultraviolet, but even the false, visual range peak will usually appear so shifted.

Like the O/B stars, the early B-type stars are still very hot. They range from approximately 26,000K down to around 17,000K⁽¹²⁾. They are massive, coming in between 11 and 5.5 times the mass of our Sun⁽¹²⁾. They are also very bright, with luminosities between 13,500 and 975 times that of our Sun⁽¹²⁾. As with the O/B stars, these specimens burn through their nuclear fuel quickly, commonly staying on the main sequence for only about 75 Myr⁽⁷⁾. Again, the neutral helium lines are the calling cards of these stars. In addition, some ionized metals can often be visible, including silicon, oxygen, carbon, magnesium, iron, and nitrogen.

The star chosen as an example of this subtype is Epsilon Cassiopeiae, better known as Segin, in the constellation of Cassiopeia, the Queen. This star is a main sequence star, and so should provide a good example of the features commonly present in these stars.

The spectrum of Epsilon Cassiopeiae (Segin) is presented here, with a rectified version appearing in red.

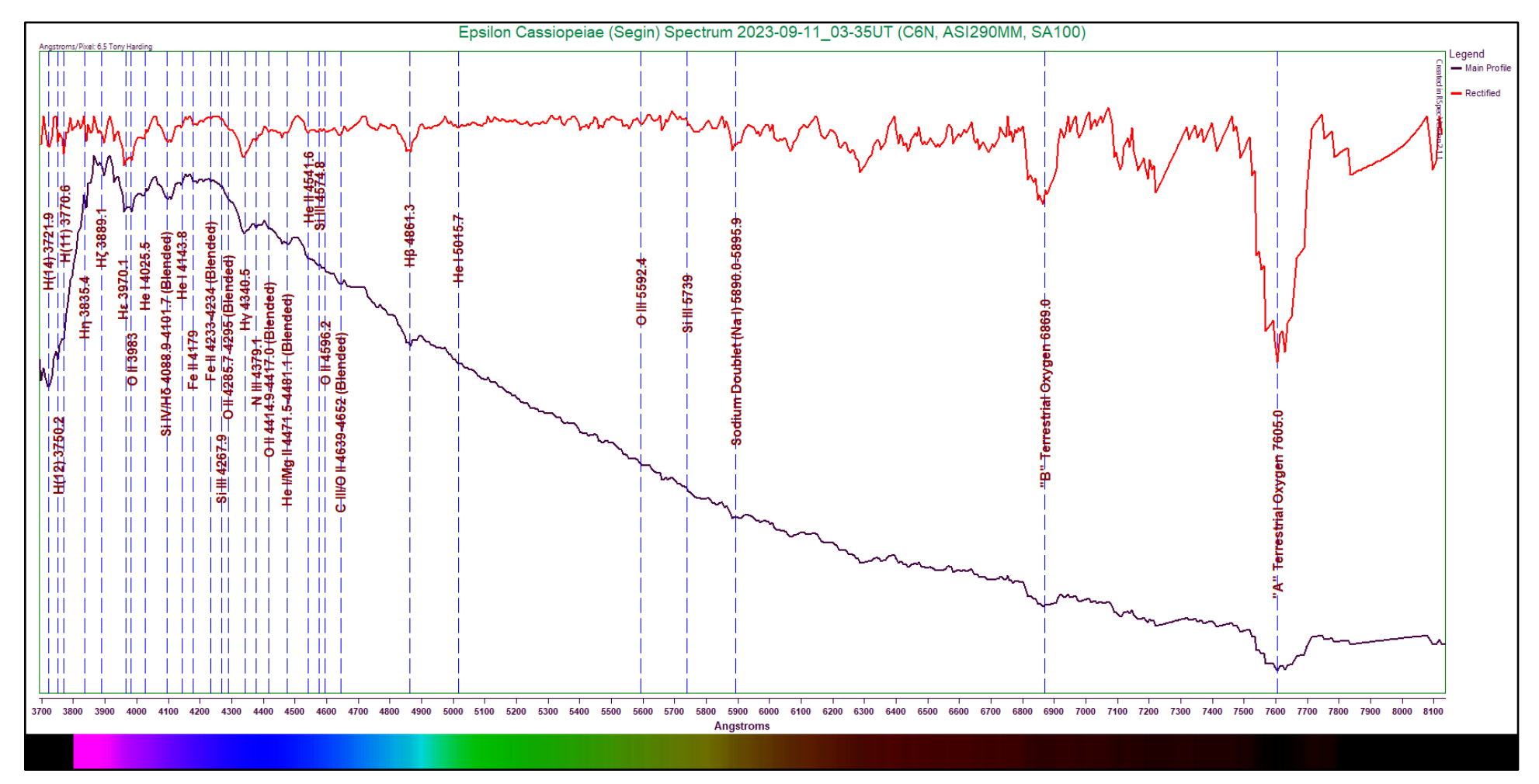


Figure 5.5: Epsilon Cassiopeiae (Segin) Spectrum (6.2 Angstroms/pixel)
Capture Details: Exposure 474ms, Gain 149, 50% of 511 frames stacked, Integration Time 121s

The hydrogen Balmer absorptions continue to appear somewhat weakly here, with the H α absorption buried in the continuum noise. A good number of neutral helium lines, plus one ionized helium line, are visible at 4025.5, 4143.8, 4471.5 (blended with Mg II), 4541.6,

and 5015.7 Angstroms. The sodium doublet at 5890.0-5895.9 Angstroms is visible clearly, but the helium line often just below it is missing. Additional metals are labeled, including oxygen, silicon, iron, nitrogen, magnesium, and carbon. Most of these are extremely faint and can be difficult to identify in low-resolution spectra, so great caution must be exercised with these, as some may be erroneous identifications.

The following table shows the indicated absorption features of the Epsilon Cassiopeiae (Segin)spectrum.

Table 5.6 - Epsilon Cassiopeiae (Segin) Line Identification Details

Feature	Wavelength	Comments
	(Angstroms)	
H(14)	3721.9	Higher order neutral hydrogen absorption; moderately strong here
H(12)	3750.2	Weak higher order neutral hydrogen line
H(11)	3770.6	Very weak higher order neutral hydrogen line
Ηη	3835.4	Weak hydrogen Balmer line
Нζ	3889.1	Somewhat weak, but distinctive hydrogen Balmer line
Ηε	3970.1	Moderately strong hydrogen Balmer absorption
OII	3983	Moderately strong ionized oxygen line
He I	4025.5	Weak neutral helium line
Si IV/Hδ	4088.9-4101.7	Blended hydrogen Balmer line; somewhat weak
He I	4143.8	Weak neutral helium absorption
Fe II	4179	Very weak ionized iron line; more common in cooler stars
Fe II	4233-4234	Extremely weak ionized iron absorption; more common in cooler stars
Si III	4267.9	Extremely weak doubly-ionized silicon line
OII	4285.7-4295	Extremely subtle ionized oxygen blend; only causing small dip in continuum
Нү	4340.5	Moderately strong hydrogen Balmer line
N III	4379.1	Very weak doubly-ionized nitrogen line
OII	4414.9-4417.0	Very weak ionized oxygen blend
He I/Mg II	4471.5-4481.1	Moderate neutral helium/ionized magnesium blend
He II	4541.6	Weak ionized helium absorption
Si III	4574.8	Extremely weak doubly-ionized silicon line; dubious identification
OII	4596.2	Extremely weak ionized oxygen line; dubious identification
C III/O II	4639-4652	Weak blend of doubly-ionized carbon and ionized oxygen
Нβ	4861.3	Moderately strong hydrogen Balmer line
He I	5015.7	Extraordinarily weak neutral helium line; very dubious identification
O III	5592.4	Very weak doubly-ionized oxygen line
Si III	5739	Exceptionally weak doubly-ionized silicon line; dubious identification
Sodium Doublet (Na I)	5890.0-5895.9	Blended Fraunhofer "D1" and "D2" blend; relatively weak here
Telluric Oxygen	6869.0	Fraunhofer "B" absorption due to atmospheric oxygen
I olidilo oxygon		

Like other B-type stars, this subtype emits most of its radiation in the ultraviolet region. Since our camera is unable to penetrate very far into this wavelength region, and due to the Balmer jump masking the continuum at the extreme low end of our graph, our curve will

indicate a "false peak" near the lower end of the spectrum. For consistency, we will calculate the temperature according to Wien's Law and compare this to our expected value.

Following is the continuum curve for Epsilon Cassiopeiae (Segin), along with the main spectrum. The labels have been removed to facilitate easier identification of the apparent peak wavelength.

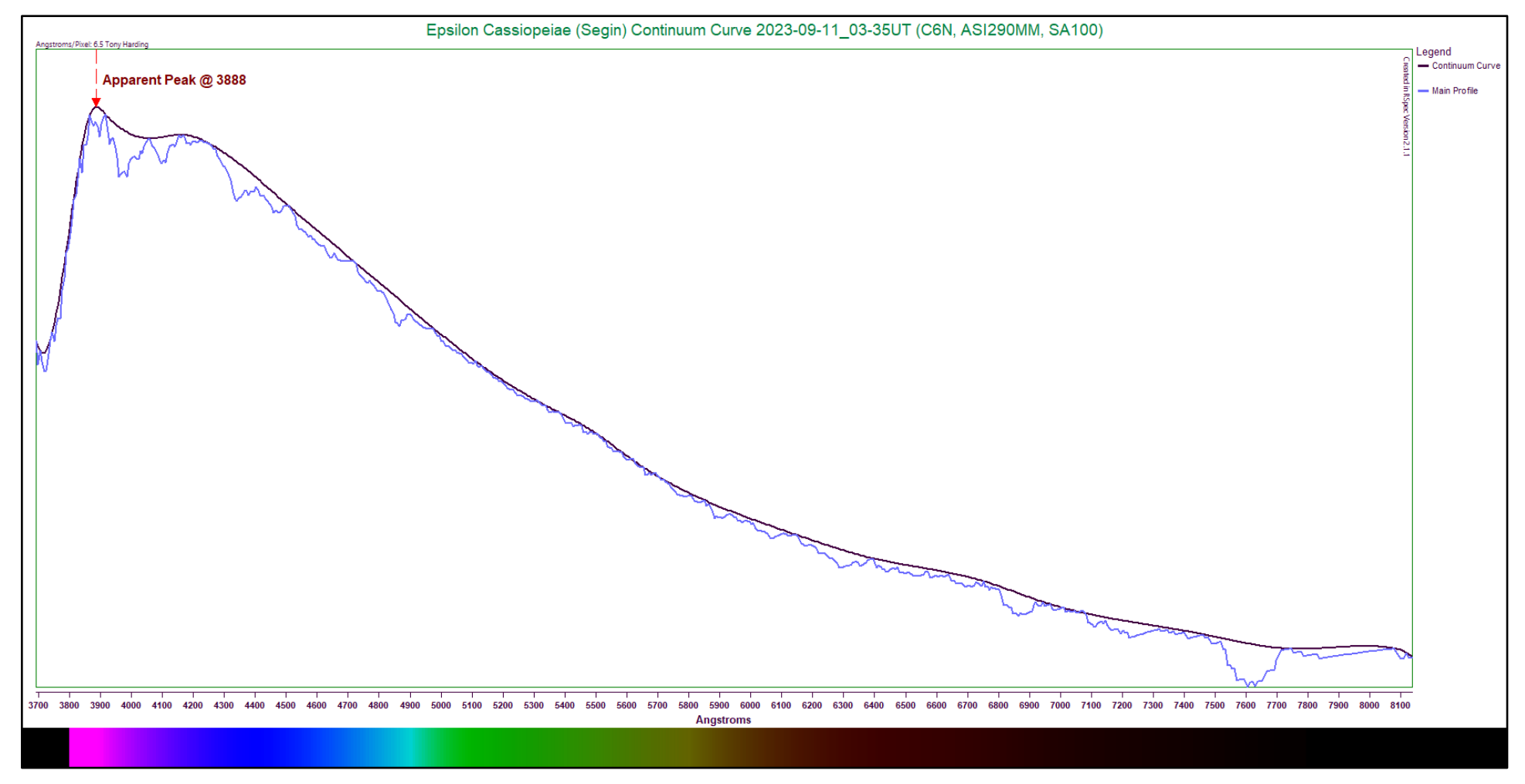


Figure 5.6 - Continuum Curve Plot (Epsilon Cassiopeiae)

From our drawn continuum curve, the peak would appear to lie at 3888 Angstroms. Adopting this value, Wien's Law provides a temperature estimate of 7,453K. Indeed, this is far removed from the anticipated temperature range of 26,000K-17,000K. Compared to the median value of our expected range (21,500K), the calculation is in error by a factor of approximately 2.88. The professionally determined temperature of the star is 15,174K⁽¹⁴⁾. This value is actually slightly below our expected range, slightly more than 12% below the lower expended temperature of 17,000K. Reconsidering our temperature estimate with respect to the established value, our estimate is off by a factor of 2.04–better, but still incredibly inaccurate.

Middle B-Type Stars

The middle B-type stars represent the beginning of a transition, where the neutral helium lines begin to fade while some ionized metals typical in A-type stars begin to emerge. These metals are not always visible, and they can be difficult to identify due to their extreme weakness. The temperatures of these stars will show a slight decline from their early B-type cousins.

Like all B-type stars, the middle B-types are still hot, with these coming in at approximately 16,500K to 14,500K⁽¹²⁾. They are still quite massive, as well, typically having 5.1 to 4.3 times the mass of our Sun⁽¹²⁾. They shine between 775 down to about 370 times solar luminosity⁽¹²⁾. Their lower mass allows them to live longer on the main sequence than the earlier stars, typically for approximately 150 Myr⁽⁷⁾. Spectroscopically, the neutral helium lines are the identifying characteristics of these stars, but (as mentioned above) a number of extremely weak ionized metals can often be seen peeking through the continuum. The hydrogen Balmer lines still appear subdued, but may be gaining more definition in the spectra.

The representative star chosen for the middle B-types is Nu Andromedae in the constellation of Andromeda, the Chained Maiden. This star is a main sequence star, but it is also a spectroscopic binary. Its companion, however, is much dimmer, shining with a luminosity that is almost 300 times less than the primary. This being the case, the companion shouldn't make any practical contribution to our low-resolution spectrum.

The spectrum of Nu Andromedae is presented here, along with a rectified spectrum appearing in red.

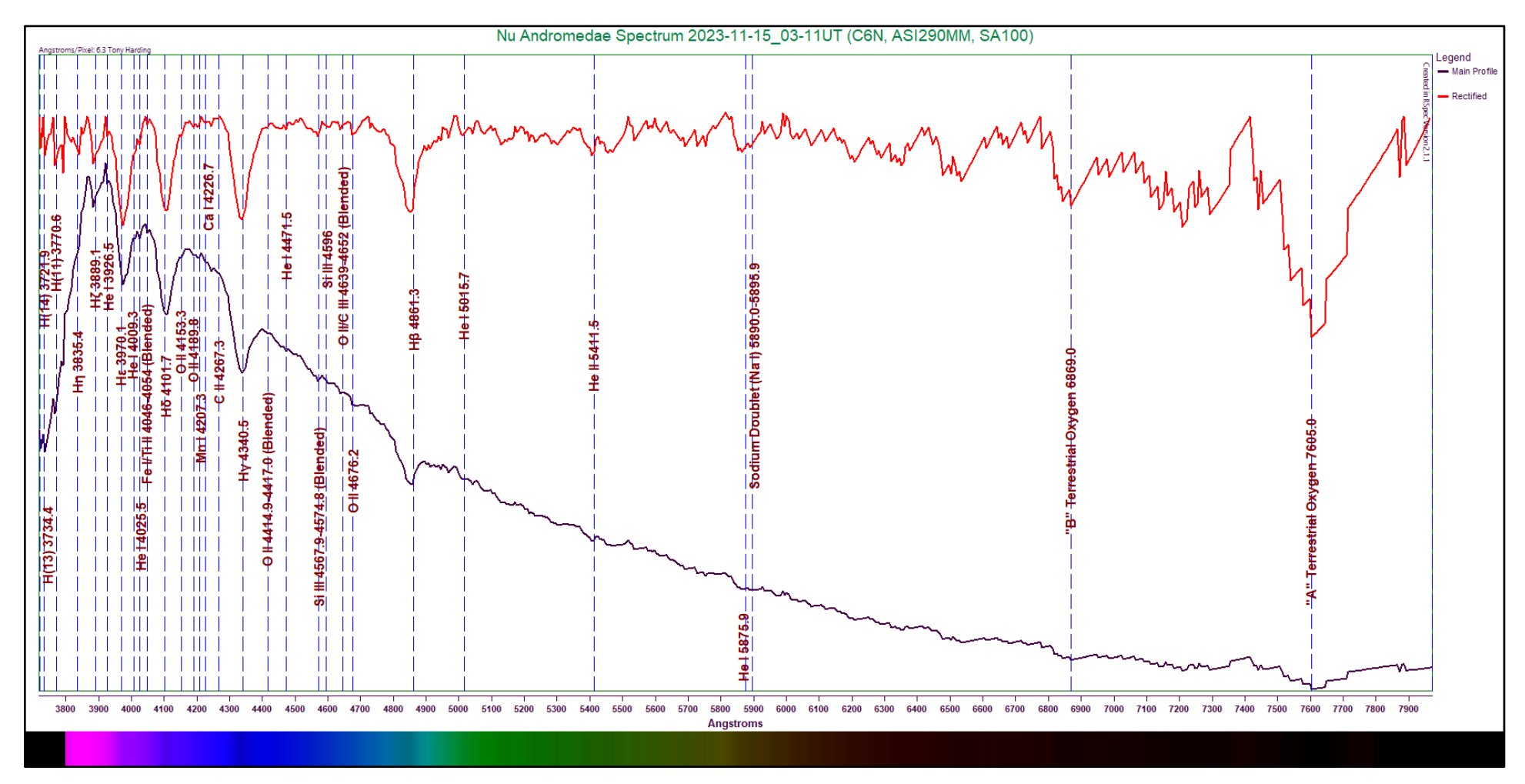


Figure 5.7: Nu Andromedae Spectrum (6.2 Angstroms/pixel)
Capture Details: Exposure 760ms, Gain 113, 80% of 324 frames stacked, Integration Time 196s

The hydrogen Balmer lines do appear a bit more pronounced than in the O-type and earlier B-type stars. However, the Hα absorption is not clearly visible here. A good number of helium lines are present, 3926.5, 4009.3, 4025.5, 4471.5, 5015.7, 5411.5, and 5875.6

Angstroms. The sodium doublet at 5890.0-5895.9 Angstroms is visible, appearing broadened by the neutral helium line just below it. This presence is weak, indicating a possible interstellar source for the absorption, but it appears quite broad. Other metals visible include iron, oxygen, manganese, carbon, calcium, and silicon.

The following table shows the indicated absorption features of the Nu Andromedae spectrum.

Table 5.7 - Nu Andromedae Line Identification Details

Feature	Wavelength (Angstroms)	Comments
H(14)	3721.9	Higher order hydrogen Balmer line; appears here hugging the left edge of the graph
H(13)	3734.4	Higher order hydrogen Balmer line; weak but clear
H(11)	3770.6	Higher order hydrogen Balmer line; weak but clear
Ηη	3835.4	Very weak hydrogen Balmer line; only causing small diversion in continuum
Hζ	3889.1	Weak but notable hydrogen Balmer line
He I	3926.5	Very weak neutral helium line
Ηε	3970.1	Strong hydrogen Balmer absorption
He I	4009.3	Extremely weak neutral helium line
He I	4025.5	Very weak to weak neutral helium line
Fe I/Ti II	4046-4054	Very weak iron/titanium blend; much more common in cooler stars
Нδ	4101.7	Strong hydrogen Balmer blend line
OII	4153.3	Extremely weak ionized oxygen line
OII	4189.8	Extremely weak ionized oxygen line
Mn I	4207.3	Very weak neutral manganese line; more common in cooler stars
Ca I	4226.7	Extremely weak but common neutral calcium line
CII	4267.2	Extremely subtle ionized carbon line; only causing small dip in continuum; dubious identification
Нү	4340.5	Strong hydrogen Balmer absorption
OII	4414.9-4417.0	Very subtle ionized oxygen blend; only causing small dip in continuum
He I	4471.5	Extremely weak neutral helium line
Si III	4567.9-4574.8	Weak doubly-ionized silicon absorption
Si III	4596	Very weak doubly-ionized silicon absorption
O II/C III	4639-4652	Very weak oxygen/carbon blend
OII	4676.2	Very weak ionized oxygen line
Нβ	4861.3	Fairly strong hydrogen Balmer line
He I	5015.7	Very weak neutral helium line
He II	5411.5	Very weak ionized helium line
He I	5875.6	Common but extremely faint neutral helium line; contributing to broad dip with sodium doublet
Sodium Doublet (Na I)	5890.0-5895.9	Fraunhofer "D1" and "D2" neutral sodium blend; may be interstellar in nature here; broadened by He I below
Telluric Oxygen	6869.0	Fraunhofer "B" absorption due to atmospheric oxygen
Telluric Oxygen	7605.0	Fraunhofer "A" absorption due to atmospheric oxygen

When considering this star's temperature, we will again observe that since the star's peak energy output actually lies in the ultraviolet range, our use of Wien's Law will produce a woefully inadequate answer. The capacities of the camera used, along with the Balmer

jump eradicating the continuum at the lowest wavelength range of our spectrum, will conspire to produce an apparent false spectrum peak. To demonstrate, this calculation will be carried out and compared to temperatures typical of middle B-type stars.

The continuum curve for Nu Andromedae is presented here, along with the spectrum in blue. The labels have been removed to enable a better view of the curves, and the apparent peak energy wavelength has been labeled.

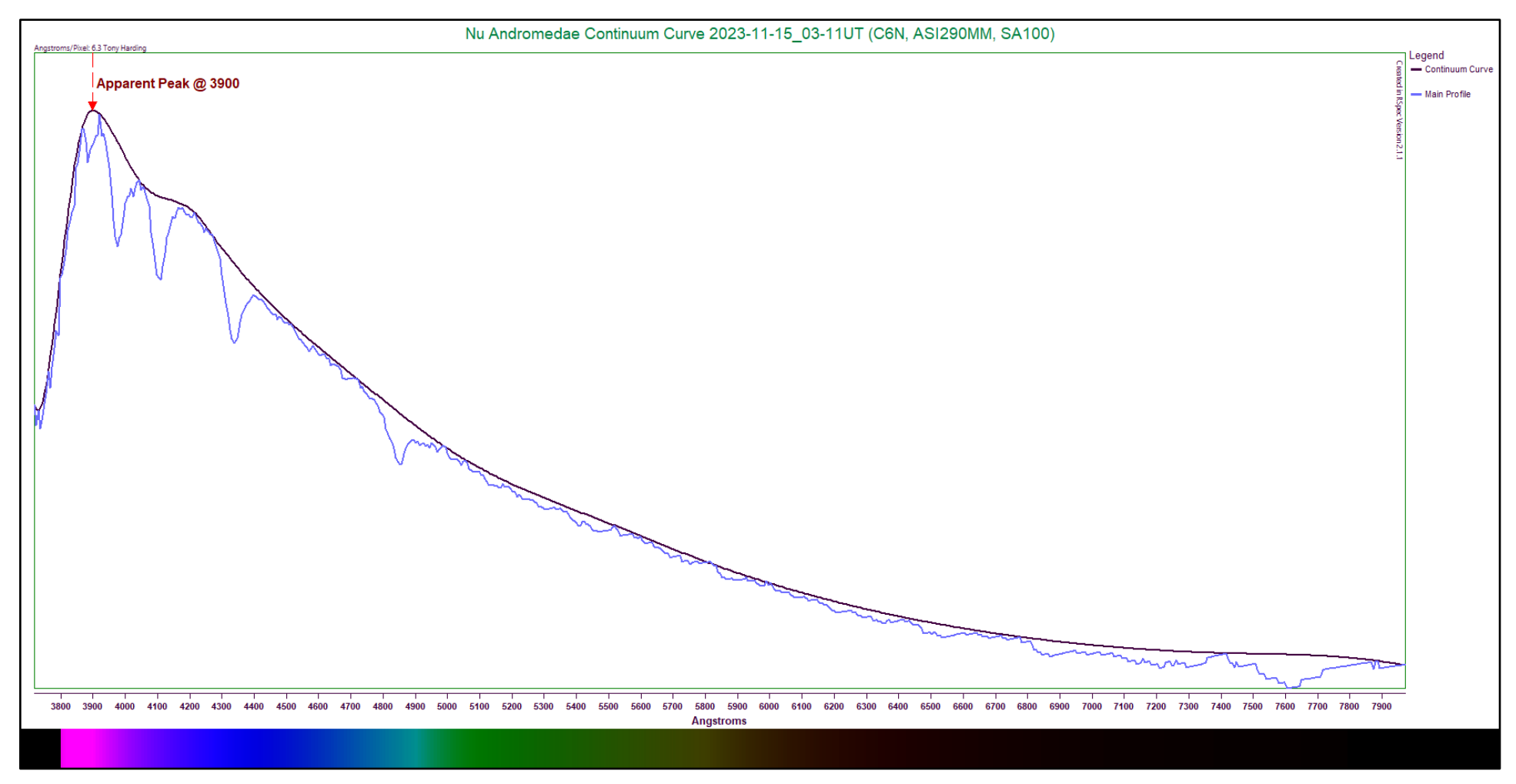


Figure 5.8 - Continuum Curve Plot (Nu Andromedae)

Using the data available to us, the peak energy wavelength appears to lie at 3900 Angstroms. Adopting this value, we use Wien's Law to calculate a temperature of 7,430K. Again, we see that our estimate is incredibly short of the expected value between 16,500K and 14,500K. The estimate is short of the median of the range (15,500K) by a factor of 2.09. The professionally determined temperature of the star is 14,851K⁽¹⁵⁾. Comparing our estimate to this actual value, we are still off by a factor of 2.00.

Late B-Type Stars

Late B-type stars begin to show characteristics very similar to the A-types. The neutral helium lines continue to diminish in number, while the strength of the faint metals grows. The hydrogen Balmer lines continue to grow in strength here, making the curve more strongly resemble that of an A-type star. The temperature continues to decline.

Though somewhat cooler than the middle B-types, these stars remain quite hot. They range in effective temperature from about 14,000K down to about 12,000K⁽¹²⁾. Compared to our Sun, they are massive, ranging from 4 to 3.3 times solar mass⁽¹²⁾. Their luminosities range from roughly 300 down to about 150 times that of our Sun⁽¹²⁾, making them still quite bright. They remain longer on the main sequence than earlier B-types, having stays of approximately 225 Myr ⁽⁷⁾. The spectra of these late B-types typically show moderately strong hydrogen Balmer lines, with several neutral helium lines still present. Some other neutral and ionized metals can often be seen, though these remain weak to very weak in strength. These can include iron, manganese, calcium, and silicon. Of course, the presence and strength of these features will vary from one specimen to another, and some may not be present at all.

The star chosen to represent the late B-types is Zeta Pegasi, also called Homam, in the constellation of Pegasus, the Winged Horse.

The spectrum of Zeta Pegasi (Homam) is presented here, along with a rectified spectrum in red.

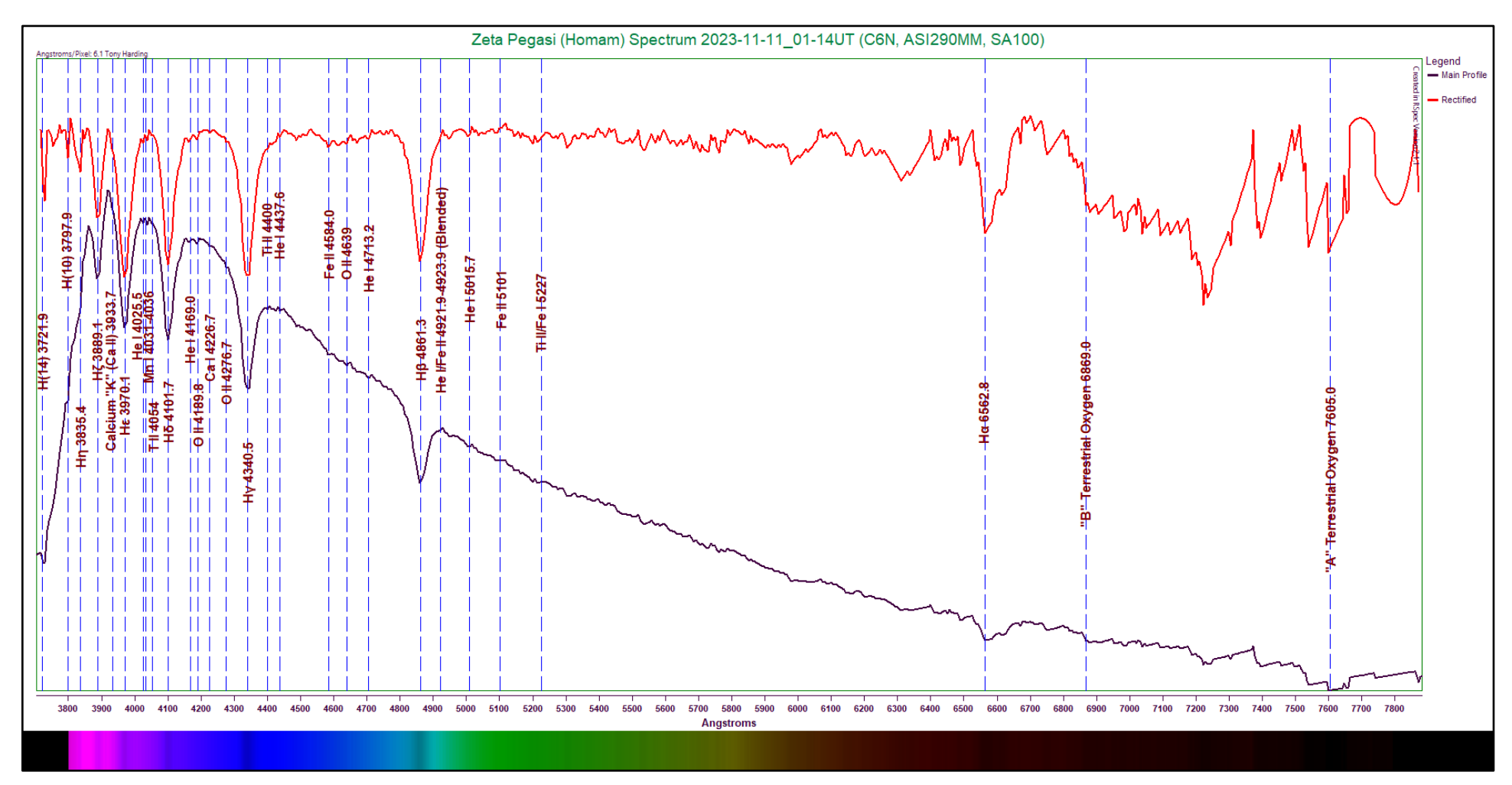


Figure 5.9: Zeta Pegasi (Homam) Spectrum (6.3 Angstroms/pixel)
Capture Details: Exposure 441ms, Gain 95, 40% of 422 frames stacked, Integration Time 74s

The first characteristic of note is the strength and definition of the hydrogen Balmer lines. The lines appear clear and strong. Even the Hα absorption appears distinctly here. We can see a few helium lines present, at 4025.5, 4169.0, 4437.6, 4713.2, 4921.9 (blended with Fe II) Angstroms. A very subtle bump occurs at 3933.7 Angstroms, which is the emergence of the calcium "K" line. (This will continue to grow into the G-type stars.) Several other faint or very faint metals are marked, including manganese, titanium, oxygen, and calcium. These appear in varying stages of ionization.

The following table shows the indicated absorption features of the Zeta Pegasi (Homam) spectrum.

Table 5.8 - Zeta Pegasi (Homam) Line Identification Details

Feature Wavelength (Angstroms) Higher order hydrogen Balmer line; weak, but well defined	Table 5.8 - Zeta Pegasi	}	
H(14) 3721.9 Higher order hydrogen Balmer line; weak, but well defined	Feature	Wavelength	Comments
H(10) 3797.9 Very weak higher order hydrogen Balmer line			
Hη 3835.4 Subtle hydrogen Balmer absorption Hζ 3889.1 Moderately strong hydrogen Balmer line Ca II 3933.7 Fraunhofer "K" line for ionized calcium; just barely beginning to emerge Hε 3970.1 Strong hydrogen Balmer line He I 4025.5 Common neutral helium line; extremely weak here Mn I 4031-4036 Extremely weak neutral manganese blend Tī III 4054 Extremely weak ionized titanium absorption; dubious identification Hδ 4101.7 Strong hydrogen Balmer line He I 4169.0 Very weak neutral helium line O III 4189.8 Very weak neutral helium line Ca I 4226.7 Extremely weak ionized oxygen line Ca I 4276.7 Extremely weak ionized oxygen line Hγ 4340.5 Very strong hydrogen Balmer Tī III 4400 Extremely weak ionized dixpliam basorption He I 4437.6 Extremely weak ionized titanium absorption He I 4437.6 Extremely weak ionized iron line O II 4639 Extremely weak ionized oxygen line He I 4713.2 Very weak ionized iron line He I 4713.2 Very weak ionized iron line He I 4921.9-4923.9 Very subtle helium/iron blend; dubious identification Ti II/Fe II 5015.7 Extremely weak neutral helium line Extremely weak neutral helium line Extremely weak neutral helium line		3721.9	Higher order hydrogen Balmer line; weak, but well defined
Hζ 3889.1 Moderately strong hydrogen Balmer line Ca II 3933.7 Fraunhofer "K" line for ionized calcium; just barely beginning to emerge Hε 3970.1 Strong hydrogen Balmer line He I 4025.5 Common neutral helium line; extremely weak here Mn I 4031-4036 Extremely weak neutral manganese blend Ti III 4054 Extremely weak ionized titanium absorption; dubious identification Hδ 4101.7 Strong hydrogen Balmer line He I 4169.0 Very weak neutral helium line O III 4189.8 Very weak ionized oxygen line Ca I 4226.7 Extremely weak neutral calcium line; common line O II 4276.7 Extremely weak ionized oxygen line Hγ 4340.5 Very strong hydrogen Balmer Ti II 4400 Extremely weak ionized titanium absorption He I 4437.6 Extremely weak ionized titanium absorption Fe II 4584.0 Very weak ionized iron line O II 4639 Extremely weak ionized oxygen line He I 4713.2 Very weak ionized oxygen line He I 4921.9-4923.9 Very subtle helium line Fe II 4921.9-4923.9 Very subtle helium/iron blend; dubious identification Ti II/Fe II 5227 Extremely weak inoized iron absorption; dubious due to noise in the continuum here	H(10)	3797.9	Very weak higher order hydrogen Balmer line
Ca II 3933.7 Fraunhofer "K" line for ionized calcium; just barely beginning to emerge Hε 3970.1 Strong hydrogen Balmer line He I 4025.5 Common neutral helium line; extremely weak here Mn I 4031-4036 Extremely weak neutral manganese blend Ti II 4054 Extremely weak ionized titanium absorption; dubious identification H8 4101.7 Strong hydrogen Balmer line He I 4169.0 Very weak ionized oxygen line O II 4189.8 Very weak ionized oxygen line Ca I 4226.7 Extremely weak ionized oxygen line O II 4276.7 Extremely weak ionized oxygen line Hy 4340.5 Very strong hydrogen Balmer Ti II 4400 Extremely weak ionized titanium absorption He I 4437.6 Extremely weak ionized itinnium absorption He I 4584.0 Very weak neutral helium line G II 4639 Extremely weak ionized iron line He I 4713.2 Very weak neutral helium line He I 4921.9-4923.9 Very subtle helium/iron blend; dubious identification He I 5015.7 Extre	Ηη	3835.4	Subtle hydrogen Balmer absorption
Hε 3970.1 Strong hydrogen Balmer line He I 4025.5 Common neutral helium line; extremely weak here Mn I 4031-4036 Extremely weak neutral manganese blend Ti II 4054 Extremely weak ionized titanium absorption; dubious identification Hδ 4101.7 Strong hydrogen Balmer line He I 4169.0 Very weak neutral helium line O II 4189.8 Very weak ionized oxygen line Ca I 4226.7 Extremely weak ionized oxygen line O II 4276.7 Extremely weak ionized oxygen line Hγ 4340.5 Very strong hydrogen Balmer Ti II 4400 Extremely weak ionized titanium absorption He I 4437.6 Extremely weak neutral helium line Fe II 4584.0 Very weak ionized ion line O II 4639 Extremely weak ionized oxygen line He I 4713.2 Very weak ionized oxygen line He I 4713.2 Very weak neutral helium line He I/Fe II 4921.9-4923.9 Very subtle helium/iron blend; dubious identification Fe II 5015.7 Extremely weak neutral helium line Fe II 5101 Extremely weak neutral helium line	Нζ	3889.1	Moderately strong hydrogen Balmer line
He I 4025.5 Common neutral helium line; extremely weak here Mn I 4031-4036 Extremely weak neutral manganese blend Ti II 4054 Extremely weak ionized tiralum absorption; dubious identification Hδ 4101.7 Strong hydrogen Balmer line He I 4169.0 Very weak neutral helium line O II 4189.8 Very weak ionized oxygen line Ca I 4226.7 Extremely weak neutral calcium line; common line O II 4276.7 Extremely weak ionized oxygen line Hγ 4340.5 Very strong hydrogen Balmer Ti II 4400 Extremely weak ionized titanium absorption He I 4437.6 Extremely weak ionized titanium absorption Fe II 4584.0 Very weak ionized oxygen line O II 4639 Extremely weak ionized oxygen line He I 4713.2 Very weak ionized oxygen line He I 4921.9-4923.9 Very subtle helium line He I/Fe II 4921.9-4923.9 Very subtle helium/iron blend; dubious identification Fe II 5101 Extremely weak ionized iron absorption; dubious due to noise in the continuum here	Ca II	3933.7	Fraunhofer "K" line for ionized calcium; just barely beginning to emerge
Mn I 4031-4036 Extremely weak neutral manganese blend Ti II 4054 Extremely weak ionized titanium absorption; dubious identification Hδ 4101.7 Strong hydrogen Balmer line He I 4169.0 Very weak neutral helium line O II 4189.8 Very weak ionized oxygen line Ca I 4226.7 Extremely weak neutral calcium line; common line O II 4276.7 Extremely weak ionized oxygen line Hγ 4340.5 Very strong hydrogen Balmer Ti II 4400 Extremely weak ionized titanium absorption He I 4437.6 Extremely weak neutral helium line Fe II 4584.0 Very weak ionized iron line O II 4639 Extremely weak ionized oxygen line He I 4713.2 Very weak neutral helium line Hβ 4861.3 Strong hydrogen Balmer line He I/Fe II 4921.9-4923.9 Very subtle helium/iron blend; dubious identification He I 5015.7 Extremely weak neutral helium line Fe II 5101 Extremely weak neutral helium line Ti II/Fe I 5227 Extremely weak ittanium/iron blend; very	Ηε	3970.1	Strong hydrogen Balmer line
Ti II 4054 Extremely weak ionized titanium absorption; dubious identification Hδ 4101.7 Strong hydrogen Balmer line He I 4169.0 Very weak neutral helium line O II 4189.8 Very weak ionized oxygen line Ca I 4226.7 Extremely weak neutral calcium line; common line O II 4276.7 Extremely weak ionized oxygen line Hγ 4340.5 Very strong hydrogen Balmer Ti II 4400 Extremely weak ionized titanium absorption He I 4437.6 Extremely weak neutral helium line Fe II 4584.0 Very weak ionized in line O II 4639 Extremely weak ionized oxygen line He I 4713.2 Very weak neutral helium line Hβ 4861.3 Strong hydrogen Balmer line He I/Fe II 4921.9-4923.9 Very subtle helium/iron blend; dubious identification Fe II 5101 Extremely weak ionized iron absorption; dubious due to noise in the continuum here	He I	4025.5	Common neutral helium line; extremely weak here
Hδ 4101.7 Strong hydrogen Balmer line He I 4169.0 Very weak neutral helium line O II 4189.8 Very weak ionized oxygen line Ca I 4226.7 Extremely weak neutral calcium line; common line O II 4276.7 Extremely weak ionized oxygen line Hγ 4340.5 Very strong hydrogen Balmer Ti II 4400 Extremely weak ionized titanium absorption He I 4437.6 Extremely weak ionized titanium ine Fe II 4584.0 Very weak ionized iron line O II 4639 Extremely weak ionized oxygen line He I 4713.2 Very weak ionized oxygen line He I 4921.9-4923.9 Very subtle helium/iron blend; dubious identification Fe II 5015.7 Extremely weak neutral helium line Fe II 5101 Extremely weak ionized iron absorption; dubious identification Ti II/Fe I 5227 Extremely weak itianium/iron blend; very dubious due to noise in the continuum here	Mn I	4031-4036	Extremely weak neutral manganese blend
He I 4169.0 Very weak neutral helium line O II 4189.8 Very weak ionized oxygen line Ca I 4226.7 Extremely weak neutral calcium line; common line O II 4276.7 Extremely weak ionized oxygen line Hγ 4340.5 Very strong hydrogen Balmer Ti II 4400 Extremely weak ionized titanium absorption He I 4437.6 Extremely weak neutral helium line Fe II 4584.0 Very weak ionized iron line O II 4639 Extremely weak ionized oxygen line He I 4713.2 Very weak neutral helium line Hβ 4861.3 Strong hydrogen Balmer He I/Fe II 4921.9-4923.9 Very subtle helium/iron blend; dubious identification Fe II 5015.7 Extremely weak neutral helium line Fe II 5101 Extremely weak ionized iron absorption; dubious identification Ti II/Fe I 5227 Extremely weak ionized iron absorption; dubious due to noise in the continuum here	Ti II	4054	Extremely weak ionized titanium absorption; dubious identification
O II 4189.8 Very weak ionized oxygen line Ca I 4226.7 Extremely weak neutral calcium line; common line O II 4276.7 Extremely weak ionized oxygen line Hγ 4340.5 Very strong hydrogen Balmer Ti II 4400 Extremely weak ionized titanium absorption He I 4437.6 Extremely weak neutral helium line Fe II 4584.0 Very weak ionized iron line O II 4639 Extremely weak ionized oxygen line He I 4713.2 Very weak neutral helium line Hβ 4861.3 Strong hydrogen Balmer line He I/Fe II 4921.9-4923.9 Very subtle helium/iron blend; dubious identification He I 5015.7 Extremely weak neutral helium line Fe II 5101 Extremely weak ionized iron absorption; dubious identification Ti II/Fe I 5227 Extremely weak titanium/iron blend; very dubious due to noise in the continuum here	Ηδ	4101.7	Strong hydrogen Balmer line
Ca I 4226.7 Extremely weak neutral calcium line; common line O II 4276.7 Extremely weak ionized oxygen line Hy 4340.5 Very strong hydrogen Balmer Ti II 4400 Extremely weak ionized titanium absorption He I 4437.6 Extremely weak neutral helium line Fe II 4584.0 Very weak ionized iron line O II 4639 Extremely weak ionized oxygen line He I 4713.2 Very weak neutral helium line HB 4861.3 Strong hydrogen Balmer line He I/Fe II 4921.9-4923.9 Very subtle helium/iron blend; dubious identification He I 5015.7 Extremely weak neutral helium line Fe II 5101 Extremely weak ionized iron absorption; dubious identification Ti II/Fe I 5227 Extremely weak titanium/iron blend; very dubious due to noise in the continuum here	He I	4169.0	Very weak neutral helium line
O II 4276.7 Extremely weak ionized oxygen line Hγ 4340.5 Very strong hydrogen Balmer Ti II 4400 Extremely weak ionized titanium absorption He I 4437.6 Extremely weak neutral helium line Fe II 4584.0 Very weak ionized iron line O II 4639 Extremely weak ionized oxygen line He I 4713.2 Very weak neutral helium line Hβ 4861.3 Strong hydrogen Balmer line He I/Fe II 4921.9-4923.9 Very subtle helium/iron blend; dubious identification He I 5015.7 Extremely weak ionized iron absorption; dubious identification Ti II/Fe I 5227 Extremely weak titanium/iron blend; very dubious due to noise in the continuum here	OII	4189.8	Very weak ionized oxygen line
Hγ 4340.5 Very strong hydrogen Balmer Ti II 4400 Extremely weak ionized titanium absorption He I 4437.6 Extremely weak neutral helium line Fe II 4584.0 Very weak ionized iron line O II 4639 Extremely weak ionized oxygen line He I 4713.2 Very weak neutral helium line Hβ 4861.3 Strong hydrogen Balmer line He I/Fe II 4921.9-4923.9 Very subtle helium/iron blend; dubious identification He I 5015.7 Extremely weak neutral helium line Fe II 5101 Extremely weak ionized iron absorption; dubious identification Ti II/Fe I 5227 Extremely weak titanium/iron blend; very dubious due to noise in the continuum here	Ca I	4226.7	Extremely weak neutral calcium line; common line
Ti II 4400 Extremely weak ionized titanium absorption He I 4437.6 Extremely weak neutral helium line Fe II 4584.0 Very weak ionized iron line O II 4639 Extremely weak ionized oxygen line He I 4713.2 Very weak neutral helium line Hβ 4861.3 Strong hydrogen Balmer line He I/Fe II 4921.9-4923.9 Very subtle helium/iron blend; dubious identification He I 5015.7 Extremely weak neutral helium line Fe II 5101 Extremely weak ionized iron absorption; dubious identification Ti II/Fe I 5227 Extremely weak titanium/iron blend; very dubious due to noise in the continuum here	OII	4276.7	Extremely weak ionized oxygen line
He I 4437.6 Extremely weak neutral helium line Fe II 4584.0 Very weak ionized iron line O II 4639 Extremely weak ionized oxygen line He I 4713.2 Very weak neutral helium line Hβ 4861.3 Strong hydrogen Balmer line He I/Fe II 4921.9-4923.9 Very subtle helium/iron blend; dubious identification He I 5015.7 Extremely weak neutral helium line Fe II 5101 Extremely weak ionized iron absorption; dubious identification Ti II/Fe I 5227 Extremely weak titanium/iron blend; very dubious due to noise in the continuum here	Нү	4340.5	Very strong hydrogen Balmer
Fe II 4584.0 Very weak ionized iron line O II 4639 Extremely weak ionized oxygen line He I 4713.2 Very weak neutral helium line Hβ 4861.3 Strong hydrogen Balmer line He I/Fe II 4921.9-4923.9 Very subtle helium/iron blend; dubious identification He I 5015.7 Extremely weak neutral helium line Fe II 5101 Extremely weak ionized iron absorption; dubious identification Ti II/Fe I 5227 Extremely weak titanium/iron blend; very dubious due to noise in the continuum here	Ti İI	4400	Extremely weak ionized titanium absorption
O II 4639 Extremely weak ionized oxygen line He I 4713.2 Very weak neutral helium line Hβ 4861.3 Strong hydrogen Balmer line He I/Fe II 4921.9-4923.9 Very subtle helium/iron blend; dubious identification He I 5015.7 Extremely weak neutral helium line Fe II 5101 Extremely weak ionized iron absorption; dubious identification Ti II/Fe I 5227 Extremely weak titanium/iron blend; very dubious due to noise in the continuum here	He I	4437.6	Extremely weak neutral helium line
He I 4713.2 Very weak neutral helium line Hβ 4861.3 Strong hydrogen Balmer line He I/Fe II 4921.9-4923.9 Very subtle helium/iron blend; dubious identification He I 5015.7 Extremely weak neutral helium line Fe II 5101 Extremely weak ionized iron absorption; dubious identification Ti II/Fe I 5227 Extremely weak titanium/iron blend; very dubious due to noise in the continuum here	Fe II	4584.0	Very weak ionized iron line
Hβ 4861.3 Strong hydrogen Balmer line He I/Fe II 4921.9-4923.9 Very subtle helium/iron blend; dubious identification He I 5015.7 Extremely weak neutral helium line Fe II 5101 Extremely weak ionized iron absorption; dubious identification Ti II/Fe I 5227 Extremely weak titanium/iron blend; very dubious due to noise in the continuum here	OII	4639	Extremely weak ionized oxygen line
He I/Fe II 4921.9-4923.9 Very subtle helium/iron blend; dubious identification He I 5015.7 Extremely weak neutral helium line Fe II 5101 Extremely weak ionized iron absorption; dubious identification Ti II/Fe I 5227 Extremely weak titanium/iron blend; very dubious due to noise in the continuum here	He I	4713.2	Very weak neutral helium line
He I 5015.7 Extremely weak neutral helium line Fe II 5101 Extremely weak ionized iron absorption; dubious identification Ti II/Fe I 5227 Extremely weak titanium/iron blend; very dubious due to noise in the continuum here	Нβ	4861.3	Strong hydrogen Balmer line
Fe II 5101 Extremely weak ionized iron absorption; dubious identification Ti II/Fe I 5227 Extremely weak titanium/iron blend; very dubious due to noise in the continuum here	He I/Fe II	4921.9-4923.9	Very subtle helium/iron blend; dubious identification
Ti II/Fe I 5227 Extremely weak titanium/iron blend; very dubious due to noise in the continuum here	He I	5015.7	Extremely weak neutral helium line
	Fe II	5101	Extremely weak ionized iron absorption; dubious identification
Hα 6562.8 Moderately strong hydrogen Balmer line	Ti II/Fe I	5227	Extremely weak titanium/iron blend; very dubious due to noise in the continuum here
	Ηα	6562.8	Moderately strong hydrogen Balmer line

Feature	Wavelength	Comments
	(Angstroms)	
H(14)	3721.9	Higher order hydrogen Balmer line; weak, but well defined
H(10)	3797.9	Very weak higher order hydrogen Balmer line
Нη	3835.4	Subtle hydrogen Balmer absorption
Нζ	3889.1	Moderately strong hydrogen Balmer line
Ca II	3933.7	Fraunhofer "K" line for ionized calcium; just barely beginning to emerge
Ηε	3970.1	Strong hydrogen Balmer line
He I	4025.5	Common neutral helium line; extremely weak here
Mn I	4031-4036	Extremely weak neutral manganese blend
Ti II	4054	Extremely weak ionized titanium absorption; dubious identification
Ηδ	4101.7	Strong hydrogen Balmer line
He I	4169.0	Very weak neutral helium line
OII	4189.8	Very weak ionized oxygen line
Ca I	4226.7	Extremely weak neutral calcium line; common line
OII	4276.7	Extremely weak ionized oxygen line
Нү	4340.5	Very strong hydrogen Balmer
Ti II	4400	Extremely weak ionized titanium absorption
He I	4437.6	Extremely weak neutral helium line
Fe II	4584.0	Very weak ionized iron line
OII	4639	Extremely weak ionized oxygen line
He I	4713.2	Very weak neutral helium line
Нβ	4861.3	Strong hydrogen Balmer line
Telluric Oxygen	6869.0	Fraunhofer "B" absorption due to atmospheric oxygen; appears weakly here
Telluric Oxygen	7605.0	Fraunhofer "A" absorption due to atmospheric oxygen

Even though the late B-type stars have reduced effective temperatures compared to their hotter brethren, they still emit most of their light in the ultraviolet wavelength range. This combined with the Balmer jump will once more produce a false peak in our curve. We will demonstrate this by using Wien's Law to calculate a temperature, then compare this with the expected value.

The continuum curve for Zeta Pegasi (Homam) is presented here, along with the spectrum in blue. The labels have been removed to enable a better view of the curves, and the apparent peak energy wavelength has been labeled.

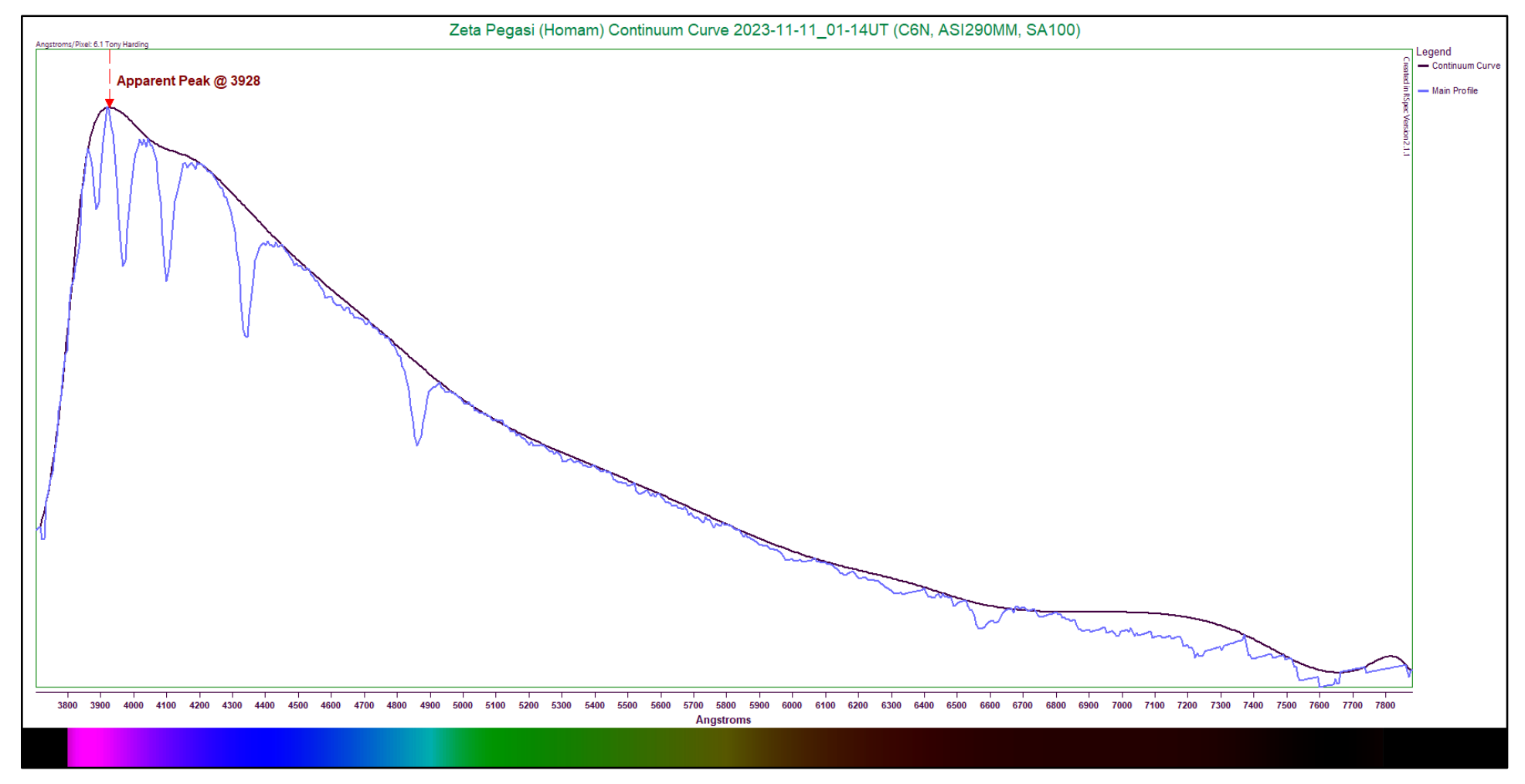


Figure 5.10 - Continuum Curve Plot (Zeta Pegasi)

From the continuum curve presented above, the peak energy output appears to lie at 3928 Angstroms. Plugging this value into Wien's Law results in a temperature estimate of 7,377K. This is a far cry from the expected temperature of 14,000K to 12,000K. This puts our estimate off by a factor of 1.76 from the median value of 13,000K. The professionally determined temperature of the star is listed as approximately 12,300K⁽¹⁶⁾. With respect to this value, our estimate is off by a factor of 1.67.

Be Stars

These special stars are typically hot B-types which throw off material due to their rapid rotation. This material absorbs the intense ultraviolet radiation from the parent star, exciting the hydrogen therein. The excited atoms then de-excite and emit radiation. This shows up as one or more emission lines in the spectrum, showing distinct spikes above the continuum level.

The B-types capable of doing this are usually to be found among the O/B stars or the earlier B-type stars. Specimens are known down into the late B-types, but most are earlier.

We will briefly examine one example of this type of star. The star chosen is Gamma Cassiopeiae, also known as Navi, in the Constellation of Cassiopeiae, the Queen. This star was the first one identified to be of this type and to have its emission lines explained. Unlike our other examinations, we will forego detailed accounts of all the absorption lines in this specimen and focus on the distinctive emission lines. We will also not calculate the star's effective temperature based on the appearance of the spectrum obtained.

The spectrum of Gamma Cassiopeiae (Navi) is presented here, along with a rectified spectrum in red. Unlike the other entries in this Atlas, this rectified spectrum will appear below the main profile. This mutes the absorption features, but better shows the emission characteristics of the star.

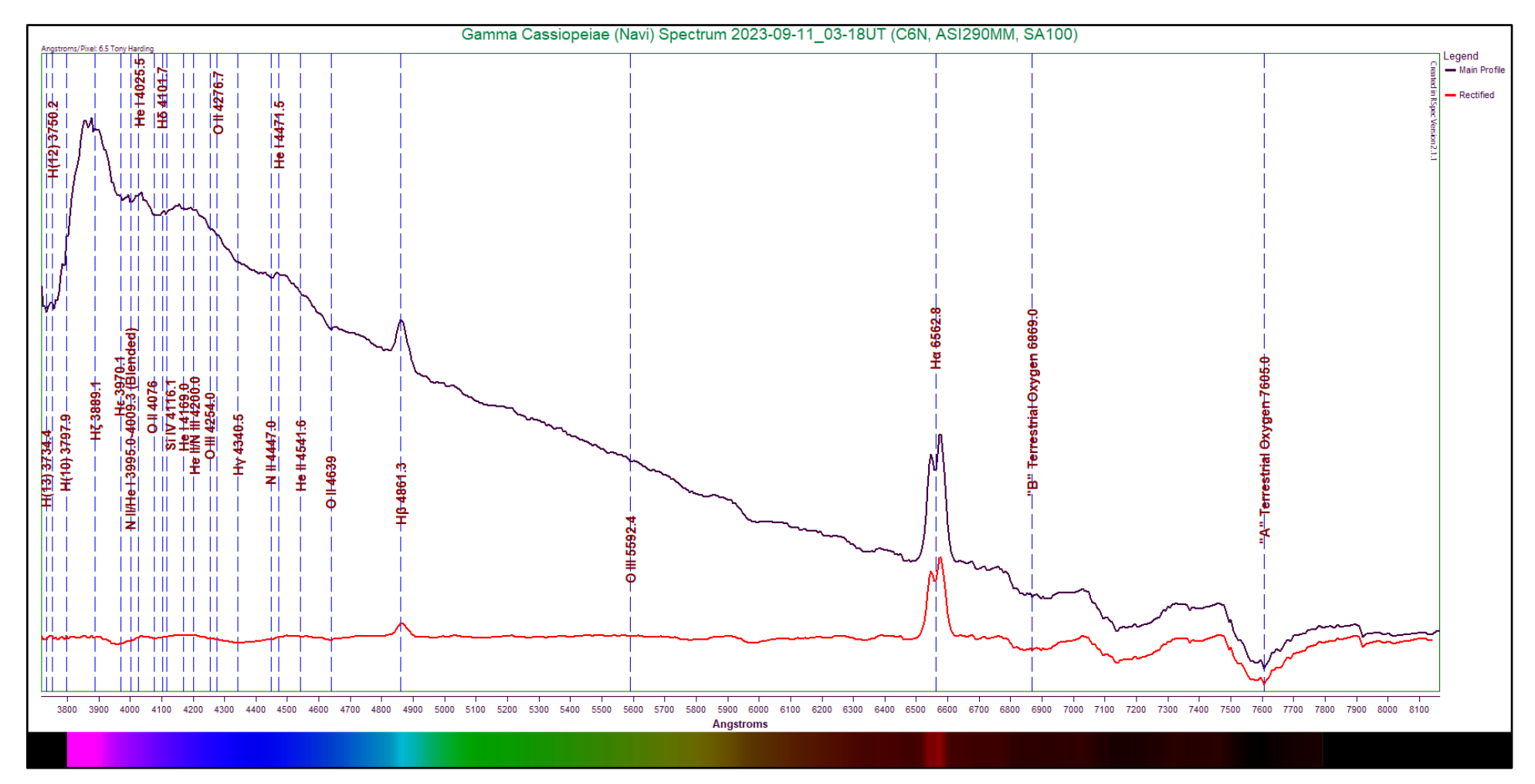


Figure 5.11: Gamma Cassiopeiae (Navi) Spectrum (6.3 Angstroms/pixel)
Capture Details: Exposure 310ms, Gain 110, 50% of 397 frames stacked, Integration Time 573s

At a glance we notice several broad dips in the continuum; these are caused by closely spaced, blended absorptions which tend to mask the continuum in the local vicinity. Also, many of the labeled absorption features appear extremely weak and are therefore questionable. We can see several hydrogen Balmer absorption lines, but we can also clearly see that two of these lines—the H β and the H α lines—are shown in emission. The H β line appears crisp and clear. The H α line, however, shows a double-peak in the middle. This curious characteristic is caused due to the motion of the hydrogen gas around the star relative to our viewing angle. From our point of view, some of the gas is moving toward us in its orbit of the star, and is therefore blue-shifted. Another part is moving away from us in its orbit, and appears red-shifted. The result is a double-peak, with a valley in the middle that indicates the central wavelength.

Some caution is required when these peaks are encountered. In addition to the emission features explained, they can also be caused by unnoticed field stars that may lie along the line of the spectrum when the data is collected. Their light pollutes the spectrum, making it appear as though an emission is present. If this is suspected, rotating the telescope tube and recapturing data will confirm what is actually happening.

5.4 Spectral Type B/A Stars (Very Late B and Very Early A)

Stars in this custom category typically show strong hydrogen Balmer lines. They also commonly demonstrate a few of the neutral helium lines found mostly in the B-type stars. They shine with a bright, white light, and are more common than the hotter O-types and B-types.

The B/A stars typically have temperatures between 10,700K and 9,700K^(12,17). They are fairly massive stars, weighing in at approximately 2.75 to 2.2 times solar mass. They are also bright stars, shining with luminosities ranging from approximately 72 down to 38 times solar luminosity^(12,17). As mentioned above, they show prominent hydrogen Balmer absorptions, making them ideal for the creation of response curves. They burn more slowly than the more massive B-types, usually staying on the main sequence of hydrogen burning for about 300 Myr ⁽⁷⁾. Other very faint metals are often visible, but these are usually weak in appearance, so great care must be taken when trying to identify them. There is usually a combination of neutral and ionized metals present in these spectra.

Spectroscopically, the dominant features are their strong hydrogen Balmer lines. These are commonly mixed with some neutral helium lines more prominently seen in hotter B-types. A growing number of other, fainter metal lines begin to emerge.

The star chosen to represent this type is indicated here:

Table 5.9 - Representative B/A Star

Subtype	Star
Very Late B/Very Early A	Sigma Piscium

B/A Stars (Very Late B and Very Early A)

The very late B-type and very early A-type stars can be tricky to differentiate based solely on low-resolution spectra. Their spectral curves are typically smooth in appearance, and they can show small neutral helium lines along with prominent hydrogen Balmer absorptions and a smattering of other, very faint metals.

Their temperatures are still quite high, around 10,000K^(12,17), making the application of Wien's Law ill-advised. Though the error in the calculation grows smaller as we work toward the A-type stars, the specimens still emit a lot of radiation in the ultraviolet range, throwing off estimates. This will be demonstrated for each specimen. Their masses hover around 2.5 times solar mass^(12,17), while they shine with luminosities averaging about 55 times the solar value^(12,17). As noted previously, they remain on the main sequence for approximately 300 Myr⁽⁷⁾.

The specimen chosen to represent this customized classification is Sigma Piscium, in the constellation of Pisces, the Fishes. The star is a spectroscopic binary, but both stars are estimated to be the exact same type. For the purposes of a low-resolution example, it should suffice nicely. However, the star is dim, so longer exposures were needed to capture its spectrum. This may lessen some of the detail visible.

The spectrum of Sigma Piscium is shown here; included is a rectified spectrum in red.

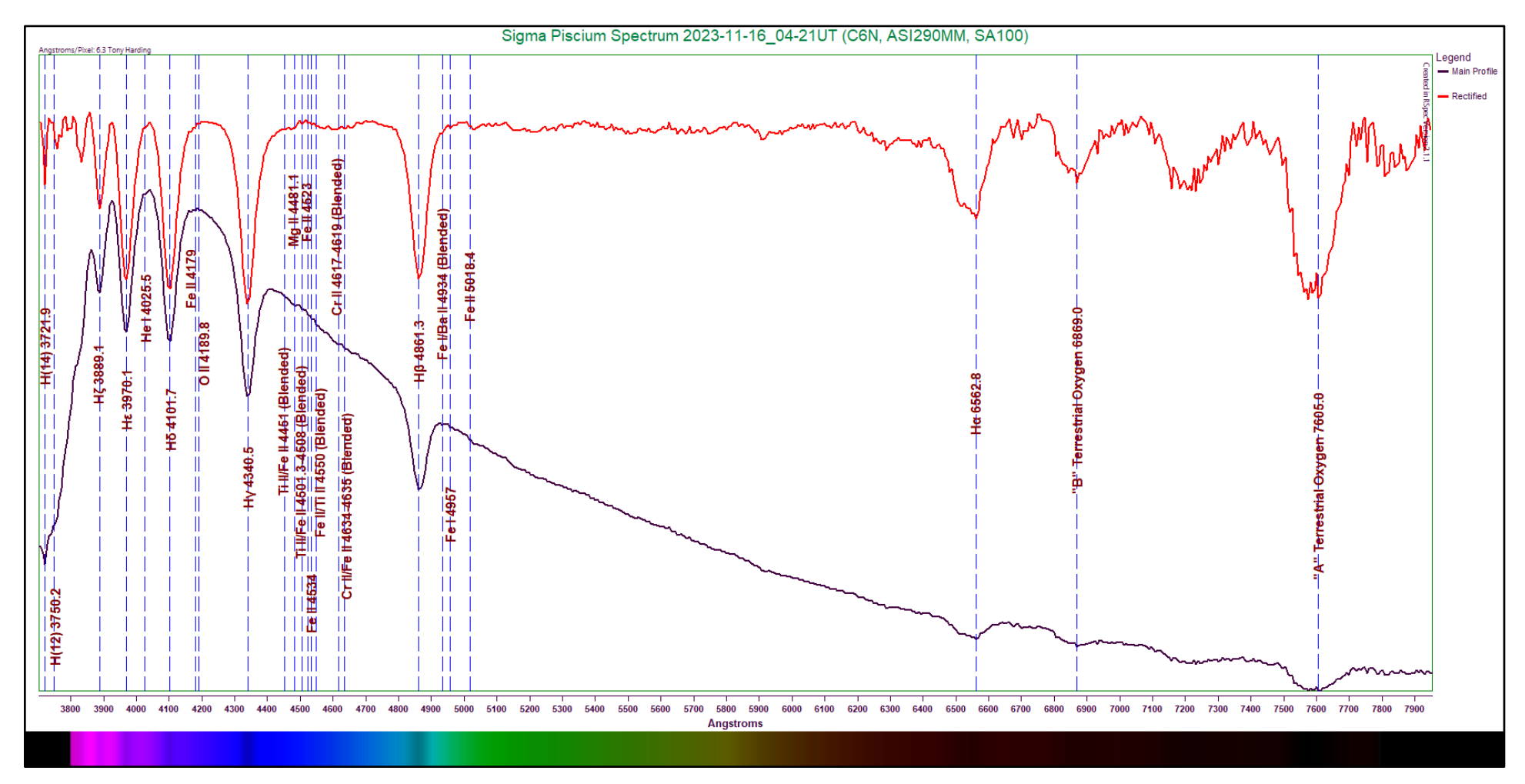


Figure 5.12: Sigma Piscum Spectrum (6.3 Angstroms/pixel)
Capture Details: Exposure 3s, Gain 154, 90% of 80 frames stacked, Integration Time 216s

Indeed, this spectrum appears quite smooth overall. The hydrogen Balmer absorptions are very strong, even the H α feature. Only one neutral helium line is labeled here, at 4025. Angstroms. A number of other very faint neutral and ionized metals are labeled, but they

are extremely weak at best, and so must be regarded with a healthy dose of suspicion. These include iron, oxygen, titanium, magnesium, and chromium.

The following table shows the indicated absorption features of the Sigma Piscium spectrum.

Table 5.10 - Sigma Piscium Line Identification Details

Feature	Wavelength	Comments
	(Angstroms)	
H(14)	3721.9	Higher order hydrogen Balmer line; moderately strong here
H(12)	3750.2	Higher order hydrogen Balmer absorption; very weak
Нζ	3889.1	Fairly strong hydrogen Balmer line
Ηε	3970.1	Very strong hydrogen Balmer line
He I	4025.5	Very faint neutral helium line
Ηδ	4101.7	Very strong hydrogen Balmer line
Fe II	4179	Extremely faint ionized iron absorption
OII	4189.4	Extremely faint ionized oxygen line
Нү	4340.5	Exceptionally strong hydrogen Balmer line; very clear and sharp
Ti II/Fe II	4451	Extremely subtle titanium/iron blend; dubious identification at best
Mg II	4481.1	Common ionized magnesium line; very weak here
Ti II/Fe II	4501.3-4508	Exceptionally weak titanium/iron blend; dubious identification
Fe II	4523	Exceptionally weak ionized iron absorption; dubious identification
Fe II	4534	Exceptionally weak ionized iron absorption; dubious identification
Fe II/Ti II	4550	Common iron/titanium blend; extremely subtle; dubious identification
Cr II	4617-4619	Very weak ionized chromium absorption; somewhat common
Cr II/Fe II	4634-4635	Extremely weak chromium/iron absorption
Нβ	4861.3	Very strong hydrogen Balmer line
Fe I/Ba II	4934	Extremely faint iron/barium absorption; fairly common
Fe I	4957	Extremely weak neutral iron line
Fe II	5018.4	Very weak ionized iron line
Ηα	6562.8	Fairly strong hydrogen Balmer absorption
Telluric Oxygen	6869.0	Fraunhofer "B" absorption due to atmospheric oxygen; appears weak and shallow here
Telluric Oxygen	7605.0	Fraunhofer "A" absorption due to atmospheric oxygen

We will again employ Wien's Law to gather an effective temperature estimate. As before, our estimate is guaranteed to be too low due to the ultraviolet range of the actual peak energy wavelength and the Balmer jump. Nonetheless, the demonstration will be carried out.

The continuum curve for Sigma Piscium is shown here, along with the spectrum line in blue. The labels have been removed to enable a better view of the curves, and the apparent peak energy wavelength has been labeled.

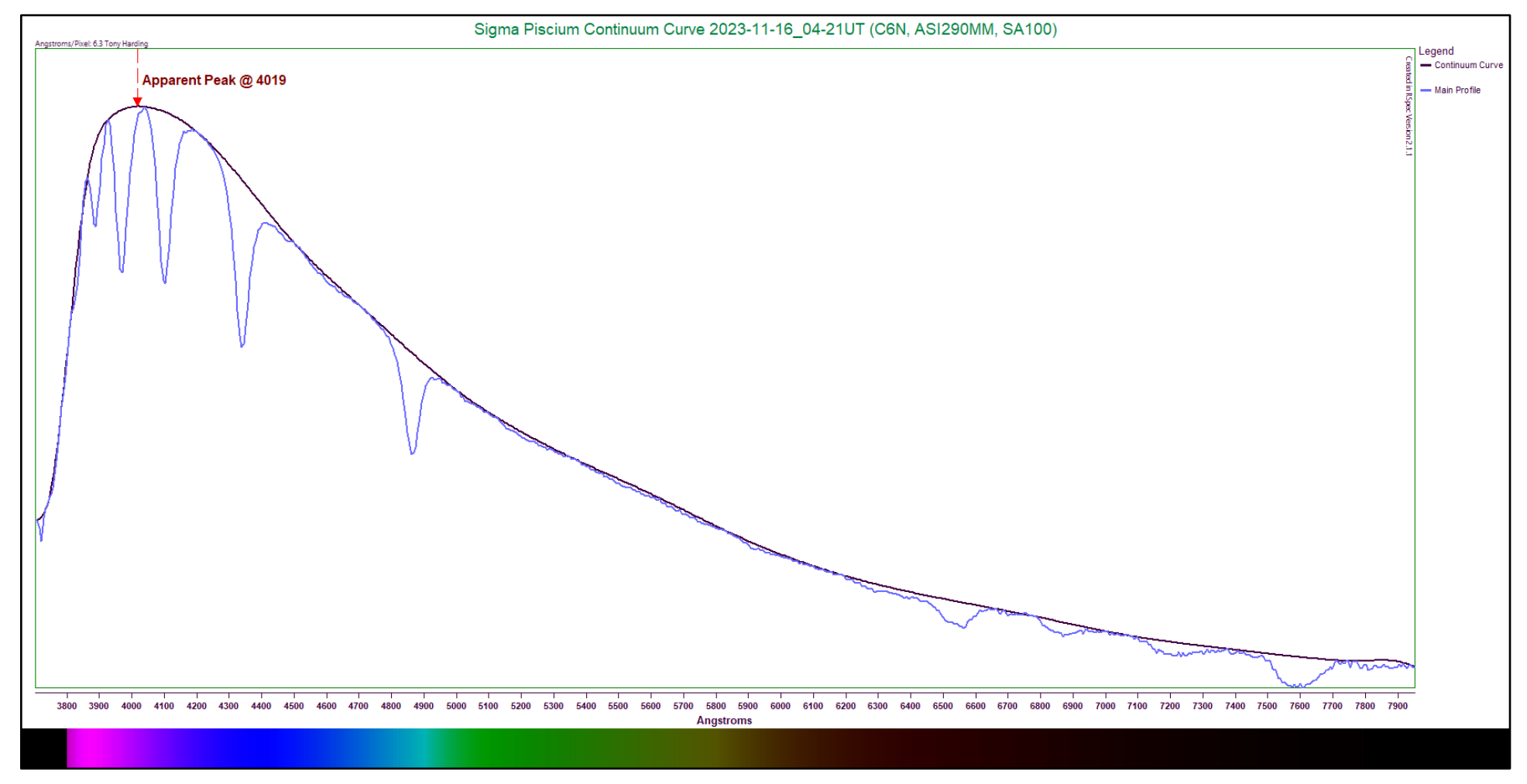


Figure 5.13 - Continuum Curve Plot (Sigma Piscium)

The apparent peak in the flux curve appears to lie at 4019 Angstroms. Using Wien's Law, this value returns an effective temperature estimate of 7210K. As expected, our answer falls very short of the expected temperature of 10,000K. Our estimate in this case is off the mark by a factor of approximately 1.39. The star's professionally determined temperature is listed as 10,795K⁽¹⁸⁾. Comparing our estimate to this temperature, we find our estimate is off by a factor of 1.50.

5.5 Spectral Type A Stars

The A-type stars rank third in decreasing order of temperature on the MK scale, superseded only by the hotter B-types and the extremely hot O-types. Stars of this type appear visually white, and can paint a striking visage through a telescope. Some of the most beautiful stars in the sky are bright examples of A-type stars. Stars such as Vega and Sirius are prime examples.

A-type stars have typical masses ranging between about 2.0 and 1.7 times solar mass⁽¹⁷⁾. The main sequence lifespans of these stars vary from about 500 Myr to 1,700 Myr⁽⁷⁾. The cooler varieties are able to stay longer on the main sequence, as their hydrogen fuel is consumed much more slowly. Their luminosities are considerably more than that of our Sun, ranging from 30 down to 9 times solar luminosity⁽¹⁷⁾. They are usually destined to become white dwarfs as they age. Compared to our own Sun, these stars are short-lived.

These stars range in temperature from about 9,000K down to approximately 7,500K⁽¹⁷⁾, and so are still considered hot. Their peak energy emission occurs in the near ultraviolet range, which is often not detectable by amateur astronomy cameras. This peak falls within the Balmer jump, where the continuum is effectively masked by tightly spaced absorption lines. This skews any attempts to estimate temperatures via Wien's Law by observing the lower visual wavelength range. For the selected stars of this type, we will calculate these estimates to show how inaccurate they are, but also to show that as the stars get cooler within the type, the estimates start edging closer to the actual values. This trend continues into the F-types, where the estimates more accurately begin to reflect the actual temperatures of the stars.

Spectroscopically, the dominant features of these stars are their very strong hydrogen Balmer lines. A-type stars (particularly the early ones) show the strongest such lines, making them ideal for use as reference stars. In addition to these loud and proud hydrogen Balmer lines, some fainter metals can typically be seen, particularly later in the type. Iron and other elements begin to emerge more strongly as the temperatures decrease. More and stronger metal lines emerge toward the end of the sequence. The general shape of the continuum curves of these stars shows a visual peak near the lower wavelength range. As noted above, this is deceptive due to the Balmer jump, which masks the continuum in that area.

The stars chosen to represent the various subtypes are presented here:

Table 5.11 - Representative A-Type Stars

	J 1
Subtype	Star
Early	Beta Leonis (Denebola)
Middle	Mu Andromedae
Late	Lambda Piscium

Early A-Type Stars

When the first alphabetical classification system was implemented, it was based solely on the prominence of the hydrogen Balmer series of absorption lines. A-types had the strongest such lines, followed by B-Types, then C-Types, and so on. When it was realized that the order could be rearranged to represent a temperature scale, many of the classes were omitted, but the A-type stars remained and were ranked third in line on a decreasing scale of temperature, behind both the O-types and B-types. The early A-type stars nonetheless show the strongest hydrogen Balmer lines among stellar spectra.

As noted, the early A-type stars are where the signature hydrogen Balmer lines are most strongly evident. The lines are quite pronounced and very easy to recognize. When moving progressively toward either earlier or later stellar types, these lines gradually lose prominence.

These stars are still quite hot, falling in the 9,300K to 8,600K range⁽¹⁷⁾. Much of their light is still emitted in the near ultraviolet range. They typically shine with a visible white light, making some of the nearest ones appear like diamonds against the dark sky. Their masses are typically about 2 times solar mass⁽¹⁷⁾, and they shine with luminosities ranging from 30 to 17 times the luminosity of our Sun⁽¹⁷⁾. They are somewhat shorter lived than our own Sun, existing for approximately 500 Myr⁽⁷⁾.

As previously noted, the hydrogen Balmer lines reach their peak in this type. Some additional metals can be evident, and may appear a bit stronger as we move to later A-types. These visible metals may include iron, titanium, magnesium, and calcium. Not all of these will be visible in low-resolution spectra, and their presence and prominence can certainly vary from one star to another. These lines can also appear as blends of multiple absorption lines if they are very close together.

The star chosen to represent this type is Beta Leonis, more commonly known as Denebola (in the constellation of Leo, the Lion). It is a main sequence star, providing an excellent example of this type.

The spectrum of Beta Leonis (Denebola) is presented here. The rectified spectrum is included in red.

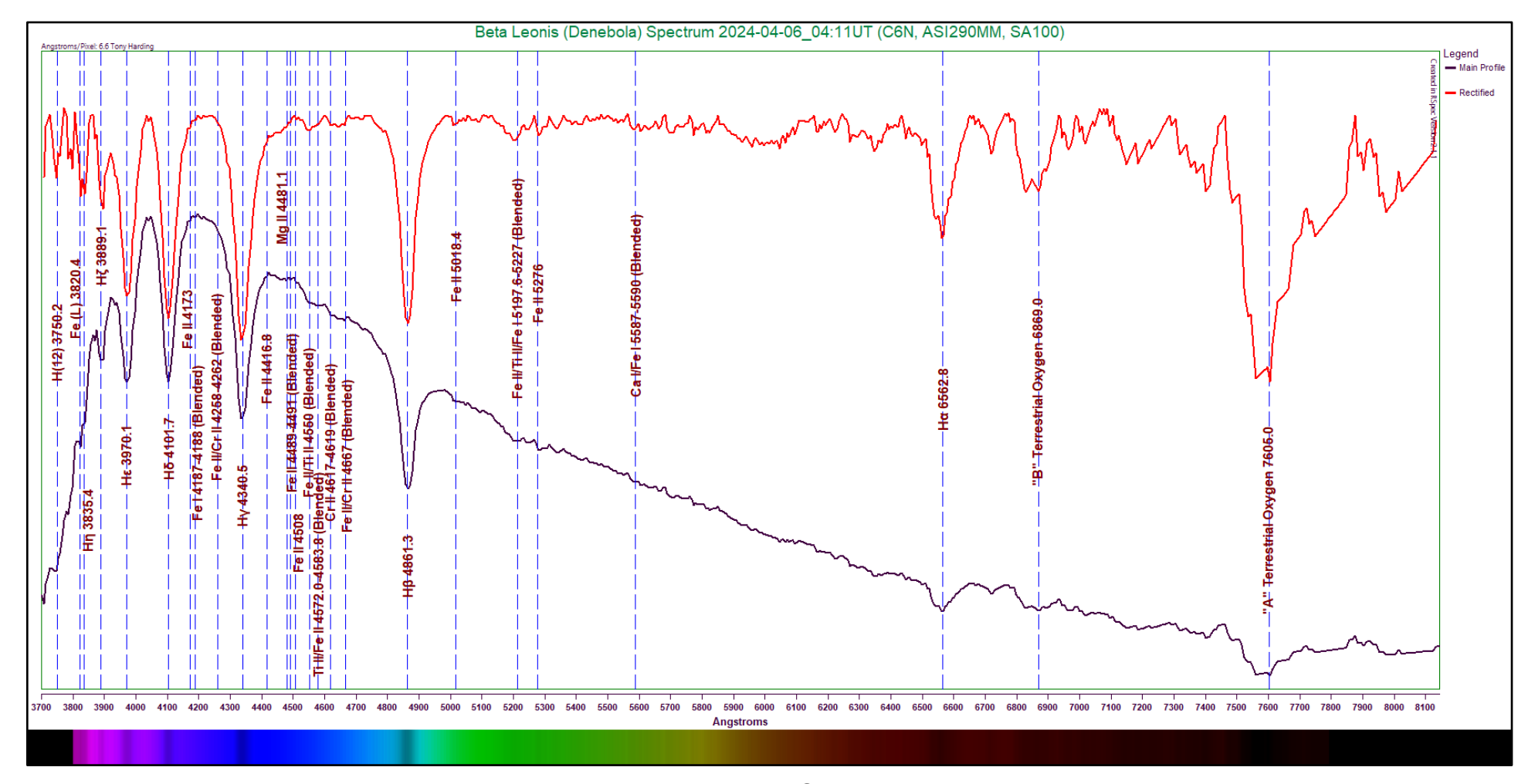


Figure 5.14: Beta Leonis (Denebola) Spectrum (6.3 Angstroms/pixel)
Capture Details: Exposure 296ms, Gain 48, 40% of 822 frames stacked, Integration Time: 97s

The hydrogen Balmer lines are indeed quite profound, as expected. These are by far the strongest features, especially in the rectified profile above (excluding the Fraunhofer "A" absorption due to atmospheric oxygen). Additionally, several much fainter metal absorptions

are noted, including iron, magnesium, titanium, and calcium in various states of ionization. These faint absorptions cannot compete with the much more prominent hydrogen Balmer lines, but (especially in the rectified profile) they can be seen carving out small but distinct dips in the continuum. However, some of these are extremely weak, and therefore must be regarded dubiously.

The following table shows the indicated absorption features of the Beta Leonis (Denebola) spectrum.

Table 5.12 - Beta Leonis (Denebola) Line Identification Details

Feature	Wavelength	Comments
	(Angstroms)	
H(12)	3750.2	Higher order hydrogen Balmer line
Fe I	3820.4	Fraunhofer "L" neutral iron line; weak but notable
Ηη	3835.4	Very weak hydrogen Balmer line; only causing small deviation in continuum on main profile
Нζ	3889.1	Somewhat weak hydrogen Balmer line
Ηε	3970.1	Strong hydrogen Balmer line
Ηδ	4101.7	Extremely strong hydrogen Balmer line
Fe II	4173	Extremely weak ionized iron line
Fe I	4187-4188	Extremely weak neutral iron blend
Fe II/Cr II	4258-4262	Extremely subtle ionized iron/chromium blend; dubious identification
Нү	4340.5	Extremely strong hydrogen Balmer line
Fe II	4416.8	Extremely weak ionized iron line
Mg II	4481.1	Common ionized magnesium line; extremely weak here
Fe II	4489-4491	Very weak ionized iron blend
Fe II	4508	Very weak ionized iron absorption
Fe II/Ti II	4550	Fairly weak iron/titanium blend
Ti II/Fe II	4572.0-4583.8	Weak titanium/iron blend
Cr II	4617-4619	Weak ionized chromium blend
Fe II/Cr II	4667	Common iron/chromium blend; appears weak here
Нβ	4861.3	Extremely strong hydrogen Balmer line
Fe II	5018.4	Weak ionized iron line
Fe II/Ti II/Fe I	5197.6-5227	Weak iron/titanium blend
Fe II	5276	Weak ionized iron line
Ca I/Fe I	5887-5890	Common calcium/iron blend; extremely weak here; possibly dubious identification
Ηα	6562.8	Strong hydrogen Balmer absorption
Telluric Oxygen	6869.0	Fraunhofer "B" absorption due to atmospheric oxygen
Telluric Oxygen	7605.0	Fraunhofer "A" absorption due to atmospheric oxygen

Stars of this type still have a peak energy output in the ultraviolet wavelength range, which our equipment cannot detect. Again, the Balmer Jump will interfere with obtaining an accurate peak energy wavelength for the spectrum. Applying Wien's Law, we can attempt to calculate the star's effective temperature based on the apparent peak in the visible wavelength range, but we must again expect our estimate to fall short of the actual temperature.

The continuum curve for Beta Leonis (Denebola) is plotted here, along with the main spectrum. The labels have been removed so that an easier comparison can be made between the two curves.

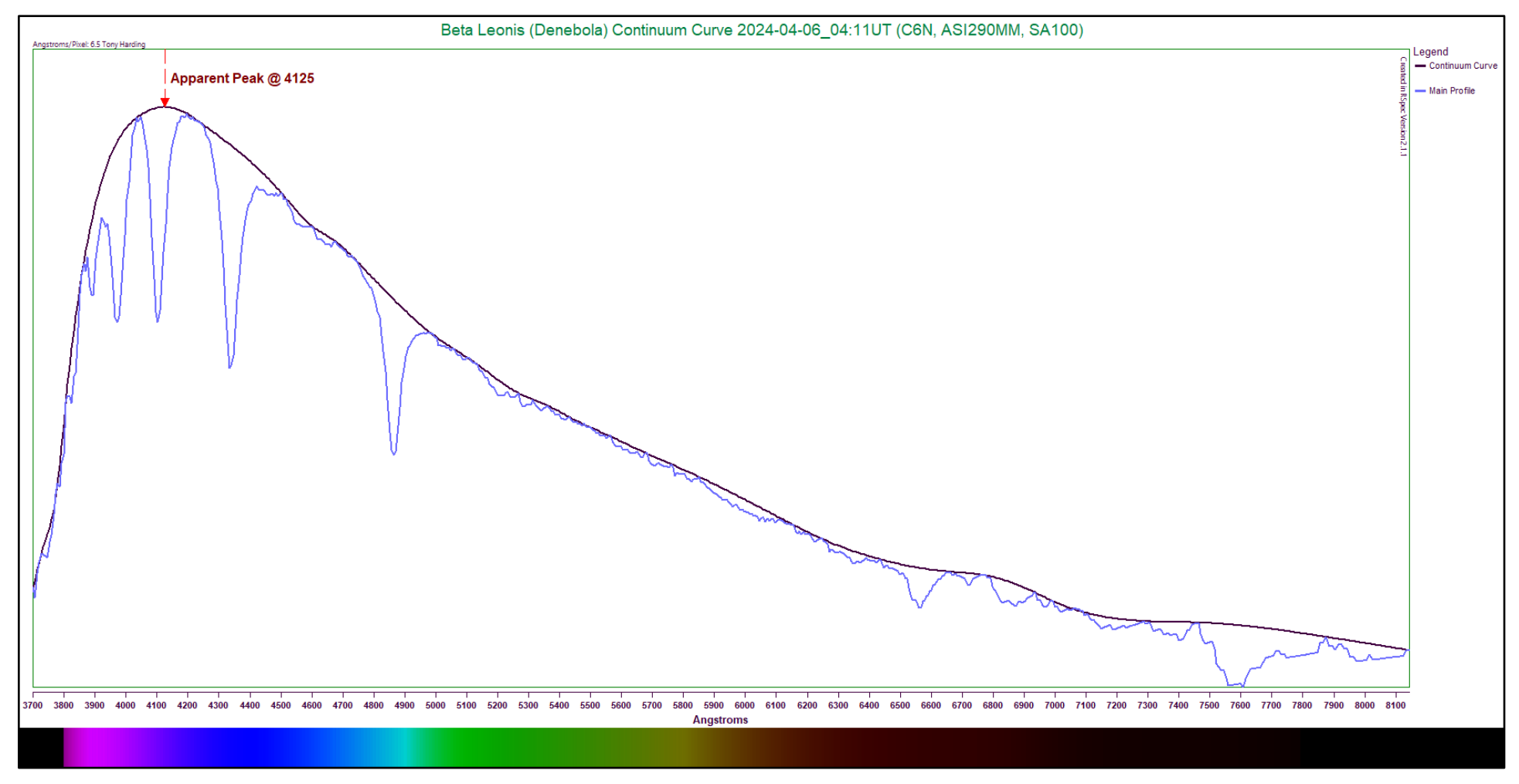


Figure 5.15 - Continuum Curve Plot (Beta Leonis)

The plotted continuum curve indicates a peak energy value at approximately 4125 Angstroms (labeled above). This results in a temperature estimate of 7025K. As expected, this falls significantly short of the typical temperature for a star of this type (9,300K-8,600K). Comparing our estimate to the median value of this range (8950K), we find the estimate is off by a factor of 1.27. The professionally determined temperature for the star is approximately 8,262K⁽¹⁹⁾. This is actually about 4% less than the expected temperature for the star in question. However, comparing our result to the professional temperature still shows it is off by a factor of 1.18.

Middle A-Type Stars

As we move into the middle A-type stars, we will begin to see the hydrogen Balmer lines start to decline in strength. This will be subtle at first, but will become much more evident the farther we delve into progressively cooler stars. The hydrogen Balmer lines in these stars are still quite striking, but they will start to become mixed with an increasing number of metal lines, particularly iron.

These stars are still considered hot, typically falling in the 8,200K to 7,900K range⁽¹⁷⁾. The peak energy wavelength is nearer the visible range, but still falls within the near ultraviolet. They have masses of approximately 1.85 times the solar value⁽¹⁷⁾, and shine with luminosities ranging from 13 down to about 11 times that of the Sun⁽¹⁷⁾. They have life spans on the order of 1,000 Myr⁽⁷⁾.

As noted above, the hydrogen Balmer lines are still impressively strong in these stars. The metals present in the spectrum will be slightly stronger than in the early A-types, and more of them will be apparent. These metals can include iron, magnesium, titanium, and others. Of course, the presence and strength of these fainter absorptions will vary between specimens. Some of the weakest lines may be absent, or appear blended together if closely spaced.

The star chosen to represent this type is Mu Andromedae, in the constellation of Andromeda, the Chained Maiden. It is a main sequence star, again providing a good example of the type.

The spectrum of Mu Andromedae is presented here, along with the rectified spectrum in red.

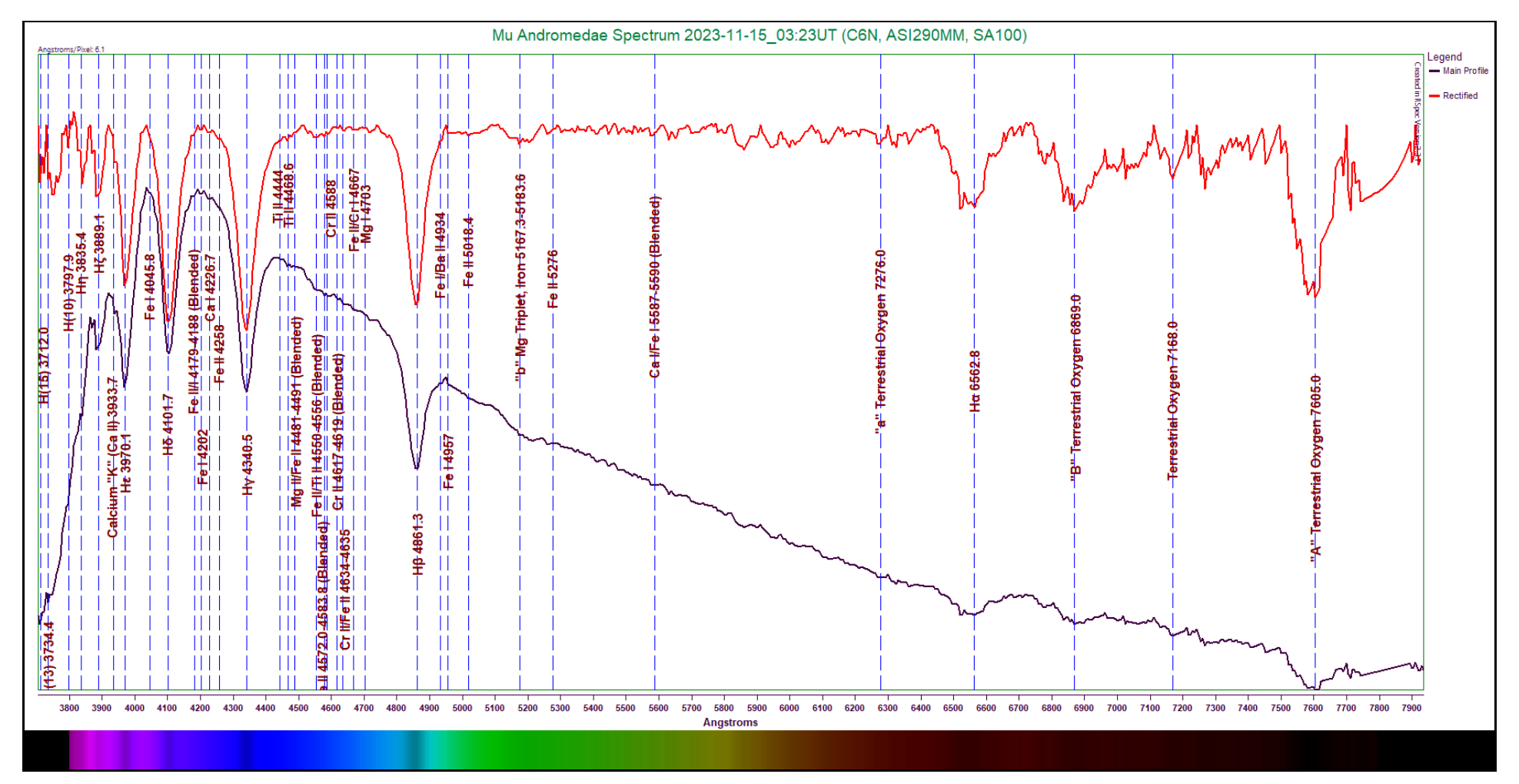


Figure 5.16: Mu Andromedae Spectrum (6.2 Angstroms/pixel)
Capture Details: Exposure 702ms, Gain 119, 75% of 262 frames stacked, Integration Time 137s

The hydrogen Balmer lines remain very strong here, as expected. Even a cursory examination of the spectrum shows a greater number of very faint metal lines becoming apparent, often in blends, and often with iron as a component. The magnesium triplet at 5167.3-5183.6 absorption is also faint, but provides evidence that other metals will become more prevalent as stellar temperatures continue to fall. Among these faint metals are calcium, iron, titanium, magnesium, and chromium. Many are closely spaced, so take care when tracing the labels.

The following table lists all the labeled absorptions in the spectrum of Mu Andromedae.

Table 5.13 - Mu Andromedae Line Identification Details

Feature	Wavelength	Comments
	(Angstroms)	
H(15)	3712.0	Higher order hydrogen Balmer line; very weak; hugging the left border of the graph
H(13)	3734.4	Higher order hydrogen Balmer line; very weak
H(10)	3797.9	Higher order hydrogen Balmer line; very subtle; only causing small deviation in continuum
Ηη	3835.4	Very weak hydrogen Balmer line
Нζ	3889.1	Moderately strong hydrogen Balmer absorption
Ca II	3933.7	Common ionized calcium line; appears very weak here; more pronounced in cooler stars
Ηε	3970.1	Very strong hydrogen Balmer line
Ηδ	4101.7	Extremely strong hydrogen Balmer line
Fe II/I	4179-4188	Very weak iron blend
Fe I	4202	Weak neutral iron absorption
Ca I	4226.7	Very common neutral calcium line; weak but distinct
Fe II	4258	Extremely weak ionized iron absorption
Ηγ	4340.5	Extremely strong hydrogen Balmer line
Ti II	4444	Extremely weak ionized titanium absorption
Ti II	4468.6	Very weak ionized titanium line
Mg II/Fe II	4481-4491	Very weak but broad magnesium/iron blend
Fe II/Ti II	4550-4556	Weak iron/titanium blend
Ti II/Fe II	4570.2-4583.8	Very weak ionized titanium/iron blend
Cr II	4588	Very weak ionized chromium absorption
Cr II	4617-4619	Extremely weak ionized chromium blend
Cr II/Fe II	4634-4635	Very weak ionized chromium/iron blend
Fe II/Cr I	4667	Common iron/chromium absorption; extremely weak here
Mg I	4703	Common neutral magnesium absorption; extremely subtle here; dubious identification
Ηβ	4861.3	Very strong hydrogen Balmer line
Fe I/Ba II	4634	Fairly common iron/barium blend; extremely weak here
Fe I	4957	Weak neutral iron absorption
Fe II	5018.4	Extremely weak ionized iron line
Mg I Triplet	5167.3-5183.6	Common magnesium triplet with iron; appears weak here; more pronounced in cooler stars
Telluric Oxygen	7276.0	Fraunhofer "a" absorption due to atmospheric oxygen
Ηα	6562.8	Moderately strong hydrogen Balmer line
Telluric Oxygen	6869.0	Fraunhofer "B" absorption due to atmospheric oxygen
Telluric Oxygen	7168.0	Absorption due to atmospheric oxygen; weak, but distinct
Telluric Oxygen	7605.0	Fraunhofer "A" absorption due to atmospheric oxygen

As with the early A-type stars, the middle A-types actually have a peak energy wavelength in the near ultraviolet. The Balmer jumper in the lower wavelength range of our results obscures this peak. However, to demonstrate the inaccuracy of applying it to such stars, we will proceed to employ Wien's Law to the apparent peak in the spectrum and calculate a temperature based on this. We will again see that such an estimate will fall short of the actual value.

Here is presented the plotted continuum curve of Mu Andromedae, along with the spectrum curve. The labels have been removed in order to enable a cleaner comparison of the two curves.

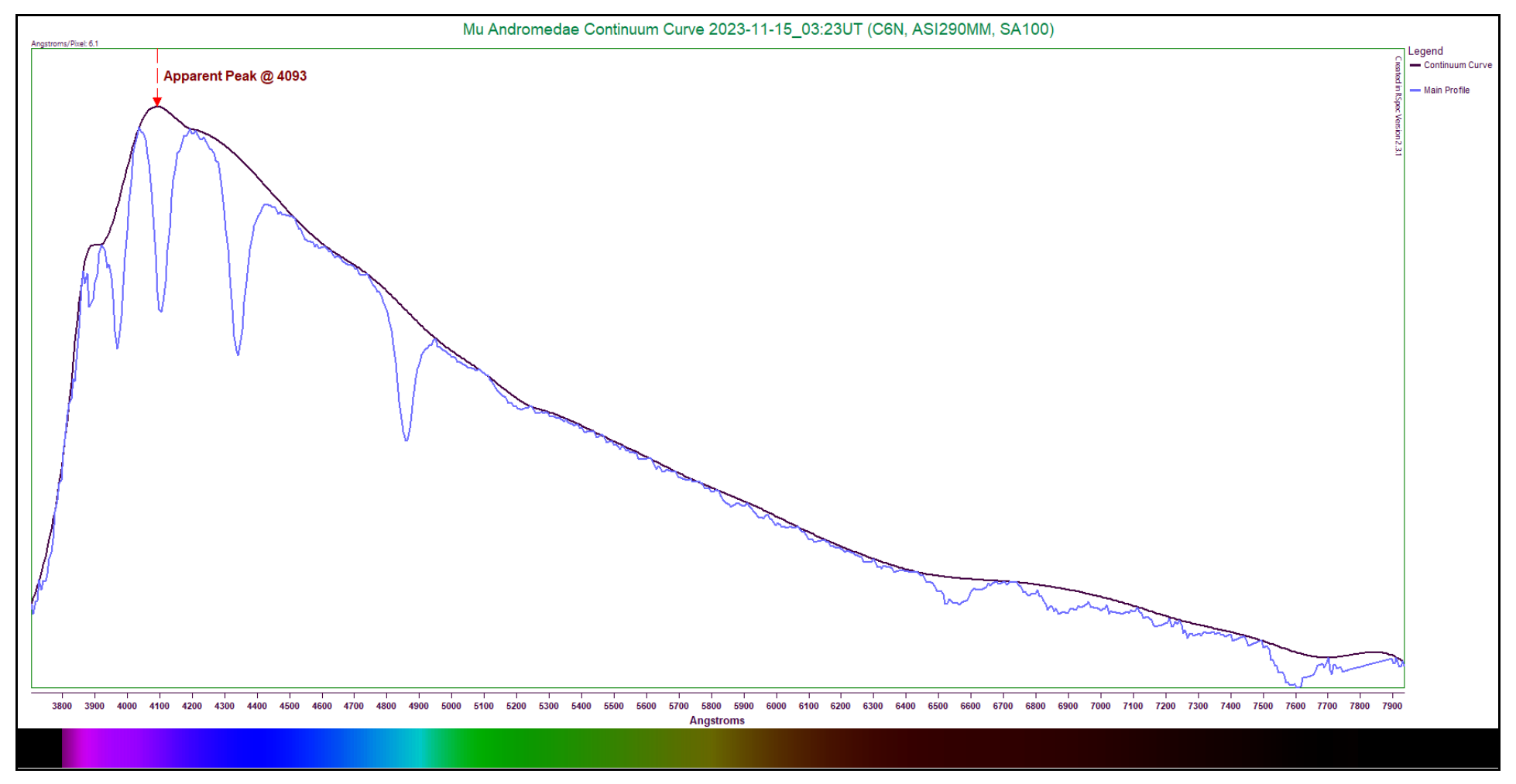


Figure 5.17 - Continuum Curve Plot (Mu Andromedae)

This one presented some oddities when attempting to construct a continuum line near the peak section. The peak energy wavelength from the curve appears to lie at 4093 Angstroms. If we use this value and apply Wien's Law, we obtain a temperature estimate of approximately 7080K. Obviously, this falls far short of the expected temperature range of 8,300K-7,900K. Our estimated effective temperature is off by a factor of 1.14 from the median expected value (8,100K). The professionally derived temperature of the star is listed as 8,320K⁽²⁰⁾. Based on this value, our estimate is off by a factor of 1.18.

Late A-Type Stars

Traveling into the late A-type stars, the previous trends in absorption lines continue. The hydrogen Balmer lines continue to become slightly less pronounced, with numbers of faint metal lines continuing to increase. The general shape of the continuum curve is not significantly different from the other A-type stars, though the apparent peak energy wavelength is shifted slightly toward longer wavelengths.

These stars are slightly cooler, though still hot, coming in at approximately 7,800K to 7,500⁽¹⁷⁾. They range in mass between approximately 1.8 and 1.75 times solar mass⁽¹⁷⁾. Their luminosities typically range between 10 and 9 times that of our Sun⁽¹⁷⁾. These stars have main-sequence lifespans averaging approximately 1,500 Myr⁽⁷⁾.

The same basic spectroscopic properties will be visible in these stars as in the middle A-types, with a slightly lower temperature. The hydrogen Balmer lines are still obvious here, with numerous fainter metals present. These can include iron, magnesium, carbon, and silicon, among others. Of course, the visibility of these elements will vary from one star to another, some being altogether absent. As before, some of the weaker lines may appear blended.

The star chosen as an example of this type is Lambda Piscium, in the constellation of Pisces, the Fishes. It is a main sequence star, but is moderately dim (at apparent magnitude 4.45). This may indicate that fewer details can be made out, but the general characteristics are on display.

The spectrum of Lambda Piscium is presented here; the red rectified profile is also included.

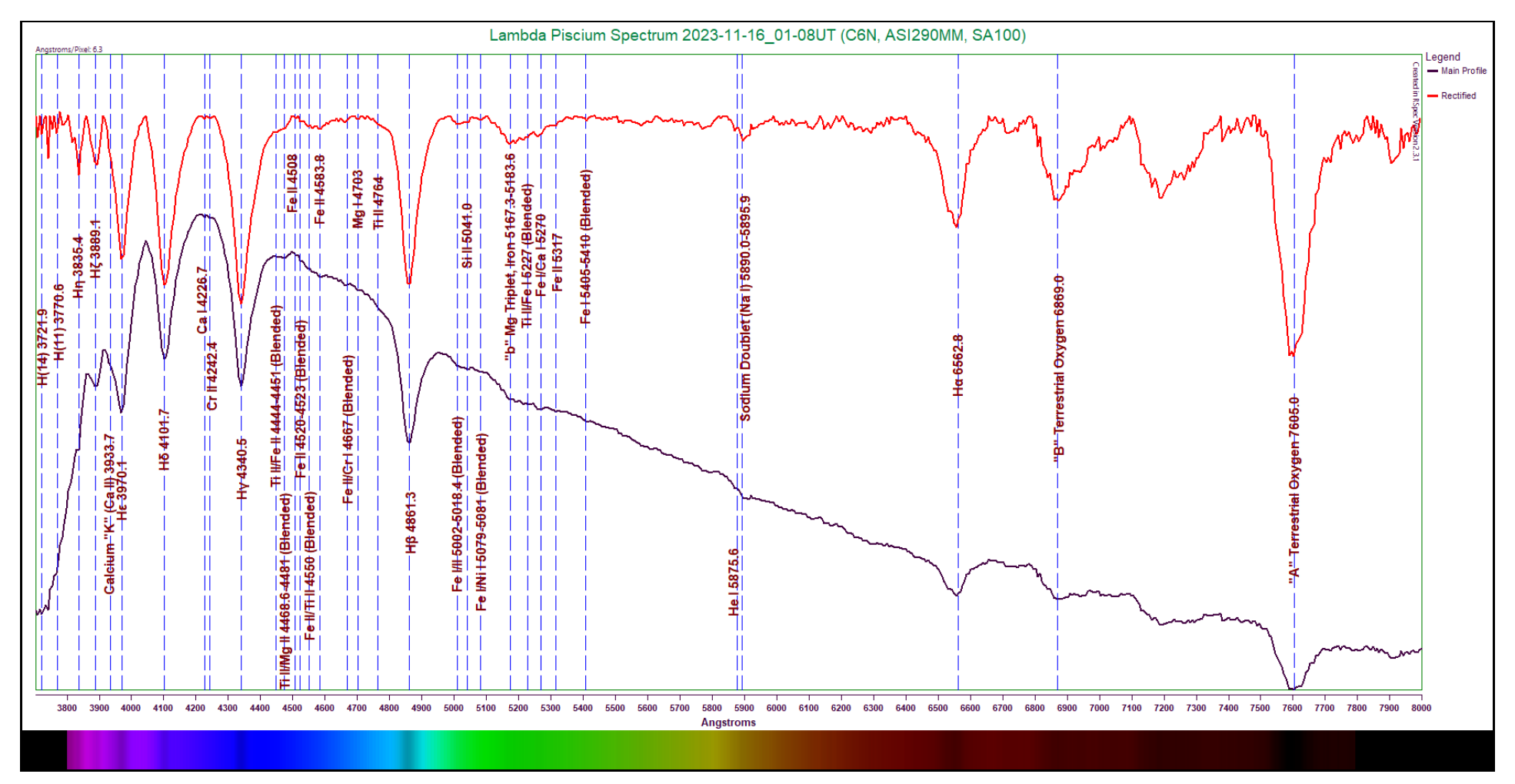


Figure 5.18: Lambda Piscium Spectrum (6.3 Angstroms/pixel)
Capture Details: Exposure 1s, Gain 208, 50% of 225 frames stacked, Integration Time 112s

The spectrum above shows an overall familiar shape. The hydrogen Balmer lines appear clearly and sharply. The Fraunhofer calcium "K" line is visible at 3933.7 Angstroms, but it is very subtle, only causing a small diversion along the lower wings of the Hε line. The magnesium triplet at 5167.3-5183.6 Angstroms is visible, though not terribly strong. The adjacent titanium/iron absorption at 5227 Angstroms serves to broaden the feature. The sodium doublet is visible at 5890.0-5895.9 Angstroms, along with the neutral helium line just below it at 5875.6 Angstroms. Some other labeled metals include calcium, chromium, titanium, iron, magnesium, and silicon.

The following table lists the absorptions labeled in the Lambda Piscium spectrum.

Table 5.14 - Lambda Piscium Line Identification Details

Feature	Wavelength	Comments
	(Angstroms)	
H(14)	3721.9	Very weak higher order hydrogen Balmer line
H(11)	3770.6	Extremely weak higher order hydrogen Balmer line
Ηη	3835.4	Very small hydrogen Balmer line
Ηζ	3889.1	Weak hydrogen Balmer line
Ca II	3933.7	Very subtle Fraunhofer "K" ionized calcium line
Ηε	3970.1	Moderately strong hydrogen Balmer line
Ηδ	4101.7	Very strong hydrogen Balmer line
Ca I	4226.7	Common neutral calcium line; appears very weak here
Cr II	4242.4	Very weak ionized chromium line
Ηγ	4340.5	Extremely strong hydrogen Balmer line
Ti II/Fe II	4444-4451	Weak titanium/iron blend; broadened with titanium/magnesium absorption above it
Ti II/Mg II	4468.8-4481	Weak titanium/magnesium blend; broadened with titanium/iron absorption below it
Fe II	4508	Exceptionally weak ionized iron absorption
Fe II	4520-4523	Exceptionally weak ionized iron blend
Fe II/Ti II	4550	Weak ionized iron/titanium blend
Fe II	4583.9	Weak ionized iron line
Fe II/Cr I	4667	Fairly common iron/chromium absorption; appears very weak here
Mg I	4703	Fairly common neutral magnesium absorption; extremely weak
Ti II	4764	Extremely subtle ionized titanium absorption; only causing small deviation in continuum; dubious identification
Нβ	4861.3	Very strong hydrogen Balmer line
Fe I/II	5002-5018.4	Weak iron blend
Si II	5041.0	Weak ionized silicon line
Fe I/Ni I	5079-5081	Very weak iron/nickel blend
Magnesium Triplet	5167.3-5183.6	Common magnesium/iron absorption; weak to moderate strength
Ti II/Fe I	5227	Weak titanium/iron blend; causing broadening of dip near magnesium triplet
Fe I/Ca I	5270	Common iron/calcium blend; appears weak but distinct
Fe II	5317	Extremely weak ionized iron absorption
Fe I	5405-5410	Extremely weak neutral iron absorption
He I	5875.6	Common but very weak neutral helium line; not always distinctly visible
Na I Doublet	5890.0-5895.9	Fraunhofer "D1" and "D2" neutral sodium blend; weak to moderate in strength
Ηα	6562.8	Strong hydrogen Balmer line
Telluric Oxygen	6869.0	Fraunhofer "B" absorption due to atmospheric oxygen
Telluric Oxygen	7605.0	Fraunhofer "A" absorption due to atmospheric oxygen

We will continue to observe that Wien's Law provides greatly inaccurate stellar temperature estimates for these late A-type stars. We will compute the apparent effective temperature and compare it to the expected temperature to demonstrate.

Presented here is a plotted continuum curve for Lambda Piscium, along with its normal spectrum. The labels are removed in order to facilitate a clean comparison of the two.

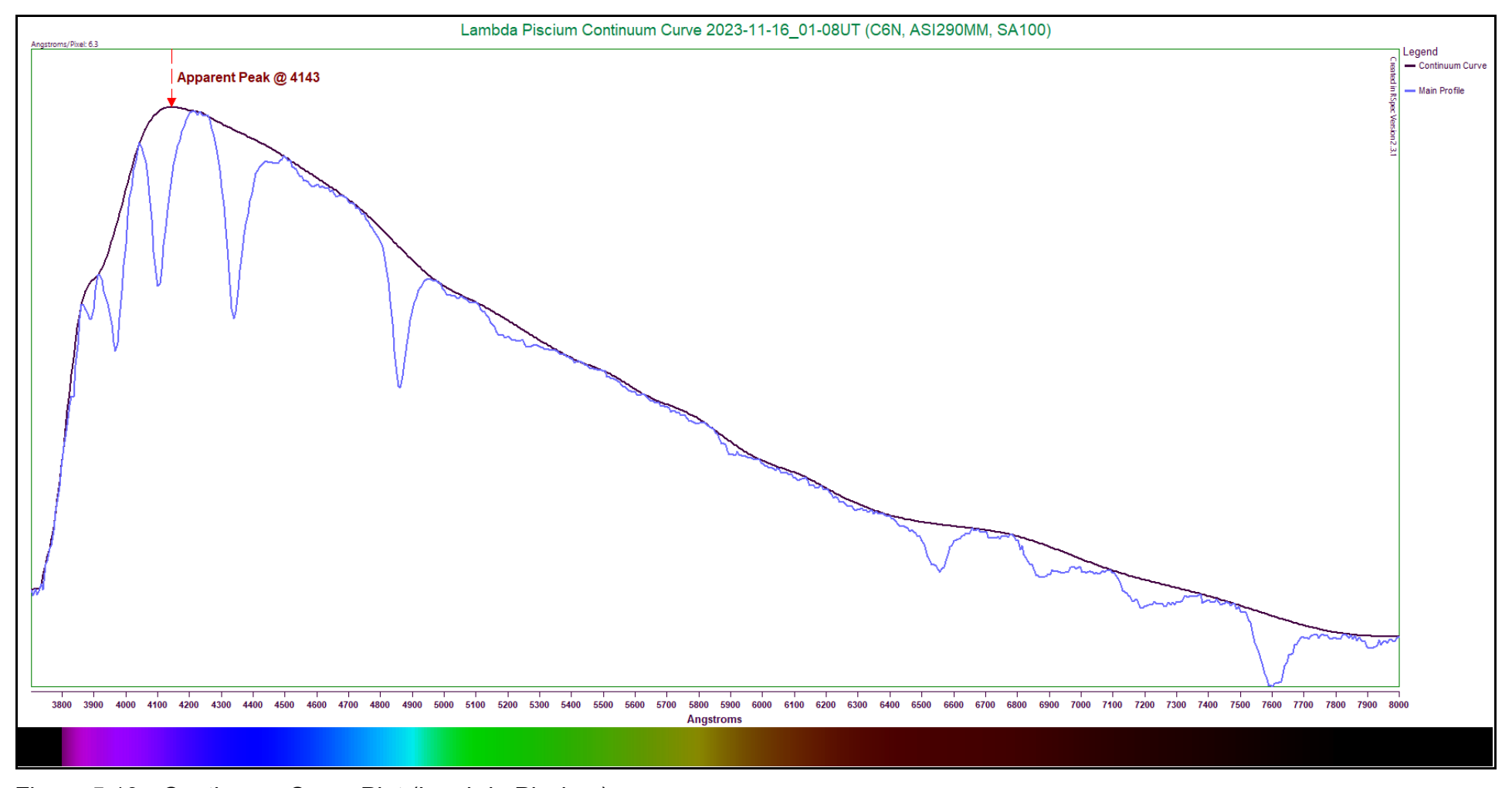


Figure 5.19 - Continuum Curve Plot (Lambda Piscium)

Again, we see that the peak energy wavelength appears to lie near the lower wavelength range. In this case, the visible peak lies at 4143 Angstroms. Using this value, Wien's Law provides us with an estimated temperature of approximately 6,994K. This is significantly short of the expected temperature of 7,800K-7,500K. Our estimate is off from the expected median temperature value (7650K) by a factor of approximately 1.09. The star's professionally determined temperature is listed as 7,734K⁽²²⁾. Comparing our estimate to this number, we find we are off by a factor of 1.13. Despite the fact that our estimates continue to come in too low, we can also see that the gaps between our estimates and the actual values are beginning to dwindle as the temperatures decrease. As we progress into the F-type stars, the estimates will become more accurate.

5.6 Spectral Type A/F Stars (Very Late A and Very Early F)

Stars in this custom category continue to show easily identifiable hydrogen Balmer lines, but here is where the Fraunhofer "H" ionized calcium line begins to overtake the Hε absorption. The number of metal lines also continues to grow. They continue to visually shine with an apparent white light, but not as brilliant as the earlier A-types.

The A/F stars typically have temperatures between 7,400K and 7,200K^(17,22). They are fairly massive stars, weighing in at 1.75 to 1.6 times solar mass^(17,22). Their luminosities range between 8.3 to 7.2 times that of our Sun^(17,22). Because of their lower mass, they burn somewhat more slowly than the earlier A-types, usually staying on the main sequence for approximately 2,000 Myr⁽⁷⁾. Smaller metal lines become more numerous.

Spectroscopically, these stars still show good hydrogen Balmer absorptions, but will also show an increased mixture of metals among and between the hydrogen Balmer lines. The apparent peak energy wavelength continues to shift slowly toward longer wavelengths, but Wien's Law remains unable to calculate an effective temperature with accuracy.

The star chosen to represent this type is indicated here:

Table 5.15 - Representative A/F Star

Subtype	Star
Very Late A/Very Early F	Zeta Leonis (Adfhafera)

A/F Stars (Very Late A and Very Early F)

The A/F stars in our customized classification scheme remain fairly hot, as noted above. Their spectra show fairly strong hydrogen Balmer lines. The magnesium triplet and the sodium doublet become slightly stronger. Other typical spectral features include metals such as iron, calcium, magnesium, and others. Line strengths will vary from specimen to specimen, and blended lines become more common.

These stars are still somewhat hot, coming in at around 7,300K^(17,22). Their masses hover around 1.6 times solar mass^(17,22), and they shine with luminosities around 8 times that of our Sun^(17,22). They remain on the main sequence for approximately 2,000 Myr⁽⁷⁾.

The star Zeta Leonis, also called Adfhafera, was chosen to demonstrate this subtype. The star is a giant, which may cause the strengths of the absorptions to appear somewhat diminished, but the main features should still be readily visible.

The spectrum of Zeta Leonis (Adfhafera) is presented here, along with a rectified profile in red.

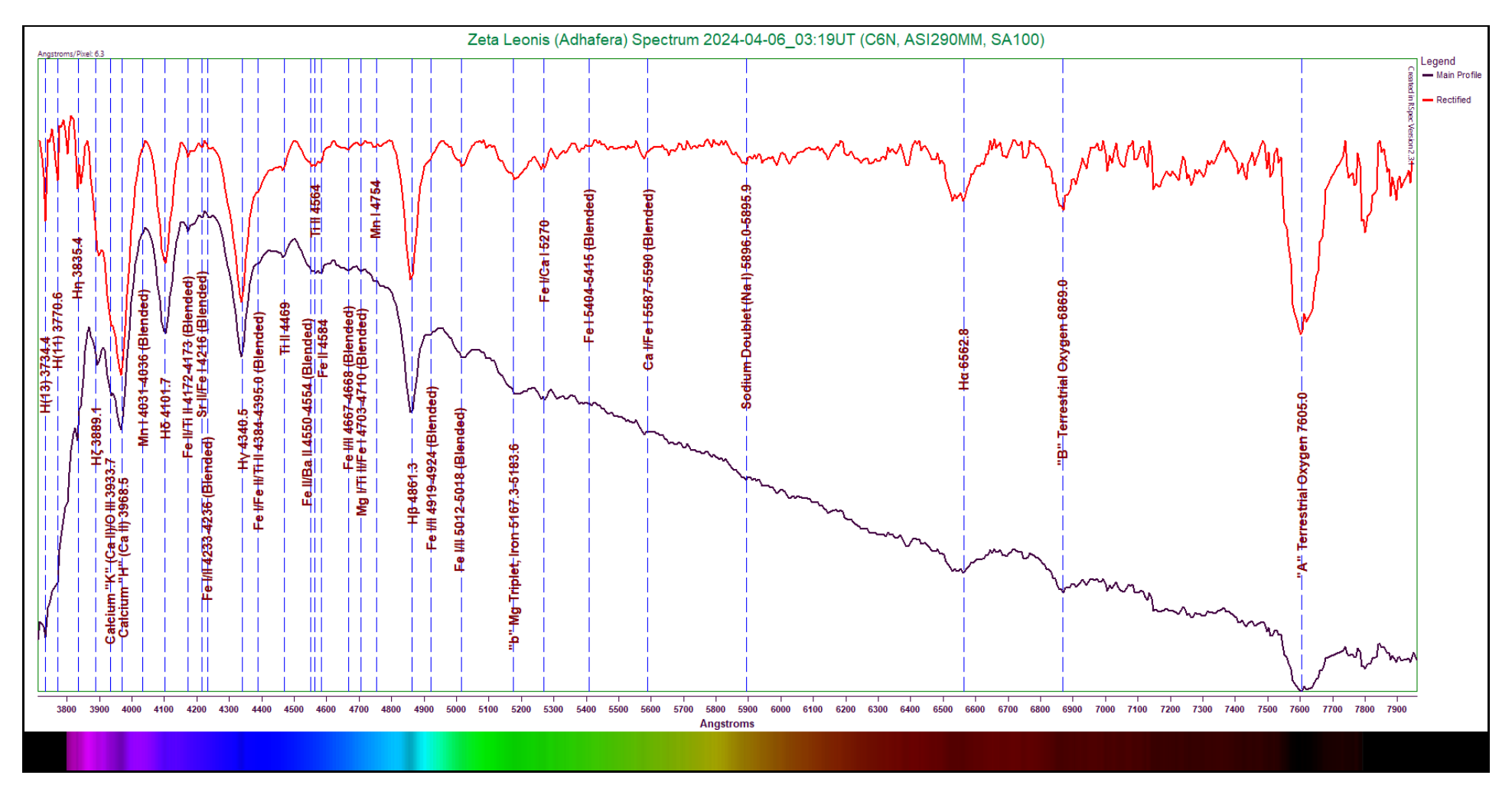


Figure 5.20: Zeta Leonis (Adhafera) Spectrum (6.3 Angstroms/pixel)
Capture Details: Exposure 332ms, Gain 178, 40% of 735 frames stacked, Integration Time 97s

Most of the hydrogen Balmer lines appear moderately strong in this spectrum. The Fraunhofer "K" and "H" ionized calcium lines at 3933.7 and 3968.5 Angstroms respectively can be easily seen. A notable dip in the continuum occurs at 4550-4584 Angstroms due to absorptions of iron, barium, and titanium. The magnesium triplet absorption at 5167.3-5183.6 Angstroms is fairly prominent here. The neutral sodium doublet at 5890.0-5895.9 Angstroms is also visible, though only very weakly. Other labeled metals include manganese, iron, titanium, magnesium, and calcium.

The following table lists the absorptions labeled in the Zeta Leonis (Adfhafera) spectrum.

Table 5.16 - Zeta Leonis (Adfhafera) Line Identification Details

Feature	Wavelength	Comments
	(Angstroms)	
H(13)	3734.4	Moderately strong higher order hydrogen Balmer line
H(11)	3770.6	Weak higher order hydrogen Balmer line
Ηη	3835.4	Weak hydrogen Balmer line
Ηζ	3889.1	Weak to moderate strength hydrogen Balmer line
Ca II	3933.7	Fraunhofer "K" ionized calcium line
Ca II	3968.5	Fraunhofer "H" ionized calcium line
Mn I	4031-4036	Common neutral manganese absorption; extremely subtle here; dubious identification
Ηδ	4101.7	Moderately strong hydrogen Balmer line
Fe II/Ti II	4172-4173	Weak ionized iron/titanium blend
Sr II/Fe I	4216	Very weak strontium/iron absorption
Fe I/II	4233-4236	Very weak iron blend
Ηγ	4340.5	Strong hydrogen Balmer line
Fe I/Fe II/Ti II	4384-4395	Subtle but clear dip due to iron and titanium
Ti II	4469	Moderate ionized titanium absorption
Fe II/Ba II	4550-4554	Weak ionized iron/barium blend; part of local dip in continuum
Ti II	4564	Weak ionized titanium absorption; part of local dip in continuum
Fe II	4584	Weak ionized iron absorption; part of local dip in continuum
Fe I/II	4667-4668	Weak iron blend
Mg I/Ti II/Fe I	4703-4710	Weak magnesium/titanium/iron blend
Mn I	4754	Very weak manganese absorption
Нβ	4861.3	Strong hydrogen Balmer line
Fe I/II	4919-4924	Very weak iron blend
Fe I/II	5012-5018	Moderate iron blend
Mg I Triplet	5167.3-5183.6	Fraunhofer "b" magnesium triplet with ionized iron; very common line; moderately strong here
Fe I/Ca I	5270	Weak to moderate iron/calcium absorption; common
Fe I	5404-5415	Extremely weak iron blend; dubious identification
Ca I/Fe I	5587-5590	Weak calcium/iron absorption; common
Na I Doublet	5890.0-5895.9	Common neutral sodium doublet; extremely weak here
Ηα	6562.8	Moderately strong hydrogen Balmer line
"B" Telluric Oxygen	6869.0	Fraunhofer "B" absorption due to atmospheric oxygen
"A" Telluric Oxygen	7605.0	Fraunhofer "A" absorption due to atmospheric oxygen

As mentioned earlier, it is among the F-type stars that Wien's Law will begin to provide decent effective temperature estimates. For the A/F stars, however, the estimates will still reflect a considerable error. To demonstrate, we will calculate an effective temperature for Zeta Leonis and compare this to the expected value.

The plotted continuum curve for Zeta Leonis (Adfhafera) is found below. Along with this curve, an unlabeled version of the spectrum is plotted. The apparent peak energy wavelength of the continuum curve is marked.

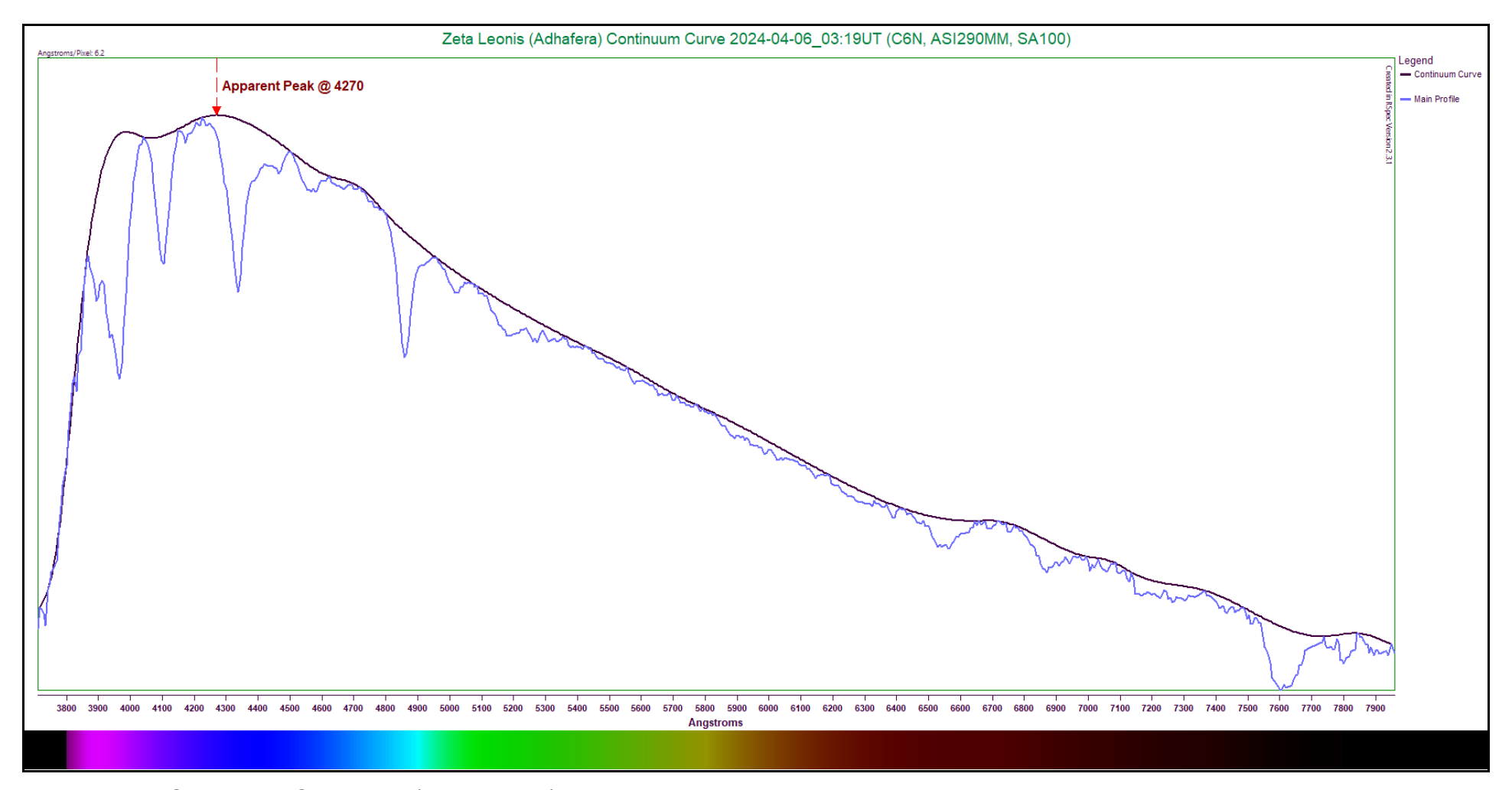


Figure 5.21 - Continuum Curve Plot (Zeta Leonis)

The apparent peak of the energy distribution curve appears to lie at 4270 Angstroms. With this value, Wien's Law returns a temperature estimate of 6,786K. This indeed falls short of the expected temperature of roughly 7,300K. This puts our estimate off by approximately 7.04%. The star's professionally determined temperature is listed at 6,900K⁽²³⁾. This is rather lower than expected, but brings our calculated estimate to within 1.7% of the actual value—very close.

5.7 Spectral Type F Stars

Type-F stars rank fourth on the MK temperature scale, representing a median between the hot A-types and the cooler G-types. These stars appear white or dirty-white through a telescope.

These stars are slightly more massive than our Sun, ranging from 1.5 down to about 1.2 times solar mass⁽²²⁾. They are content on the main sequence for approximately 6,000 Myr to 3,000 Myrs depending on their masses⁽⁷⁾. Their luminosities are greater than that of our Sun, ranging roughly from 6 to 2 times the solar value⁽²²⁾. When these stars reach their old age, they are destined to follow a path not dissimilar to that awaiting our own Sun; they will swell into red giants, then puff off their outer layers, leaving a white dwarf behind.

The temperatures of the F-type stars range from 7,000K to 6,200K, again depending upon their masses⁽²²⁾. It is amidst this type that the peak energy wavelength begins to fall into the visible range—usually in the middle F-types. This means that as we progress from earlier to later subtypes, Wien's Law will begin to reflect crudely accurate temperatures.

The spectra of the F-type stars also reflect an intermediate stage between the A-type and G-type stars. The hydrogen Balmer absorptions remain fairly strong, but more and stronger metal lines begin to appear. Additionally, the Ca II "K" and "H" lines will grow in strength, becoming a dominant feature in the G-types. The magnesium triplet and sodium doublet also slowly increase in strength.

The stars chosen to represent the various F-type stars are listed here:

Table 5.17 - Representative A-Type Stars

Subtype	Star
Early	Delta Aquilae (Almizan I)
Middle	lota Pegasi
Late	lota Piscium

Early F-Type Stars

Early F-type stars continue to show reductions in temperature, but the hydrogen Balmer lines continue to be fairly strong. The exception to this is the Hε line, which is overtaken by the Fraunhofer "H" line. The shape of the energy distribution curves show a slow drift of the peak energy wavelength to longer wavelengths. Wien's Law now becomes a reasonably accurate tool for measuring stellar temperatures, usually providing an answer within a few percent of the actual value.

These stars remain pretty hot, ranging in temperature from 7,000K down to about 6,750K⁽²²⁾. They usually remain on the main sequence for approximately 3,000 Myr⁽⁷⁾. They range in mass between about 1.5 and 1.4 times the mass of the Sun⁽²²⁾. They are also more luminous than our Sun, shining at between 6 and 4.5 times that of our Sun⁽²²⁾. Spectroscopic characteristics include fairly strong hydrogen Balmer lines, as well as the growing calcium II "K" and "H" lines mentioned previously. The magnesium triplet and sodium doublet are typically slightly stronger here, and a growing number of other metals continue to be evident, with blended lines being common.

The star chosen to represent this subtype is Delta Aquilae, also known as Almizan I, in the constellation of Aquila, the Eagle. The star is a subgiant and a rapid rotator, which may cause a slight reduction in the apparent strengths of the absorption features, but these effects may not even be noticeable in our low-resolution results.

The spectrum of Delta Aquilae (Almizan I) is presented here, along with a rectified profile in red.

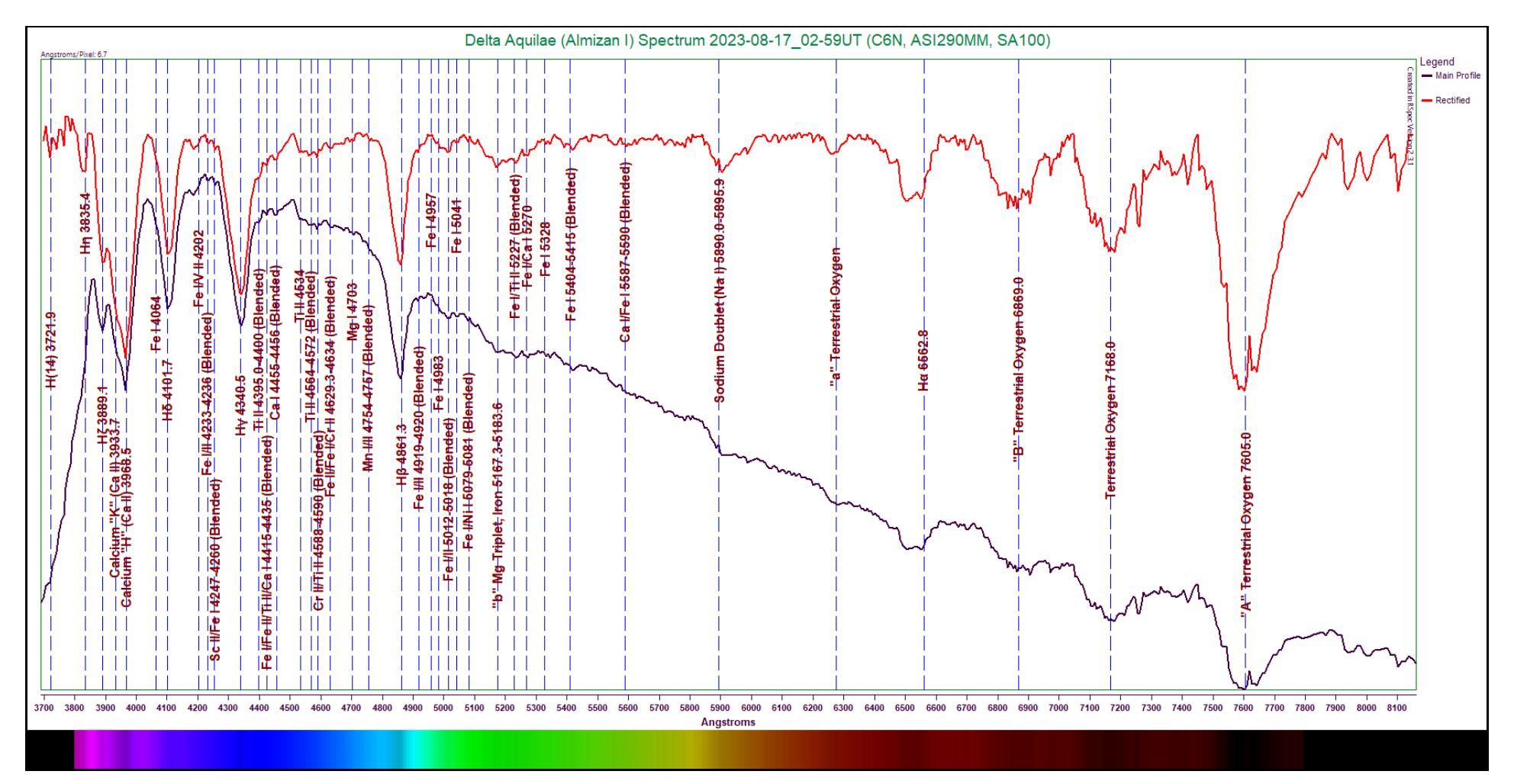


Figure 5.22: Delta Aquilae (Almizan I) Spectrum (6.3 Angstroms/pixel)
Capture Details: Exposure 343ms, Gain 184, 80% of 420 frames stacked, Integration Time 115s

Most of the moderately strong hydrogen Balmer absorptions that are visible remain easily identifiable. The Hη absorption is extremely subtle here, causing only a small deviation in the continuum line. A cursory glance at the spectrum reveals a good number of iron absorptions, many of which are blends. The magnesium triplet at 5167.3-5183.6 Angstroms appears as a significant dip, broadened by the adjacent iron lines. The sodium doublet at 5890.0-5895.9 Angstroms is also a significant dip. A good number of additional metals are evident, including iron, scandium, calcium, titanium, chromium, magnesium, and manganese.

The following table lists the labeled absorptions noted in the Delta Aquilae (Almizan I) spectrum.

Table 5.18 - Delta Aquilae (Almizan I) Line Identification Details

Feature	Wavelength	Comments
	(Angstroms)	
H(14)	3721.9	Weak higher order hydrogen line
Ηη	3835.4	Weak hydrogen Balmer line
Ca II	3933.7	Fraunhofer "H" ionized calcium line; appears very weak here
Ca II	3968.5	Fraunhofer "K" ionized calcium line; moderately strong and masking Ηε absorption
Fe I	4064	Very subtle neutral iron absorption
Ηδ	4101.7	Moderately strong blended hydrogen Balmer line
Fe I/V II	4202	Weak iron/vanadium blend
Fe I/II	4233-4236	Very weak iron blend
Sc II/Fe I	4247-4260	Weak scandium/iron blend
Нү	4340.5	Strong hydrogen Balmer line
Ti II	4395.0-4400	Weak ionized titanium blend
Fe I/Fe II/Ca I	4415-4435	Very weak iron/calcium blend
Ca I	4455-4456	Weak neutral calcium blend
Ti II	4534	Weak ionized titanium absorption
Ti II	4564-4572	Very weak ionized titanium blend
Cr II/Ti II	4588-4590	Weak chromium/titanium blend
Mg I	4703	Common but very weak neutral magnesium absorption
Mn I/II	4754-4757	Weak blend of neutral and ionized manganese
Нβ	4861.3	Strong hydrogen Balmer line
Fe I/II	4919-4920	Common but very weak iron blend
Fe I	4957	Extremely weak neutral iron absorption
Fe I	4983	Weak neutral iron absorption
Fe I/II	5012-5018	Weak to moderate iron blend; common
Fe I	5041	Very weak neutral iron absorption; fairly common
Fe I/Ni I	5079-5081	Very weak iron/nickel blend
Fe II/S II	5100.8-5103.3	Very weak blend; Fe II dominates @ 5100.8Å
Mg I Triplet	5167.3-5183.6	Fraunhofer "b" magnesium and iron blend; broadened by adjacent iron absorptions
Fe I/Ti II	5227	Weak but common iron/titanium blend
Fe I/Ca I	5270	Weak but common iron/calcium blend
Fe I	5328	Fairly common neutral iron absorption; appears weak here
Fe I	5404-5410	Weak neutral iron blend; fairly common
Ca I/Fe I	5587-5590	Common calcium/iron blend; extremely weak here; dubious identification
Na I Doublet	5890.0-5895.9	Fraunhofer "D2" and "D1" neutral sodium blend; moderately strong here

Feature	Wavelength	Comments
	(Angstroms)	
"a" Telluric Oxygen	6276.0	Fraunhofer "a" absorption due to atmospheric oxygen
Ηα	6562.8	Fairly strong hydrogen Balmer line
Telluric Oxygen	6869.0	Fraunhofer "B" absorption due to atmospheric oxygen
Telluric Oxygen	7168.0	Absorption due to atmospheric oxygen
Telluric Oxygen	7605.0	Fraunhofer "A" absorption due to atmospheric oxygen

We will ascertain an approximate peak energy wavelength for the spectrum and apply Wien's Law to calculate a temperature estimate for the star. For these early F-type stars, our estimate is sure to be a little too low, but it should be closer to the expected temperature as the gap between our estimates and the real values gets smaller.

The plotted continuum curve for Delta Aquilae (Almizan I) can be found here. Along with the continuum curve, an unlabeled version of the spectrum is plotted in blue. The apparent peak energy wavelength of the continuum curve is marked in red.

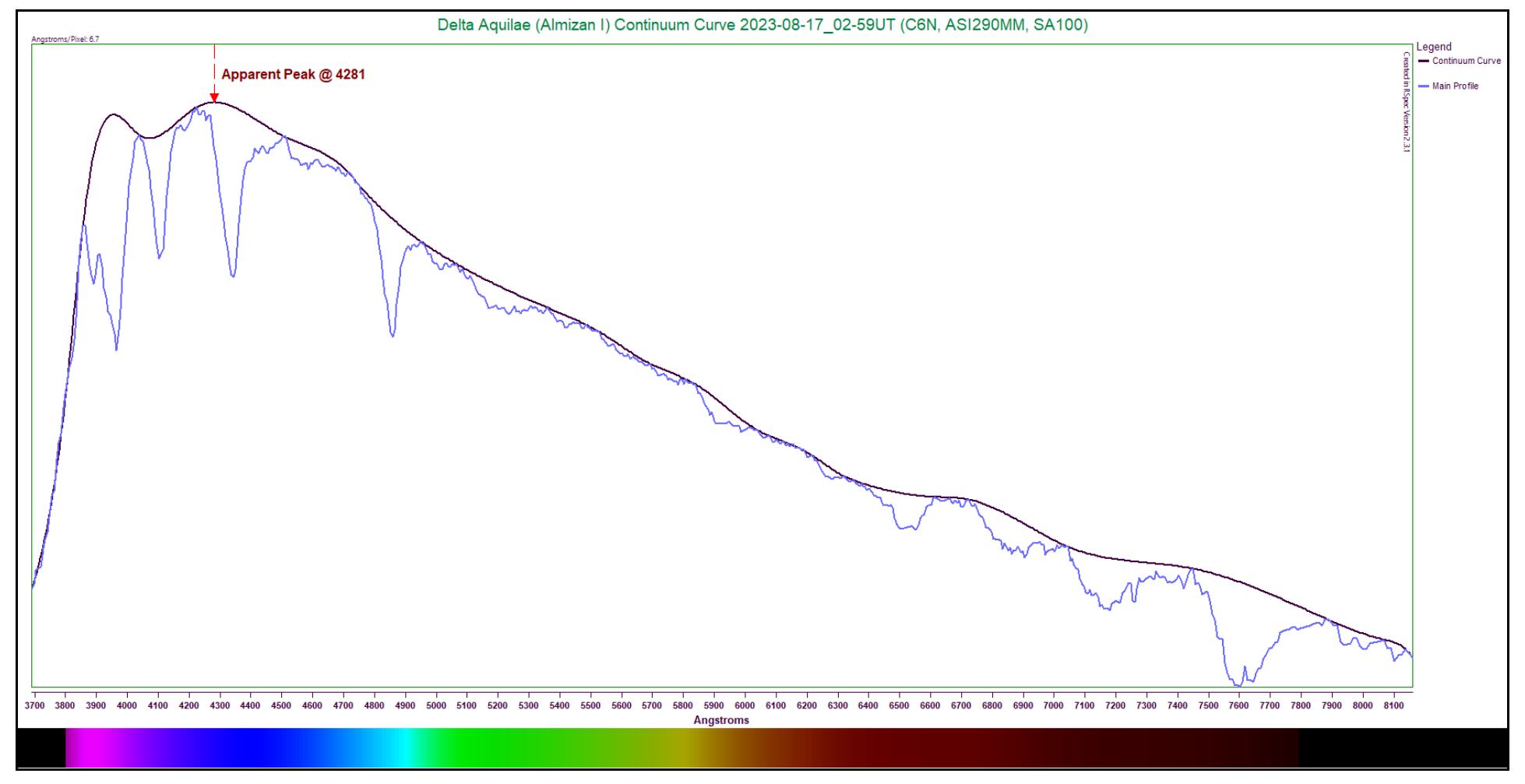


Figure 5.23 - Continuum Curve Plot (Delta Aquilae)

The apparent peak energy wavelength appears to be 4281 Angstroms. Applying Wien's Law using this value, we calculate a temperature estimate of 6,769K. This does fall within our expected range (between 7,000K and 6,750K). As mentioned previously, the star is a subgiant, which serves to reduce the temperature somewhat. This makes our temperature estimate come out quite close; using the median expected temperature (6,875K), we find our estimate is only off by 1.54%. The professionally determined temperature of the star is listed as 6,958K⁽²⁴⁾. Comparing our estimate to this value, we find our estimate comes within 2.72%.

Middle F-Type Stars

The middle F-type stars demonstrate a continued decrease in temperature. Wien's Law continues to be more useful for temperature estimates in low-resolution spectra. The Fraunhofer "K" ionized calcium line grows in strength, and the Fraunhofer "H" ionized calcium line becomes more dominant. The magnesium triplet and sodium doublet also slowly increase in prominence. The presence of additional metal lines continues to grow as well, with many blended lines appearing.

Middle F-type stars commonly come in between 6,650K and 6,350K, making them still significantly hotter than our Sun⁽²²⁾. These stars typically stay on the main sequence for approximately 4,500 Myr⁽⁷⁾. They range in mass from approximately 1.35 down to 1.25 times solar mass⁽²²⁾. They shine with luminosities ranging from roughly 4 times down to about 2.5 times that of the Sun⁽²²⁾. Spectroscopic features continue the trends of earlier subtypes—the Fraunhofer "K" and "H" lines continue to strengthen, the magnesium triplet and sodium doublet remain identifiable, and the number and strengths of other metals increases. The likelihood of blended lines also increases in low-resolution spectra.

The representative star chosen for this subtype is lota Pegasi in the constellation of Pegasus, the Winged Horse. It is a main sequence star, and so should provide an excellent example.

The spectrum of lota Pegasi is presented here, along with a rectified profile in red.

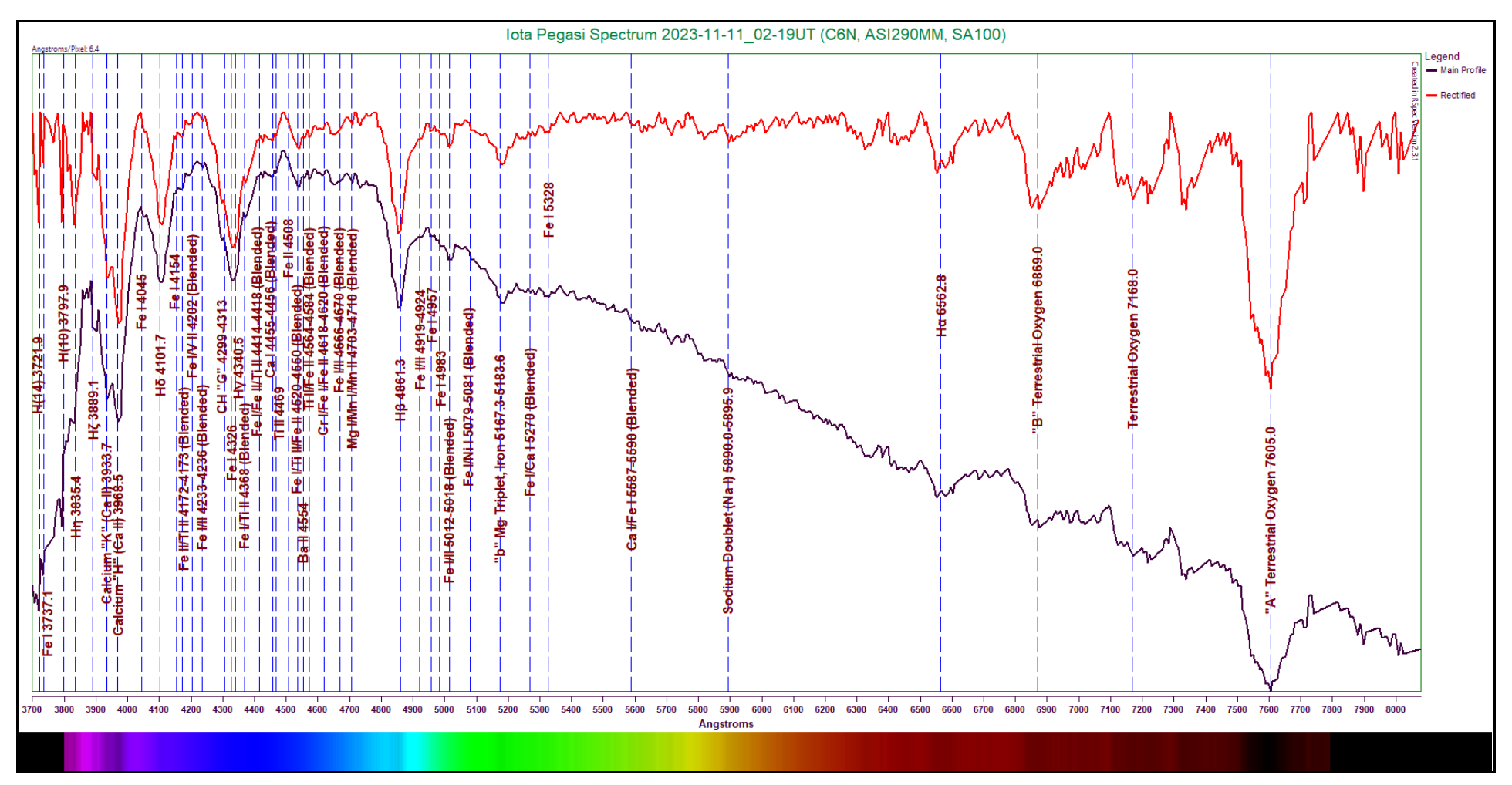


Figure 5.24: Iota Pegasi Spectrum (6.3 Angstroms/pixel)
Capture Details: Exposure 815ms, Gain 113, 50% of 307 frames stacked, Integration Time 125s

As you can see, most of the hydrogen Balmer absorptions are visible, but slightly reduced in strength compared to the early F-types. The Fraunhofer "K" and "H" lines due to ionized calcium are clear, and are almost but not quite equal in strength. We see in this star the first clear instance of a molecular absorption, the Fraunhofer "G" absorption due to the CH molecule at 4299-4313 Angstroms, just below the Hγ absorption. The Fraunhofer "b" neutral magnesium triplet (with iron) appears as a moderate strength feature here. The sodium doublet at 5890.0-5895.9 Angstroms appears extremely weak here, and is difficult to separate from the noise of the continuum, making the identification rather dubious. A fairly large number of additional weak to very weak metal lines are labeled, including iron, calcium, titanium, barium, chromium, magnesium, and manganese. As anticipated, a good number of the marked absorptions are blends, with the vast majority including iron. The absorptions are also becoming more closely crowded together, so exercise caution when tracing the labels.

The following table lists the absorptions labeled in the spectrum of lota Pegasi.

Table 5.19 - Iota Pegasi Line Identification Details

Feature	Wavelength	Comments
	(Angstroms)	
H(14)	3721.9	Weak higher order hydrogen Balmer line
Fe I	3737.1	Very weak neutral iron line
H(10)	3797.9	Moderately strong higher order hydrogen Balmer line
Ηη	3835.4	Hydrogen Balmer line; weak but well-defined
Hζ	3889.1	Relatively weak hydrogen Balmer line; appears broadened here
Ca II	3933.7	Fraunhofer "K" ionized calcium line
Ca II	3968.5	Fraunhofer "H" ionized calcium line
Fe I	4045	Very weak neutral iron absorption
Нδ	4101.7	Moderate strength hydrogen Balmer line
Fe I	4154	Extremely weak neutral iron absorption
Fe I/Ti II	4172-4173	Very weak iron/titanium blend
Fe I/V II	4202	Very weak iron/vanadium blend
CH	4299-4313	Fraunhofer "G" molecular absorption; extremely weak here
Fe I	4326	Neutral iron line; broadened due to adjacent Hγ absorption
Ηγ	4340.5	Hydrogen Balmer line; slightly broadened by adjacent iron absorption
Fe I/Ti II	4414-4418	Extremely weak iron/titanium blend
Ca I	4455-4456	Weak neutral calcium blend
Ti II	4469	Exceptionally subtle ionized titanium absorption; dubious identification
Fe I/Ti II/Fe II	4520-4550	Weak iron/titanium blend
Ba II	4554	Extremely weak ionized barium absorption
Ti II/Fe II	4564-4584	Weak ionized titanium/iron absorption
Cr I/Fe I/Fe II	4618-4620	Weak chromium/iron blend
Fe I/II	4666-4670	Weak iron blend
Mg I/Mn I/Mn II	4703-4710	Weak magnesium/manganese blend
Нβ	4861.3	Moderately strong hydrogen Balmer line
Fe I/II	4919-4924	Very weak iron blend
Fe I	4957	Extremely weak neutral iron absorption
Fe I	4983	Extremely weak neutral iron absorption
Fe I/II	5012-5018	Common iron blend; appears broadened here
Fe I/Ni I	5079-5081	Common iron/nickel blend; appears extremely weak here
Mg I Triplet	5167.3-5183.6	Fraunhofer "b" magnesium triplet with iron
Fe I/Ca I	5270	Common iron/calcium blend; not clear and therefore dubious
Fe I	5328	Very weak neutral iron absorption

Feature	Wavelength	Comments
	(Angstroms)	
Ca I/Fe I	5587-5590	Common calcium/iron blend; appears extremely weak; dubious identification
Na I Doublet	5890.0-5895.9	Common absorption due to neutral sodium; extremely weak; dubious identification
Ηα	6562.8	Weak to moderate hydrogen Balmer line
"B" Telluric Oxygen	6869.0	Fraunhofer "B" absorption due to atmospheric oxygen
Telluric Oxygen	7168.0	Absorption due to atmospheric oxygen
"A" Telluric Oxygen	7605.0	Fraunhofer "A" absorption due to atmospheric oxygen

As noted previously, Wien's Law can provide reasonably accurate temperature estimates for these middle F-type stars. We will determine the approximate peak energy wavelength, then calculate the temperature. This will then be compared to the professionally determined temperature.

The continuum curve for lota Pegasi is presented here. The spectrum is indicated in blue, and the labels have been removed for clarity.

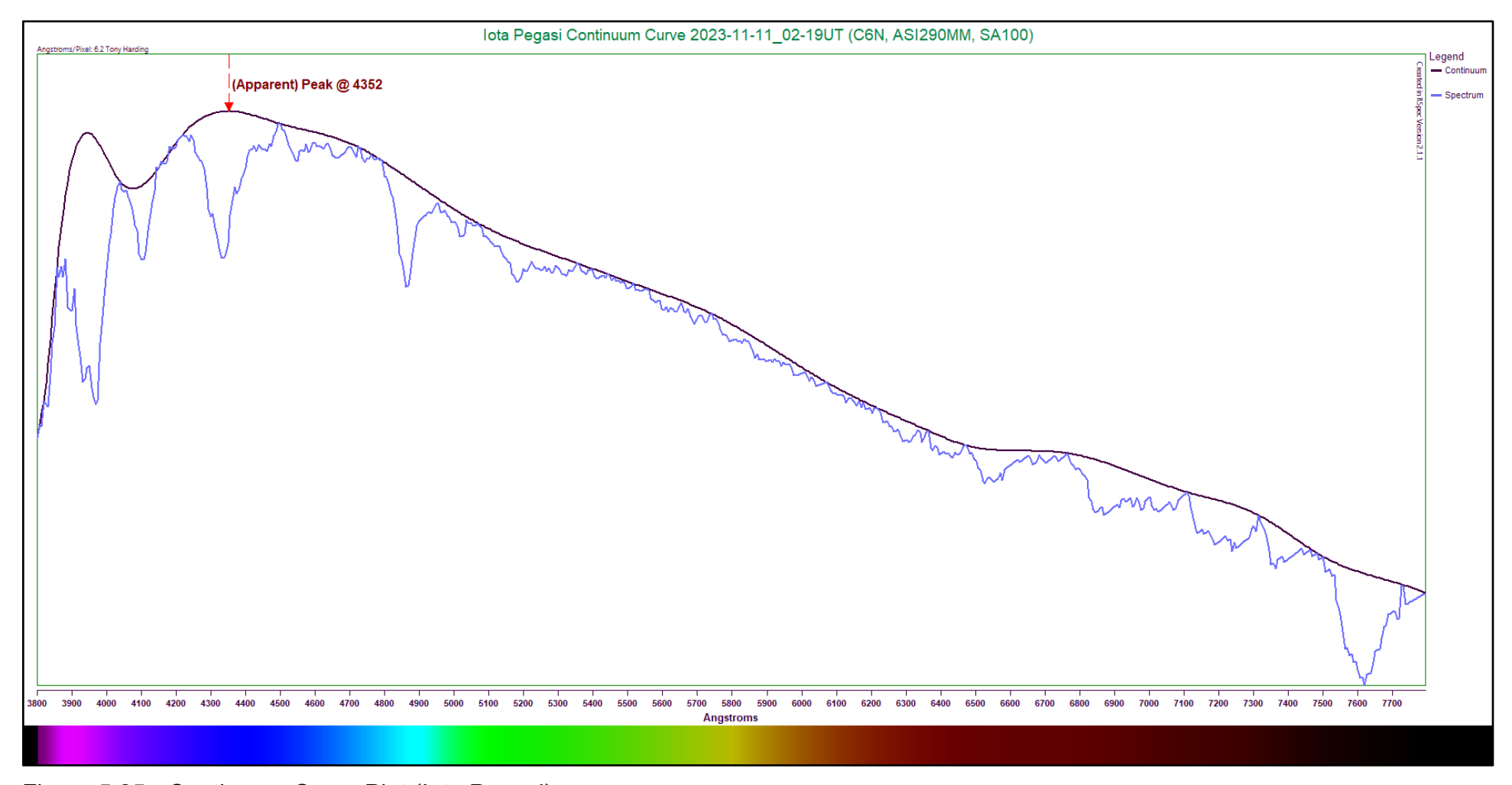


Figure 5.25 - Continuum Curve Plot (Iota Pegasi)

The peak energy wavelength appears to be 4440 Angstroms. Using this value for Wien's Law, we calculate an effective temperature of 6,527K. This is within our expected temperature range of 6,650K-6,350K. Our estimate is off the median expected temperature of

(6,450K) by approximately 1.19%. The professionally determined temperature of the star is listed as 6,580K⁽²⁵⁾. Comparing our estimate to this value, we find we are only off by 0.81%. In both cases, our estimate is fairly close, demonstrating that Wien's Law is now more accurate.

Late F-Type Stars

These stars continue the trends apparent in the last few subtypes. The temperatures continue to fall, the calcium "K" line continues to strengthen, and the metals—particularly iron—become more numerous.

Late F-type stars range in temperature from about 6,250K down to approximately 6,150K⁽²²⁾. They typically stay on the main sequence for about 5,500 Myr⁽⁷⁾. They are slightly less massive than the middle F-types, coming in at 1.3 to 1.2 times the mass of our Sun⁽²²⁾. They shine with an approximate luminosity of 2.5 to 1.9 times that of our Sun⁽²²⁾. Common spectroscopic features continue to include moderate strength hydrogen Balmer lines and stronger Fraunhofer "K" and "H" ionized calcium lines. The magnesium triplet and sodium doublet continue to slowly strengthen as well, while the profusion of additional faint metal lines is evident. Many of the fainter lines will appear blended, and be more closely spaced. We can expect a high number of iron absorptions.

The star chosen to represent the Late F-type stars is lota Piscium in the constellation of Pisces, the Fishes. It is a main sequence star and will be a good demonstration of the typical features.

The spectrum of lota Piscium is presented here, along with a rectified profile in red.

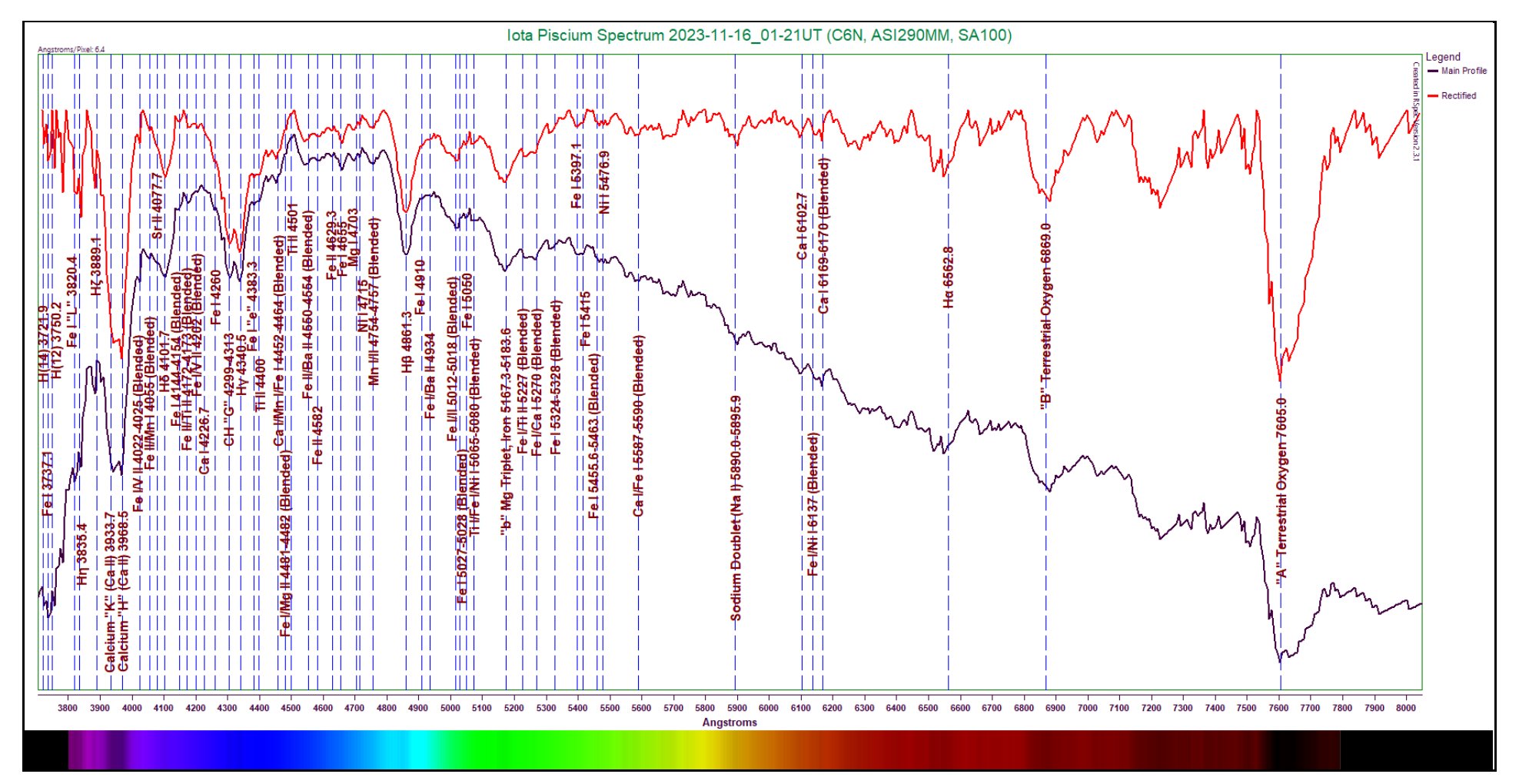


Figure 5.26: Iota Piscium Spectrum (6.3 Angstroms/pixel)
Capture Details: Exposure 1s, Gain 113, 80% of 242 frames stacked, Integration Time 193s

It can be plainly and immediately seen that the number of fine metal lines has increased! Most of the hydrogen Balmer lines are evident, though a bit reduced in strength compared to the middle F-types. The Hŋ line appears next to the Fraunhofer "L" iron line. The Fraunhofer "K" and "H" calcium II lines at 3933.7 and 3968.5 Angstroms respectively appear very close in strength. Notably, the Fraunhofer "G" molecular CH absorption at 4299-4313 Angstroms is strong. The magnesium triplet at 5167.3-5183.6 Angstroms is fairly sharp and moderately deep. The sodium doublet at 5890.0-5895.9 Angstroms appears sharp and distinct, but is a bit weaker by comparison. A large number of faint to very faint additional metal lines are present, including iron, strontium, calcium, titanium, magnesium, nickel, and manganese. (Be very careful when tracing labels, as some of the lines are crowded somewhat closely together!)

The following table lists the absorptions labeled in the lota Piscium spectrum.

Table 5.20 - lota Piscium Line Identification Details

Feature	Wavelength	Comments
	(Angstroms)	
H(14)	3721.9	Higher order hydrogen Balmer line; very weak here
Fe I	3737.1	Weak neutral iron line; not uncommon
H(12)	3750.2	Very weak higher order hydrogen Balmer line
Fe I	3820.4	Fraunhofer "L" neutral iron line; small but distinct
Ηη	3835.4	Weak hydrogen Balmer line
Нζ	3889.1	Weak hydrogen Balmer line
Ca II	3933.7	Fraunhofer "K" ionized calcium line
Ca II	3968.5	Fraunhofer "H" ionized calcium line
Fe I/V II	4022-4025	Very weak iron/vanadium blend
Fe II/Mn I	4055	Very weak iron/manganese blend
Ηδ	4101.7	Moderate strength hydrogen Balmer line
Fe I	4144-4154	Weak neutral iron blend
Fe II/Ti II	4172-4173	Common iron/titanium blend; appears weakly here
Fe I/V II	4202	Extremely weak iron/vanadium absorption
Ca I	4226.7	Very common neutral calcium line; appears extremely weak here
Fe I	4260	Very weak neutral iron absorption
CH	4299-4313	Fraunhofer "G" molecular CH absorption; strong in this specimen
Нү	4340.5	Strong hydrogen Balmer line
Fe I	4383.3	Fraunhofer "e" neutral iron line; appears weak
Ti II	4400	Weak ionized titanium absorption
Ca I/Mn I/Fe I	4452-4464	Moderate strength calcium/manganese/iron blend
Fe I/Mg II	4481-4482	Extremely subtle iron/magnesium blend; dubious identification
Ti II	4501	Extremely subtle ionized titanium absorption; dubious identification
Fe II/Ba II	4550-4554	Weak ionized iron/barium blend
Fe II	4582	Weak ionized iron absorption
Fe II	4629.3	Very weak ionized iron line
Fe I	4655	Weak neutral iron line
Mg I	4703	Common neutral magnesium absorption; weak
Ni I	4715	Extremely weak neutral nickel absorption
Mn I/II	4754-4757	Fairly common manganese blend; weak
Нβ	4861.3	Moderately strong hydrogen Balmer line
Fe I	4910	Very subtle neutral iron absorption
Fe I/Ba II	4934	Fairly common iron/barium blend; extremely weak

Feature	Wavelength	Comments
	(Angstroms)	
Fe I/II	5012-5018	Moderately strong iron blend; common
Fe I	5027-5028	Very weak neutral iron absorption
Fe I	5050	Very weak neutral iron absorption
Ti I/Fe I/Ni I	5065-5080	Weak and somewhat unusual titanium/iron/nickel blend
Mg I Triplet	5167.3-5183.6	Fraunhofer "b" neutral magnesium absorption; includes some iron; moderately strong
Fe I/Ti II	55227	Common iron/titanium blend; weak to moderate in strength
Fe I/Ca I	5270	Common iron/calcium blend; weak to moderate strength
Fe I	5324-5328	Weak neutral iron blend
Fe I	5397.1	Weak neutral iron line
Fe I	5415	Weak neutral iron line
Fe I	5455.6-5463	Weak neutral iron blend
Ni I	5476.9	Very weak neutral nickel line
Ca I/Fe I	5587-5590	Common neutral calcium/iron blend; very weak
Na I Doublet	5890.0-5895.9	Common neutral sodium blend; sharply defined but not terribly strong
Ca I	6102.7	Common neutral calcium line
Fe I/Ni I	6137	Fairly common but weak neutral iron/nickel absorption
Ca I	6169-6170	Weak calcium blend; distinct
Ηα	6562.8	Moderately strong hydrogen Balmer line
"B" Telluric Oxygen	6869.0	Fraunhofer "B" absorption due to atmospheric oxygen
"A" Telluric Oxygen	7605.0	Fraunhofer "A" absorption due to atmospheric oxygen; obvious

We will employ Wien's Law to calculate an effective temperature for the star. We will determine the approximate peak energy wavelength, then calculate the temperature and compare this with expectations.

The continuum curve for lota Piscium is presented below. The spectrum is indicated in blue, and the labels have been removed for clarity.

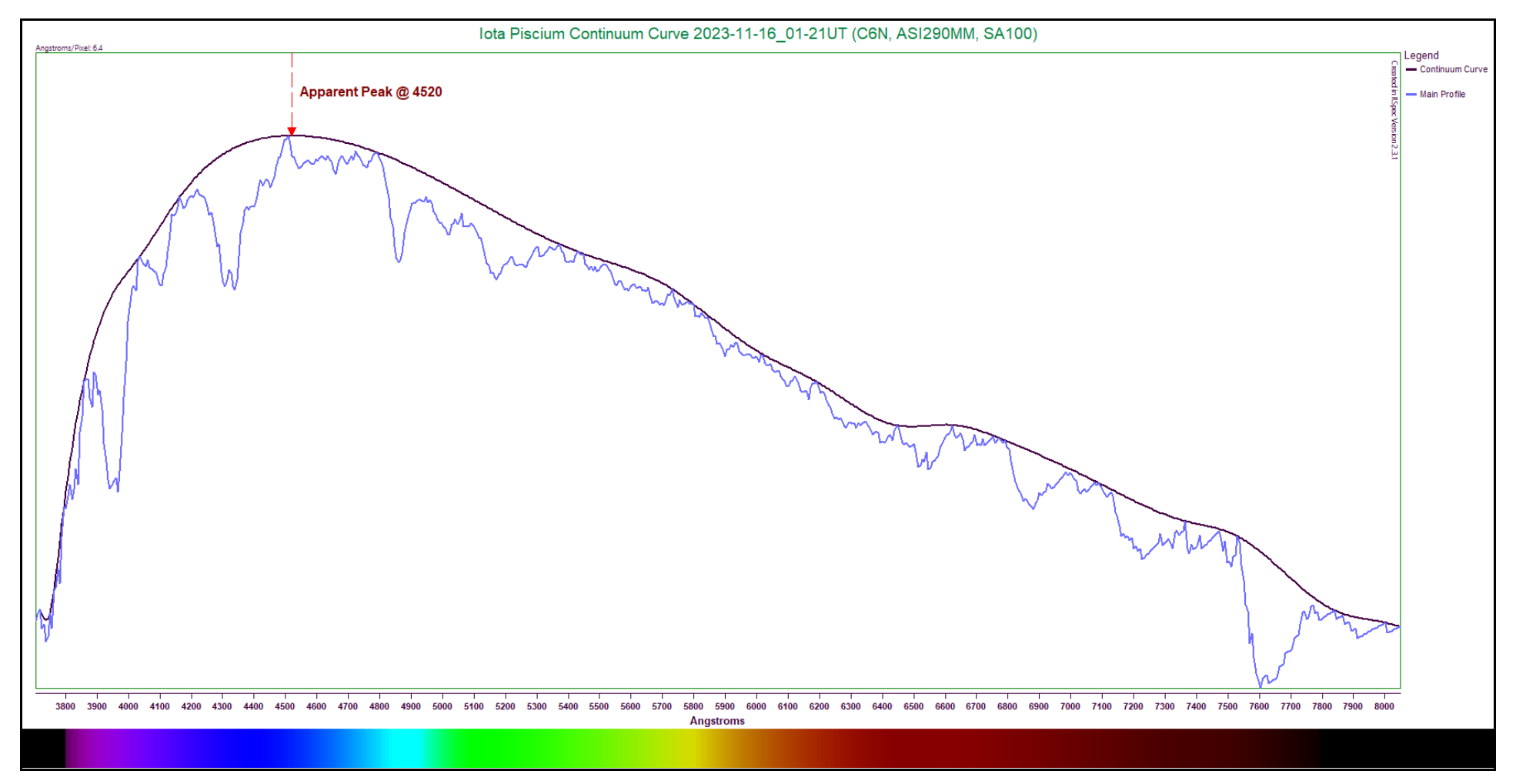


Figure 5.27 - Continuum Curve Plot (Iota Piscium)

The peak energy wavelength appears to be 4520 Angstroms. Using this value for Wien's Law, the estimated temperature comes out to approximately 6,411K. This is higher than the anticipated temperature range of 6,250K-6,150K. Comparing our estimate to the median of the expected range (6,200K) we find that we are off by approximately 3.40%. The professionally determined temperature of the star is listed as 6,288K⁽²⁶⁾. Comparing our estimate to this value, we find we are off by only 1.96%.

5.8 Spectral Type F/G Stars (Very Late F and Very Early G)

Members of this custom category begin to more strongly demonstrate features that are more Sun-like. Most of the hydrogen Balmer lines continue to be easily identifiable, excepting of course the Hε absorption, which is completely overtaken by the Fraunhofer "K" and "H" ionized calcium lines.

When viewed through a telescope, these stars show a yellowish tinge, which can appear prominent if a complimentary-colored star is in the same field of view.

These stars have temperatures ranging from 6,050K down to about 5900K^(22,27). They possess masses only slightly higher than that of our Sun, typically in the range of 1.13 to 1.05 times solar mass^(22,27). Because of this lower mass, they are fairly long-lived stars, staying on the main sequence for about 7,000 Myr⁽⁷⁾. Their luminosities range from approximately 1.65 times down to around 1.35 times solar^(22,27). Like our own star, these specimens will puff up to become red giants near the end of their lives, then throw off a planetary nebula, leaving behind a white dwarf.

Spectroscopically, they show a great mixture of metals among the hydrogen Balmer lines. These metals typically include lots of iron, titanium, nickel, and calcium, plus some others. The apparent peak energy wavelength continues to shift into the visible wavelength range, meaning that temperature estimates with Wien's Law remain roughly accurate.

The star chosen to represent this type is indicated here:

Table 5.21 - Representative F/G Star

Subtype	Star
Very Late F/Very Early G	Eta Boötis (Muphrid)

F/G Stars (Very Late F and Very Early G)

As noted previously, the very late F-type stars and very early G-type stars appear very Sun-like. The hydrogen Balmer lines are typically weak but mostly still visible, while the Fraunhofer "K" and "H" lines are very strong. The magnesium triplet and sodium doublet also continue to grow in apparent strength, and a plethora of metals will be visible.

Stars of this subtype have effective temperatures around 6,000K^(22,27). They are fairly slow-burning stars, living on the main sequence for approximately 7,000 Myr⁽⁷⁾. Their masses lie near 1.1 times the mass of our Sun, and they shine with about 1.5 times solar luminosity^(22,27). The most impressive spectroscopic features visible are the Fraunhofer "K" and "H" ionized calcium lines, the magnesium triplet, and the sodium doublet. Additionally, these stars show lots of neutral iron absorptions, a great number of which will appear blended in low-resolution spectra. Some other metals are also commonly visible, including calcium, magnesium, titanium, and others. Of course, these will vary in apparent strength and abundance between specimens.

The representative star chosen as representative of the F/G stars is Eta Boötis, also known by the common name Muphrid, in the constellation of Boötes the Herdsman. This star is actually a subgiant, just beginning to make its way toward the red giant stage. This may cause some of the absorptions to appear slightly weakened, but the spectrum should still demonstrate features typical of this subtype.

The labeled spectrum of Eta Boötis (Muphrid) is presented below, with a rectified profile accompanying it in red.

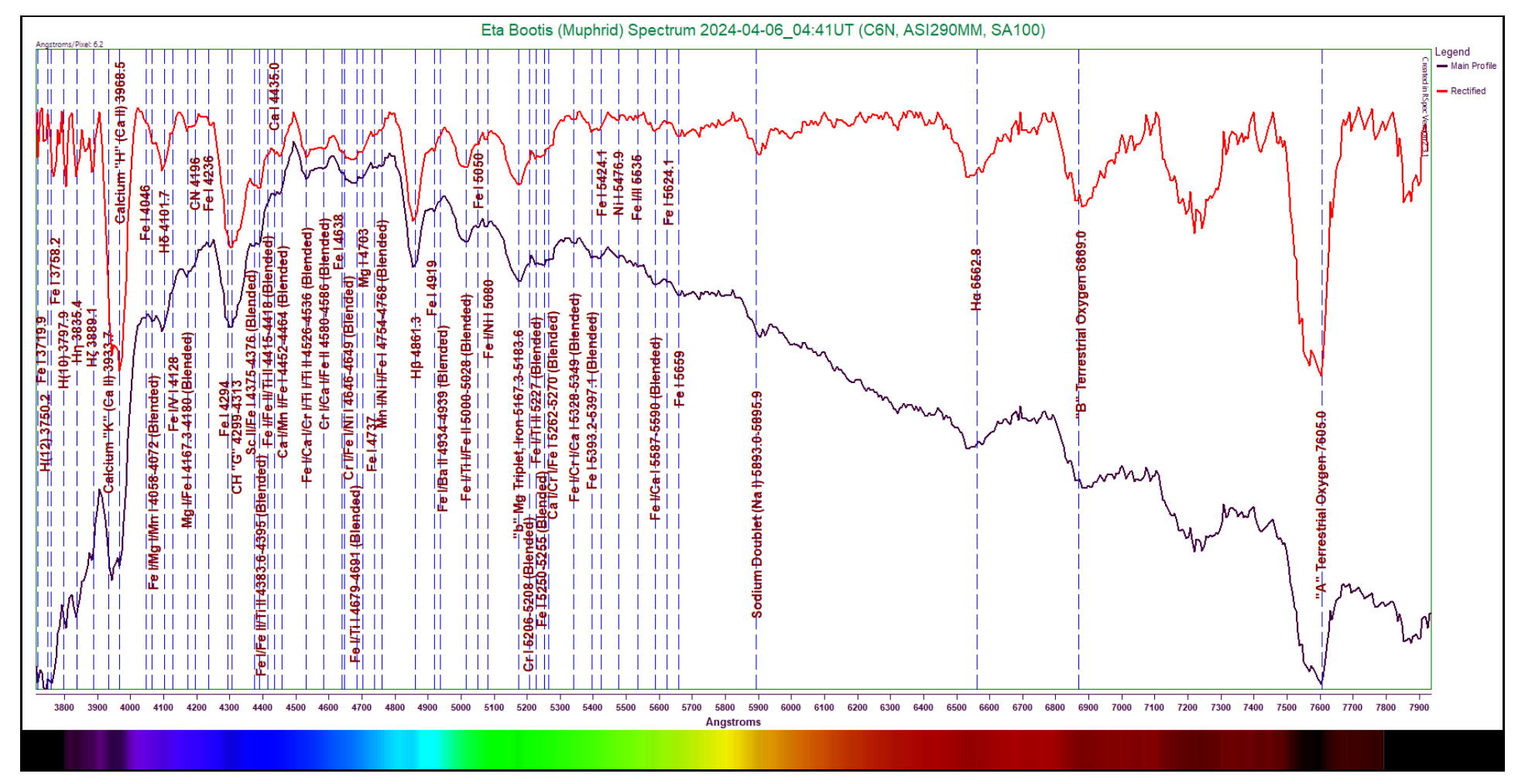


Figure 5.28: Eta Boötis (Muphrid) Spectrum (6.3 Angstroms/pixel)
Capture Details: Exposure 383ms, Gain 119, 60% of 638 frames stacked, Integration Time 146s

The first notable thing about this spectrum is how closely some of the absorptions are spaced. Be careful when tracing labels! Secondly, most of the labeled absorptions are blends rather than individual features. Many of the hydrogen Balmer lines are visible

here; the Hβ line is the strongest, but even it appears weakened compared to earlier stars. The Fraunhofer "K" and "H" ionized calcium lines at 3933.7 and 3968.5 Angstroms respectively are very deep. The Fraunhofer "G" molecular CH absorption is quite strong here, with a noticeable iron absorption just below it at 4294 Angstroms. The magnesium triplet at 5167.3-5183.6 Angstroms is strong and distinct also. Together with the chromium, iron, and calcium blends just above it, a fairly large gouge is taken out of the continuum. The sodium doublet at 5890.0-5895.9-96 Angstroms is well defined here, if not terribly deep. A fairly large number of additional metal lines and blends are labeled, including iron, a CN molecular absorption, magnesium, scandium, calcium, chromium, manganese, and nickel.

The following table shows the absorption features found in the spectrum of Eta Boötis (Muphrid).

Table 5.22 - Eta Boötis (Muphrid) Line Identification Details

Table 0.22 Eta Dootis (iviupililu) Lille lui	entification Details
Feature	Wavelength	Comments
	(Angstroms)	
Fe I	3719.9	Very weak neutral iron line
H(12)	3750.2	Weak higher order hydrogen Balmer line
Fe I	3758.2	Weak neutral iron line
H(10)	3750.2	Weak higher order hydrogen Balmer line
Ĥη	3835.4	Weak hydrogen Balmer line
Нζ	3889.1	Very weak hydrogen Balmer line
Ca II	3933.7	Fraunhofer calcium II "K" line; extremely strong here
Ca II	3968.5	Fraunhofer calcium II "H" line; extremely strong here
Fe I	4046	Extremely weak neutral iron absorption
Fe I/Mg I/Mn I	4058-4072	Weak blend of iron, magnesium, and manganese
Ηδ	4101.7	Moderate hydrogen Balmer line
Fe I/V II	4128	Extremely weak iron/vanadium blend
Mg I/Fe I	4167.3-4180	Weak magnesium/iron blend; a somewhat unusual blend
CN	4196	Very weak molecular CH absorption
Fe I	4236	Very weak neutral iron absorption
Fe I	4294	Strong neutral iron absorption; causing broadened feature with adjacent CH feature
CH	4299-4313	Fraunhofer "G" molecular CH absorption; appears broadened with adjacent iron feauture
Sc II/Fe I	4475-4376	Weak to moderate scandium/iron blend
Fe I/Fe II/Ti II	4383.6-4395	Weak to moderate iron/titanium blend
Fe I/Fe II/Ti II	4415-4418	Extremely weak iron/titanium blend; only causing small diversion on the continuum; dubious identification
Ca I	4435.0	Extremely weak neutral calcium line
Ca I/Mn I/Fe I	4452-4464	Weak to moderate calcium/manganese/iron blend
Fe I/Ca I/Cr I/Ti I/Ti II	4526-4536	Moderate strength iron/calcium/chromium/titanium blend
Cr I/Ca I/Fe II	4580-4586	Weak blend of chromium, calcium, and ionized iron
Fe I	4638	Very weak neutral iron absorption
Cr I/Fe I/Ni I	4646-4649	Moderate strength chromium/iron/nickel blend
Fe I	4638	Extremely weak neutral iron absorption
Fe I/Ti I	4679-4691	Moderate strength iron/titanium blend
Mg I	4703	Moderate neutral magnesium absorption
Fe I	4737	Very weak neutral iron absorption
Mn I/Ni I/Fe I	4754-4768	Very weak blend of manganese, nickel, and iron
Нβ	4861.3	Moderately strong hydrogen Balmer line
Fe I	4919	Very weak neutral iron line

Feature	Wavelength	Comments
	(Angstroms)	
Fe I/Ba II	4934-4939	Extremely weak blend of neutral iron and ionized barium
Fe I/Ti I/Fe II	5000-5028	Common blend of iron and titanium
Fe I	5050	Very weak neutral iron absorption
Fe I/Ni I	5080	Very weak iron/nickel blend
Mg I Triplet	5167.3-5183.6	Fraunhofer "b" neutral magnesium absorption, with iron; moderately strong and sharp
Cr I	5206-5208	Fairly common but extremely weak chromium blend
Fe I/Ti II	5227	Common iron/titanium absorption; weak here
Fe I	5250-5255	Weak neutral iron absorption; common
Ca I/Cr I/Fe I	5262-5270	Weak blend of calcium, chromium, and iron
Fe I/Cr I/Ca I	5328-5349	Weak iron/chromium/calcium blend
Fe I	5424.1	Weak neutral iron line
Ni I	5476.9	Very weak neutral nickel line
Fe I/II	5535	Extremely weak iron absorption; dubious identification due to continuum noise
Fe I/Ca I	5587-5590	Common blend of neutral iron and calcium; weak
Fe I	5624.1	Extremely weak neutral iron line
Fe I	5659	Weak neutral iron absorption
Na I Doublet	5890.0-5895.9	Common neutral sodium blend
Ηα	6562.8	Moderate hydrogen Balmer line
"B" Telluric Oxygen	6869.0	Fraunhofer "B" absorption due to atmospheric oxygen
"A" Telluric Oxygen	7605.0	Fraunhofer "A" absorption due to atmospheric oxygen

We will employ Wien's Law to calculate the effective temperature of the star. We will then compare this with our expectations to determine how close to the mark our estimate comes.

The continuum curve for Eta Boötis is presented below. The spectrum is in blue, and the labels have been removed for clarity. The apparent peak energy wavelength is marked.

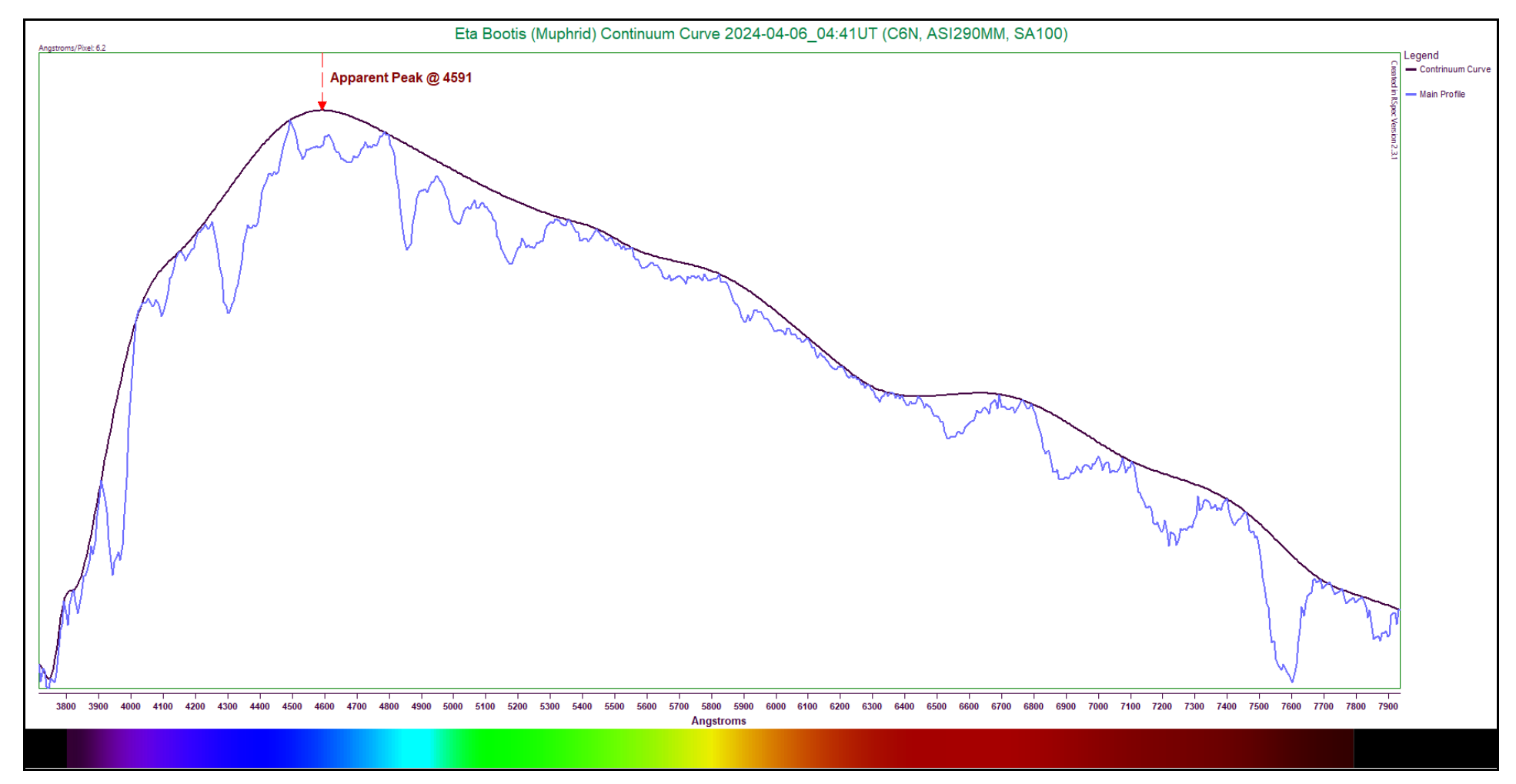


Figure 5.29 - Continuum Curve Plot (Eta Boötis)

From the apparent continuum curve, it appears that the peak energy wavelength lies at 4591 Angstroms. Using this value, Wien's Law returns an effective temperature of 6,311K. This is higher than expected, as we were hoping for an answer closer to 6,000K. We must bear in mind, however, that this star is a subgiant and not a main sequence star. In this case, our estimate is off by approximately 5.18%. The professionally determined temperature of the star is listed as 6,161⁽²⁸⁾. Using this value, we find our estimate is only off by 2.43%.

5.9 Spectral Type G Stars

The G-type stars are of particular interest to astronomers, mainly due to the fact that our own Sun is a member of this type. Studying others can serve to tell us more about our own star, as well as what phases it will go through as it evolves. These stars rank fifth in the decreasing MK temperature sequence. Hotter stars are often considered to be earlier types, whereas cooler ones are considered later types. Through a telescope, these stars typically shine with a distinct yellow tint.

G-type stars encompass the mass range including the Sun, typically having 1.03 down to 0.94 times solar mass⁽²⁹⁾. G-type stars stay on the main sequence happily fusing hydrogen in their cores from between 8,000 and 19,000 Myr⁽⁷⁾. (Our own Sun is estimated to have a total lifespan of approximately 10,000 Myr.) Their luminosities cover a range of approximately 1.2 to 0.7 times the luminosity of our local star⁽²⁹⁾. As these stars age, they swell into red giants, then throw off their outer layers and become planetary nebulae with white dwarfs left behind.

The temperature range of the G-type stars varies from about 5,850K down to about 5,450K⁽²⁹⁾. Their peak energy wavelength falls well within the optical range, which would leave one to believe that Wien's Law will continue to provide fairly accurate temperature estimates (or as accurate as is possible with low-resolution spectra) throughout the type. This situation is complicated, however, by the fact that the spectra are often saturated with fine absorption lines that can veil the true peak energy wavelength. Even a visual inspection of such stars' spectra often involves some confusion about exactly where the peak lies. This will be demonstrated.

The main spectroscopic features of these stars are primarily the huge numbers of small metal absorptions, particularly neutral iron which can be seen in abundance. Blended lines are extremely common. The hydrogen Balmer lines continue to weaken in this type as the temperatures cool. The Fraunhofer "K" and "H" Ca II lines reach their peak in the G-types, showing profound valleys in the spectra. The Fraunhofer "G" molecular CH absorption grows in strength, and the CN molecular band appears more strongly. The magnesium triplet and sodium doublet continue to grow in strength as well.

The stars chosen to represent the various G-type stars are listed here by subtype:

Table 5.23 - Representative G-Type Stars

Subtype	Star
Early	35 Leonis
Middle	Delta Coronae Borealis
Late	Eta Piscium (Alpherg)

Early G-Type Stars

The early G-type stars represent stars like our Sun. The temperatures of these stars continue to fall, shifting the apparent peak of their spectrum curves a bit farther to the right. The hydrogen Balmer lines continue their slow weakening, while the ionized Fraunhofer "K" and "H" lines are very strong. Lots of iron, often in blends, can be expected herre.

These stars have temperatures ranging from around 5,850K down to around 5,720K⁽²⁹⁾. They are fairly stable stars, staying on the main sequence for approximately 10,000 Myr⁽⁷⁾. They resemble our Sun in terms of mass as well, possessing between 1.03 and 0.99 times the solar mass. They shine with luminosities between 1.20 and 0.98 times the solar value⁽²⁹⁾. Spectroscopic features remain similar to those of the F/G stars, with weakening hydrogen Balmer lines, very strong Fraunhofer "K" and "H" lines, and a great number of iron absorptions visible. Many of the absorptions will appear as a blending of elements in low-resolution spectra. Some other metals are typically visible, including manganese, calcium, magnesium, chromium, and titanium. These will vary in number and strength from one star to another.

The specimen chosen as an example of this subtype is 35 Leonis in the constellation of Leo, the Lion. Though the star is beginning to move off the main sequence, it is still very close to it. The star is considered to be between a dwarf and a subgiant. It can still provide us with plenty of features typical of the main sequence variety.

The spectrum of 35 Leonis is shown below, with a rectified profile in red.

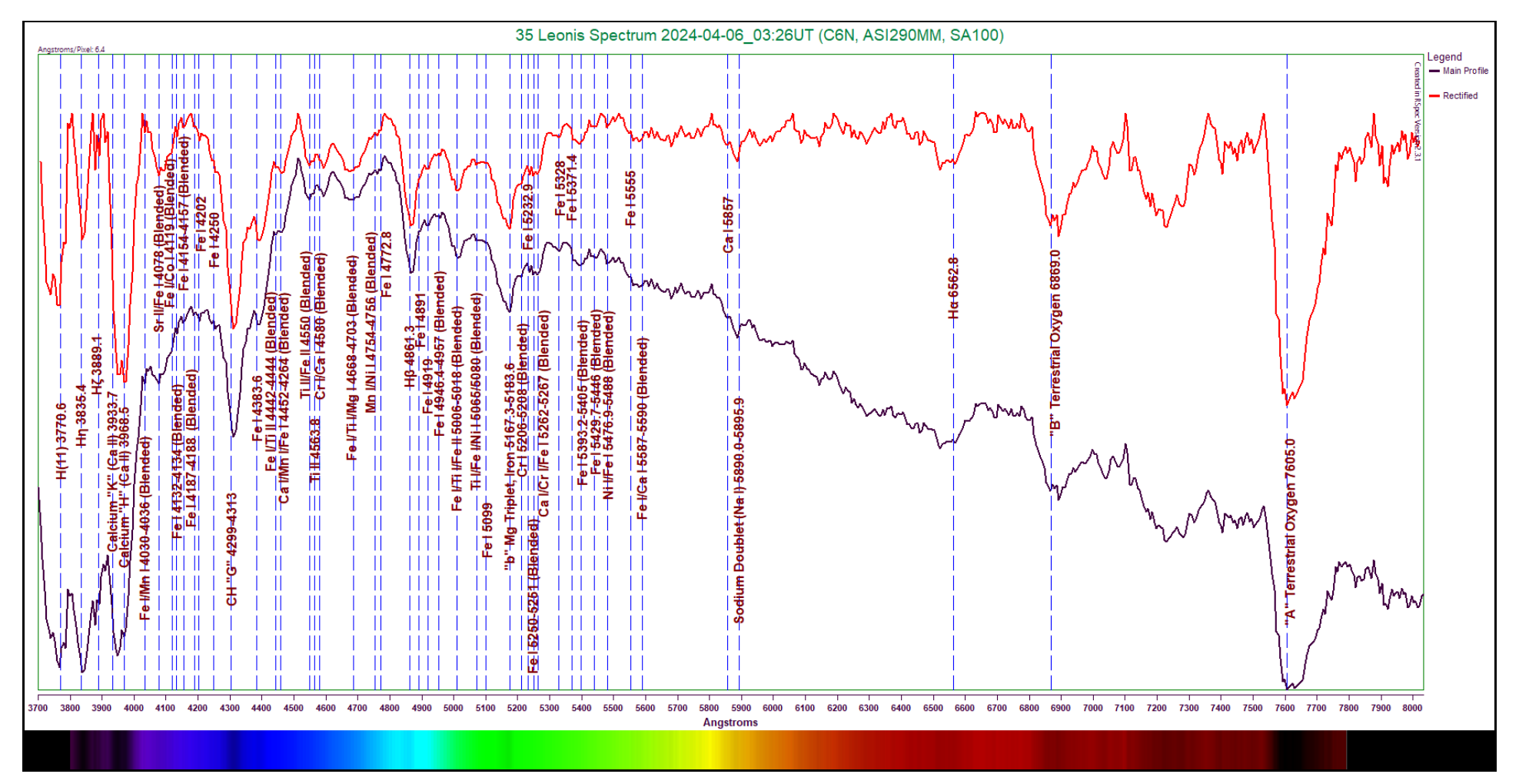


Figure 5.30: 35 Leonis Spectrum (6.3 Angstroms/pixel)
Capture Details: Exposure 3s, Gain 196, 75% of 117 frames stacked, Integration Time 263s

This specimen provided some difficulty in getting a good calibration. This is evident in several of the labeled absorptions. We can see a pretty high number of faint metal lines and blends in this spectrum, often spaced closely together. Tracing the labels can be difficult, so take care when doing so. Several of the hydrogen Balmer lines are visible, including H η , H ζ , H δ , H β , and H α . The H ϵ line has of course been overtaken by the profound Fraunhofer "K" and "H" ionized calcium lines. The H γ line is overtaken mainly by the Fraunhofer "G" molecular CH absorption. The H β absorption is the strongest and clearest hydrogen Balmer line. The Fraunhofer "K" and "H" ionized calcium lines at 3933.7 and 3968.5 Angstroms respectively appear very clear and deep here, as expected. The Fraunhofer "G" molecular CH absorption at 4299-4313 Angstroms is also very strong. A very broad and notable absorption occurs at 4668-4703 Angstroms due to a strong blend of iron, titanium, and magnesium. The magnesium triplet at 5167.3-5183.6 Angstroms is quite notable, appearing deep, and attended by the chromium, iron, and calcium absorptions above it. The sodium doublet at 5890.0-5895.9 Angstroms is also visible, being not terribly deep, but sharply defined. A neutral calcium absorption just below it at 5857 Angstroms is a somewhat common feature in stars of this type. A great number of faint metal lines are marked, including lots of iron, strontium, calcium, titanium, chromium, and manganese.

The following table lists the absorptions labeled in the spectrum of 35 Leonis.

Table 5.24 - 35 Leonis Line Identification Details

Feature	Wavelength	Comments
	(Angstroms)	
H(11)	3770.6	Very well-defined higher order hydrogen Balmer line
Ηη	3835.4	Strong hydrogen Balmer line
Нζ	3889.1	Weak hydrogen Balmer line
Ca II	3933.7	Fraunhofer "K" ionized calcium line; extremely strong here
Ca II	3968.5	Fraunhofer "H" ionized calcium line; extremely strong here
Fe I/Mn I	4030-4036	Very weak iron/manganese blend
Sr II/Fe I	4078	Weak strontium/iron absorption
Fe I/Co I	4119	Extremely weak iron/cobalt absorption
Fe I	4132-4134	Extremely weak neutral iron blend
Fe I	4154-4157	Very weak neutral iron blend
Fe I	4187-4188	Extremely weak neutral iron blend
Fe I	4202	Common but weak neutral iron absorption
Fe I	4250	Very weak neutral iron absorption
CH	4299-4313	Fraunhofer "G" absorption due to molecular CH; common; very strong here
Fe	4383.6	Strong neutral iron line
Fe I/Ti II	4442-4444	Very weak iron/titanium blend
Ca I/Mn I/Fe I	4452-4464	Weak blend of calcium, manganese, and iron
Ti II/Fe II	4550	Common titanium/iron blend; moderately strong
Ti II	4569.8	Very weak ionized titanium line
Cr I/Ca I	4580	Extremely weak neutral chromium/calcium absorption
Fe I/Ti I/Mg I	4668-4703	Moderately strong blend of iron, titanium, and magnesium; very broad
Mn I/Ni I	4754-4756	Common manganese/nickel blend; weak
Fe I	4772.8	Weak neutral iron line
Нβ	4861.3	Fairly strong hydrogen Balmer line
Fe I	4891	Extremely subtle neutral iron absorption; only causing small deviation in curve; dubious identification
Fe I	4919	Weak neutral iron absorption; common
Fe I	4946.4-4957	Very weak neutral iron blend
Fe I/Ti I/Fe II	5006-5018	Common forest of blended iron and titanium; moderate in strength here
Ti I/Fe I/Ni I	5065-5080	Weak blend of titanium, iron, and nickel
Fe I	5099	Extremely weak neutral iron absorption
Mg I Triplet	5167.3-5183.6	Fraunhofer "b" absorption due to neutral sodium, plus iron; moderate to strong here
Cr I	5206-5208	Common neutral chromium blend, appears weak here
Fe I	5232.9	Fairly common neutral iron line; very weak

Feature	Wavelength	Comments
	(Angstroms)	
Fe I	5250-5251	Common neutral iron blend
Ca I/Cr I/Fe I	5262-5267	Weak blend of calcium, chromium, and iron
Fe I	5328	Very common neutral iron absorption; very weak
Fe I	5371.4	Extremely weak neutral iron line
Fe I	5393.2-5405	Weak to moderate strength iron blend
Fe I	5429.7-5446	Weak neutral iron blend
Ni I/Fe I	5476.9-5488	Weak nickel/iron blend
Ca I	5857	Weak neutral calcium feature; small but distinct
Na I Doublet	5890.0-5895.9	Fraunhofer "D2" and "D1" blended neutral sodium absorption
Ηα	6562.8	Moderately strong but ill-defined hydrogen Balmer line
"B" Telluric Oxygen	6869.0	Fraunhofer "B" absorption due to atmospheric oxygen
"A" Telluric Oxygen	7605.0	Fraunhofer "A" absorption due to atmospheric oxygen

Wien's Law will be used to obtain a temperature estimate. Once done, we will compare this with the expected values to ascertain how accurate the estimate is.

The continuum curve for 35 Leonis is presented below. The spectrum is in blue, and the labels have been removed for clarity. The apparent peak energy wavelength is marked.

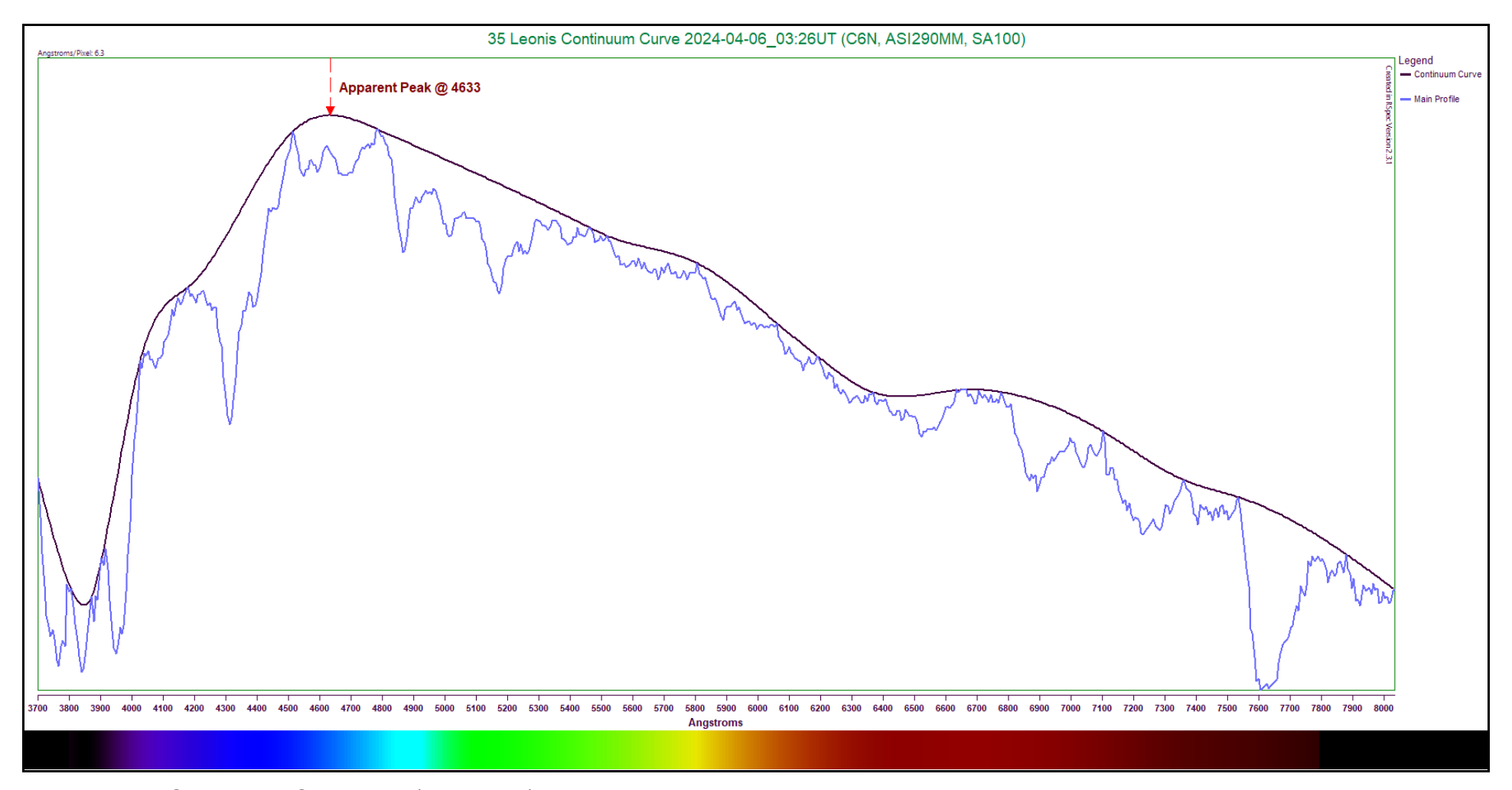


Figure 5.31 - Continuum Curve Plot (35 Leonis)

The apparent peak energy wavelength appears to lie at 4633 Angstroms. Using this value, we calculate an effective temperature of 6,255K. This estimate is a bit high from our expected range between 5,850K and 5,720K. Adopting the median value for comparison purposes (5,785K), our estimate is off by approximately 8.12%. The professionally determined temperature of the star is listed at 5,480K⁽³⁰⁾. Compared to this value, our temperature estimate is off by 14.14%.

Middle G-Type Stars

This subtype is where we begin to see temperatures cooler than that of our Sun. The Fraunhofer "K" and "H" ionized calcium lines remain very strong, and plenty of neutral iron absorptions will remain prevalent.

The middle G-type main sequence stars range in temperature between about 5,700K and 5,600K⁽²⁹⁾. These stars remain stable, staying on the main sequence for approximately 13,500 Myr⁽⁷⁾. They are still fairly close to our Sun in mass, weighing in between 0.985 and 0.970 times solar mass⁽²⁹⁾. They typically shine with luminosities between 0.9 and 0.8 times solar luminosity⁽²⁹⁾. Spectroscopically, these stars show very similar features to those of the early G-types. The hydrogen Balmer lines are weak, with the Fraunhofer "K" and "H" ionized calcium lines remaining very strong. The Fraunhofer "G" absorption due to molecular CH is also strong. Both the magnesium triplet and sodium doublet show gradual increases in strength. Other absorptions typically seen include lots of neutral iron, titanium, magnesium, calcium, and nickel. These weaker lines will vary in number and strength between specimens.

The star chosen as an example of this type is Delta Coronae Borealis in the constellation of Corona Borealis, the Northern Crown. This star is a yellow giant variable star. As such, the spectrum may show reduced line strengths, plus it may also give us a curve representing a lower temperature than expected. However, most of the main features should still be present.

The spectrum of Delta Coronae Borealis is presented below, along with a rectified profile in red.

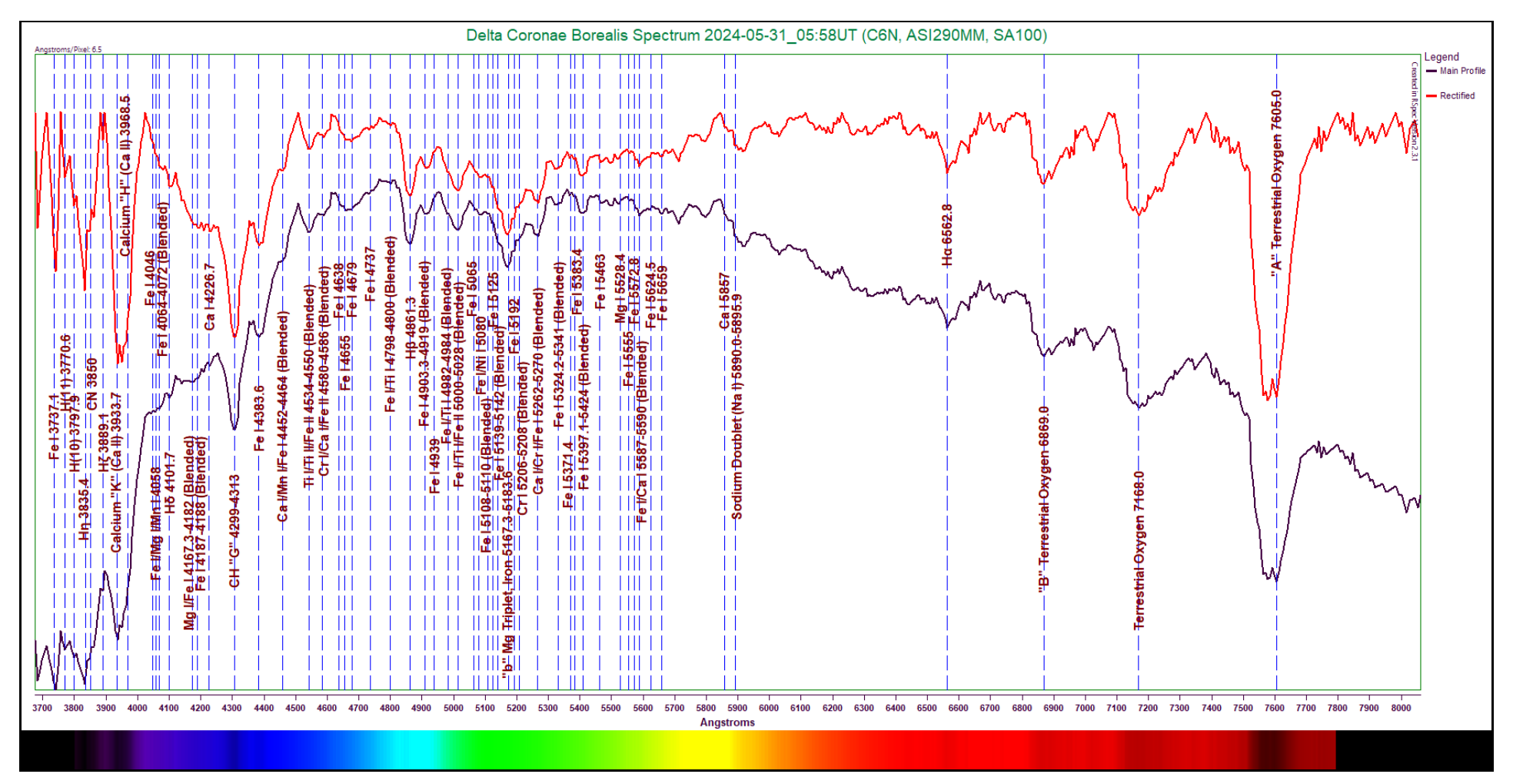


Figure 5.32: Delta Coronae Borealis Spectrum (6.3 Angstroms/pixel)
Capture Details: Exposure 637ms, Gain 196, 71% of 403 frames stacked, Integration Time 182s

Again, we see a spectrum that contains a high number of closely spaced lines, with many of them being iron blends. Be very careful when tracing labels, as it is too easy to lose track of the lines when they are so close together. We can see an exceptionally weak molecular CN absorption at 3850 Angstroms, just above the Hŋ line. The hydrogen Balmer lines that are visible appear only weak to moderate in strength. The Fraunhofer "K" and "H" lines at 3933.7 and 3968.5 Angstroms respectively are exceptionally strong, carving out a distinctive trench in the continuum. The Fraunhofer "G" molecular CH absorption at 4299-4313 Angstroms is also quite strong. The magnesium triplet at 5167.3-5183.6 Angstroms is strong as well, with several of its flanking iron lines very weakly evident around it. The sodium doublet at 5890.0-5895.9 Angstroms is moderately strong as well, with the neutral calcium line at 5857 Angstroms visible just below it. A high number of other, fainter metals are indicated here, including iron, magnesium, calcium, titanium, and chromium.

The following table shows the labeled absorptions found in the Delta Coronae Borealis spectrum.

Table 5.25 - Delta Coronae Borealis Line Identification Details

Feature	Wavelength	Comments
	(Angstroms)	
Fe I	3737.1	Moderately strong neutral iron line
H(11)	3770.6	Very weak higher order hydrogen Balmer line
H(10)	3797.9	Extremely weak higher order hydrogen Balmer line
Ηη	3835.4	Strong hydrogen Balmer line
CN	3850	Extremely weak molecular CN absorption
Нζ	3889.1	Very weak hydrogen Balmer line
Ca II	3933.7	Fraunhofer "K" ionized calcium line; extremely strong
Ca II	3968.5	Fraunhofer "H" ionized calcium line; extremely strong
Fe I	4046	Extremely weak neutral iron absorption
Fe I/Mg I/Mn I	4058	Extremely weak blend of iron, magnesium, and manganese
Fe I	4064-4072	Extremely weak neutral iron blend
Ηδ	4101.7	Weak hydrogen Balmer line
Mg I/Fe I	4167.3-4182	Extremely weak magnesium/iron absorption
Fe I	4187-4188	Fairly common neutral iron blend; extremely weak
Ca I	4226.7	Common neutral calcium line; weak
CH	4294-4313	Strong molecular CH absorption
Fe I	4383.6	Weak to moderate neutral iron line; common
Ca I/Mn I/Fe I	4452-4464	Weak blend of calcium, manganese, and iron
Ti I/Ti II/Fe II	4534-4550	Moderate strength titanium/iron blend
Cr I/Ca I/Fe II	4580-4588	Weak blend of of chromium, calcium, and iron
Fe I	4638	Weak neutral iron absorption
Fe I	4655	Weak neutral iron absorption
Fe I	4679	Weak neutral iron absorption
Fe I	4737	Extremely weak neutral iron absorption
Fe I/Ti I	4798-4800	Extremely weak iron/titanium blend
Нβ	4861.3	Moderate strength hydrogen Balmer line
Fe I	4903.3-4919	Weak to moderate neutral iron blend
Fe I	4939	Extremely subtle neutral iron absorption; dubious identification
Fe I/Ti I	4982-4984	Extremely subtle neutral iron/titanium blend; dubious identification
Fe I/Ti I/Fe II	5000-5028	Moderate iron/titanium blend; well-defined here
Fe I	5065	Extremely weak but neutral iron absorption; dubious identification
Fe I/Ni I	5080	Weak but quite common iron/nickel blend
Fe I	5108-5110	Extremely weak neutral iron absorption; dubious identification

Feature	Wavelength	Comments
	(Angstroms)	
Fe I	5139-5142	Weak neutral iron blend
Mg I Triplet	5167.3-5183.6	Fraunhofer "b" absorption due to magnesium and iron; strong
Fe I	5192	Very weak neutral iron absorption
Cr I	5206-5208	Weak but common neutral chromium blend
Ca I/Cr I/Fe I	5262-5270	Moderately strong calcium/chromium/iron blend
Fe I	5324.2-5341	Weak to moderate neutral iron blend
Fe I	5371.4	Extremely weak neutral iron line
Fe I	5383.4	Common neutral iron line
Fe I	5397.1-5424	Weak to moderate neutral iron blend
Fe I	5463	Weak neutral iron absorption
Mg I	5528.4	Very weak neutral magnesium line
Fe I	5555	Extremely weak neutral iron absorption; common
Fe I	5572.8	Extremely weak neutral iron line; can be difficult to spot
Fe I/Ca I	5587-5590	Common iron/calcium blend; weak here
Fe I	5624.5	Extremely weak neutral iron line; dubious identification
Fe I	5659	Very weak neutral iron absorption; dubious identification due to local continuum noise
Ca I	5857	Weak neutral calcium absorption
Na I Doublet	5890.0-5895.9	Fraunhofer "D2" and "D1" neutral sodium blend, with iron
Ηα	6562.8	Notable hydrogen Balmer line; well-defined in spite of continuum noise
"B" Telluric Oxygen	6869.0	Fraunhofer "B" absorption due to atmospheric oxygen
Telluric Oxygen	7168.0	Absorption due to atmospheric oxygen
"A" Telluric Oxygen	7605.0	Fraunhofer "A" absorption due to atmospheric oxygen

We will once more apply Wien's Law to obtain an effective temperature estimate. Several items of note may affect this effort. Firstly, the G-type stars often show enough veiling to make the determination of the peak energy wavelength problematic. Secondly, the star is not a main sequence star, but is an evolved giant. Such giants are normally cooler than their main sequence cousins.

Below is shown the best approximation of the continuum curve for Delta Coronae Borealis. The spectrum line is shown in blue, with the labels removed for clarity. The peak energy wavelength is labeled.

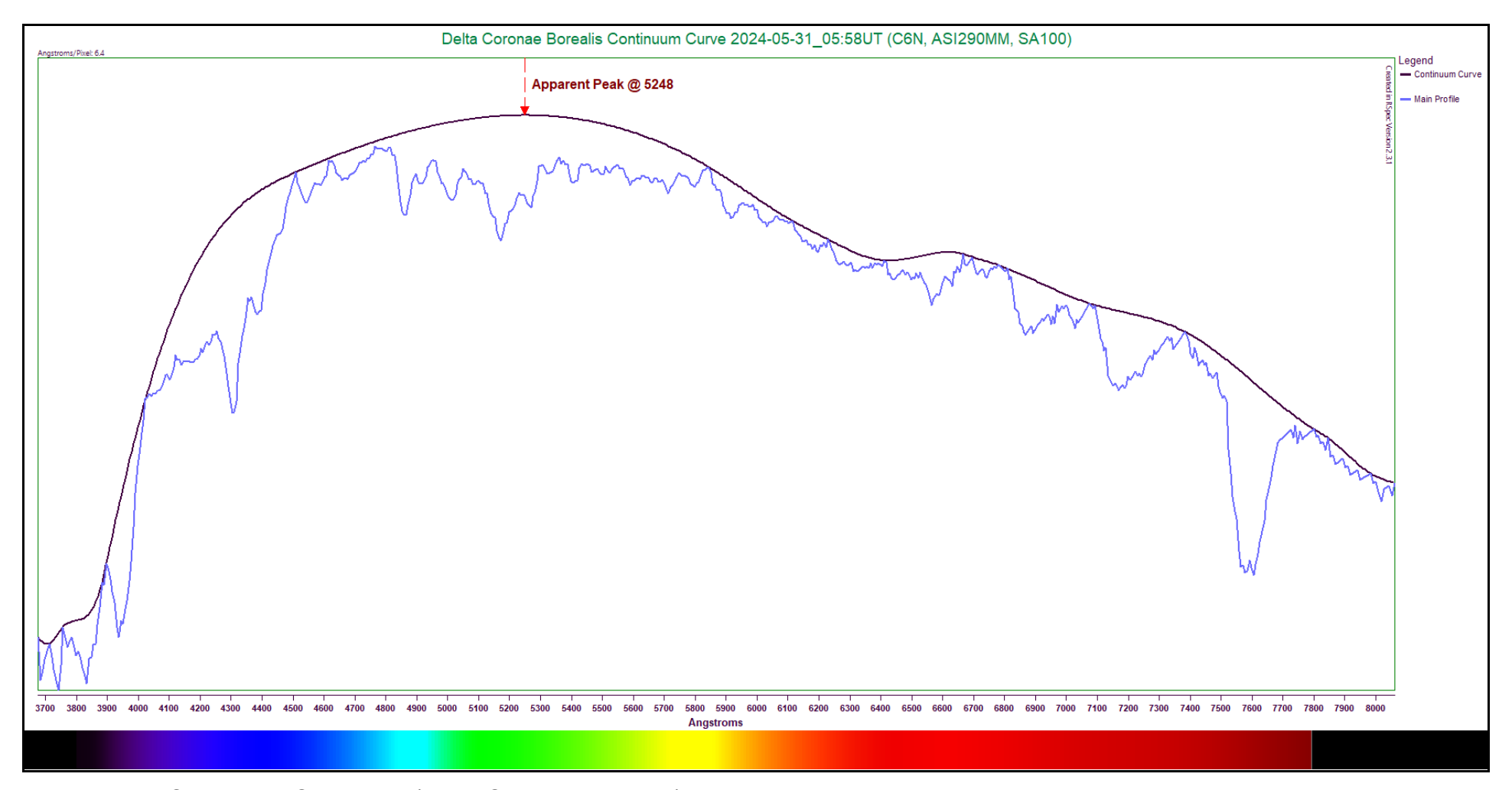


Figure 5.33 - Continuum Curve Plot (Delta Coronae Borealis)

The apparent peak energy wavelength appears to lie at 5248 Angstroms. However, it is easy to see that the tremendous amount of veiling in that area makes this a somewhat uncertain determination. Proceeding with this value, Wien's Law returns a temperature estimate of 5,521K. This is indeed a bit lower than our expected value between 5,700K and 5,600K. Using the median temperature in the expected range (5,650K), our estimate is off by approximately 2.28%. Considering the uncertainties involved, this is actually not a bad estimate. The professionally determined temperature of the star is listed as 5,180K⁽³¹⁾. Comparing the estimate to this value, we find we are off by 6.58%.

Late G-Type Stars

Late G-type stars are where we typically start to see some aspects of cooler stars begin to emerge. Molecular absorptions such as CN and CH become stronger. The Fraunhofer "K" and "H" ionized calcium lines continue to be very strong, and the spectral curve energy peak shifts farther toward longer wavelengths.

Main sequence stars of this type typically range in temperature between approximately 5,550K and 5,450K⁽²⁹⁾. They burn somewhat slowly, staying on the main sequence for approximately 16,750 Myr⁽⁷⁾. Their mass range is small, hovering between 0.95 and 0.94 times the solar value, with luminosities of approximately 0.75 down to 0.65 times that of our Sun. Their spectra begin to show some traces of the declining temperature, with ever-weakening hydrogen Balmer lines, very strong Fraunhofer "K" and "H" Ca II lines, and a very strong molecular CH absorption. The magnesium triplet and sodium doublet remain notable. The neutral iron so prevalent in earlier subtypes is tempered by more titanium, manganese, and other metals showing through.

The star chosen as an example for this type is Eta Piscium (commonly known as Alpherg) in the constellation of Pisces, the Fishes. This star is actually a binary system with a much dimmer companion of apparently undetermined type (no reference consulted at the time of writing revealed its properties). The brighter star is an evolved giant, and a variable star. Despite all of these complications, it should still yield a fair example of the subtype.

The spectrum of Eta Piscium (Alpherg) is presented below, along with a rectified profile in red.

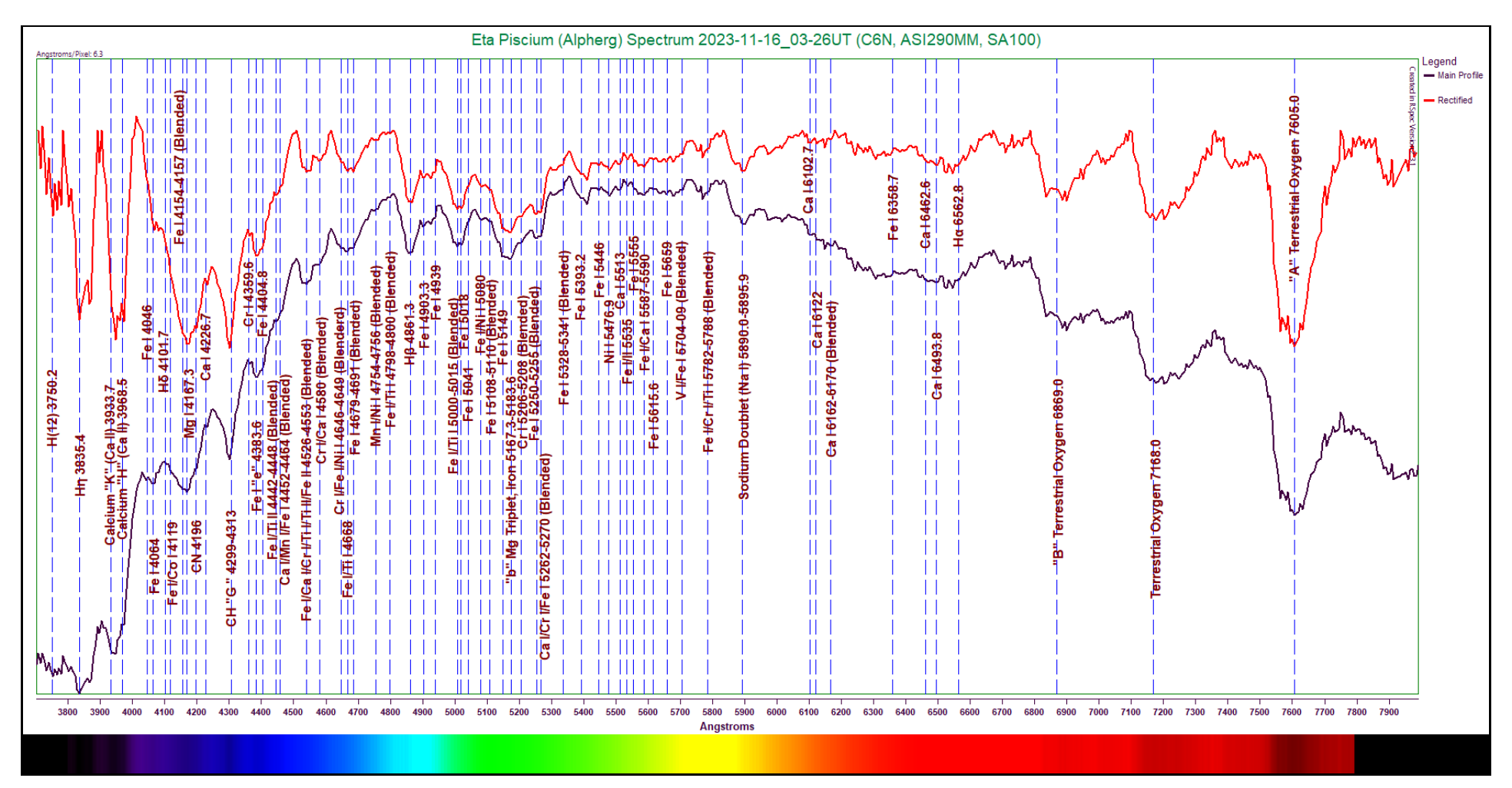


Figure 5.34: Eta Piscium (Alpherg) Spectrum (6.3 Angstroms/pixel)
Capture Details: Exposure 895ms, Gain 101, 20% of 304 frames stacked, Integration Time 54s

We can tell at a glance that the general shape of the spectral curve is shifted toward longer wavelengths compared to the earlier subtypes. The hydrogen Balmer absorptions are quite weak; even the H β line is only moderately present. The position of the H α absorption is marked, but it appears that the two neutral calcium lines below it are contributing to a broad trough. The Fraunhofer "K" and "H" lines at 3933.7 and 3968.5 Angstroms respectively are extremely strong. A mighty blend of iron and magnesium positioned at 4154-4167.3 Angstroms is carving out a respectable gouge in the continuum. The molecular CH "G" absorption appears very sharp and deep at 4299-4313 Angstroms. The magnesium triplet at 5167.3-5183.6 Angstroms is prominent, with flanking iron, chromium, and calcium absorptions serving to broaden the cut out of the continuum. The sodium doublet at 5890.0-5895.9 Angstroms is smaller, but still distinct. A good number of additional, fainter metals are indicated, many of them in the form of blended absorption features. These include iron, magnesium, molecular CN, calcium, chromium, manganese, nickel, and vanadium. Once again, the absorptions are crowded close together, so be very careful when tracing labels.

The following table shows the labeled absorptions in the spectrum of Eta Piscium (Alpherg).

Table 5.26 - Eta Piscium (Alpherg) Line Identification Details

Feature	Wavelength	Comments
	(Angstroms)	
H(12)	3750.2	Very weak higher order hydrogen Balmer line
Нη	3835.4	Weak but well-defined hydrogen Balmer line
Ca II	3934	Fraunhofer "K" ionized calcium line; extremely strong here
Ca II	3968	Fraunhofer "H" ionized calcium line; extremely strong here
Fe I	4046	Very weak neutral iron absorption
Fe I	4064	Weak neutral iron absorption
Нδ	4101.7	Extraordinarily subtle hydrogen Balmer line; dubious identification
Fe I/Co I	4119	Very subtle iron/cobalt absorption; dubious identification
Fe I	4154-4157	Very subtle neutral iron blend; dubious identification
Mg I	4167.3	Moderately strong neutral magnesium line
CN	4196	Subtle absorption due to molecular CN
Ca I	4226.7	Very common neutral calcium line; weak
CH	4299-4313	Fraunhofer "G" molecular CH absorption; strong
Cr I	4359.6	Very weak neutral chromium line
Fe I	4383.6	Fraunhofer "e" neutral iron line; very common
Fe I	4404.8	Subtle neutral iron line
Fe I/Ti II	4442-4448	Very weak iron/titanium blend
Ca I/Mn I/Fe I	4452-4464	Weak calcium/manganese/iron blend
Fe I/Ca I/Cr I/Ti I/Ti II/Fe II	4526-4553	Large and moderately strong blend of iron, calcium, chromium, and titanium
Cr I/Ca I	4580	Weak blend of chromium and calcium
Cr I/Fe I/Ni I	4646-4649	Common chromium/iron/nickel blend; weak to moderate
Fe I/Ti I	4668	Moderate strength neutral iron/titanium absorption
Fe I	4679-4691	Weak to moderate neutral iron blend
Mn I/Ni I	4754-4756	Fairly common but weak manganese/nickel absorption
Fe I/Ti I	4798-4800	Extremely weak iron/titanium blend
Нβ	4861.3	Weak to moderate hydrogen Balmer line
Fe I	4903.3	Very weak neutral iron line
Fe I	4939	Weak neutral iron absorption
Fe I/Ti I	5000-5015	Moderately strong forest of iron and titanium
Fe I	5018	Moderately strong neutral iron absorption
Fe I	5041	Very subtle neutral iron absorption; common; dubious identification
Fe I/Ni	5080	Very weak but common iron/nickel absorption
Fe I	5018-5110	Extremely weak but common iron/nickel blend

Feature	Wavelength	Comments
	(Angstroms)	
Mg I Triplet	5167.3-5183.6	Fraunhofer "b" absorption due to neutral magnesium, with iron; prominent; broadened by adjacent features
Cr I	5206-5208	Very weak neutral chromium blend; common
Fe I	5250-5255	Moderate strength neutral iron blend
Ca I/Cr I/Fe I	5262-5270	Moderately strong calcium/chromium/iron blend
Fe I	5328-5341	Weak iron blend
Fe I	5393.2	Extremely subtle iron line; dubious identification
Fe I	5446	Extremely weak neutral iron absorption
Ni I	5476.9	Weak neutral nickel line
Ca I	5513	Very weak neutral calcium absorption
Fe I/II	5535	Extremely weak iron absorption
Fe I	5555	Weak neutral iron absorption
Fe I/Ca I	5587-5590	Weak but common iron/calcium blend
Fe I	5615.6	Extremely weak neutral iron line; dubious identification
Fe I	5659	Extremely weak neutral iron absorption; very dubious identification
V I/Fe I	5704-5709	Fairly common vanadium/iron blend; weak
Fe I/Cr I/Ti I	5782-5788	Weak blend of iron, chromium, and titanium; weak
Na I Doublet	5890.0-5895.9	Very common blend of Fraunhofer "D2" and "D1" neutral sodium lines
Ca I	6102.7	Common neutral calcium line; weak
Ca I	6122	Common neutral calcium absorption; very weak
Ca I	6162-6170	Extremely weak neutral calcium blend; dubious identification due to continuum noise
Fe I	6358.7	Very weak neutral iron line
Ca I	6462.6	Very weak neutral calcium line
Ca I	6493.8	Very weak neutral calcium line
Ηα	6562.8	Weak hydrogen Balmer line; causing dip in continuum with adjacent calcium lines
"B" Telluric Oxygen	6869.0	Fraunhofer "B" absorption due to atmospheric oxygen
Telluric Oxygen	7168.0	Absorption due to atmospheric oxygen
"A" Telluric Oxygen	7605.0	Fraunhofer "A" absorption due to atmospheric oxygen

Wien's Law will be used to obtain an effective temperature estimate for the star. We must note that there is a high amount of continuum veiling occurring, which may make the peak energy wavelength difficult to nail down. Also, since the star is a giant, we can expect our answer to be a little short of what is normal for main sequence specimens.

The plotted continuum curve for Eta Piscium (Alpherg) is presented below. The spectrum line is presented in blue, with the labels removed for clarity. The apparent peak energy wavelength is indicated in red.

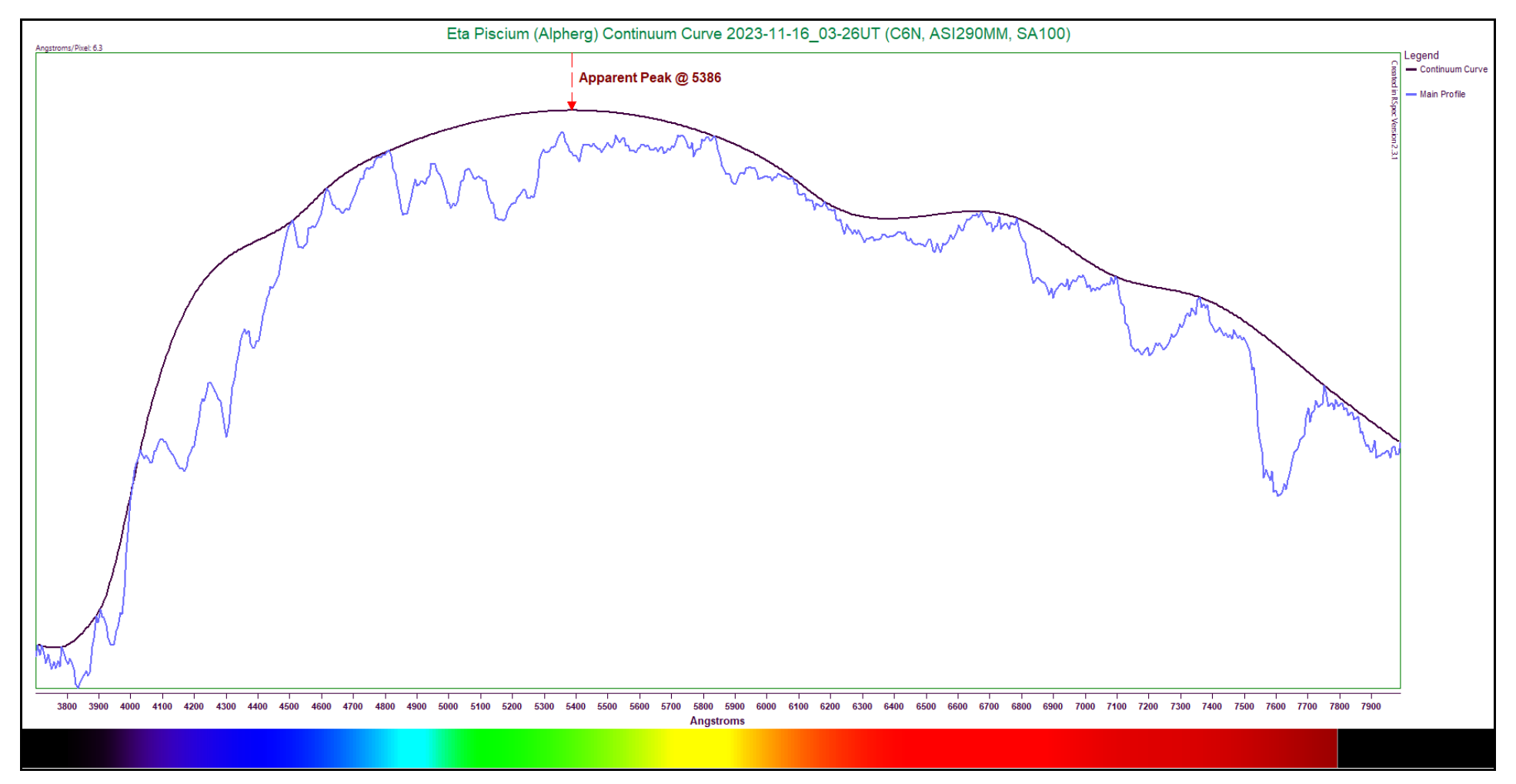


Figure 5.35 - Continuum Curve Plot (Eta Piscium)

As expected, we once again see a lot of absorptions in the area that visually seems to indicate where the peak energy wavelength resides. However, the drawn curve shows a peak wavelength of 5386 Angstroms. Using this value, Wien's Law provides an effective temperature of approximately 5,380K. This is below the expected value somewhere between 5,450K, probably due to the evolved nature of the giant star. Comparing our result with the median temperature in the expected range (5,500K), we find our estimate is off by approximately 2.18%. Not bad. The professionally determined temperature of the star is listed as 4,937K⁽³²⁾. Comparing our estimate to this value, we are off by 8.97%.

5.10 Spectral Type G/K Stars (Very Late G and Very Early K)

Stars falling into this custom category represent a midway point between yellow stars like our own Sun and the deeper orange hue of the cooler K-types. Here is where the Fraunhofer "K" and "H" lines begin to diminish in intensity. The plethora of neutral iron lines so prevalent in the G-type stars begins to thin out here, as well. When viewed through a telescope, these stars show a deep yellow or slight orange tint. This can make for attractive visual observation, especially if the star is close to a star of significantly different color.

These stars have considerably lower temperatures than our Sun, between 5,380K and 5,280K^(29,33). They have lifespans of around 20,000 Myr⁽⁷⁾. Their masses are typically between 0.90 and 0.88 times solar mass^(29,33). They are also dimmer than our star, shining with luminosities roughly between 0.55 and 0.45 times the solar value^(29,33).

The spectra show continuing diminishment of the hydrogen Balmer lines. A good number of metals, particularly iron, are still visible. Some of the molecular absorptions are more prevalent in the K-types.

The star chosen to represent this type is indicated here:

Table 5.27 - Representative FG/K Star

i dia i di a di a di a di a di a di a d	O 7. C O 10.1
Subtype	Star
Very Late G/Very Early K	Kappa Cygni (Fawaris I)

G/K Stars (Very Late G and Very Early K)

The very late G-type and very early K-type stars begin to resemble the K-types to follow. The incredibly closely packed iron absorptions typical of the G-types begin to dissipate, which makes the spectral features easier to identify. The temperatures fall, and the peak energy wavelength shifts to longer wavelengths—usually lying pretty close to the middle of the wavelength range in our results.

Main sequence specimens of this type have a temperature on the order of 5,300K^(29,33). Their stay on the main sequence is approximately 20,000 Myr⁽⁷⁾. Their masses are approximately 0.9 times that of our Sun, while their luminosities are generally about 0.5 times the solar value^(29,33). The spectra of these stars usually show several molecular bands, such as CN and CH. The ionized Fraunhofer "K" and "H" ionized lines continue to be strong, though they can appear slightly weakened compared to the earlier G-types. The magnesium triplet and sodium doublet remain fairly strong, while the hydrogen Balmer lines continue to fade; fewer of the hydrogen Balmer lines can typically be seen in these specimens. Fainter metals often visible include iron, chromium, titanium, manganese, calcium, and vanadium.

The specimen chosen to demonstrate these features is Kappa Cygni, also called Fawaris I, in the constellation of Cygnus, the Swan. This particular star is an evolved giant, which may produce a few effects in the spectrum that we need to be aware of. First, some of the lines may appear lessened in the results due to reduced gas pressure. Secondly, the star is likely to show a subnormal temperature when compared to main sequence stars of the same subtype. Still, the main characteristics should still be easily visible.

The spectrum of Kappa Cygni (Fawaris I) is presented below, along with a rectified profile in red.

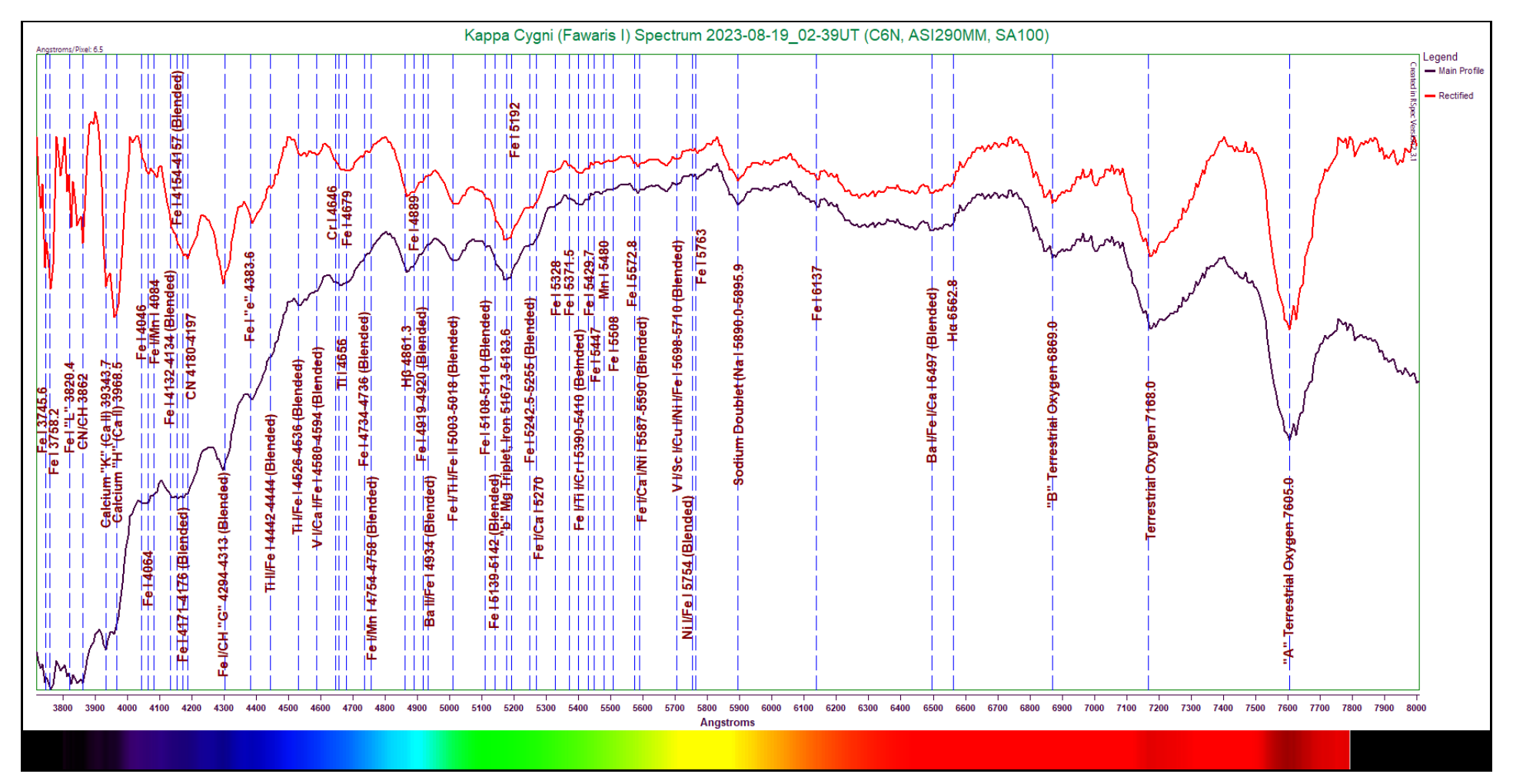


Figure 5.36: Kappa Cygni (Fawaris I) Spectrum (6.4 Angstroms/pixel)
Capture Details: Exposure 496ms, Gain 196, 55% of 369 frames stacked, Integration Time 100s

Even a cursory glance shows that the number of iron absorptions in this spectrum is greatly reduced from what was visible in the earlier G-type stars. The hydrogen Balmer absorptions are definitely weak here; the H β line continues to show a reduced profile compared to the earlier stars. The Fraunhofer "K" and "H" ionized calcium lines at 3933.7 and 3968.5 Angstroms respectively are still strong, but these also show some weakening compared to the earlier stars. The Fraunhofer "G" CH absorption in this is blended with a neutral iron line. A notable iron blend can be seen in the 5003-5018 Angstroms area. The magnesium triplet is easily recognized at 5167.3-5183.7 Angstroms, and the sodium doublet at 5890.0-5895.9 Angstroms is also well-defined. Some other faint features present include iron, molecular CN, titanium, vanadium, chromium, barium, manganese, and nickel.

The following table lists the absorptions labeled in the Kappa Cygni (Fawaris I) spectrum.

Table 5.28 - Kappa Cygni (Fawaris I) Line Identification Details

Feature	Wavelength	Comments
	(Angstroms)	
Fe I	3745.6	Extremely weak neutral iron line
Fe I	3758.2	Weak neutral iron line
Fe I	3820.4	Fraunhofer "L" neutral iron line
CN/CH	3862	Molecular absorption due to CN and CH; weak to moderate strength
Ca II	3933.7	Fraunhofer "K" ionized calcium line; still strong here
Ca II	3968.5	Fraunhofer "H" ionized calcium line; still strong here
Fe I	4046	Extremely weak neutral iron absorption
Fe I	4064	Very weak neutral iron absorption
Fe I/Mn I	4084	Weak iron/manganese absorption
Fe I	4132-4134	Weak neutral iron blend; contributing to broad dip in continuum
Fe I	4154-4157	Weak neutral iron blend; contributing to broad dip in continuum
Fe I	4171-4176	Weak neutral iron blend; contributing to broad dip in continuum
CN	4180-4197	Molecular absorption due to CN; contributing to broad dip in continuum
Fe I/CH	4294-4313	Neutral iron absorption blended with molecular CH
Fe I	4383.6	Fraunhofer "e" neutral iron line; weak to moderate strength
Ti II/Fe I	4442-4444	Very weak titanium/iron blend
Ti I/Fe I	4526-4569	Weak titanium/iron blend
V I/Ca I/Fe I	4580-4594	Weak blend of vanadium, calcium, and iron
Cr I	4646	Common but very weak neutral chromium absorption
Τi I	4656	Very weak neutral titanium absorption
Fe I	4679	Moderate strength neutral iron absorption
Fe I	4734-4736	Common but extremely weak iron blend
Fe I/Mn I	4754-4758	Common but extremely weak iron/manganese blend
Нβ	4861.3	Weak to moderate hydrogen Balmer line
Fe I	4889	Extremely weak neutral iron absorption
Fe I	4919-4920	Extremely weak iron blend
Ba II/Fe I	4934	Very subtle barium/iron absorption; dubious identification
Fe I/Ti I/Fe II	5003-5018	Weak to moderate blend of iron and titanium
Fe I	5108-5110	Very weak neutral iron blend
Mg I Triplet	5167.3-5183.6	Fraunhofer "b" absorption due to neutral magnesium, with some iron
Fel	5192	Weak to moderate neutral iron absorption
Fe I	5242.5-5255	Weak neutral iron blend
Fe I/Ca I	5270	Weak iron/calcium absorption

Feature	Wavelength	Comments
	(Angstroms)	
Fe I	5328	Weak but broad neutral iron absorption
Fe I	5371.5	Extremely weak iron line
Fe I/Ti I/Cr I	5390-5410	Very blend of iron, titanium, and chromium
Fe I	5429.7	Extremely weak neutral iron line
Fe I	5447	Extremely weak neutral iron absorption
Mg I	5480	Very weak neutral magnesium absorption
Fe I	5508	Extremely weak neutral iron absorption; dubious identification
Fe I	5572.8	Extremely weak neutral iron line
Fe I/Ca I/Ni I	5587-5590	Weak iron/calcium/nickel blend
V I/Sc I/Cu I/Ni I/Fe I	5698-5710	Weak blend of vanadium, scandium, copper, nickel, and iron
Ni I/Fe I	5754	Extremely weak nickel/iron absorption; dubious identification
Fe I	5763	Very weak neutral iron absorption
Sodium Doublet	5890.0-5895.9	Common blended Fraunhofer "D2" and "D1" neutral sodium lines
Fe I	6137	Very weak neutral iron absorption
Ba I/Fe I/Ca I	6497	Very weak barium/iron/calcium blend; more prevalent in cooler stars
Ηα	6562.8	Very weak hydrogen Balmer line
"B" Telluric Oxygen	6869.0	Fraunhofer "B" absorption due to atmospheric oxygen
Telluric Oxygen	7168.0	Absorption due to atmospheric oxygen
"A" Telluric Oxygen	7605.0	Fraunhofer "A" absorption due to atmospheric oxygen

Using Wien's Law, we will calculate an effective temperature estimate. Judging by the general shape of the spectral curve, line veiling should be less of an issue than was encountered in the previous G-types. However, we must remember that the star is a giant, and is therefore likely to have a lower temperature than expected.

The plotted continuum curve for Kapp Cygni (Fawaris I) is presented below. The spectrum line is presented in blue, with the labels removed for clarity. The apparent peak energy wavelength is indicated in red.

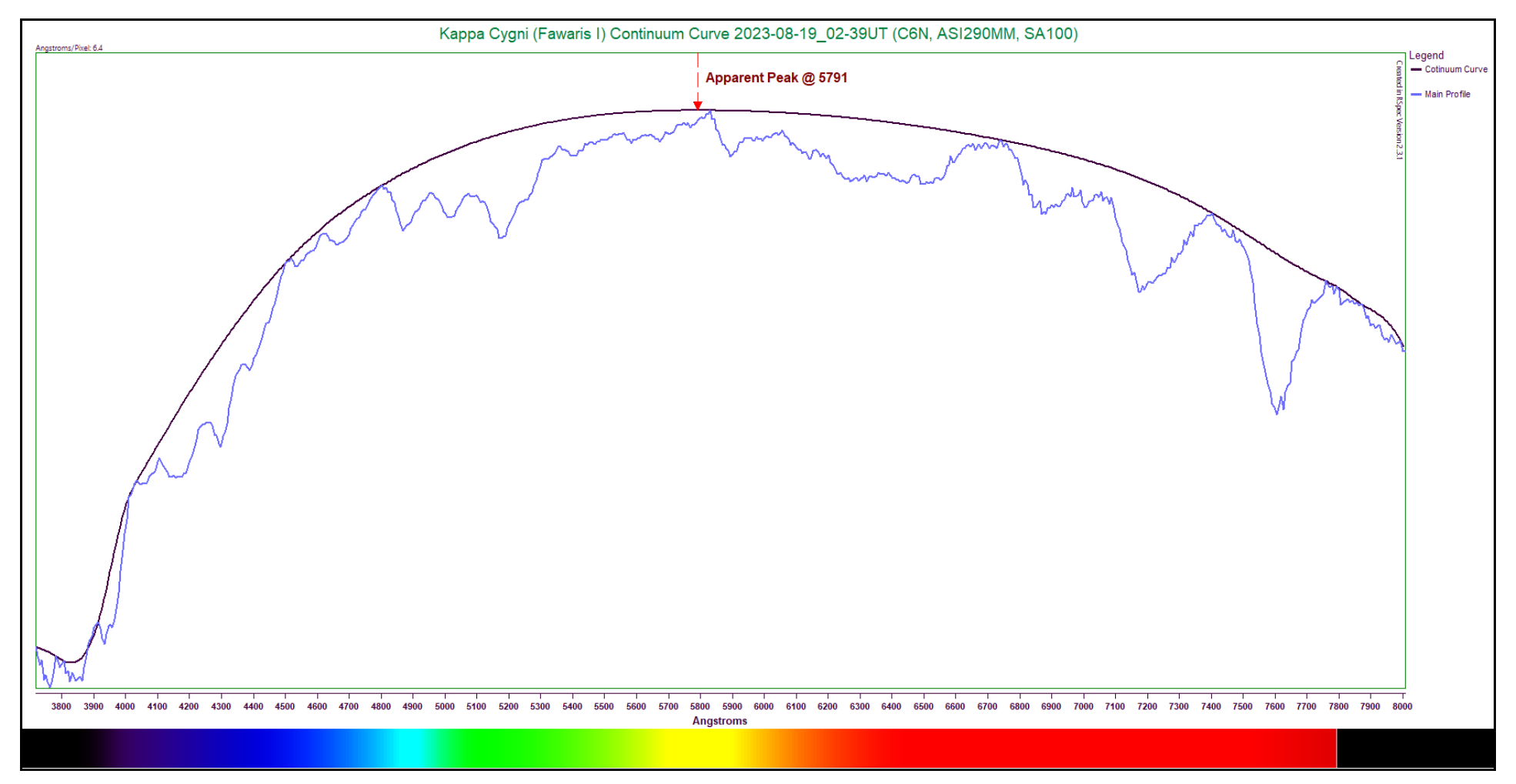


Figure 5.37 - Continuum Curve Plot (Kappa Cygni)

The continuum curve for this specimen appears elegantly smooth. The apparent peak energy wavelength is easily determined here, and appears to lie at 5791 Angstroms. Utilizing this, we calculate an effective temperature of approximately 5,004K. This is indeed lower than the typical temperature for main sequence specimens—5,300K. Our calculated temperature is approximately 5.58% off the mark. The professionally determined temperature of the star is listed as 5,021K⁽³⁴⁾. Adopting this value for comparison, we find our estimate is only off by 0.34%, or 17K!

5.11 Spectral Type K Stars

K-type stars rank sixth on the descending MK order of temperature. They are cooler than our Sun, and considerably less luminous. Through a telescope, these stars appear yellowish-orange or orange. This has led to them sometimes being called orange dwarfs.

K-type stars have typical masses ranging from 0.85 down to 0.62 times the mass of the Sun⁽³³⁾. These lower masses allow them to stay on the main sequence for quite a long time, estimated at more than 20,000 Myr⁽⁷⁾. This is longer than the estimated age of the universe, making the estimate extremely difficult to verify. They only possess a fraction of our Sun's luminosity, ranging from 0.40 to 0.09 times solar luminosity⁽³³⁾. This makes them a bit difficult to spot with amateur telescopes unless they are evolved into subgiants or giants, with a corresponding increase in luminosity. For this reason, most of the examples provided for these stars will not be main sequence specimens, but rather evolved and more luminous ones. When they die, these stars will follow much the same path as their earlier G-type cousins, only on a much longer time scale. They evolve into red giants, slough off their outer layers into planetary nebulae, and leave behind low-mass white dwarfs.

The temperatures of these stars range from approximately 5,150K down to about 4,000K⁽³³⁾. Their peak energy output lies in the longer wavelength range, especially for the later subtypes which have their energy peak very near the infrared. Still, Wien's Law can provide reasonably accurate temperature estimates for the earlier subtypes, as will be demonstrated.

K-type stars demonstrate a fairly dramatic change in spectroscopic characteristics when working from earlier subtypes to later ones. Molecular bands due to CH and CN continue to be strong, while the ionized Fraunhofer "K" and "H" ionized calcium lines weaken considerably. The hydrogen Balmer lines fade, with fewer of them being distinguishable at all. The magnesium triplet and sodium doublet continue to be evident here, though. The later subtypes begin to show TiO molecular bands, indicating a sort of transition to the later M-type stars. These later subtypes begin to strongly resemble the M-types.

No examples of late K-type stars were visible from the observer's location as the data was being collected, so there will be no example of this subtype provided.

The stars chosen to represent the various K-type stars are listed here by subtype:

Table 5.29 - Representative K Stars

Subtype	Star
Early	Alpha Arietis (Hamal)
Middle	Delta Piscium (Kuton I)
Late	None available

Early K-Type Stars

Early K-type stars continue to show a march toward ever-lower temperatures, as well as lower luminosity. The shapes of their energy distribution curves are shifted toward longer wavelengths, moving the peak energy farther to the right. The molecular absorptions from CN and CH molecules continue to be present.

The early K-type main sequence stars have temperatures in the range of approximately 5,150K down to about 4,800K⁽³³⁾. They are very long-lived stars, existing for more than 20,000 Myr⁽⁷⁾. They possess masses ranging from 0.85 down to about 0.80 times that of our Sun⁽³³⁾. They are also dim, with luminosities of only about 0.4 times down to 0.3 times solar value⁽³³⁾. The spectra of these stars show strong CN and CH molecular absorptions. The hydrogen Balmer lines are muted, with many not visible at all. The Fraunhofer "K" and "H" ionized calcium lines are still moderately strong, but appear weakened when compared to those visible in the G-type stars. Lots of neutral iron and titanium are typically visible, along with some chromium, calcium, vanadium, and barium.

The specimen chosen to demonstrate this subtype is Alpha Arietis, also called Hamal, in the constellation of Aries, the Ram. This star is not a main sequence star, but is rather a giant. This indicates a possible reduction in some of the absorptions, plus an evident temperature a bit lower than what would be expected of a main sequence star of the same subtype.

The spectrum of Alpha Arietis (Hamal) is presented below, along with a rectified profile shown in red.

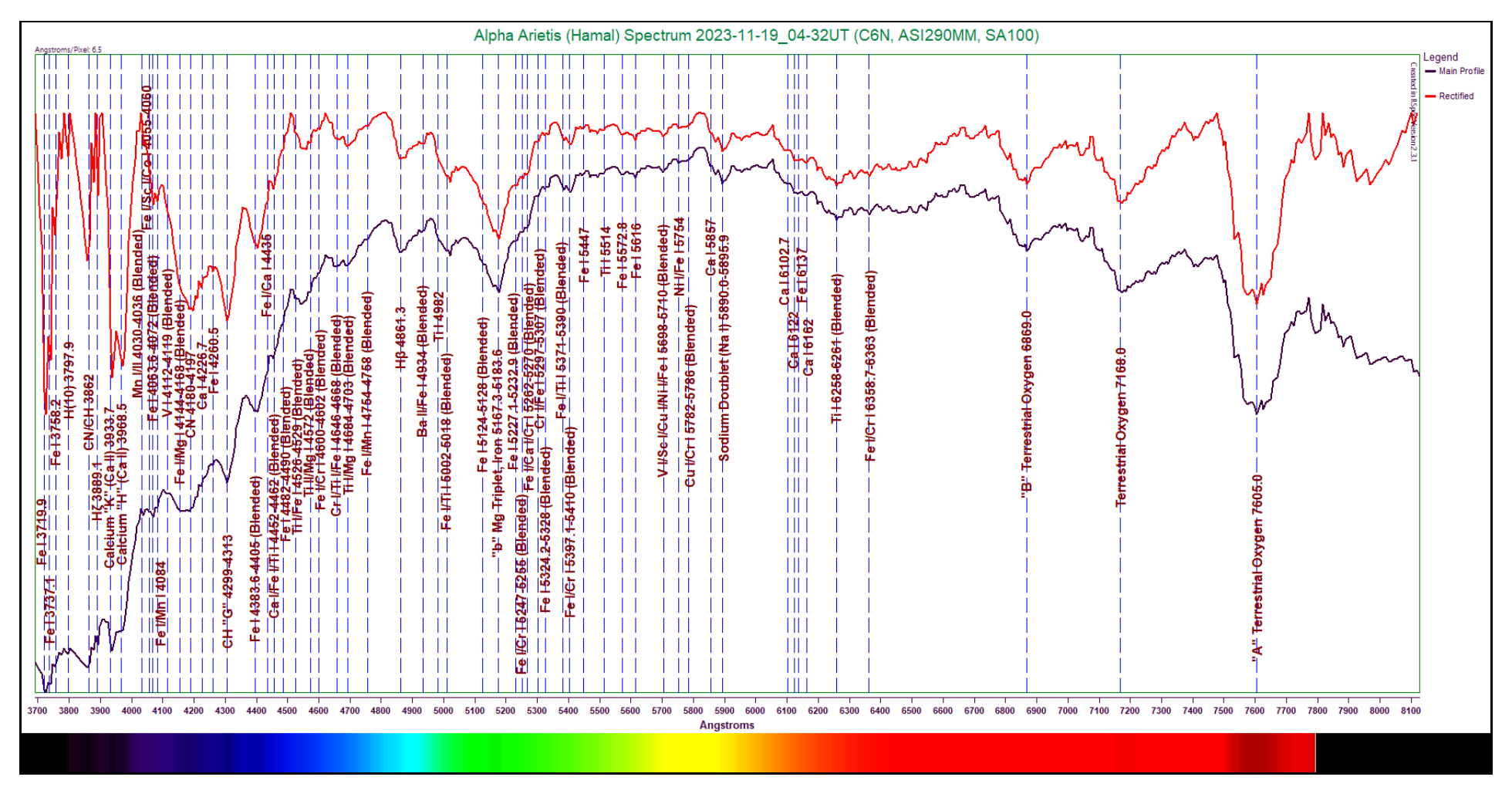


Figure 5.38: Alpha Arietis (Hamal) Spectrum (6.3 Angstroms/pixel)
Capture Details: Exposure 481ms, Gain 21, 50% of 507 frames stacked, Integration Time 121s

A glance at the overall shape of the spectrum curve indicates a peak energy wavelength near the upper-middle portion of the range. This verifies a temperature somewhat lower than that obtained for the previous G-types. Only two of the hydrogen Balmer lines are visible here—the $H\zeta$ and $H\beta$ lines, and these are definitely weak. The Fraunhofer "K" and "H" lines continue to be strong, but they do appear a little weaker than in the G-type stars. An impressive dip in the continuum can be seen in the 4144-4197 Angstroms range; this is caused by a combination of iron, magnesium, and the molecular CN absorptions. The Fraunhofer "G" absorption due to molecular CH at 4299-4313 Angstroms remains moderately sharp and deep. The magnesium triplet at 5167.3-5183.6 Angstroms is obvious here, with several iron lines flanking it. The overall effect makes the group of absorptions appear very deep. The sodium doublet at 5890.0-5895.9 Angstroms appears much smaller, but very sharp. The neutral calcium line just below it at 5857 Angstroms is also visible. Other faint metals present include iron, manganese, vanadium, calcium, titanium, chromium, barium, and copper. Many of the labeled absorptions are closely spaced, so use caution when tracing them.

The following table lists the absorptions labeled in the spectrum of Alpha Arietis (Hamal).

Table 5.30 - Alpha Arietis (Hamal) Line Identification Details

Feature	Wavelength	Comments
	(Angstroms)	
Fe I	3719.9	Moderately strong neutral iron line
Fe I	3737.1	Relatively weak neutral iron line
Fe I	3758.2	Weak neutral iron line
H(10)	3797.9	Weak to moderate higher order hydrogen Balmer line
Ĥζ	3889.1	Weak hydrogen Balmer line
CN/CH	3862	Moderate molecular absorption due to CN and CH
Ca II	3933.7	Fraunhofer "K" ionized calcium line; moderately strong
Ca II	3968.5	Fraunhofer "H" ionized calcium line; moderately strong
Mn I/II	4030-4036	Common blended manganese absorption
Fe I/Sc I/Co I	4055-4060	Very weak blend of iron, scandium, and cobalt
Fe I	4063.6-4072	Extremely weak blend of neutral iron lines
Fe I/Mn I	4084	Common but very weak iron/manganese blend
VI	4112-4119	Common neutral vanadium absorption; weak here
Fe I/Mg I	4144-4168	Moderately strong blended absorption of iron and magnesium
CN	4180-4197	Molecular CN absorption; common in cooler stars; moderately strong
Ca I	4226.7	Very weak but common neutral calcium line
Fe I	4260.5	Very weak neutral iron line
CH	4299-4313	Fraunhofer "G" absorption due to molecular CH; common in these cooler stars
Fe I	4383.6-4405	Moderate neutral iron blend
Fe I/Ca I	4435	Fairly common iron/calcium blend; subtle, only causing small diversion in continuum
Ca I/Fe I/Ti I	4452-4462	Very weak calcium/iron/titanium blend
Fe I	4482-4490	Very subtle neutral iron blend
Ti I/Fe I	4526-4529	Very weak titanium/iron blend
Ti I/Mg I	4572	Common titanium/magnesium absorption; very weak
Fe I/Cr I	4600-4602	Common iron/chromium blend; weak
Cr I/Ti I/Fe I	4646-4668	Weak blend of chromium, titanium, and iron
Ti I/Mg I	4684-4703	Weak titanium/magnesium blend
Fe I/Mn I	4754-4758	Extremely weak iron/manganese blend
Нβ	4861.3	Moderate hydrogen Balmer line
Ba II/Fe I	4934	Common barium/iron absorption; weak
Til	4982	Subtle neutral titanium absorption
Fe I/Ti I	5002-5018	Moderate iron/titanium blend; common in low-resolution spectra
Fe I	5124-5128	Very weak neutral iron blend

Feature	Wavelength	Comments
	(Angstroms)	
Mg I Triplet	5170	Fraunhofer "b" absorption due to neutral magnesium, with iron
Fe I	5227.1-5232.9	Very weak blend of neutral iron lines
Fe I/Cr I	5247-5255	Extremely weak iron/chromium blend
Fe I/Ca I/Cr I	5262-5270	Weak iron/calcium/chromium blend
Cr I/Fe I	5297-5307	Weak blend of chromium and iron
Fe I	5324.2-5328	Weak neutral iron blend
Fe I/Ti I	5371-5390	Weak iron/titanium blend
Fe I/Cr I	5397.1-5410	Weak to moderate blend of neutral iron and chromium
Fe I	5447	Very weak neutral iron absorption; common, but can be difficult to spot
Ti I	5514	Extremely weak titanium absorption
Fe I	5572.8	Weak neutral iron line
Fe I	5616	Weak but sharp neutral iron absorption
V I/Sc I/Cu I/Ni I/Fe I	5698-5710	Weak blend of vanadium, scandium, copper, nickel, and iron; common blend in low-resolution spectra
Ni I/Fe I	5754	Common but weak nickel/iron absorption
Cu I/Cr I	5782-5786	Weak blend of copper and chromium
Ca I	5857	Neutral calcium absorption; fairly common, but not always distinct
Na I Doublet	5890-96	Fraunhofer "D2" and "D1" neutral sodium blend; weak to moderate, but distinct
Ca I	6102.7	Common neutral calcium line; very weak here
Ca I	6122	Common neutral calcium absorption; weak
Fe I	6137	Fairly common neutral iron absorption; weak here; not always distinguishable
Ca I	6162	Common but weak neutral calcium absorption
Ti I	6258-6363	Weak titanium blend
Fe I/Cr I	6358.7-6363	Very weak iron/chromium blend
"B" Telluric Oxygen	6869.0	Fraunhofer "B" absorption due to atmospheric oxygen
Telluric Oxygen		Absorption due to atmospheric oxygen
"A" Telluric Oxygen	7605.0	Fraunhofer "A" absorption due to atmospheric oxygen

Making use of Wien's Law, we will calculate an effective temperature for the star. This star is an evolved giant, so we must expect the resulting temperature to be perhaps a bit lower than the expected value for a main sequence star of the same subtype.

The continuum curve for Alpha Arietis (Hamal) is presented below. The continuum curve appears in black, with the spectrum in blue for comparison. The labels have been removed for clarity. The peak energy wavelength is indicated in red.

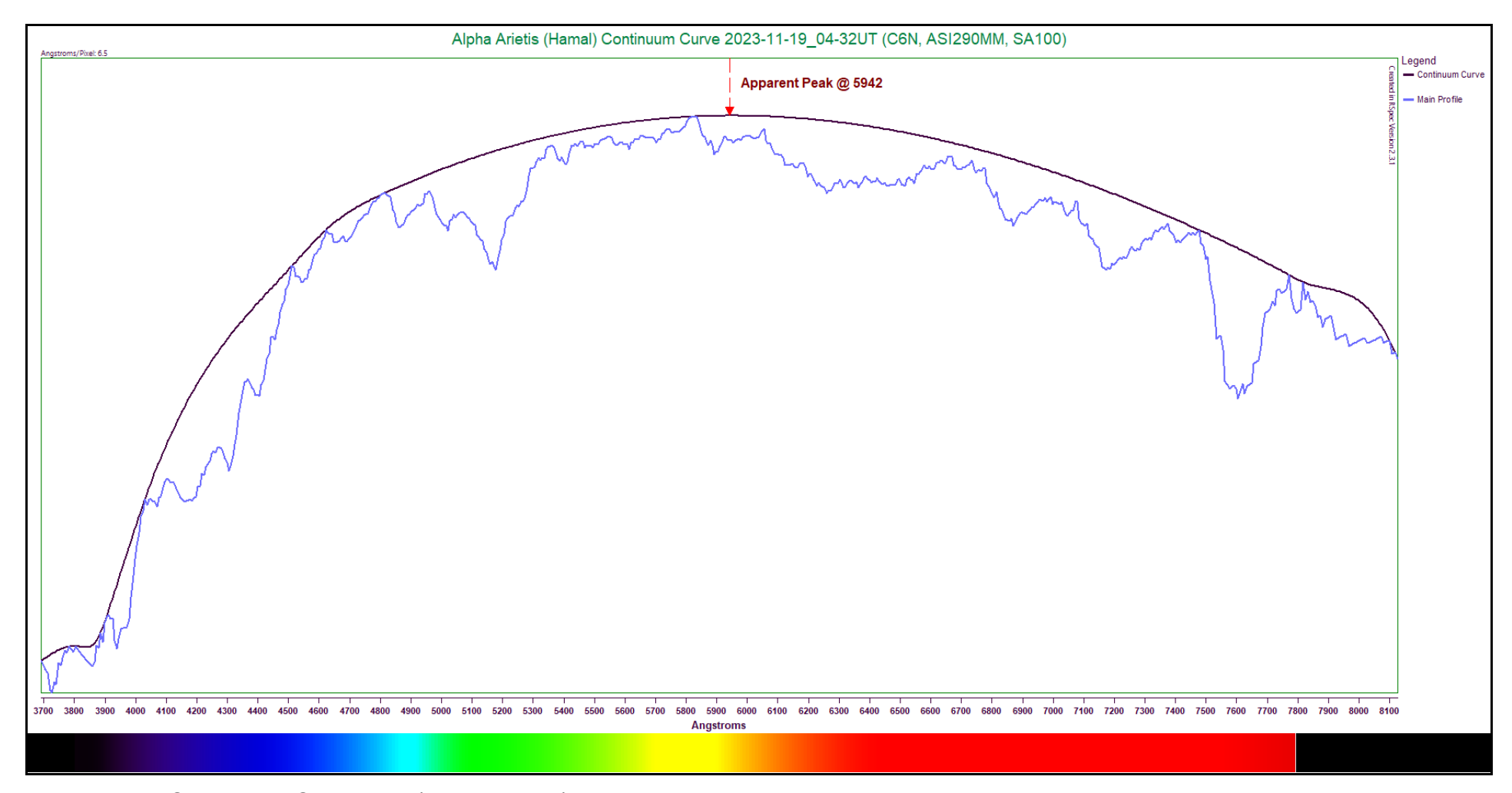


Figure 5.39 - Continuum Curve Plot (Alpha Arietis)

Examination of the continuum curve indicates a peak near 5942 Angstroms. Using this value, Wien's Law returns an effective temperature estimate of 4,877K. This result is within our expected value between 5,150K and 4,800K. Our estimate deviates from the median expected value (4,975K) by about 1.97%. The listed temperature for the star is 4,553K⁽³⁵⁾. Compared to this more precise temperature, we find our estimate is off by approximately 7.12%.

Middle K-Type Stars

The middle K-type stars show ever-decreasing temperatures. This is reflected in the shapes of their continua, with the peak energy wavelengths marching quickly toward longer wavelengths. Molecular CN and CH absorptions continue to be visible, but are reduced in intensity. Some emergent TiO bands can be evident.

Main sequence stars of this type typically show temperatures of 4,600K down to around 4,300K⁽³³⁾. They are extremely long-lived, possessing masses ranging from only 0.73 to 0.69 times the solar value⁽³³⁾. They are also very dim, having luminosities of roughly only 0.20 to 0.15 times solar luminosity⁽³³⁾. Their spectra show molecular absorptions from CN and CH, and some small TiO features can also sometimes be seen. The hydrogen Balmer lines are very weak or entirely absent, and the Fraunhofer "K" and "H" ionized calcium lines are severely reduced in strength. Other metal absorptions typically found include iron, manganese, magnesium, chromium, vanadium, and calcium.

The specimen chosen as an example of this subtype is Delta Piscium, also called Kuton 1, in the constellation of Pisces, the Fishes. This star is an evolved giant. This indicates we may see an apparent reduction in the strengths of some of the absorption features, along with a somewhat reduced temperature.

The spectrum of Delta Piscium (Kuton 1) is presented below, along with a rectified profile shown in red.

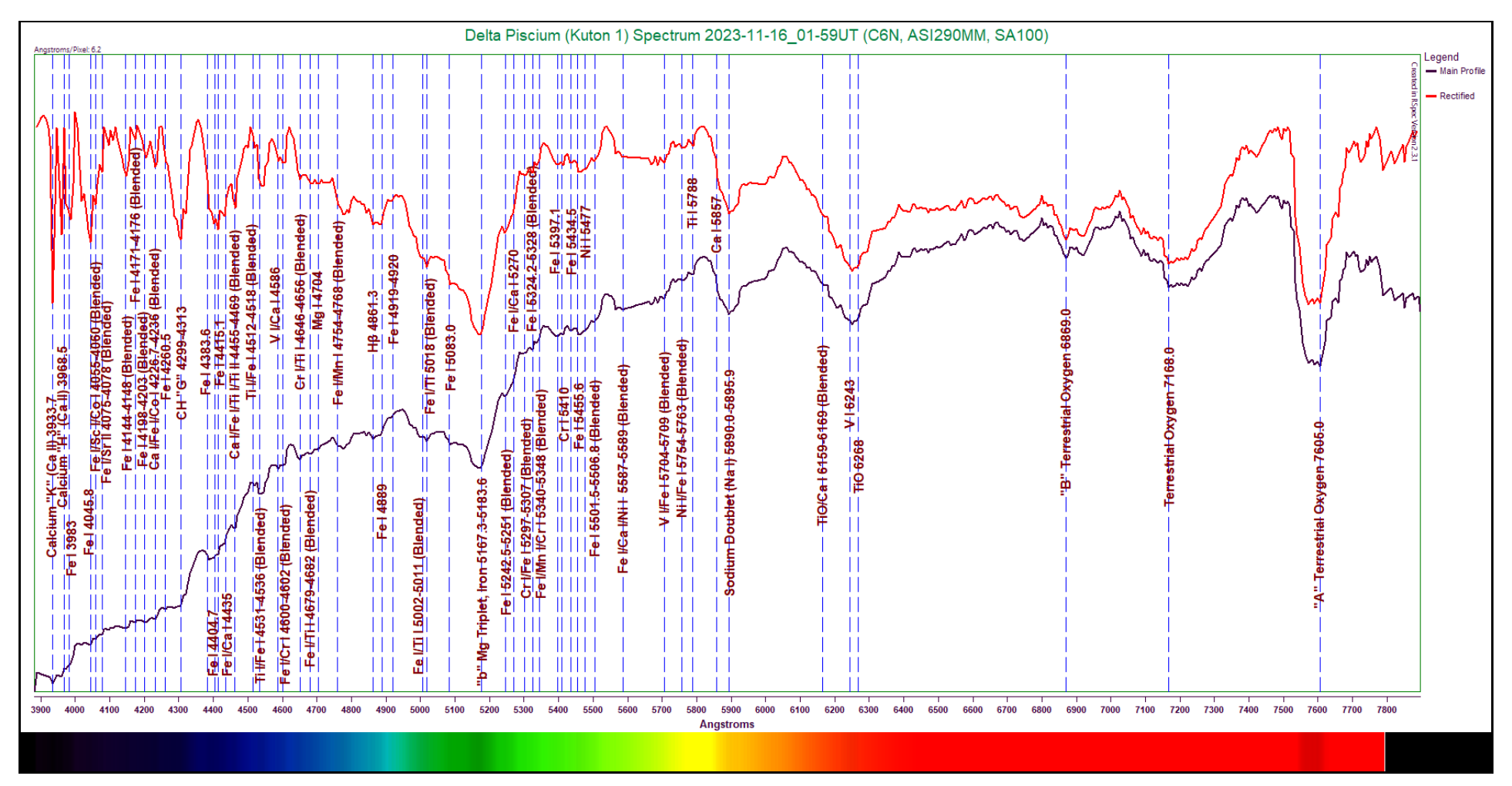


Figure 5.40: Delta Piscium (Kuton 1) Spectrum (6.3 Angstroms/pixel)
Capture Details: Exposure 1s, Gain 107, 50% of 249 frames stacked, Integration Time 124s

The shape of the curve definitely meets our expectations. The only hydrogen Balmer line visible is the Hβ line, and it appears quite weak. Near the extreme lower end of the wavelength range, we see the Fraunhofer "K" and "H" lines at 3933.7 and 3968.5 Angstroms respectively are drastically smaller than in the early K-type stars. They are identifiable, but nowhere near as strong. The Fraunhofer "G" molecular CH absorption at 4299-4313 Angstroms is visible, but is only weak to moderate in strength. Two TiO absorptions are identified; these lie at 6159 Angstroms (blended with Ca I) and 6268 Angstroms. The magnesium triplet at 5167.3-5183.6 Angstroms appears profoundly strong here. The sodium doublet at 5890.0-5895.9 Angstroms is also strong, with the neutral calcium line just visible below it at 5857 Angstroms (though it only appears to be causing a small deviation in the spectrum). Other labeled absorptions include iron, calcium, titanium, vanadium, chromium, magnesium, and nickel.

The following table lists the absorptions labeled in the spectrum of Delta Piscium (Kuton 1).

Table 5.31 - Delta Piscium (Kuton 1) Line Identification Details

Feature	Wavelength	Comments
	(Angstroms)	
Ca II	3933.7	Fraunhofer "K" ionized calcium line; weak
Ca II	3968.5	Fraunhofer "H" ionized calcium line; weak
Fe I	3983	Very weak neutral iron absorption
Fe I	4045.8	Weak neutral iron line
Fe I/Sc I/Co I	4055-4060	Extremely weak but common blend of iron, scandium, and cobalt
Fe I/Sr II	4075-4078	Extremely weak iron/strontium blend
Fe I	4144-4148	Weak neutral iron blend
Fe I	4171-4176	Extremely weak neutral iron blend
Fe I	4198-4203	Extremely weak neutral iron blend
Ca I/Fe I/Co I	4226.7-4236	Extremely weak blend of calcium, iron, and cobalt
Fe I	4260.5	Extremely weak neutral iron line
CH	4299-4313	Fraunhofer "G" absorption due to molecular CH
Fe I	4383.5	Common neutral iron line; weak to moderate here
Fe I	4404.7	Extremely weak neutral iron line
Fe I	4415.1	Extremely weak neutral iron line
Fe I/Ca I	4435	Common but weak iron/calcium absorption
Ca I/Fe I/Ti I/Ti II	4455-4469	Weak blend of calcium, iron, and titanium
Ti I/Fe I	4512-4518	Very weak titanium/iron blend
Ti I/Fe I	4531-4536	Weak to moderate strength titanium/iron blend
V I/Ca I	4586	Weak vanadium/calcium absorption; common
Fe I/Cr I	4600-4602	Common iron/calcium blend
Cr I/Ti I	4646-4656	Weak to moderate chromium/titanium blend
Fe I/Ti I	4679-4682	Very weak iron/titanium blend
Mg I	4704	Very common neutral magnesium line; extremely weak here
Fe I/Mn I	4754-4768	Weak to moderate blend of iron and manganese; sometimes visible as two separate blends
Нβ	4861.3	Weak to moderate hydrogen Balmer line
Fe I	4889	Weak to moderate neutral iron absorption
Fe I	4919-4920	Very weak neutral iron blend
Fe I/Ti I	5002-5011	Blend of neutral iron lines; often combined with Fe I/Ti I at 5018
Fe I/Ti I	5018	Very common iron/titanium absorption; often blended with others just below it
Fe I	5083.0	Moderate and fairly common neutral iron line
Mg I Triplet	5167.3-5183.6	Fraunhofer "b" neutral magnesium blend, with iron
Fe I	5242.5-5251	Blend of neutral iron lines; weak

Feature	Wavelength	Comments
	(Angstroms)	
Fe I/Ca I	5270	Common iron/calcium blend; very weak, only causing small diversion in spectrum
Cr I/Fe I	5297-5307	Small forest of chromium and iron lines; weak here
Fe I	5324.2-5328	Weak neutral iron blend
Fe I/Mn I/Cr I	5340-5348	Weak blend of iron, manganese, and chromium
Fe I	5397.1	Weak neutral iron line; common
Cr I	5410	Weak but common neutral chromium absorption
Fe I	5434.5	Very weak neutral iron line
Fe I	5455.6	Weak neutral iron line
Ni I	5477	Weak neutral nickel absorption
Fe I	5501.5-5506.8	Blend of neutral iron lines; very weak to weak
Fe I/Ca I/Ni I	5587-5589	Very common iron/calcium/nickel absorption; weak to moderate
V I/Fe I	5704-5709	Common vanadium/iron blend
Ni I/Fe I	5754-5763	Weak nickel/iron blend
Ti I	5788	Weak neutral titanium absorption
Ca I	5857	Subtle neutral calcium absorption
Na I Doublet	5890.0-5895.9	Fraunhofer "D2" and "D1" neutral sodium blend; strong here
TiO/Ca I	6159-6169	Very weak blend of molecular TiO and neutral calcium
V	6243	Strong neutral vanadium absorption
TiO	6268	Weak to moderate molecular TiO absorption
"B" Telluric Oxygen	6869.0	Fraunhofer "B" absorption due to atmospheric oxygen
Telluric Oxygen	7168.0	Absorption due to atmospheric oxygen
"A" Telluric Oxygen	7605.0	Fraunhofer "A" absorption due to atmospheric oxygen

Utilizing Wien's Law, we will calculate an effective temperature for the star. The star is an evolved giant, so we can expect our results to be a bit too low compared to those typical for a main sequence specimen.

The continuum curve for Delta Piscium (Kuton 1) is plotted below. The continuum appears in black, with the spectrum in blue for comparison. The labels have been removed for clarity, and the apparent peak energy wavelength labeled.

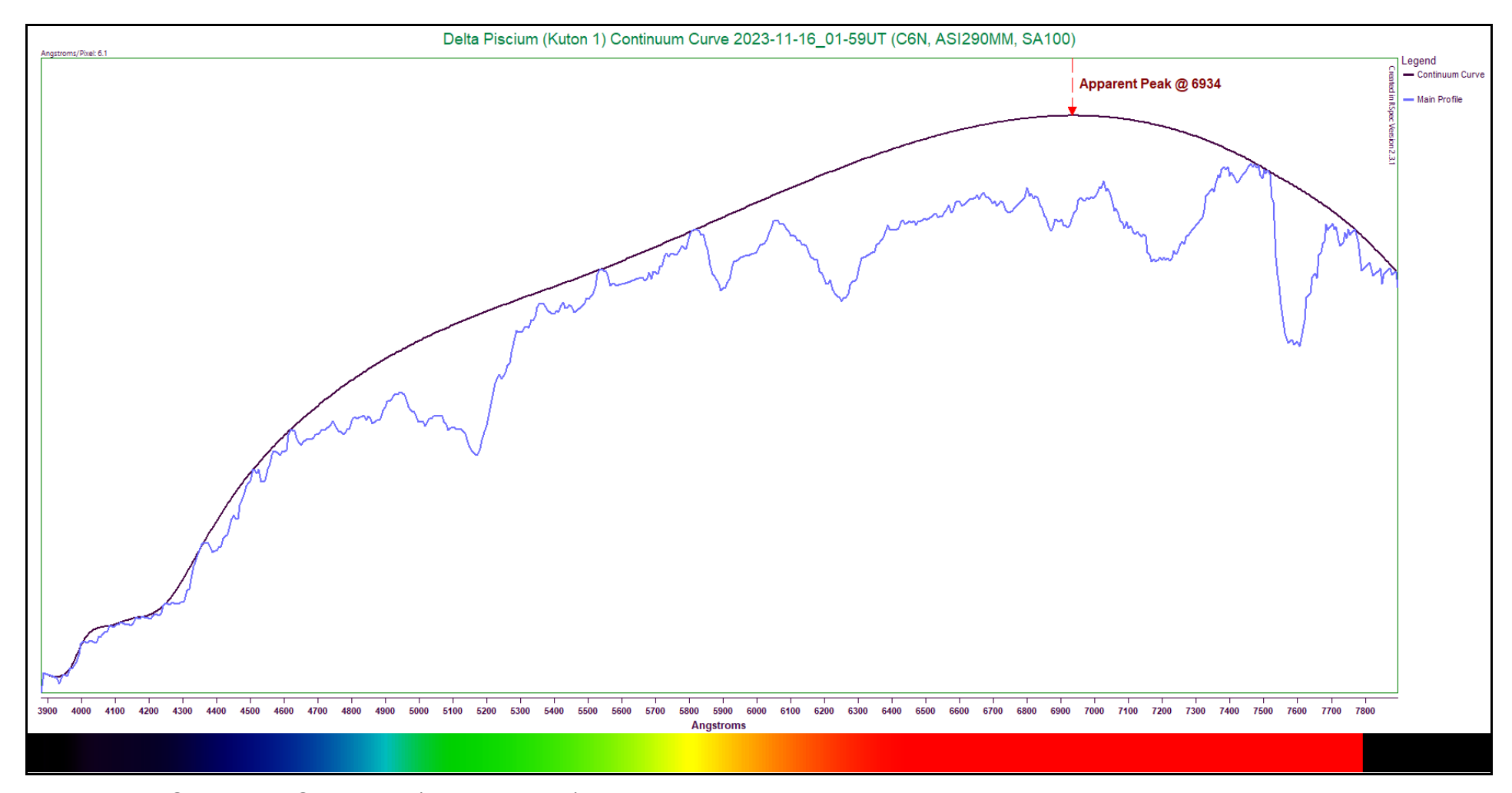


Figure 5.41 - Continuum Curve Plot (Delta Piscium)

The apparent peak of the continuum curve lies at 6934 Angstroms. Using this value, Wien's Law provides a temperature estimate of approximately 4,179K. This result is indeed lower than the expected range between 4,600K and 4,300K. The median value of the expected range is 4,450K; if we use this as our target number, then our estimate is off by approximately 6.09%. The professionally determined temperature of the star is listed as 3,868K⁽³⁶⁾. Using this value for comparison, we find our temperature estimate is off by 8.04%. This is of course a bit farther off, but still under ten percent.

5.12 Spectral Type K/M Stars (Very Late K and Very Early M)

This next specialized category encompasses stars whose temperatures have reached the point where they appear either deep orange or red in color. They are low in mass and luminosity, and can therefore be difficult to locate in amateur scopes. It is usually only the giants and supergiants that can be seen from earth.

Members of this special category have low masses, usually between 0.59 and 0.57 times the solar mass. These cooler stars usually range in temperature between about 3,950K and 3,850K (33,37). They are less luminous than previous examples, shining from 0.08 to 0.07 times the solar value(33,37).

Spectral features of these stars begin to plainly show the titanium oxide (TiO) molecular absorptions so common in the later M-types. The spectra of these stars continue to demonstrate less-visible hydrogen Balmer absorptions, and only a couple of these at best. A fair number of metals are still present, particularly in the lower wavelength region. The magnesium triplet and sodium doublet meanwhile grow in intensity.

The peak energy wavelength shifts even farther toward longer wavelengths here. For this reason, we will now extend the wavelength range in our results to 9,000 Angstroms for the remainder of the Atlas. This will allow us to identify a few near infrared absorptions, and provide a clearer evaluation of the peak energy wavelength.

The star chosen to represent this custom type is indicated here:

Table 5.32 - Representative K/M Star

	VIII - C 1511
Subtype	Star
Very Late K/Very Early M	Beta Andromedae (Mirach)

K/M Stars (Very Late K and Very Early M)

Stars of this custom category represent a sort of transition from the metal-laden K-types to the molecule-dominated M-types. A combination of these features will typically be present in the K/M stars, making them very interesting specimens to examine. The peaks of their spectral curves lie near the infrared region.

Main sequence examples of this custom type continue to show decreasing temperatures, with 3,900K being typical^(33,37). They are long-lived, and possess masses of only about 0.585 times that of our Sun^(33,37). These stars are also very dim, with luminosities of only about 0.075 times the solar value^(33,37).

Typical features include a strong magnesium triplet and sodium doublet, CH and TiO molecular absorptions (and possibly some others), along with some fainter metal absorptions, particularly in the lower wavelength regions. As the wavelength increases, the broad molecular absorptions become evident. The infrared ionized calcium triplet is also typically visible, though not always all three components.

The specimen chosen to represent this subtype is Beta Andromedae, sometimes called Mirach, in the constellation of Andromeda, the Chained Maiden. The star is a giant, which again may serve to lessen the intensities of some of the lines, but it should otherwise provide a good example.

The spectrum for Beta Andromedae (Mirach) is presented below. A rectified spectrum is shown alongside it in red.

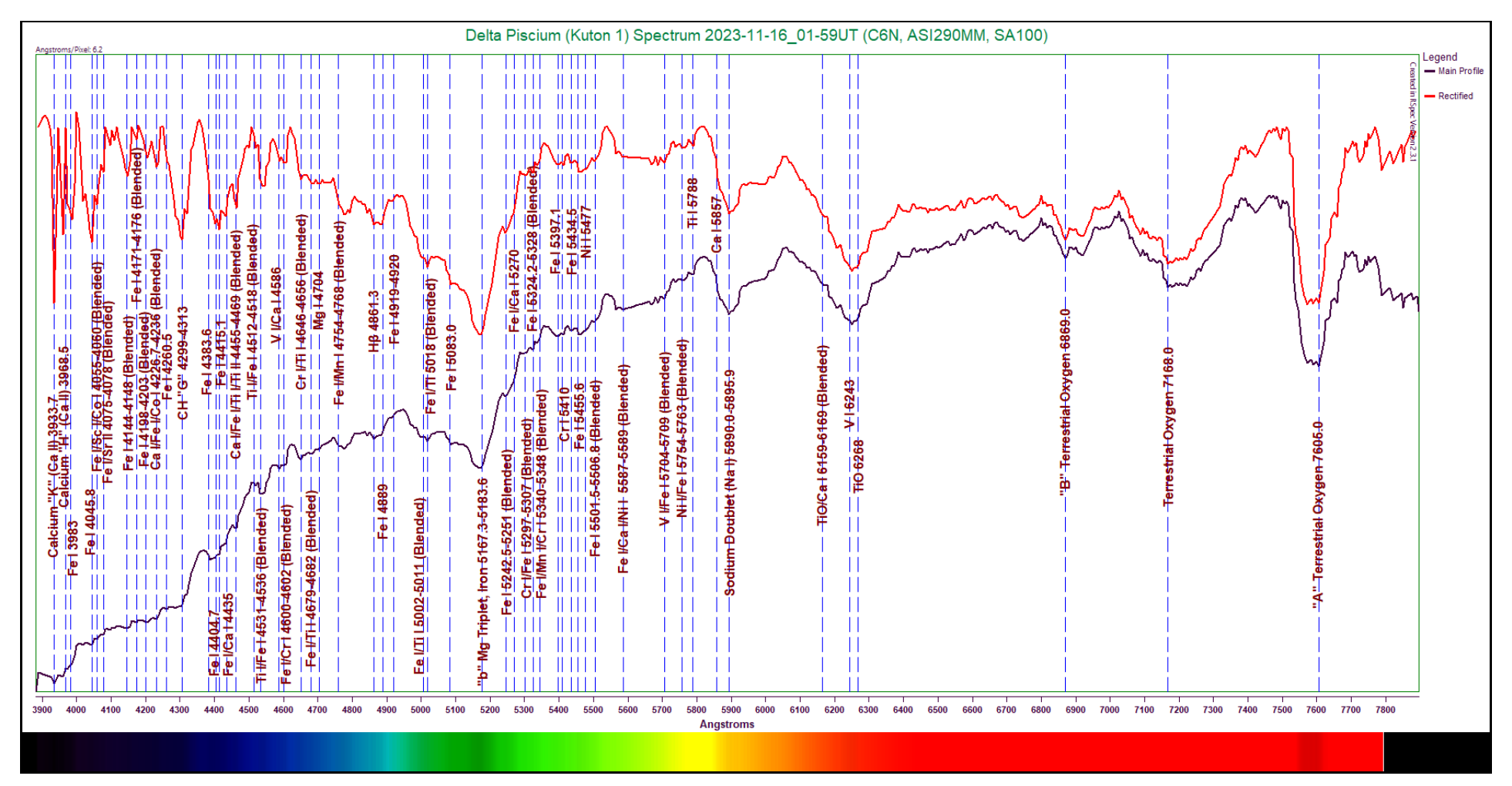


Figure 5.42: Beta Andromedae (Mirach) Spectrum (6.2 Angstroms/pixel)
Capture Details: Exposure 318ms, Gain 68, 75% of 580 frames stacked, Integration Time 138s

A cooler star is definitely represented here, with a peak energy wavelength in the red region of the spectrum. Only two of the hydrogen Balmer lines are identifiable here—H β and H α . These are both weak. The Fraunhofer "K" and "H" lines are present, but appear weak. The magnesium triplet at 5170 Angstroms is strong, with several of its typical flanking iron lines visible. Several molecular absorptions are visible in this spectrum, including CH (4299-4313 Angstroms), MgH (4780 Angstroms), several TiO absorptions (4704, 5448-5451, 5497, 5968, 5998, 6169-6180, 6358, 6681, 6715, 7054, 8254, 8430, and 8859 Angstroms), CaH (6750 Angstroms), and VO (7865 and 7939 Angstroms). The magnesium triplet at 5167.3-5183.6 Angstroms is strong; the sodium doublet at 5890.0-5895.9 Angstroms is also strong. Other fainter absorptions labeled include manganese, iron, vanadium, calcium, titanium, chromium, scandium, and barium.

The following shows the labeled features of the Beta Andromedae (Mirach) spectrum.

Table 5.33 - Beta Andromedae (Mirach) Line Identification Details

Feature	Wavelength	Comments
	(Angstroms)	
Ca II	3933.7	Fraunhofer "K" ionized calcium line; weak
Ca II	3968.5	Fraunhofer "H" ionized calcium line; weak
Mn/Fe I/Sc I/Co I	4030-4060	Very weak manganese/iron/scandium/cobalt blend
Fe I/Sr II	4075-4078	Very weak blend of neutral iron and ionized strontium
V I/Fe I/Co I	4112-4148	Small, broad blend of vanadium, iron, and cobalt; causing small plateau in continuum
Fe I/Ga I	4171-4178	Weak but notable blend of iron and gallium
Ca I	4226.7	Weak but clear neutral calcium line; common
Fe I	4260.5	Very weak neutral iron line
Ti I/Fe I	4290-4296	Weak titanium/iron blend
СН	4299-4313	Fraunhofer "G" absorption due to molecular CH
Fe I/Cr I	4384	Weak iron/chromium absorption
Fe I/V I	4405	Weak iron/vanadium absorption
Ca I/Fe I/Ti I	4455-4462	Extremely weak calcium/iron/titanium blend
Fe I	4490	Extremely weak neutral iron absorption
Ti I/Fe I/Cr I	4526-4540	Weak but notable blend of titanium, iron, and chromium
V I/Ca I	4580-4594	Very weak vanadium/calcium blend
Cr I/V I/Ni I	4646-4649	Weak chromium/vanadium/nickel blend
Fe I/Ti I	4668	Weak iron/titanium blend; common
TiO	4704	Extremely weak molecular TiO absorption; dubious identification
Fe I	4427-4737	Extremely weak neutral iron blend
MgH	4780	Weak to moderate absorption due to molecular MgH; fairly common
Нβ	4861.3	Weak to moderate hydrogen Balmer line
Fe I/Ti I	5002-5013	Moderately strong iron/titanium blend; common
Fe I	5080-5083	Weak neutral iron blend
Mg I Triplet	5167.3-5183.6	Fraunhofer "b" absorption due to neutral magnesium, with iron; strong to very strong
Fe I/Ca I/Cr I	5262-5270	Weak blend of iron, calcium, and chromium
Fe I	5324.2-5328	Weak neutral iron blend; common
Fe I/Cr I	5394-5410	Weak blend of iron and chromium
TiO	5448-5451	Weak to moderate molecular TiO blend
TiO	5497	Weak TiO absorption
Fe I/Ca I	5601-5603	Broad and fairly strong iron/calcium blend
Sc I/Cu I/Ni I/Fe I	5700-5710	Extremely weak blend of scandium, copper, nickel, and iron
Na I Doublet	5890.0-5895.9	Fraunhofer "D2" and "D1" absorption due to neutral sodium; strong to very strong

Feature	Wavelength	Comments
	(Angstroms)	
TiO	5968	Extremely weak TiO absorption; dubious identification
TiO	5998	Extremely weak TiO absorption; dubious identification
Ca I	6102.7	Extremely weak neutral calcium line
TiO	6159-6180	Strong blend of molecular TiO absorptions
TiO	6358	Very weak molecular TiO absorption
Ba I/Fe I/Ca I	6497	Weak but common barium/iron/calcium blend
Ηα	6562.8	Weak hydrogen Balmer line
TiO	6681	Extremely weak TiO absorption
TiO	6715	Moderate strength molecular TiO absorption
CaH	6750	Extremely weak molecular CaH absorption
"B" Telluric Oxygen	6869.0	Fraunhofer "B" absorption due to atmospheric oxygen
TiO	7054	Extremely weak TiO absorption; dubious identification
TiO	7088	Very weak molecular TiO absorption
TiO	7126	Strong molecular TiO absorption
"A" Telluric Oxygen	7605.0	Fraunhofer "A" absorption due to atmospheric oxygen
TiO	7821	Extremely weak TiO absorption; dubious identification due to local continuum noise
VO	7865	Extremely weak molecular VO absorption; dubious identification due to continuum noise
VO	7939	Weak molecular VO absorption
TiO	8254	Very weak TiO absorption
TiO	8430	Extremely weak TiO absorption; dubious identification
Ca II	8498	Weak to moderate ionized calcium absorption; part of infrared Ca II triplet
Ca II	8662	Weak to moderate ionized calcium absorption; part of infrared Ca II triplet
TiO	8859	Weak molecular TiO absorption; causing small plateau in continuum

Using Wien's Law, we will calculate an effective temperature for the star and compare this to our expected value. Once again, the star is a giant, so our calculated temperature is expected to be a little off.

The continuum curve for Beta Andromedae (Mirach) is presented below. The continuum appears in black, with the spectrum in blue for comparison. The labels have been removed for clarity, and the apparent peak energy wavelength labeled.

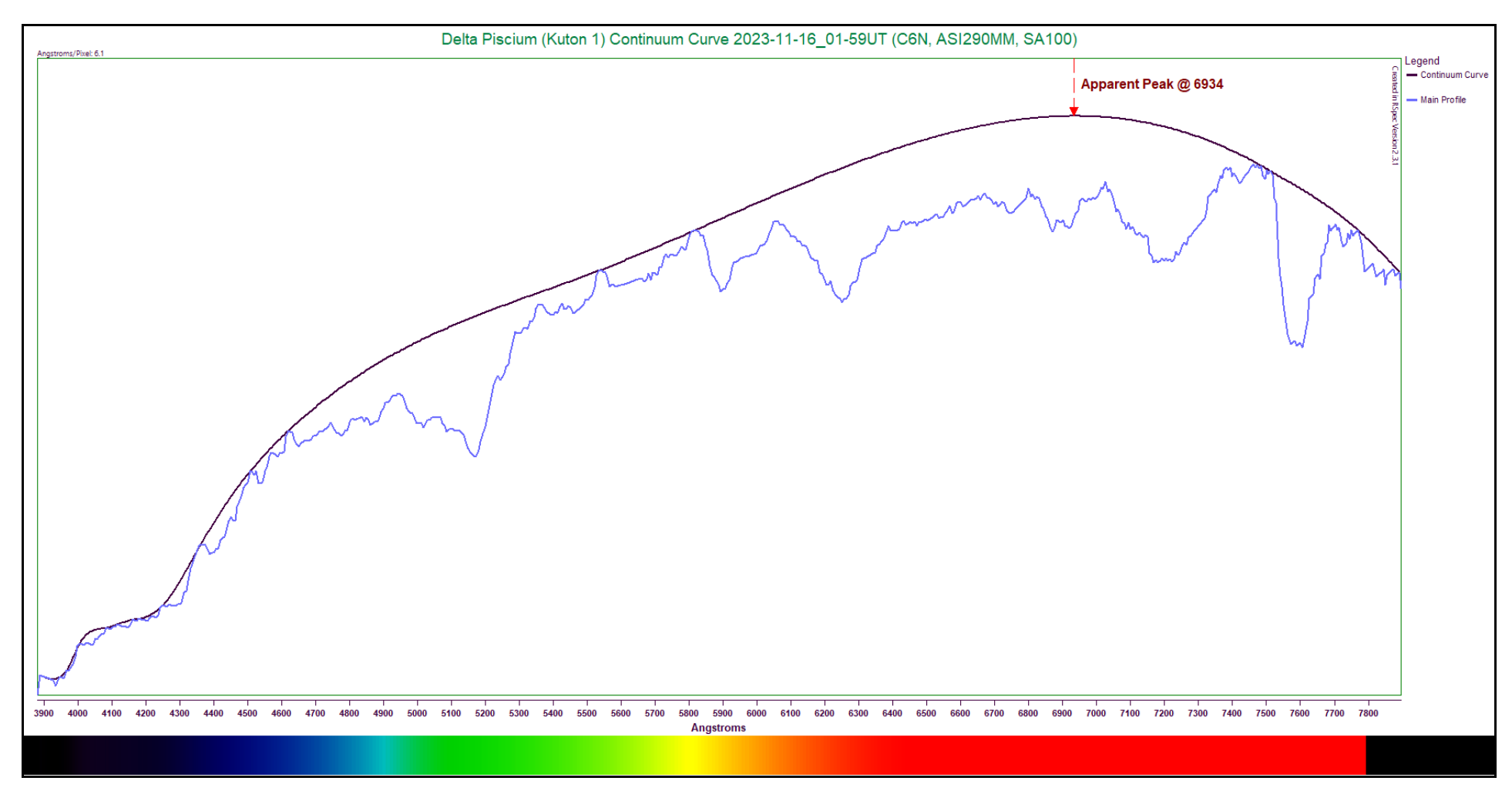


Figure 5.43 - Continuum Curve Plot (Beta Andromedae)

From the graph, the peak energy wavelength appears to lie near 7436 Angstroms. With this value, Wien's Law returns a temperature estimate of 3,897K. This is only about 13K removed from our expected value of 3,900K, making our estimate off by only 0.08%. The professional estimation of the star's temperature is listed as 3762K⁽³⁸⁾. Comparing our estimate to this value, we determine that we are off by approximately 3.59%. Still, not too shabby.

5.13 Spectral Type M Stars

M-type stars rank seventh on the descending MK temperature scale, and represent the last major type to be included in this Atlas. They are small and dim, appearing through a telescope as distinctively red in color. The main sequence stars of this type are called red dwarfs. They are estimated to be the most numerous type of star, but they are notoriously difficult to observe due to their dimness (unless they are giants or supergiants).

The M-type stars are far less massive than our Sun, ranging from only about 0.50 times down to 0.08 times the solar value⁽³⁷⁾. They are extremely long-lived stars, persisting for an estimated 100,000 Myr and more. This time frame is greater than the estimated age of the universe, so this is a mathematical estimate. Due to their low mass, they are consequently very dim, having luminosities ranging from 0.04 down to an amazingly low 0.0003 times that of our Sun⁽³⁷⁾.

The temperatures of the red dwarfs range from 3,650K down to only 2,350K⁽³⁷⁾. Their peak energy output lies very near or in the infrared region. This makes the use of Wien's Law for estimating their temperatures a questionable endeavor, as will be demonstrated.

The spectroscopic characteristics of these stars differ quite dramatically from the others. The TiO bands dominate here, causing a curve with broad, sweeping dips throughout. The magnesium triplet and sodium doublet are often still quite identifiable, though these are often blended with TiO absorptions. In the near infrared, they often show VO absorptions, plus the infrared calcium triplet becomes clearer as well.

No very late specimens were available from the observer's location when the data for the Atlas was collected, so no example of this subtype will be presented. The stars chosen to represent the other various M-types are listed here by subtype:

Table 5.34 - Representative M-Type Stars

Subtype	Star
Early	Sigma Librae (Brachium)
Middle	Rho Persei (Gorgonea Tertia)
Late	Omicron Ceti (Mira)
Very Late	None available

Early M-Type Stars

The early M-type stars typically show a decreasing number of metal absorptions, as the TiO molecular features become dominant. Their spectra take on a smoother appearance, with the peak energy wavelength continuing to shift closer to the near infrared.

Main sequence examples of this subtype typically have temperatures ranging from about 3,650K down to around 3,450K⁽³⁷⁾. These stars have very low masses, ranging from about 0.50 times down to approximately 0.35 times solar mass⁽³⁷⁾. This makes them extremely long-lived stars, and also very dim, with luminosities of only 0.041 to 0.016 times the luminosity of our Sun⁽³⁷⁾. As mentioned above, the molecular TiO absorptions become dominant here. The magnesium triplet and sodium doublet usually remain visible. Some VO absorptions can sometimes be made out, as can at least some of the infrared ionized calcium triplet.

The star chosen to represent this subtype is Sigma Librae, also referred to by the common name Brachium, in the constellation of Libra, the Scales. This specimen is a double star, but fairly widely separated, so the secondary does not interfere. However, the star is a pulsating variable and a giant. From this, we can expect some possible weakening of lines.

The spectrum for Sigma Librae (Brachium) is presented below, along with a rectified profile shown in red.

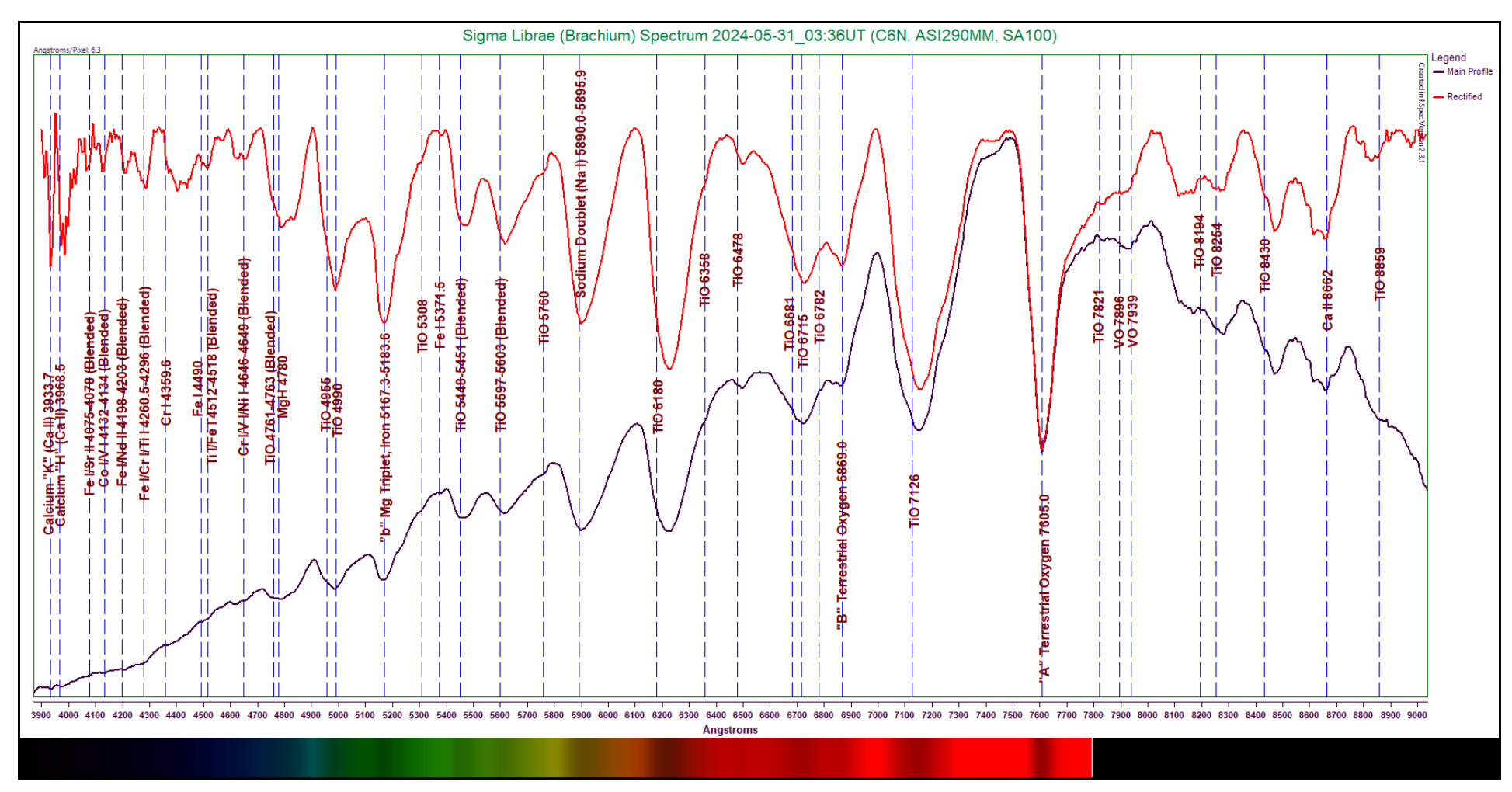


Figure 5.44: Sigma Librae (Brachium) Spectrum (6.3 Angstroms/pixel)
Capture Details: Exposure 496ms, Gain 202, 50% of 747 frames stacked, Integration Time 182s

Here we can see that most of the absorptions in the spectrum show up as smooth, sweeping curves. None of the hydrogen Balmer lines are visible. The Fraunhofer "K" and "H" lines at 3933.7 and 3968.5 Angstroms are extremely weak. In fact, all of the absorption below 4600 Angstroms are extremely subtle to very weak in strength. The magnesium triplet at 5167.3-5183.6 Angstroms is moderately strong, while the sodium doublet at 5890.0-5895.9 Angstroms is stronger. Aside from the numerous TiO molecular absorptions, we can see a few other molecules at play–MgH at 4780 Angstroms, and two VO absorptions at 7896 and 7939 Angstroms. One of the infrared ionized calcium triplet is seen at 8662 Angstroms. Additional faint metals, mostly in blends, include iron, cobalt, chromium, and titanium.

The following table lists the absorptions labeled in the Sigma Librae (Brachium) spectrum.

Table 5.35 - Sigma Librae (Brachium) Line Identification Details

Feature	Wavelength	Comments	
, catare	(Angstroms)		
Ca II	3933.7	Fraunhofer "K" ionized calcium line; extremely weak here	
Call	3968.5	Fraunhofer "H" ionized calcium line; extremely weak here	
Fe I/Sr II	4075-4078	Extremely weak iron/strontium blend; dubious identification	
Co I/V I	4132-4134	Extremely weak cobalt and vanadium blend; dubious identification	
Fe I/Nd II	4198-4203	Extremely weak iron/neodymium blend	
Fe I/Cr I/Ti I	4260.5-4296	Very weak iron/chromium/titanium blend	
Cr I	4359.6	Very weak neutral chromium line	
Fe I	4490	Extremely weak neutral iron absorption	
Ti I/Fe I	4512-4518	Very weak titanium/iron blend	
Cr I/V I/Ni I	4646-4649	Weak blend of chromium, vanadium, and nickel	
TiO	4761-4763	Blend of molecular TiO absorptions; weak	
MgH	4780	Moderate strength molecular MgH absorption	
Mg I Triplet	5167.3-5183.6	Fraunhofer "b" absorption due to neutral magnesium, with iron	
TiO	5308	Extremely weak TiO absorption; only causing small; deviation in continuum	
Fe I	5371.5	Very weak neutral iron line	
TiO	5480	Strong TiO absorption	
TiO	5448-5451	Moderate blend of molecular TiO absorptions	
TiO	5597-5603	Blended TiO absorptions; moderate strength	
TiO	5760	Weak TiO molecular absorption	
Na I Doublet	5890.0-5895.9	Blended Fraunhofer "D2" and "D1" lines of neutral sodium; strong	
TiO	6180	Strong TiO absorption	
TiO	6358	Extremely weak molecular TiO absorption; only causing small deviation in spectrum	
TiO	6478	Weak TiO absorption	
TiO	6681	Weak molecular TiO absorption	
TiO	6715	Moderate strength TiO absorption	
TiO	6782	Extremely weak molecular TiO absorption	
"B" Telluric Oxygen	6869.0	Fraunhofer "B" absorption due to atmospheric oxygen	
TiO	7126	Extremely strong TiO absorption	
"A" Telluric Oxygen	7605.0	Fraunhofer "A" absorption due to atmospheric oxygen	
TiO	7821	Very weak TiO absorption	
VO	7896	Very weak molecular VO absorption	
VO	7939	Extremely weak molecular VO absorption	
TiO	8194	Exceptionally weak TiO absorption; dubious identification	

Feature	Wavelength	Comments	
	(Angstroms)		
TiO	8254	Moderate molecular TiO absorption	
TiO	8340	Extremely weak TiO absorption	
Ca II	8662	Third ionized calcium line in infrared calcium triplet; strong	
TiO	8859	Weak molecular TiO absorption	

We will employ Wien's Law to calculate an effective temperature for the star, then compare this to our expected value range. It is typically around this subtype that these temperature estimates begin to show significant deviation from expected values, though, as the peak energy wavelength shifts into the near infrared range.

The continuum curve for Sigma Librae (Brachium) is presented below. The continuum line appears in black, with the spectrum shown in blue. The labels have been removed for clarity, and the apparent peak energy wavelength of the curve labeled.

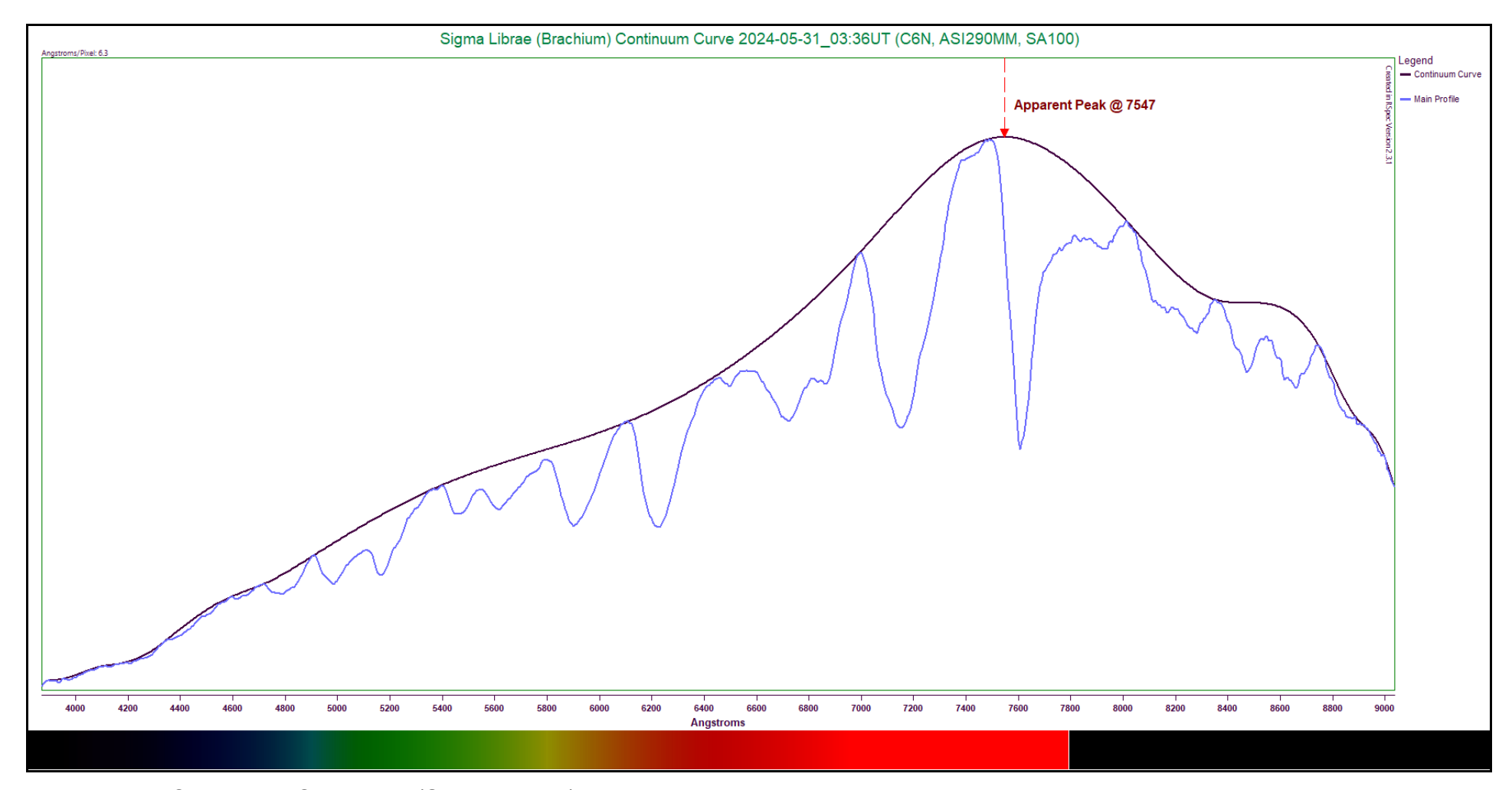


Figure 5.45 - Continuum Curve Plot (Sigma Librae)

Examining the graph above shows the apparent peak energy wavelength lies at approximately 7547 Angstroms. Plugging this value into Wien's Law results in an effective temperature estimate of 3,840K. This is indeed higher than our expected range of 3,650K to 3,450K. Comparing our result to the median of this range (3,550K), we find our estimate is off by 8.17%. The listed temperature for the star is 3,596⁽³⁹⁾. Using this value for comparison, our estimate is off by 6.79%.

Middle M-Type Stars

This subtype shows an increase in the depth and breadth of the TiO absorptions. When any finer metal absorptions are visible, they are found in the lower wavelength region and are exceptionally weak. The peak energy wavelength continues to slide deeper into the near infrared.

Middle-M main sequence stars remain quite cool, usually with temperatures between 3,200K and 2,800K⁽³⁷⁾. Their masses are also quite low, with typical stars coming in between around 0.250 and 0.100 times the mass of the Sun⁽³⁷⁾. Middle M-type stars have correspondingly low luminosities, shining with only about 0.0072 times down to 0.0010 times solar luminosity⁽³⁷⁾

The TiO absorptions continue to be dominant, on a spectrum composed of broad, deep absorption scoops. The magnesium triplet and sodium doublet continue to show well, sometimes aided by adjacent TiO absorptions. Some VO can usually be seen in the near infrared, along with components of the infrared calcium triplet.

The specimen chosen as an example of this subtype is Rho Persei, also called Gorgonea Tertia, in the constellation of Perseus, the Hero. The star is a giant, and a pulsating star, but we should still be able to make out the relevant major features of its spectrum.

The spectrum for Rho Persei (Gorgonea Tertia) is presented below, along with a rectified spectrum in red.

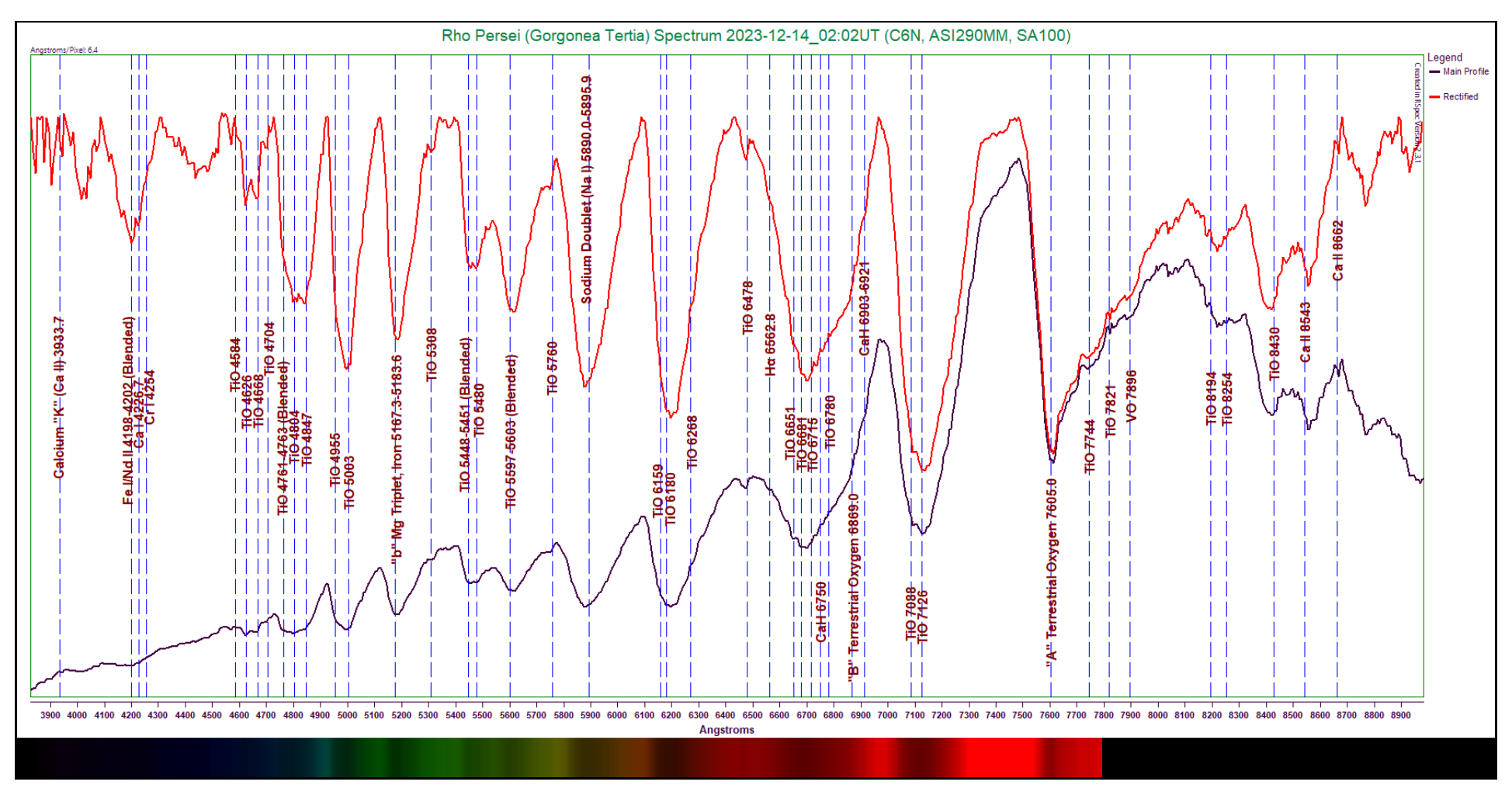


Figure 5.46: Rho Persei (Gorgonea Tertia) Spectrum (6.3 Angstroms/pixel)
Capture Details: Exposure 496ms, Gain 71, 50% of 379 frames stacked, Integration Time 93s

Indeed we can see how the spectrum appears virtually saturated with TiO absorptions! One hydrogen Balmer line can be seen here—the Hα line at 6562.8 Angstroms. This line is extremely weak. Also, the paucity of metals visible in the lower wavelength region is notable. The Fraunhofer "K" ionized calcium line is peeking through, but is exceedingly weak. The magnesium triplet at 5167.3-5183.6 Angstroms and the sodium doublet at 5890.0-5895.9 Angstroms remain strong, though. A single molecular VO absorption is presented at 7896 Angstroms. Two members of the infrared ionized calcium triplet are visible at 8543 and 8662 Angstroms respectively. We have two CaH molecular absorptions here, one at 6750 Angstroms and a second at 6903-6921 Angstroms. One distinguishing feature here is that the TiO absorptions are beginning to overtake the Fraunhofer "B" atmospheric absorption line; this B line is subdued and barely visible. Other labeled metals include iron (blended with neodymium, calcium, and chromium.

The following table lists the absorptions labeled in the Rho Persei (Gorgonea Tertia) spectrum.

Table 5.36 - Rho Persei (Gorgonea Tertia) Line Identification Details

		a) Line identification Details	
Feature	Wavelength	Comments	
	(Angstroms)		
Ca II	3933.7	Fraunhofer "K" ionized calcium line; extremely weak	
Fe I/Nd II	4198-4202	Weak blend of iron and neodymium	
Ca I	4226.7	Extremely weak neutral calcium line	
Cr I	4254	Exceedingly weak neutral chromium absorption; only causing a tiny deviation in the spectrum	
TiO	4584	Very weak molecular TiO line	
TiO	4626	Weak but distinct TiO absorption	
TiO	4668	Weak but distinct TiO absorption	
TiO	4704	Very weak molecular TiO absorption	
TiO	4761-4763	Moderately strong blend of TiO absorptions	
TiO	4804	Fairly strong TiO absorption	
TiO	4847	Moderately strong TiO absorption	
TiO	4955	Moderate molecular TiO absorption	
TiO	5003	Moderate to strong TiO absorption	
Mg I Triplet	5167.3-5183.6	Fraunhofer "b" absorption due to neutral magnesium, with iron	
TiO	5308	Very weak TiO absorption	
TiO	5448-5451	Moderately strong blend of TiO absorptions	
TiO	5480	Moderately strong molecular TiO absorption	
TiO	5597-5603	Moderately strong TiO absorption	
TiO	5760	Very weak TiO absorption	
Na I Doublet	5890.0-5895.9	Fraunhofer "D2" and "D1" blended absorption due to neutral sodium; strong	
TiO	6159	Extremely subtle TiO absorption; dubious identification	
TiO	6180	Very strong molecular TiO absorption	
TiO	6268	Very weak molecular TiO absorption	
TiO	6478	Weak to moderate TiO absorption; may be dubious identification due to band head position	
Ηα	6562.8	Very weak hydrogen Balmer line	
TiO	6651	Weak molecular TiO absorption	
TiO	6681	Very strong TiO absorption	
TiO	6715	Very weak TiO absorption	
СаН	6750	Very weak molecular CaH absorption	
TiO	6780	Extremely weak TiO absorption; dubious identification	
"B" Telluric Oxygen	6869.0	Fraunhofer "B" absorption due to atmospheric oxygen; extremely weak here	
СаН	6903-6921	Extremely weak molecular CaH absorption feature	
TiO	7088	Weak TiO absorption	
TiO TiO CaH TiO "B" Telluric Oxygen CaH	6681 6715 6750 6780 6869.0 6903-6921	Very strong TiO absorption Very weak TiO absorption Very weak molecular CaH absorption Extremely weak TiO absorption; dubious identification Fraunhofer "B" absorption due to atmospheric oxygen; extremely weak here Extremely weak molecular CaH absorption feature	

Feature	Wavelength	Comments	
	(Angstroms)		
TiO	7126	Very strong molecular TiO absorption	
"A" Telluric Oxygen	7605.0	Fraunhofer "A" absorption due to atmospheric oxygen	
TiO	7744	Weak TiO absorption	
TiO	7821	Extremely weak and narrow TiO absorption; dubious identification	
VO	7896	Weak molecular VO absorption	
TiO	8194	Very subtle molecular TiO absorption; dubious identification	
TiO	8254	Extremely weak and noisy TiO absorption; dubious identification	
TiO	8430	Moderate to strong TiO absorption	
Ca II	8543	Second of infrared ionized calcium triplet; weak to moderate in strength	
Ca II	8662	Last of infrared ionized calcium triplet; very weak	

Using Wien's Law, we will compute an effective temperature for the star and compare this to the expected temperature range for this subtype. As with the previous M-type example, we can expect the estimate to be a little farther off due to the peak energy wavelength drifting deeper into the infrared.

The following graph shows the continuum curve for Rho Persei (Gorgonea Tertia). The approximated continuum curve appears in black, with the spectrum in blue for comparison. The labels have been removed, and the apparent peak of the curve is indicated in red.

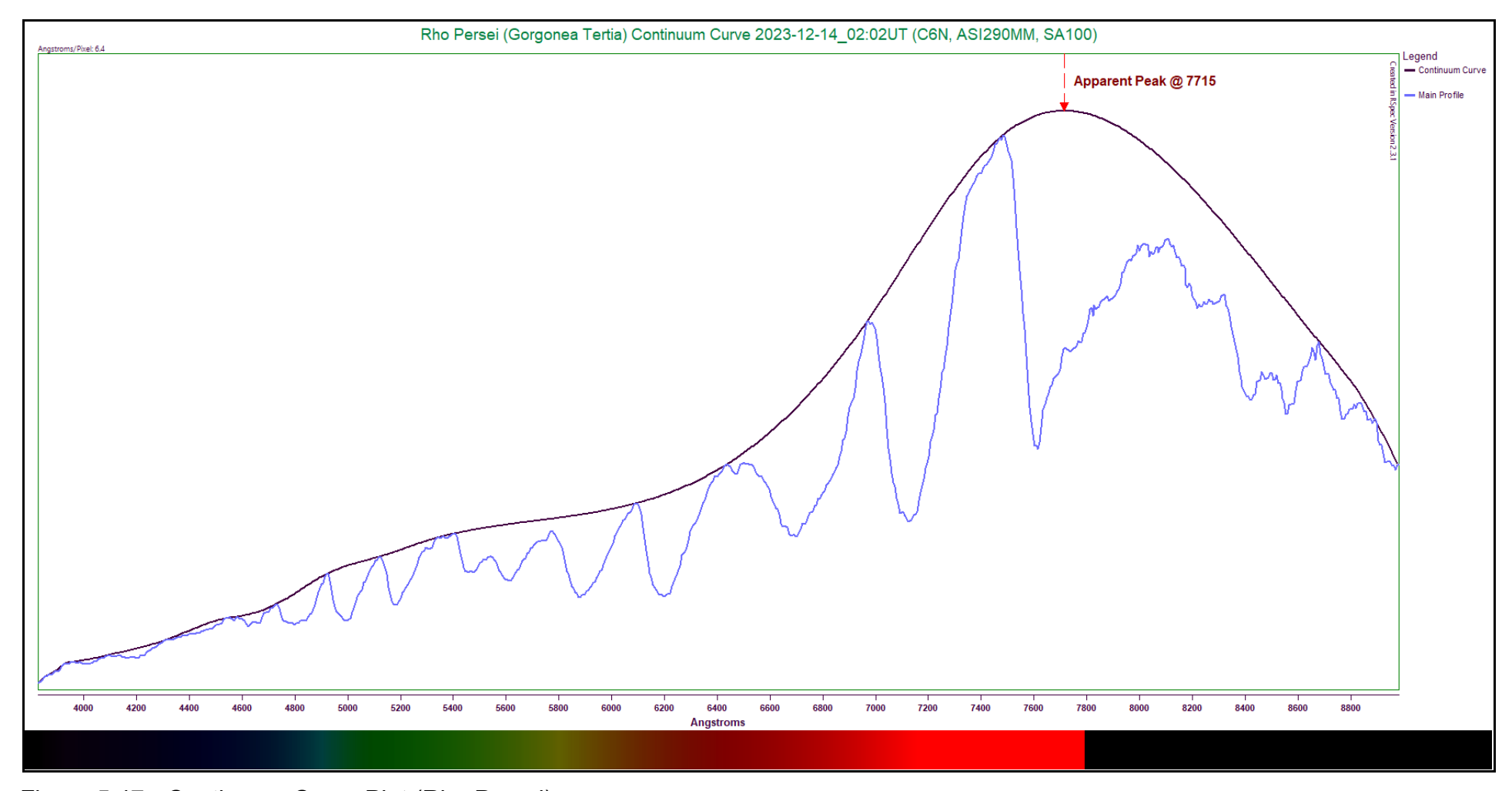


Figure 5.47 - Continuum Curve Plot (Rho Persei)

From this, the peak energy wavelength appears to lie at 7715 Angstroms. Using this value, Wien's Law returns an effective temperature estimate of 3,756K. This is significantly higher than our expected value between 3,200K and 2,800K. Adopting the median temperature value in our expected range (3,000K), we find our estimate is off by a factor of 1.25. The professionally determined temperature of the star is listed as 3,479K⁽⁴⁰⁾. This value is also a little outside the expected range. Using this value for comparison, we find our estimate is off by only 7.96%.

Late M-Type Stars

The late M-type stars are our final stop along this tour of stellar spectra. They show a substantial shift in energy output toward the infrared. The TiO lines still dominate, but little else can be discerned. The peak energy output occurs well into the near infrared region.

The main sequence specimen stars of this type are very cool, with temperatures typically of only 2,680K to 2,580K⁽³⁷⁾. They are extremely low-mass, weighing in at around 0.90 to 0.85 times the solar mass⁽³⁷⁾. They are also very dim, with luminosities of only about 0.00065 to 0.00052 times the solar value⁽³⁷⁾. The TiO bands overwhelmingly dominate these spectra. Some VO can sometimes be seen, as well as members of the infrared ionized calcium triplet, but the overall definition of these additional absorption features is reduced.

The star chosen as representative of this subtype is Omicron Ceti, better known as Mira, in the constellation of Cetus, the Whale. The star is a pulsating variable star, and is also quite dim visually. The spectrum presented below lacks some detail as a result due to the longer exposures needed and the limitations of the equipment used.

The spectrum of Omicron Ceti (Mira) is presented in black, along with a rectified spectrum in red.

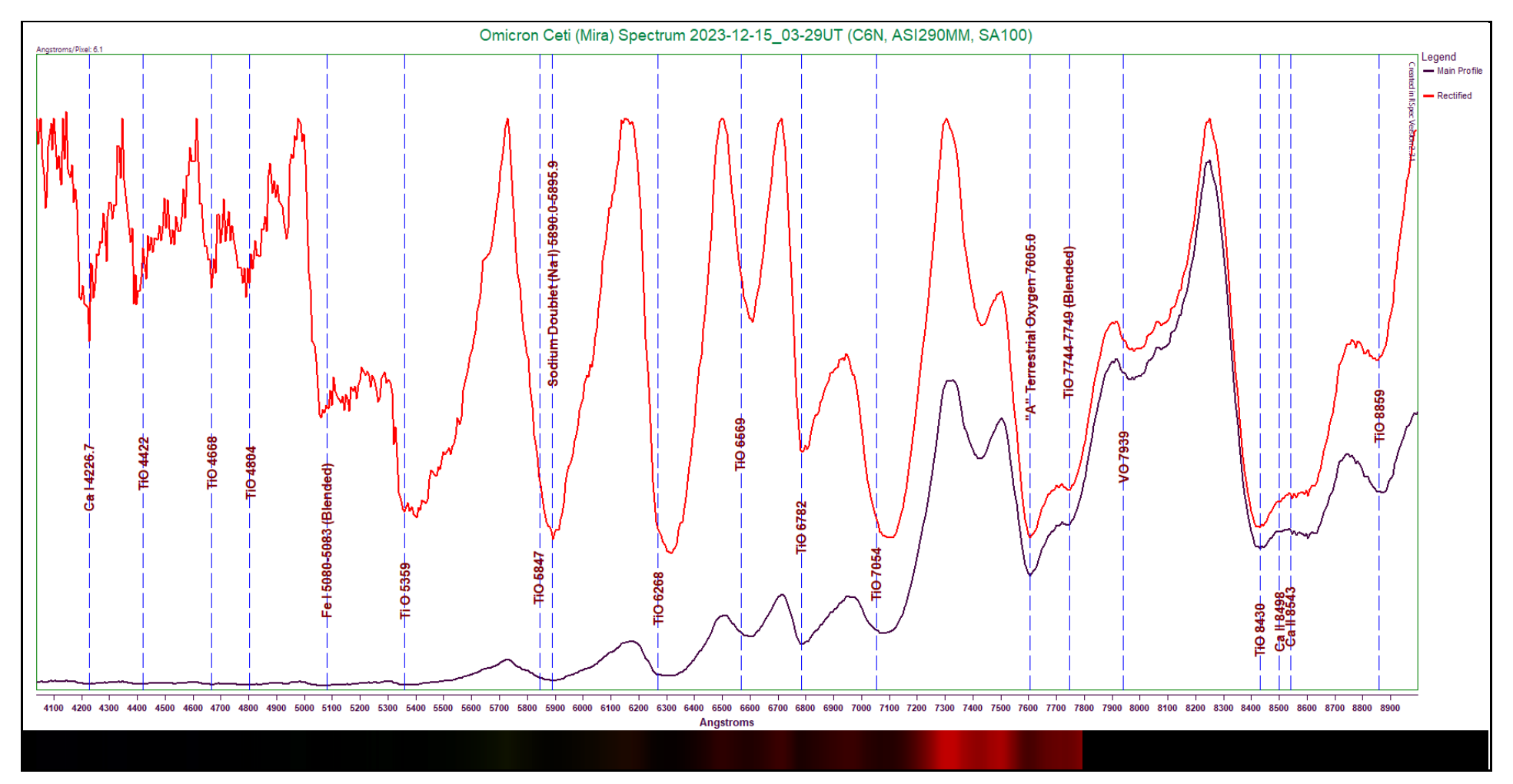


Figure 5.48: Omicron Ceti (Mira) Spectrum (6.1 Angstroms/pixel)
Capture Details: Exposure 3s, Gain 196, 80% of 80 frames stacked, Integration Time 192s

The shift towards the infrared is very easy to see here. There are only traces of features visible below 5000 Angstroms. The four absorptions below this point are suspect due to their weakness (though they do appear more clearly in the rectified profile). The first weak feature that appears seems to be a blended iron absorption at 5080-5083 Angstroms. The magnesium triplet has been absorbed by the continuum, but the sodium doublet at 58990.0-5895.9 Angstroms is still strong. A TiO absorption just below it is labeled, but it is certainly unclear if this is accurate. A single VO molecular absorption is visible at 7939 Angstroms, and two members of the infrared calcium triplet are noted, though they appear extremely weak. The peak of the curve is well into the near infrared.

The following table lists the features indicated in the Omicron Ceti (Mira) spectrum.

Table 5.37 - Omicron Ceti (Mira) Line Identification Details

Feature	Wavelength (Angstroms)	Comments	
Ca I	4226.7	Extremely weak neutral calcium line; common line; dubious identification	
TiO	4422	Extremely weak TiO absorption; dubious identification	
TiO	4668	Extremely weak TiO absorption; dubious identification	
Fe I	5080-5083	Very weak neutral iron blend	
TiO	5359	Very weak TiO absorption	
TiO	5847	Possible bandhead of TiO absorption; questionable identification	
Na I Doublet	5890.0-5895.9	Fraunhofer "D2" and "D1" absorption due to neutral sodium	
TiO	6268	Strong TiO absorption	
TiO	6569	Moderate TiO absorption	
TiO	6782	Strong molecular TiO absorption	
TiO	7054	Moderate to strong TiO absorption	
"A" Telluric Oxygen	7605.0	Fraunhofer "A" absorption due to atmospheric oxygen	
TiO	7744-7749	Blend of molecular TiO absorptions	
VO	7939	Weak molecular VO absorption	
TiO	8430	Extremely strong and common TiO absorption	
Ca II	8498	First of infrared calcium triplet; extremely weak	
Ca II	8543	Second of infrared calcium triplet; extremely weak	
TiO	8859	Moderate and common molecular TiO absorption	

Making use of Wien's Law, we will calculate an effective temperature for the star and compare the result to the expected values. Since the energy peak of this star is far into the near infrared, we must expect some significant error in our computation.

The following graph shows the continuum curve for Omicron Ceti (Mira), along with the spectrum indicated in blue. The labels have been removed, and the peak energy wavelength marked in red.

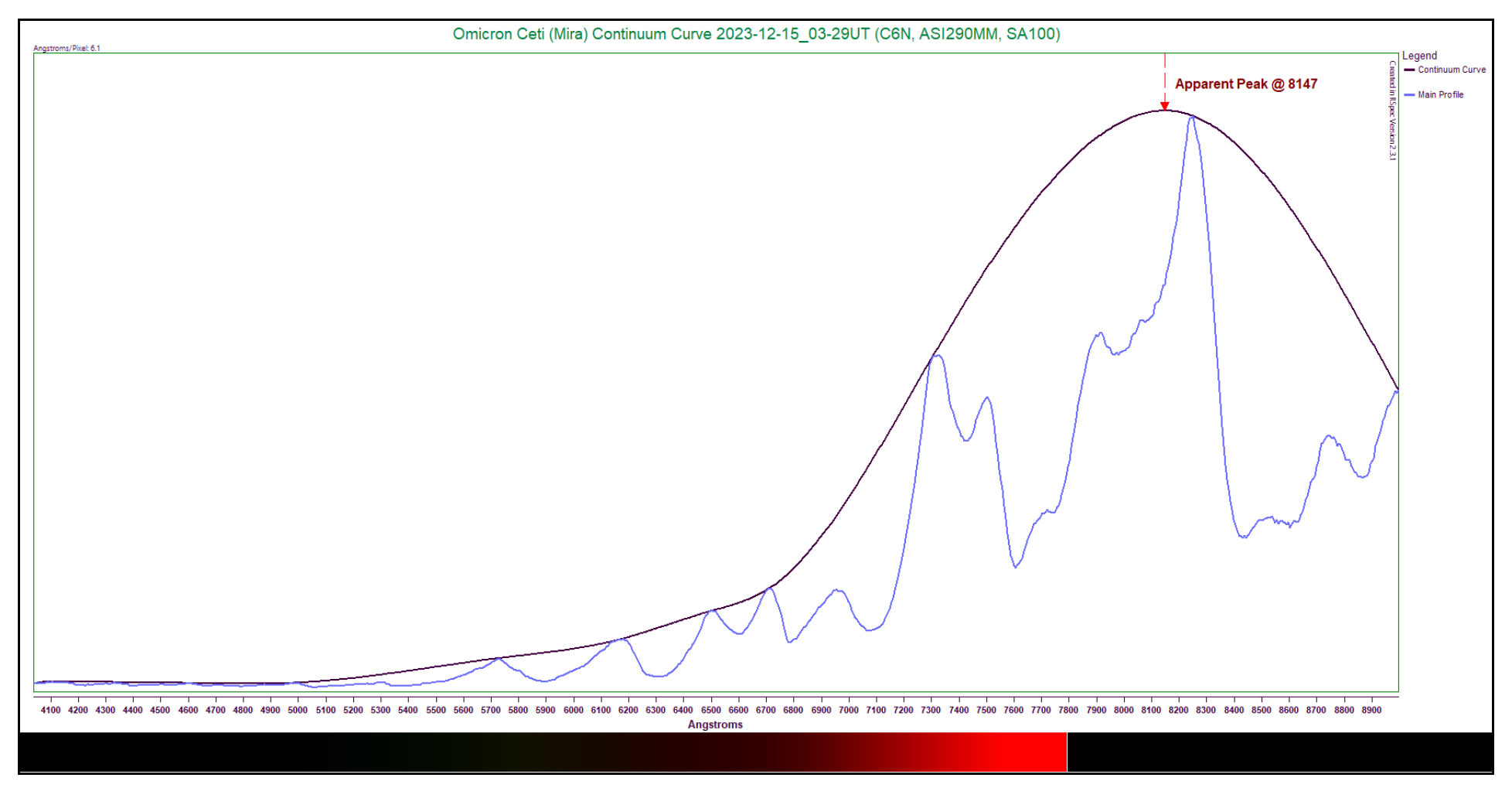


Figure 5.49 - Continuum Curve Plot (Omicron Ceti)

This plot of the continuum curve indicates a peak at 8147 Angstroms. Using this value, Wien's Law provides an effective temperature estimate of approximately 3,557K—quite far off from our expected value near 2,680K to 2,580K. Using the median value of the expected range (2,630K) for comparison, our estimate is found to be in error by a factor of 1.35. There are two main contributing factors to this error. The first is that the star is actually a pulsating giant, not a main sequence star. The second main contribution to the error is the presence of so many broad molecular absorptions, which makes ascertaining a continuum curve very uncertain. The sources available list the temperature for the star as fluctuating between 2,918K and 3,192K⁽⁴¹⁾. Both of these values exceed the expected temperature, but the average value in this range is 3,055K. Recalculating the error based on this value, we find our estimate is still off, but only by a factor of 1.16.

6. Acknowledgements

We wish to thank the following individuals who provided review and comment on the contents of this document:

- Paul Hemphill for his technical review and comments on the initial draft of this document.
- Matthew Underwood for review and comments on formatting and presentation style.
- Tom Field for his technical review and comments on the final draft of this document.

7. References

- 1. Allen, C. W., (1981). Astrophysical Quantities, Third Edition. Athlone Press
- 2. Emerson, D., (1997). Interpreting Astronomical Spectra, John Wiley and Sons
- 3. Harrison, Ken M, (2011). Astronomical Spectroscopy for Amateurs. Springer
- 4. Hirschfield, Alan (2014). Starlight Detectives, Bellevue Literary Press
- Kramida, A., Ralchenko, Yu., Reader, J. and <u>NIST ASD Team</u> (2024). *NIST Atomic Spectra Database* (version 5.12), [Online]. Available: https://physics.nist.gov/asd. National Institute of Standards and Technology, Gaithersburg, MD. DOI: https://doi.org/10.18434/T4W30F
- 6. Osterbrock, Donald E. (1989). Astrophysics of Gaseous Nebulae and Active Galactic Nuclei, University Science Books
- 7. Walker, Richard (2017). *Spectral Atlas for Amateur Astronomers*. Cambridge University Press
- 8. The Infrared Spectral Classification of M-Type Stars, Steward Sharpless (US Naval Observatory), Astrophysical Journal, vol. 124, p.342 (SAO/NASA Astrophysics Data System), 5/10/1956,
 - https://articles.adsabs.harvard.edu/full/1956ApJ...124..342S
- 9. *O-type main-sequence star*, Wikipedia, 2/12/2025, https://en.wikipedia.org/wiki/O-type main-sequence star
- 10. Xi Persie, Wikipedia, 8/22/2024, https://en.wikipedia.org/wiki/Xi Persei
- 11. O-type main-sequence star, Wikipedia, 2/12/2025, https://en.wikipedia.org/wiki/O-type main-sequence star
- 12. B-type main-sequence star, Wikipedia, 7/21/2024, https://en.wikipedia.org/wiki/B-type main-sequence star
- 13. Alnitak, Wikipedia, 2/25/2025, https://en.wikipedia.org/wiki/Alnitak

- 14. *Epsilon Cassiopeiae*, Wikipedia, 10/26/2024, https://en.wikipedia.org/wiki/Epsilon Cassiopeiae
- 15. Nu Andromedae, Wikipedia, 3/23/2025, https://en.wikipedia.org/wiki/Nu Andromedae
- 16. Zeta Pegasi, Wikipedia, 1/27/2025, https://en.wikipedia.org/wiki/Zeta Pegasi
- 17. A-type main-sequence star, Wikipedia, 3/15/2025, https://en.wikipedia.org/wiki/A-type main-sequence star
- 18. σ Piscium (*sigma Piscium*), The Sky Live, https://theskylive.com/sky/stars/sigma-piscium-star
- 19. Denebola, Wikipedia, 8/21/2024, https://en.wikipedia.org/wiki/Denebola
- 20. *Mu Andromedae*, Wikipedia, 3/23/2025, https://en.wikipedia.org/wiki/A-type-main-sequence-star
- 21. *Lambda Piscium*, Wikipedia, 11/15/2024, https://en.wikipedia.org/wiki/Lambda_Piscium
- 22. *F-type main-sequence star*, Wikipedia, 1/22/2025, https://en.wikipedia.org/wiki/F-type main-sequence star
- 23. Zeta Leonis, Wikipedia, 3/31/2025, https://en.wikipedia.org/wiki/Zeta Leonis
- 24. Delta Aquilae, Wikipedia, 10/26/2024, https://en.wikipedia.org/wiki/Delta Aquilae
- 25. Iota Pegasi, Wikipedia, 1/27/2025, https://en.wikipedia.org/wiki/lota Pegasi
- 26. Iota Piscium, Wikipedia, 1/11/2024, https://en.wikipedia.org/wiki/lota Piscium
- 27. *G-type main sequence star*, Wikipedia, 7/19/2025, https://en.wikipedia.org/wiki/G-type main-sequence star
- 28. Eta Bootis, Wikipedia, 5/26/2025, https://en.wikipedia.org/wiki/Eta Bo%C3%B6tis
- 29. *G-type main sequence stars*, Wikipedia, 7/19/25, https://en.wikipedia.org/wiki/G-type main-sequence star
- 30. 35 Leonis, Wikipedia, 5/26/2025, https://en.wikipedia.org/wiki/35_Leonis
- 31. *Delta Coronae Borealis*, Wikipedia, 4/13/2025, https://en.wikipedia.org/wiki/Delta Coronae Borealis
- 32. Eta Piscium, Wikipedia, 7/16/2025, https://en.wikipedia.org/wiki/Eta Piscium
- 33. *K-type main sequence star,* Wikipedia, 7/19/2025, https://en.wikipedia.org/wiki/K-type_main-sequence_star
- 34. Kappa Cygni, Wikipedia, 6/5/2025, https://en.wikipedia.org/wiki/Kappa_Cygni
- 35. Hamal, Wikipedia, 7/16/2025, https://en.wikipedia.org/wiki/Hamal
- 36. Delta Piscium, Wikipedia, 5/16/2025, https://en.wikipedia.org/wiki/Delta_Piscium
- 37. Red dwarf, 7/20/2025, https://en.wikipedia.org/wiki/Red_dwarf
- 38. Mirach, Wikipedia, 6/8/2025, https://en.wikipedia.org/wiki/Mirach
- 39. Sigma Librae, Wikipedia, 7/11/2025, https://en.wikipedia.org/wiki/Sigma Librae
- 40. Rho Persei, Wikipedia, 1/1/2025, https://en.wikipedia.org/wiki/Rho Persei
- 41. Mira, Wikipedia, 7/13/2025, https://en.wikipedia.org/wiki/Mira

42. David R. Lide, ed., CRC Handbook of Chemistry and Physics, Internet Version 2005, http://www.hbcpnetbase.com, CRC Press, Boca Raton, FL, 2005

8. Appendices

Appendix 1 - Physical Constants

Constant	Symbol	Value	Units
Velocity of light	С	2.99792458 x 10 ⁸	m/s
Boltzmann's constant	k _b	1.3806505 x 10 ⁻²³	joules/Kelvin
Planck constant	h	6.6260693 x 10 ⁻³⁴	joule-seconds
Wien's displacement constant	b	2.8978 x 10 ⁶	nm⋅K

(CRC Handbook of Chemistry and Physics)

Appendix 2 - Representative Temperatures of Main Sequence Stars

Temperatures in degrees Kelvin (K)

	Type O	Type B	Type A	Type F	Type G	Type K	Туре М
0		23,422	11,470	7,554	5,617	4,464	3,699
1		21,232	10,908	7,303	5,476	4,373	3,637
2		19,412	10,397	7,068	5,342	4,287	3,577
3		17,876	9,932	6,848	5,214	4,204	3,518
4		16,562	9,506	6,640	5,092	4,123	3,461
5	47,828	15,426	9,115	6,445	4,975	4,046	3,407
6	39,640	14,434	8,754	6,261	4,864	3,972	3,353
7	33,820	13,560	8,420	6,087	4,757	3,900	3,302
8	29,474	12,785	8,111	5,922	4,655	3,831	3,252
9	26,107	12,092	7,823	5,765	4,557	3,764	3,203

(University of Northern Iowa, "Spectral Type Characteristics",

sites.uni.edu/morgans/astro/course/Notes/section2/spectraltemps.html)

Appendix 3 - Temperatures of Peak Line Intensities of the 20 Most Abundant Elements in the Solar Spectrum

Element	Neutral	Singly Ionized	Doubly lonized	Triply Ionized
Н	9,000			
He	16,000	47,000		
0	8,000	25,500	50,000	Tmax > 55,000 K
С	7,000	19,500	39,000	Tmax > 55,000 K
N	8,500	22,000	42,000	Tmax > 55,000 K
Ne	12,500	30,500	Tmax > 55,000 K	Tmax > 55,000 K
Fe	4,500	11,000	25,000	No Lines in Visible Range
Si	4,500	12,000	24,000	39,500
Mg	4,000	10,000	Tmax > 55,000 K	Tmax > 55,000 K
S	6,000	15,500	28,500	46,500
Ar	8,500	18,500	No Lines in Visible Range	No Lines in Visible Range
Al	3,500	11,500	21,500	Tmax > 55,000 K
Ca	3,250	6,500	36,500	No Lines in Visible Range
Ni	4,500	No Lines in Visible Range	No Lines in Visible Range	No Lines in Visible Range
Na	3,000	33,500	Tmax > 55,000 K	Tmax > 55,000 K
Cr	4,000	10,000	No Lines in Visible Range	No Lines in Visible Range
CI	7,500	17,000	31,000	No Lines in Visible Range
Р	6,000	13,500	26,500	43,500
Mn	4,000	10,000	No Lines in Visible Range	No Lines in Visible Range
Ti	3,500	9,000	21,500	44,500

(From calculations by S. Donnell and NIST spectral line data)

Appendix 4 - Elements and Ions by Spectral Type

Spectral Type O > 30,000 K

Element/Ion	Peak Temperature (K)
O III	50,000
He II	47,000
SIV	46,500
Ti IV	44,500
PIV	43,500
N III	42,000
Si IV	39,500
C III	39,000
Ca III	36,500
Na II	33,500
CI III	31,000
Ne II	30,500

Spectral Type B 10,000 - 35,000 K

Element/Ion	Peak Temperature (K)
S III	28,500
P III	26,500
OII	25,500
Fe III	25,000
Si III	24,000
N II	22,000
Ti III	21,500
Al III	21,500
CII	19,500
Ar II	18,500
CI II	17,000
He I	16,000
SII	15,500
PII	13,500
Ne I	12,500
Si II	12,000
Al II	11,500
Fe II	11,000

Spectral Type A 7,500 - 10,000 K

Element/lon	Peak Temperature (K)
Mg II	10,000
Mn II	10,000
Cr II	10,000
Ti II	9,000
HI	9,000
01	8,500
ΝI	8,500
Ar I	8,000

Spectral Type F 6,000 - 7,500 K

Element/Ion	Peak Temperature (K)
CII	7,500
CI	7,000

Spectral Type G 5,200 - 6,500 K

Element/Ion	Peak Temperature (K)
Ca II	6,500
SI	6,000
PI	6,000

Spectral Type K 3,700 - 5,200 K

Element/Ion	Peak Temperature (K)
Ni I	4500
Fel	4500
Si I	4500
Cr I	4000
Mg I	4000
Mn I	4000

Spectral Type M 2,400 - 3,700 K

Element/lon	Peak Temperature (K)
TI	3,500
Al I	3,500
Ca I	3,250
Na I	3,000

(Wikipedia)

Appendix 5 - Element Profiles and Spectral Lines

Following are profiles for neutral elements and their ions over the temperature range 3,000 K to 55,000 K corresponding to spectral types M through O. Shown for each element or ion is the calculated Balmer/Saha temperature profile and corresponding spectral lines within the visible range.

Temperature profiles are generated by S. Donnell from equations for Boltzmann excitations and Saha ionizations.

- 1. Boltzmann excitations use the average energy level difference and statistical weights for lines in the range 380 nm to 780 nm.
- 2. Saha electron number density is determined by an empirical fit of a set of elements with known maximum temperature. Electron densities for all elements use the same density profile.
- 3. Peak temperature for each profile is noted.
- 4. Plots for most neutral elements and lower ionization stages have a temperature range of 3,000 K to 30,000 K. Plots for higher ionization stages of elements may have a temperature range of 3,000 55,000 K
- 5. All profile plots generated by S. Donnell

Spectral Lines are generated from the NIST ASD

- 1. Wavelength range 380 nm to 780 nm
- 2. Electron temperature determined from profile peak temperature
- 3. Electron density is the density at the peak temperature.
- 4. Observed wavelengths and allowed transitions only.
- 5. Output is relative line intensities with spectral lines plotted on a relative scale where the strongest line in the series has a value of 1.
- 6. Lines with relative intensities greater than 0.05 for each element are listed in the table accompanying each element, the exceptions being H I in which the Balmer series from H α through H η are listed or where the maximum table length is reached. Lines with relative intensities less than 0.05 may appear in the plot, but are not listed in the table

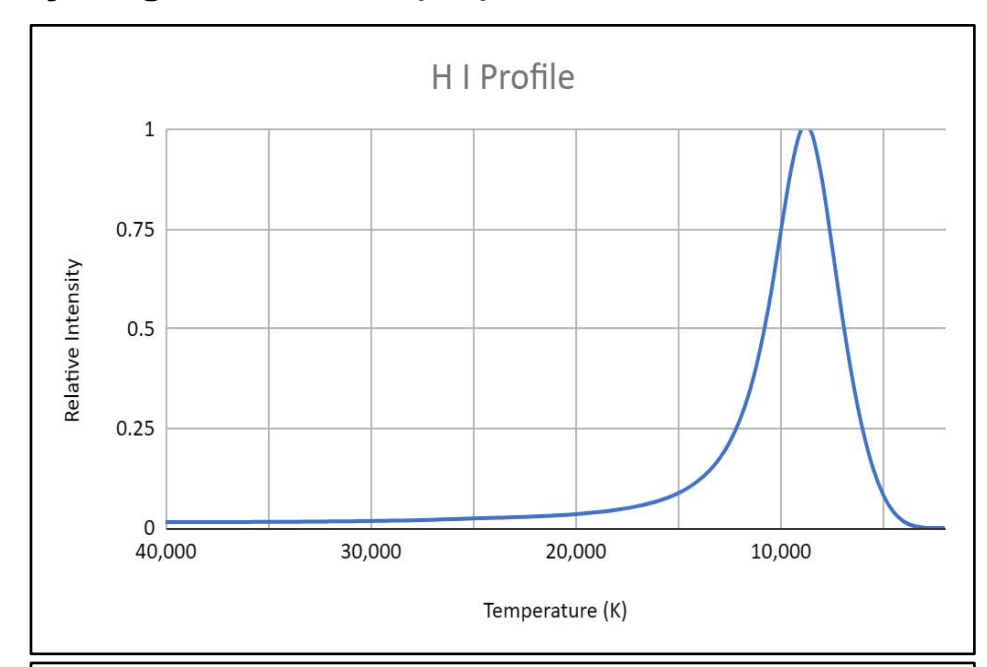
Stars are complex, and factors other than temperature and density can affect the calculated temperature profile, the strengths of the observed spectral lines, and even if an element or ion shows visible lines in a stellar spectrum at all. The information presented here is intended to inform the user of what spectral features may be expected in a spectrum with the understanding that this may differ from observations of individual stars.

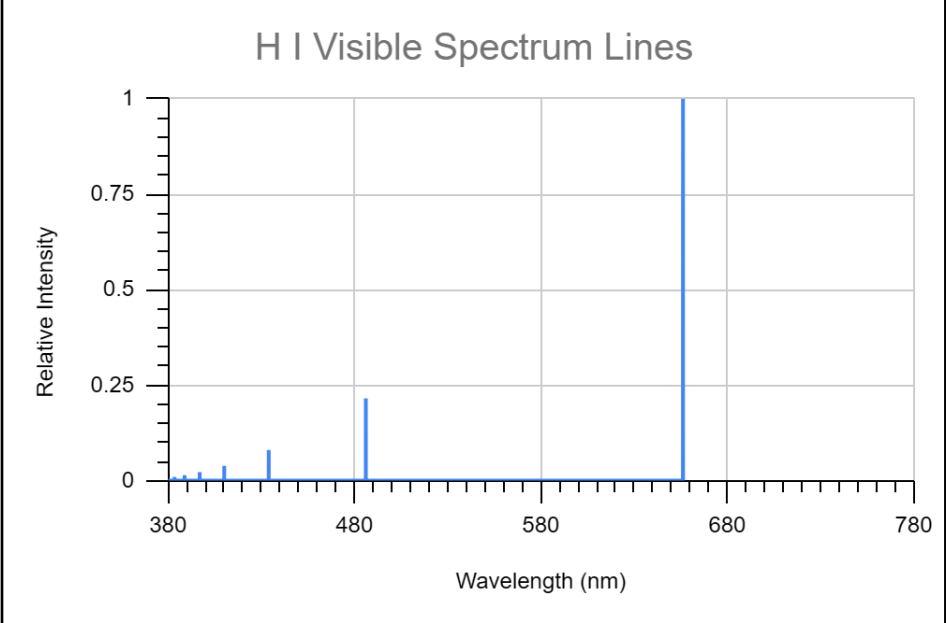
Index to Element Profiles and Spectral Lines

Element	Neutral	Singly lonized	Doubly Ionized	Triply Ionized
Hydrogen	<u>H1</u>			
Helium	He I	He II		
Oxygen	01	<u>O II</u>	<u>O III</u>	
Carbon	<u>C I</u>	<u>C II</u>	<u>C III</u>	
Nitrogen	<u>N I</u>	<u>N II</u>	<u>N III</u>	
Neon	<u>Ne I</u>	Ne II		
Iron	<u>Fe I</u>	<u>Fe II</u>	Fe III	
Silicon	<u>Si I</u>	<u>Si II</u>	<u>Si III</u>	<u>Si IV</u>
Magnesium	Mg I	Mg II		
Sulfur	<u>S I</u>	<u>S II</u>	<u>S III</u>	SIV
Argon	<u>Ar I</u>	<u>Ar II</u>		
Aluminum	<u>Al I</u>	Al II	<u>Al III</u>	
Calcium	<u>Ca I</u>	<u>Ca II</u>	<u>Ca III</u>	
Nickel	<u>Ni I</u>			
Sodium	<u>Na I</u>	<u>Na II</u>		
Chromium	<u>Cr I</u>	<u>Cr II</u>		
Chlorine	CII	<u>CI II</u>	<u>CI III</u>	
Phosphorus	<u>P I</u>	PII	<u>P III</u>	PIV
Manganese	Mn I	Mn II		
Titanium	<u>Ti l</u>	<u>Ti II</u>	<u>Ti III</u>	<u>Ti IV</u>

Hydrogen - Neutral (H I)







H I Profile:

Peak Temperature: 9,000 K

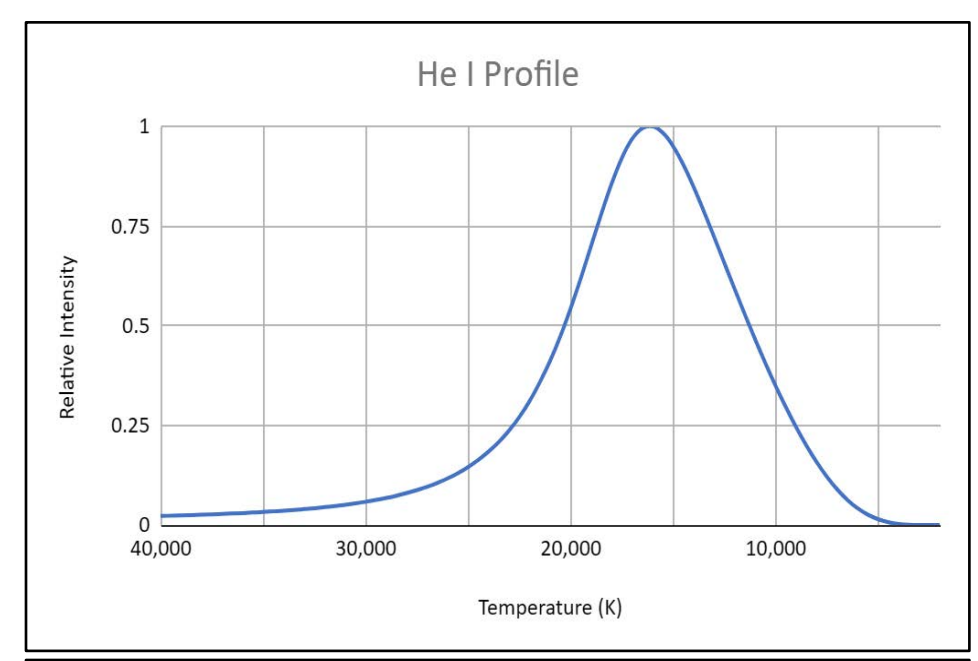
H I Visible Spectrum Lines:

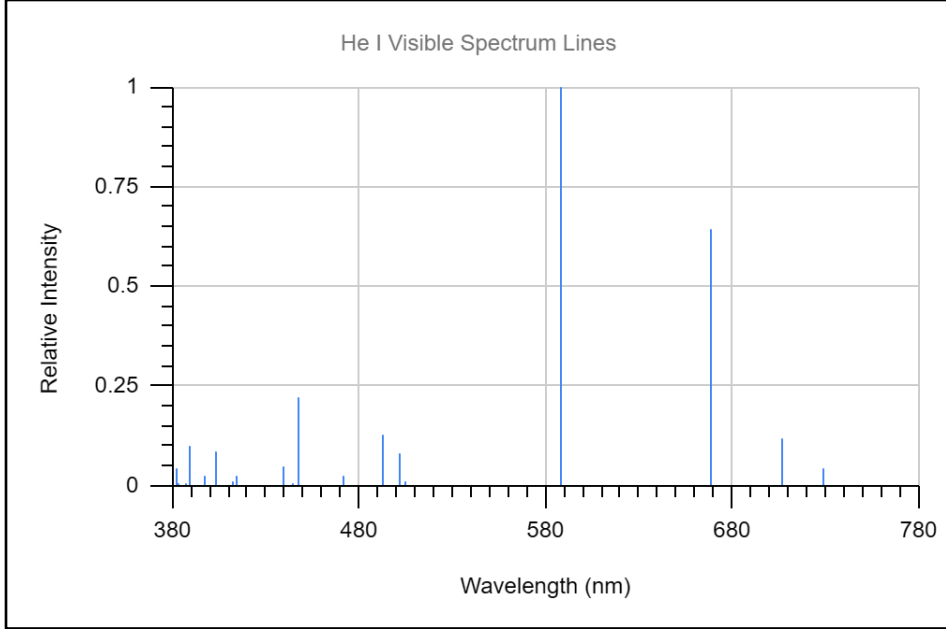
Electron Temperature: 0.78 T (eV) Electron Density: 9.28E+13 (cm⁻³)

λ (nm)	Rel Intensity	Balmer Designation
383.54	0.01	Нη
388.91	0.01	Нζ
397.01	0.02	Ηε
410.17	0.04	Нδ
434.05	0.08	Нγ
486.13	0.22	Нβ
656.28	1.00	Ηα

Helium - Neutral (He I)

(Return to Index)





He I Profile:

Peak Temperature: 16,000 K

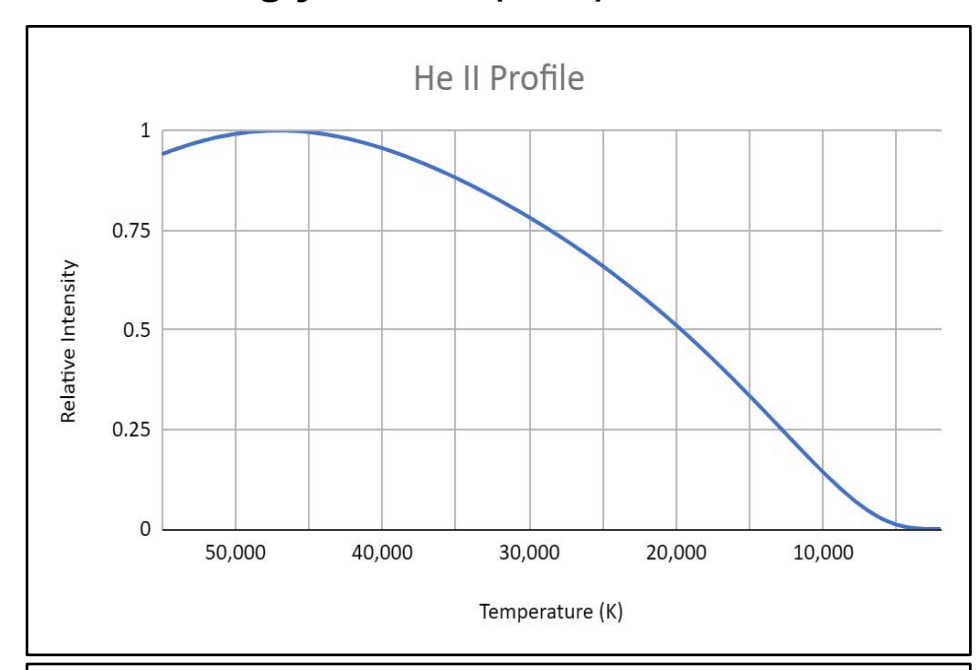
He I Visible Spectrum Lines:

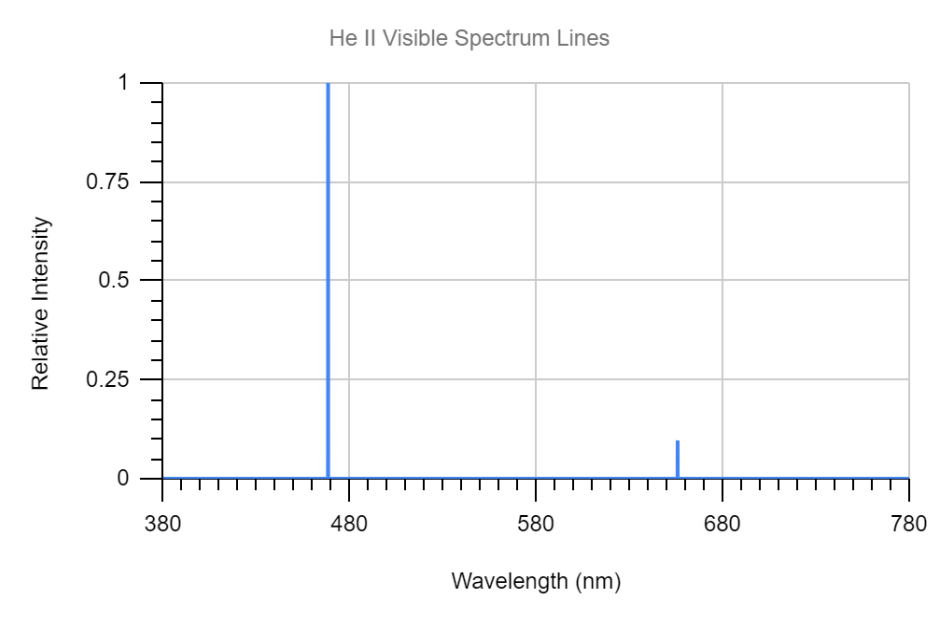
Electron Temperature: 1.38 T (eV) Electron Density: 2.36E+15 (cm⁻³)

λ (nm)	Rel Intensity	λ (nm)	Rel Intensity
388.86	0.06	501.57	0.08
388.86	0.10	587.56	0.18
402.62	0.08	587.56	1.00
402.62	0.05	587.56	0.18
438.79	0.05	587.56	0.54
447.15	0.22	667.82	0.64
447.15	0.12	706.52	0.12
492.19	0.13	706.52	0.07

Helium - Singly Ionized (He II)

(Return to Index)





He II Profile:

Peak Temperature: 47,000 K

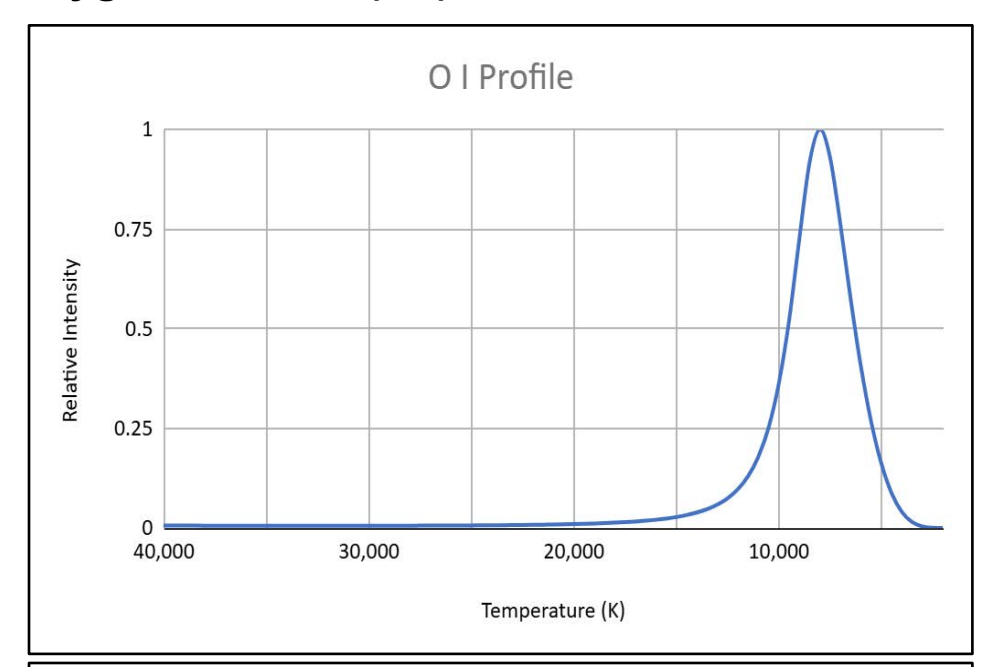
He II Visible Spectrum Lines:

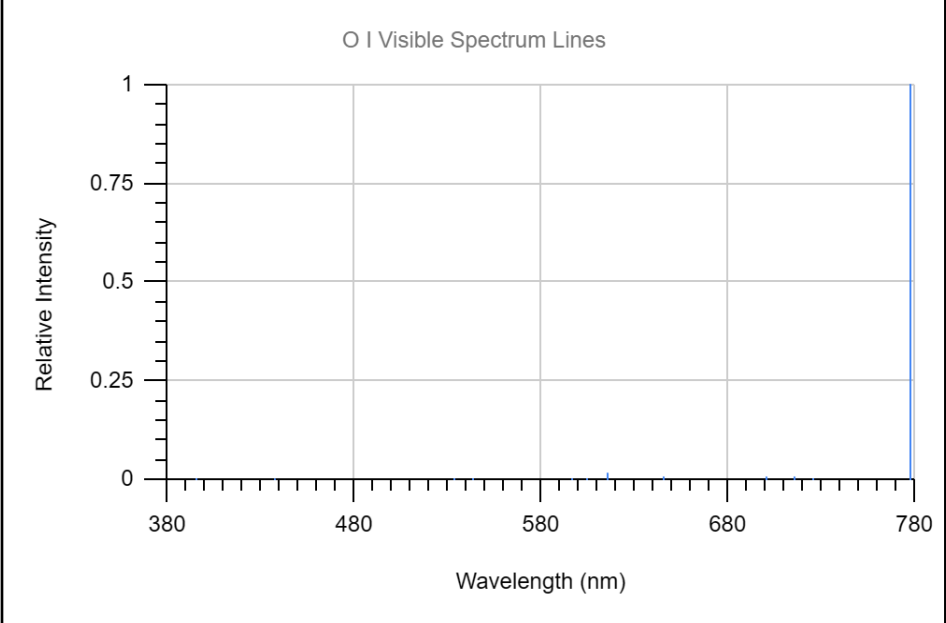
Electron Temperature: 4.05 T (eV) Electron Density: 9.10E+17 (cm⁻³)

_			
λ (nm)	Rel Intensity	λ (nm)	Rel Intensity
468.54	0.21	468.59	0.02
468.54	0.11	468.59	0.01
468.55	0.01	655.98	0.02
468.56	0.06	655.98	0.01
468.57	0.70	655.99	0.01
468.57	0.38	656.01	0.04
468.58	0.04	656.01	0.03
468.58	1.00	656.01	0.06
468.58	0.05	656.01	0.06
468.59	0.01	656.02	0.08

Oxygen - Neutral (O I)

(Return to Index)





O I Profile:

Peak Temperature: 8,000 K

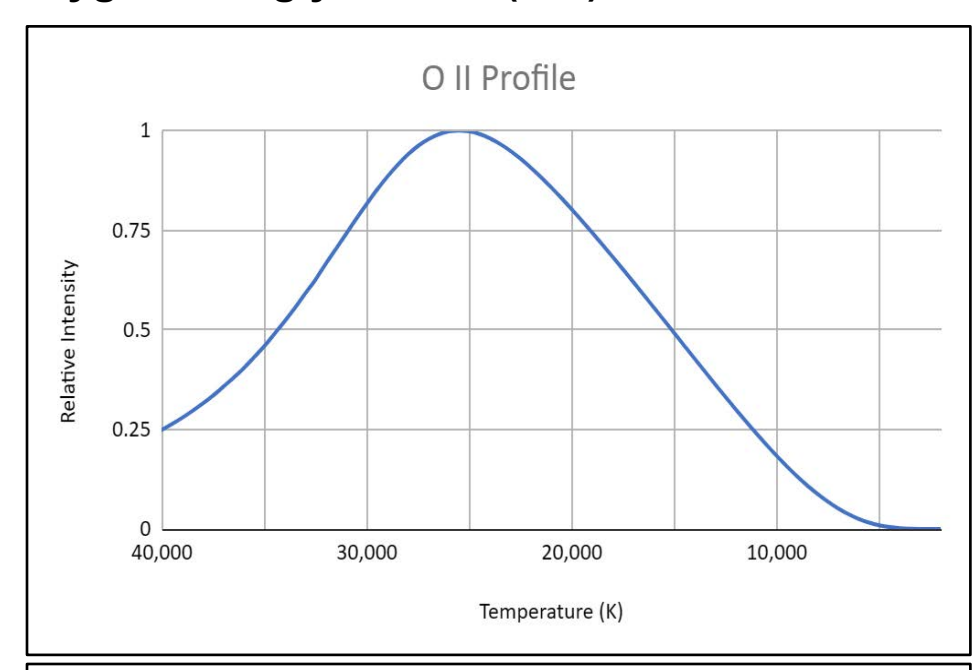
O I Visible Spectrum Lines:

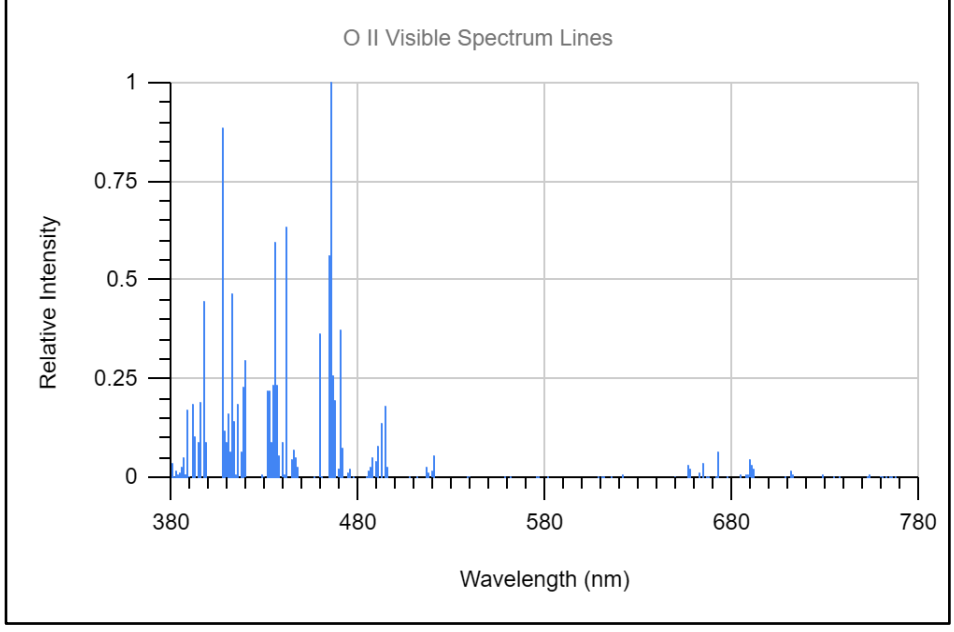
Electron Temperature: 0.69 T (eV) Electron Density: 5.12E+13 (cm⁻³)

λ (nm)	Rel Intensity	λ (nm)	Rel Intensity
777.19	1.00		
777.42	0.71		
777.54	0.43		

Oxygen - Singly Ionized (O II)

(Return to Index)





O II Profile:

Peak Temperature: 25,500 K

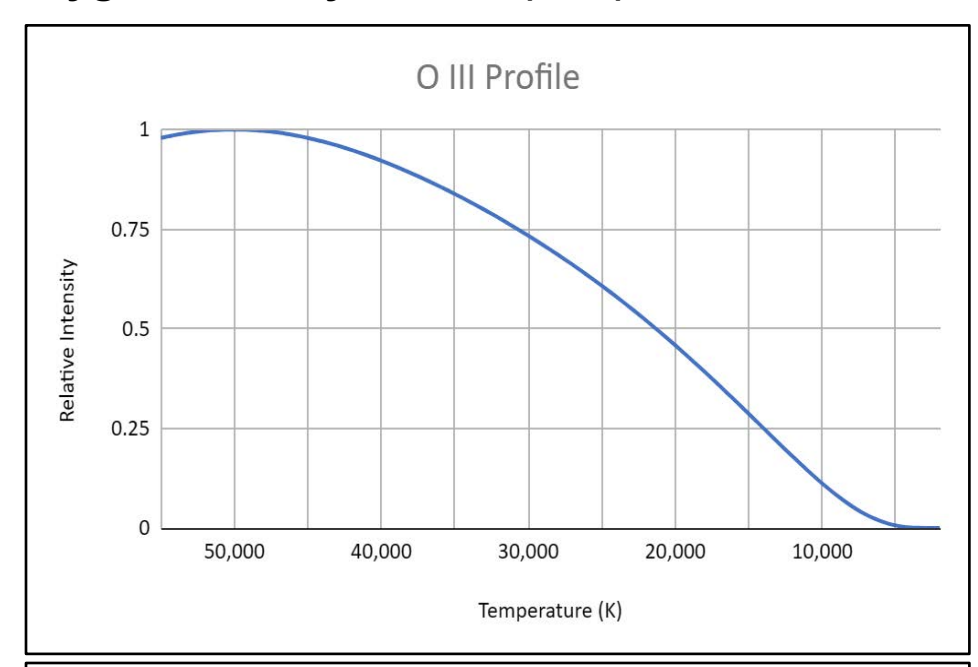
O II Visible Spectrum Lines:

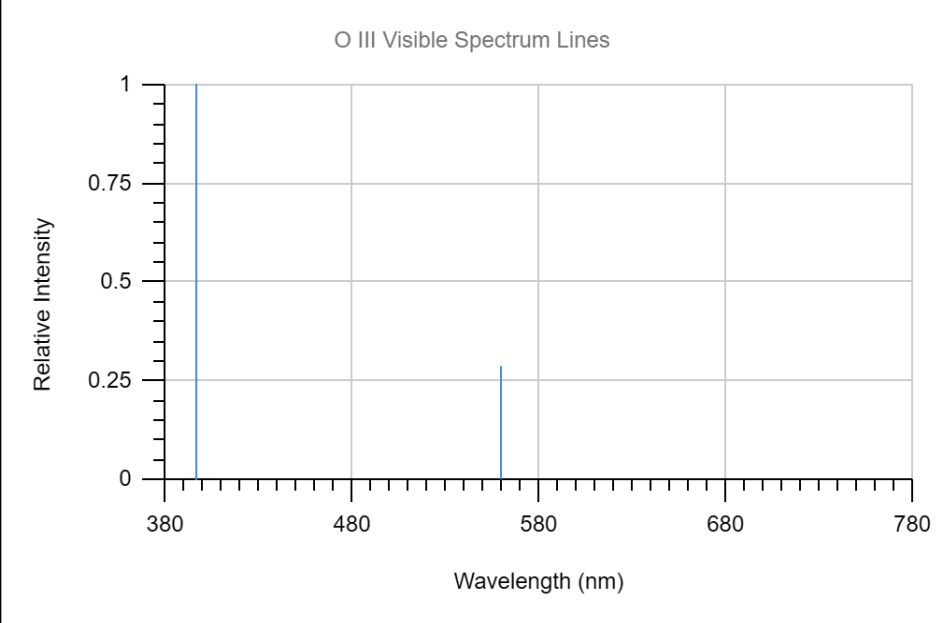
Electron Temperature: 2.20 T (eV) Electron Density: 3.10E+16 (cm⁻³)

λ (nm)	Rel Intensity	λ (nm)	Rel Intensity
388.22	0.17	434.74	0.18
391.20	0.19	434.94	0.60
391.93	0.10	435.13	0.29
395.44	0.19	436.69	0.23
397.33	0.45	441.49	0.64
406.96	0.26	441.70	0.36
406.99	0.40	459.10	0.37
407.22	0.64	459.62	0.26
407.59	0.89	463.89	0.23
408.51	0.12	464.18	0.56
410.50	0.16	464.91	1.00
411.92	0.47	465.08	0.22
413.28	0.14	466.16	0.26
415.33	0.19	467.62	0.20
418.54	0.23	469.90	0.13
418.98	0.29	469.92	0.24
431.71	0.22	470.53	0.38
431.96	0.22	492.45	0.14
434.56	0.24	494.30	0.18

Oxygen - Doubly Ionized (O III)

(Return to Index)





O III Profile:

Peak Temperature: 50,000 K

O III Visible Spectrum Lines:

Electron Temperature: 4.31 T (eV) Electron Density: 1.28E+18 (cm⁻³)

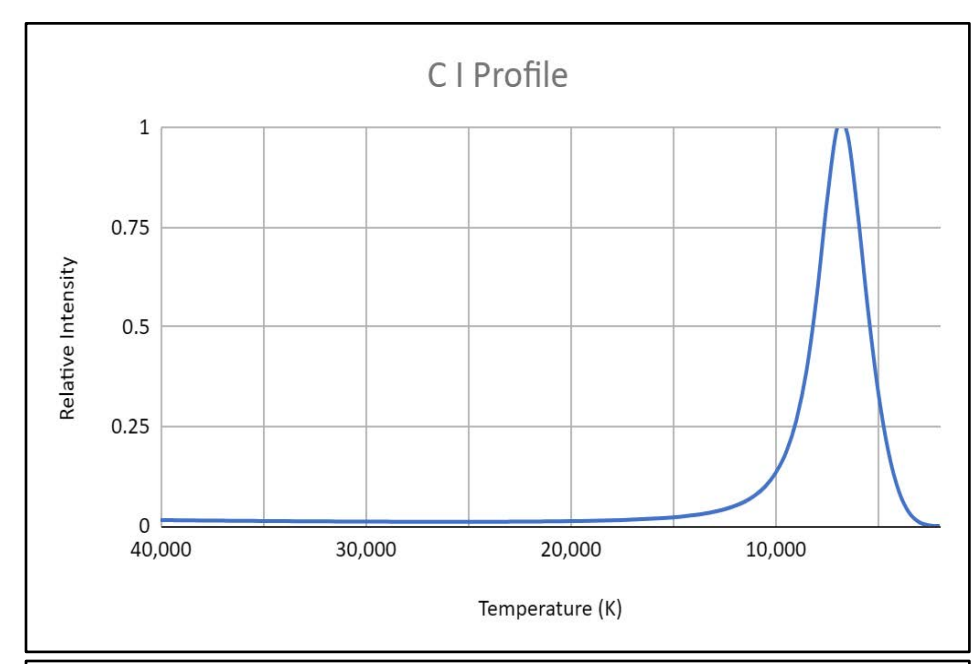
λ (nm)	Rel Intensity	λ (nm)	Rel Intensity
396.16	1.00		
559.23	0.29		

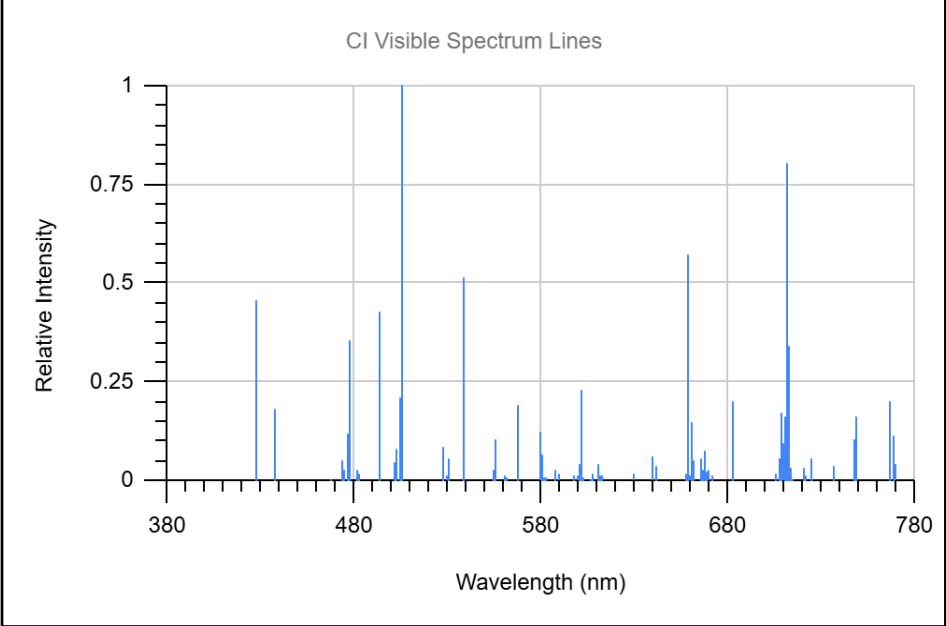
Notes:

1. O III line at 396.16 nm is close to and may be masked by H ϵ line at 397.01

Carbon - Neutral (C I)

(Return to Index)





C I Profile:

Peak Temperature: 7,000 K

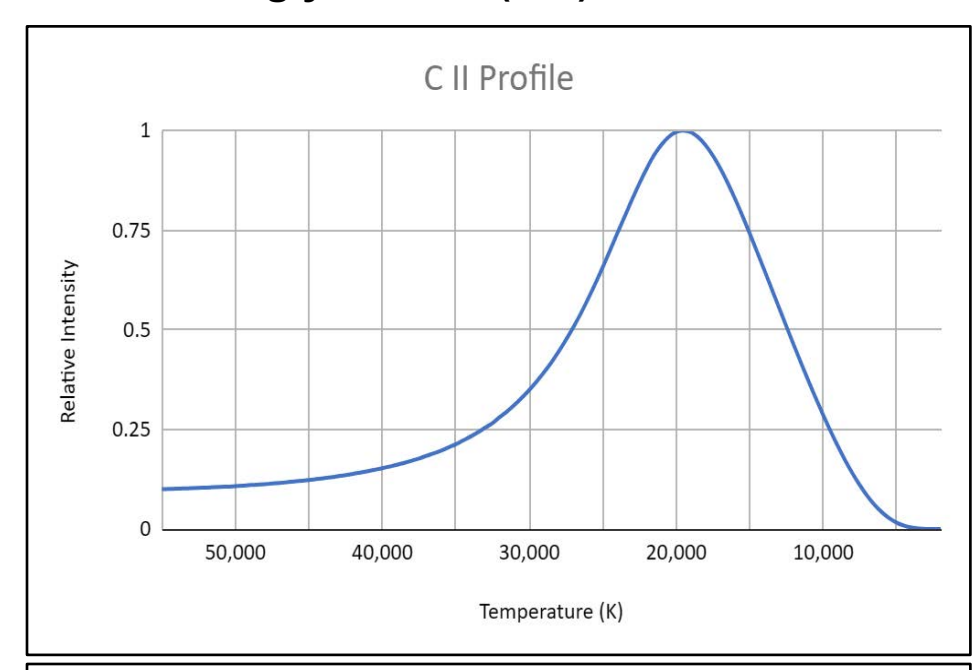
C I Visible Spectrum Lines:

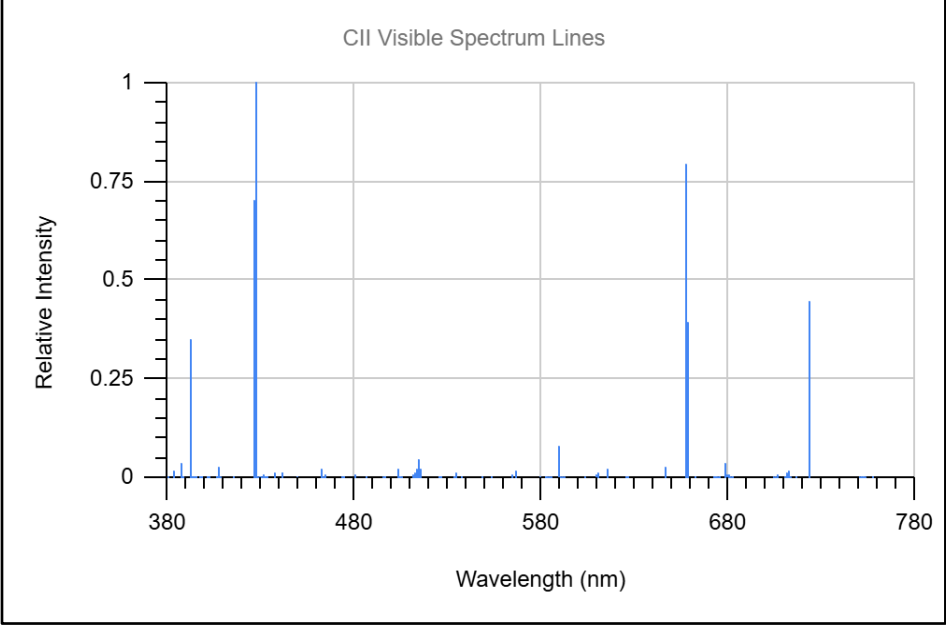
Electron Temperature: 0.61 T (eV) Electron Density: 2.45E+13 (cm⁻³)

λ (nm)	Rel Intensity	λ (nm)	Rel Intensity
426.90	0.46	601.33	0.10
437.14	0.18	601.48	0.12
476.23	0.09	658.76	0.57
476.25	0.12	660.24	0.15
477.00	0.10	682.81	0.20
477.17	0.36	708.78	0.17
477.59	0.13	709.33	0.10
493.20	0.43	710.01	0.16
502.38	0.08	710.89	0.12
503.91	0.21	711.15	0.40
504.15	0.13	711.32	0.80
504.18	0.12	711.52	0.16
505.21	1.00	711.52	0.56
526.90	0.08	711.70	0.60
538.03	0.52	711.97	0.34
555.10	0.10	747.62	0.10
566.89	0.19	748.34	0.16
579.31	0.12	766.24	0.20
601.32	0.23	768.52	0.12

Carbon - Singly Ionized (C II)

(Return to Index)





C II Profile:

Peak Temperature: 19,500 K

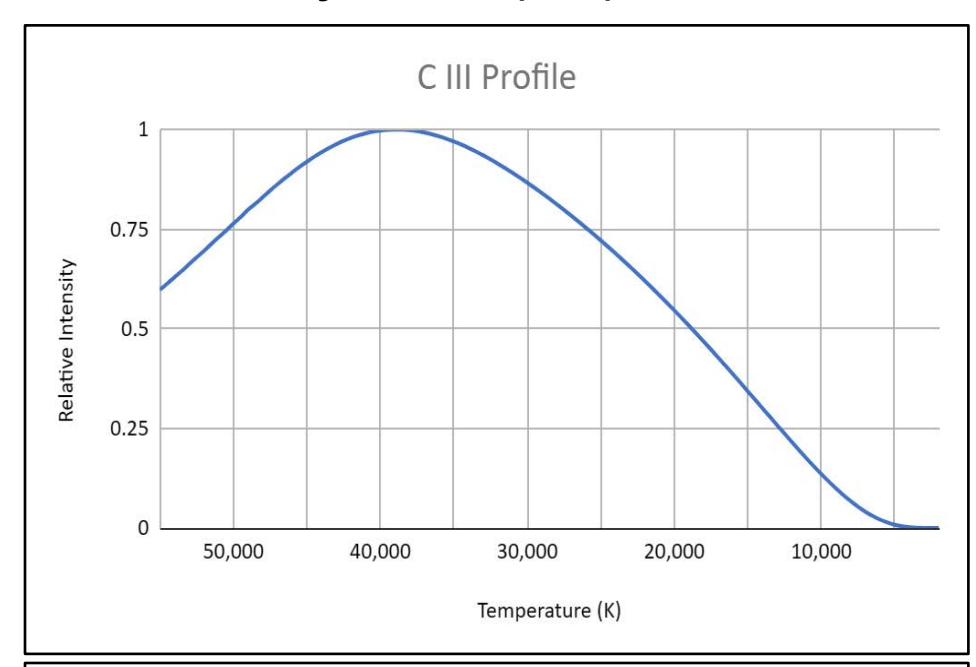
C II Visible Spectrum Lines:

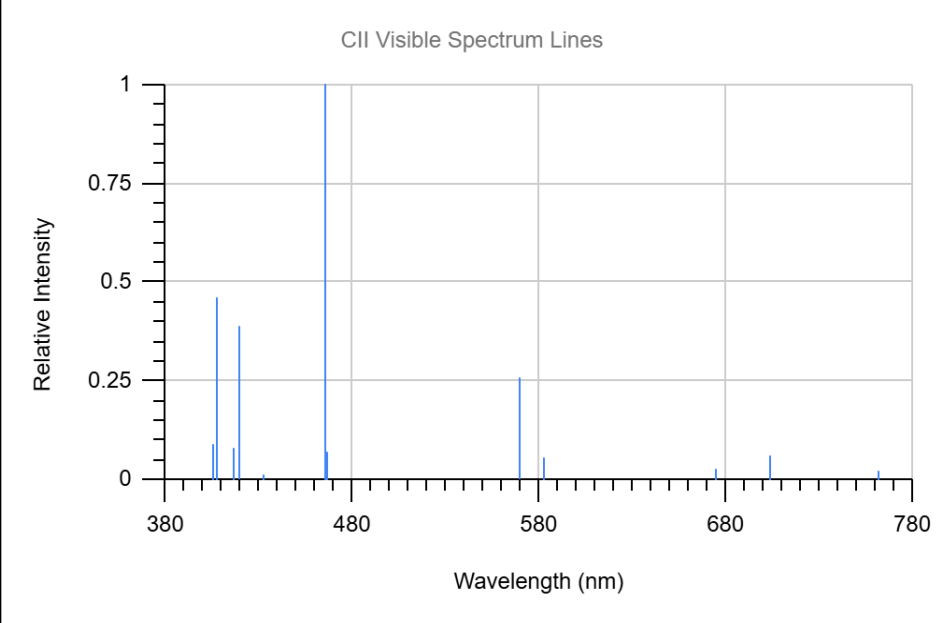
Electron Temperature: 1.68 T (eV) Electron Density: 7.04E+15 (cm⁻³)

λ (nm)	Rel Intensity	λ (nm)	Rel Intensity
391.90	0.18	588.98	0.08
392.07	0.35	657.80	0.79
426.70	0.70	658.29	0.40
426.72	1.00	723.13	0.25
426.73	0.05	723.64	0.45
514.52	0.05	723.72	0.05

Carbon - Doubly Ionized (C III)

(Return to Index)





C III Profile:

Peak Temperature: 39,000 K

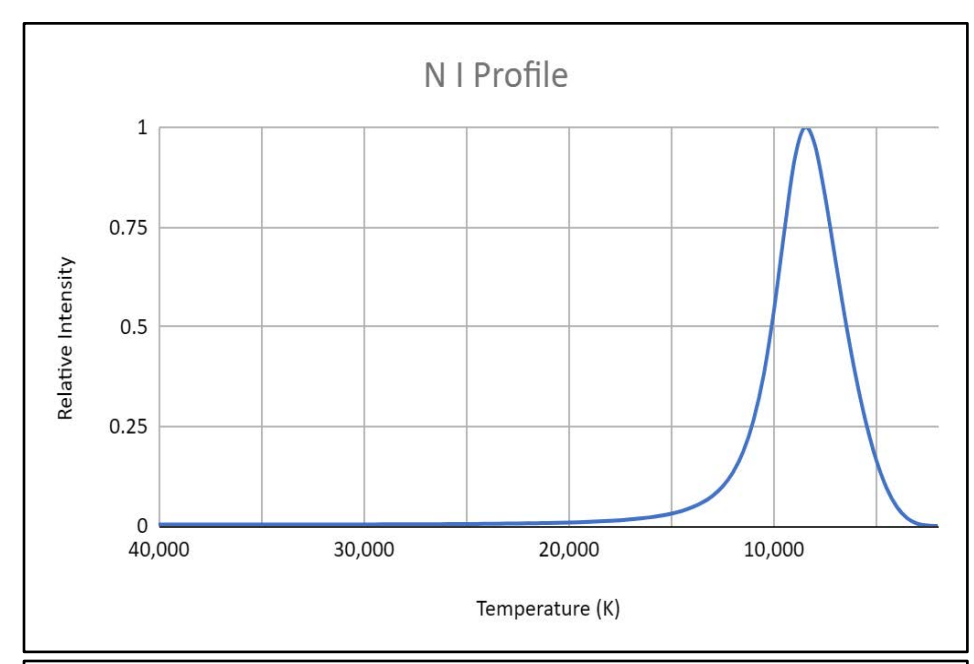
C III Visible Spectrum Lines:

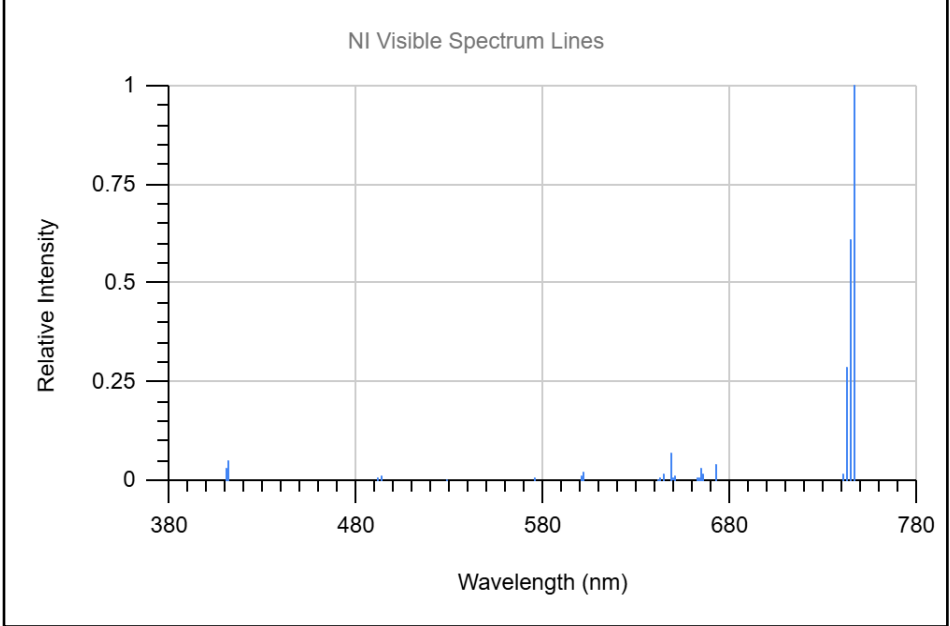
Electron Temperature: 3.36 T (eV) Electron Density: 3.24E+17 (cm⁻³)

λ (nm)	Rel Intensity	λ (nm)	Rel Intensity
405.61	0.09	465.02	0.60
406.79	0.27	465.15	0.20
406.89	0.35	466.59	0.07
407.03	0.46	569.59	0.26
416.29	0.08	582.64	0.06
418.69	0.39	703.73	0.06
464.74	1.00		

Nitrogen - Neutral (N I)

(Return to Index)





N I Profile:

Peak Temperature: 8,500 K

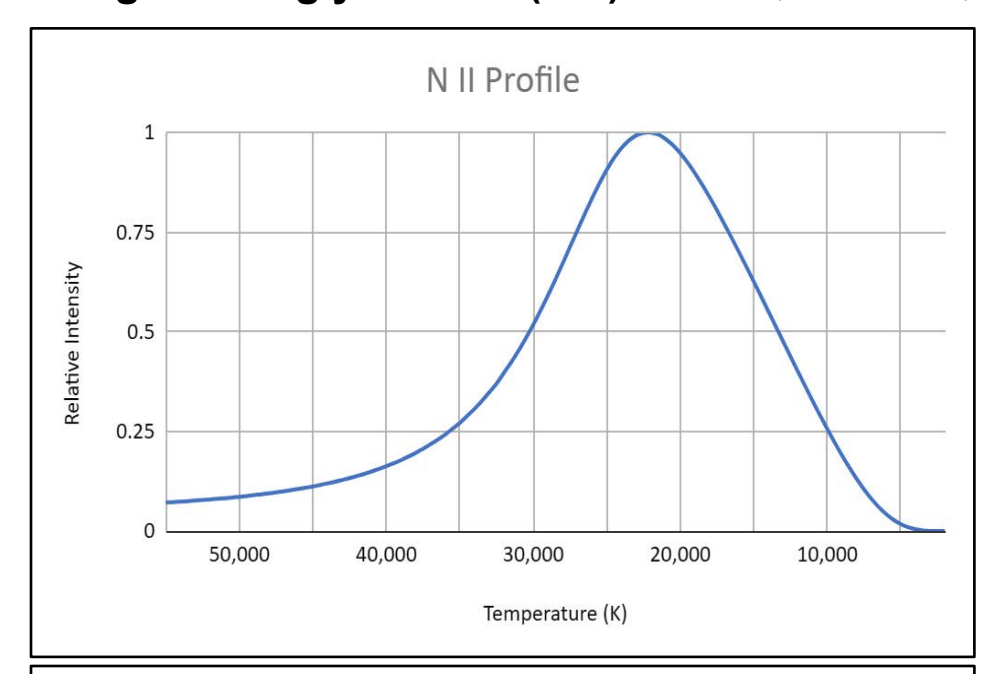
N I Visible Spectrum Lines:

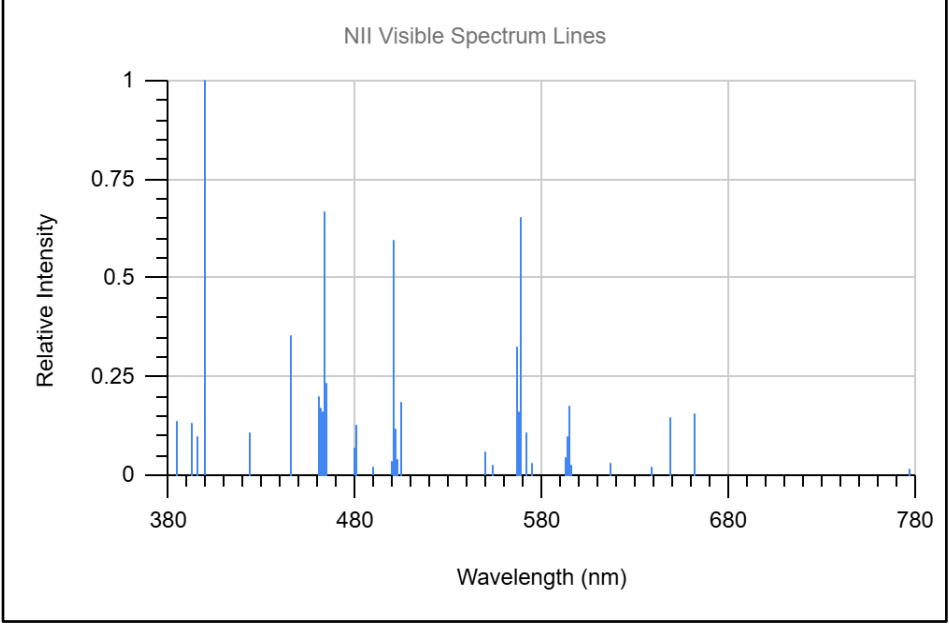
Electron Temperature: 0.73 T (eV) Electron Density: 7.16E+13 (cm⁻³)

λ (nm)	Rel Intensity	λ (nm)	Rel Intensity
410.99	0.05	742.36	0.29
648.27	0.07	744.23	0.61
648.48	0.05	746.83	1.00

Nitrogen - Singly Ionized (N II)

(Return to Index)





N II Profile:

Peak Temperature: 22,000 K

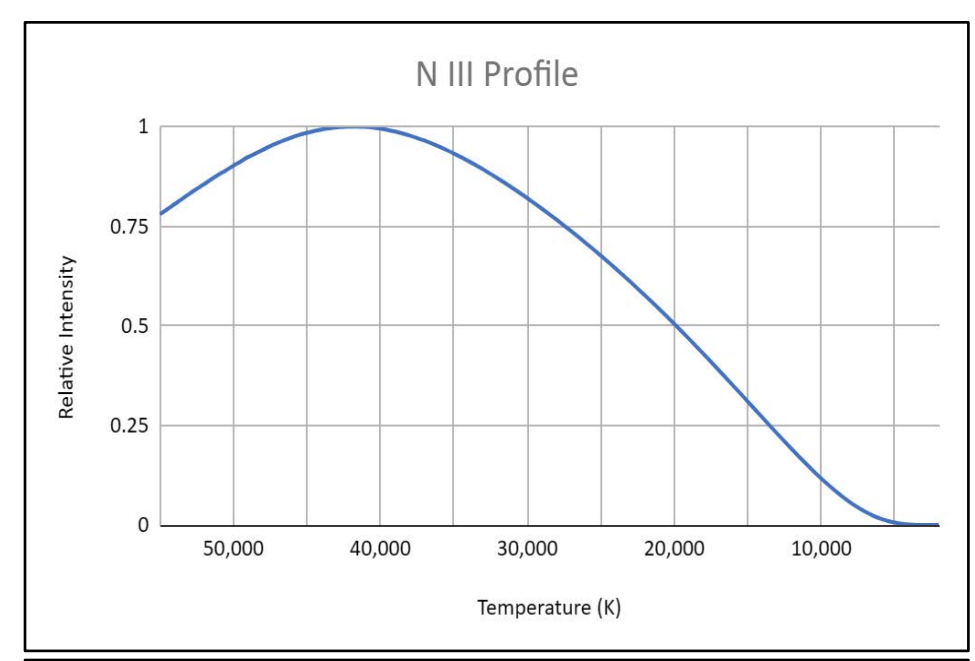
N II Visible Spectrum Lines:

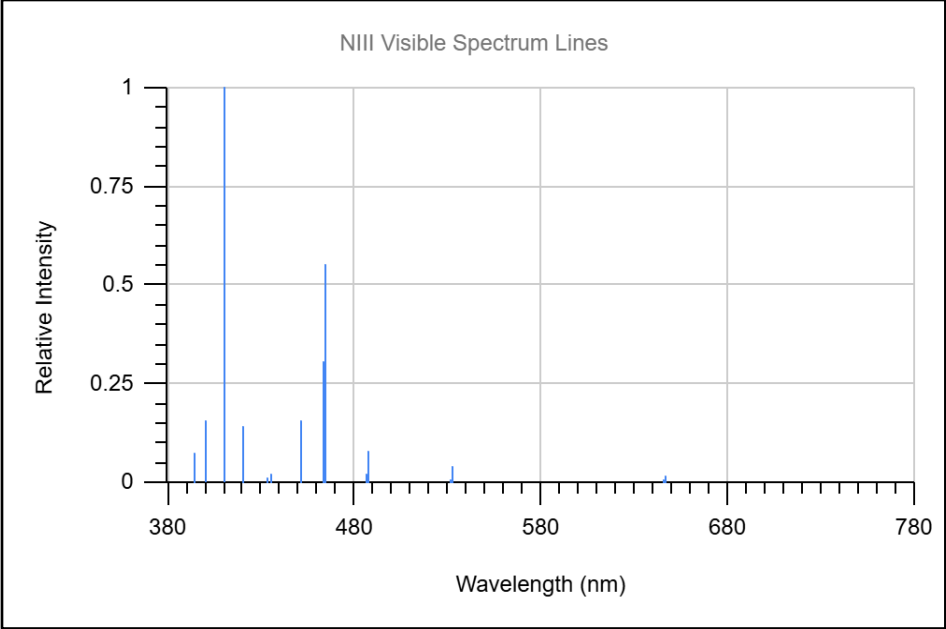
Electron Temperature: 1.90 T (eV) Electron Density: 1.37E+16 (cm⁻³)

λ (nm)	Rel Intensity	λ (nm)	Rel Intensity
383.84	0.14	500.52	0.60
391.90	0.13	500.73	0.19
395.59	0.10	501.06	0.12
399.50	1.00	501.64	0.05
422.77	0.11	504.51	0.19
444.70	0.36	549.57	0.06
460.15	0.20	566.66	0.33
460.72	0.17	567.60	0.16
461.39	0.11	567.96	0.65
462.14	0.16	568.62	0.10
463.05	0.67	571.08	0.11
464.31	0.24	593.18	0.10
478.81	0.07	594.17	0.18
480.33	0.13	648.21	0.15
500.15	0.43	661.06	0.16
500.27	0.05		

Nitrogen - Doubly Ionized (N III)

(Return to Index)





N III Profile:

Peak Temperature: 42,000 K

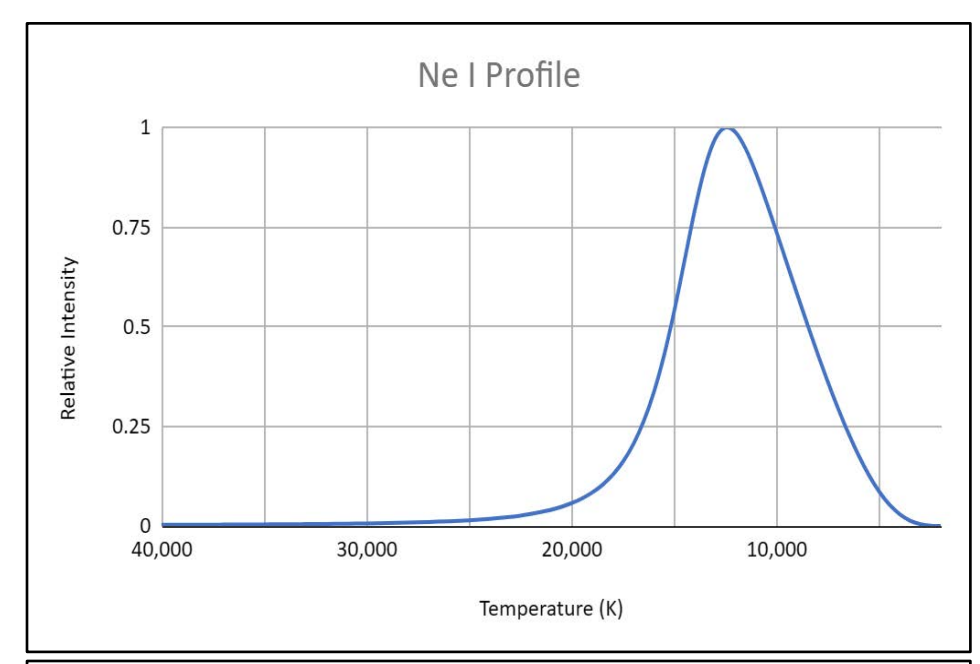
N III Visible Spectrum Lines:

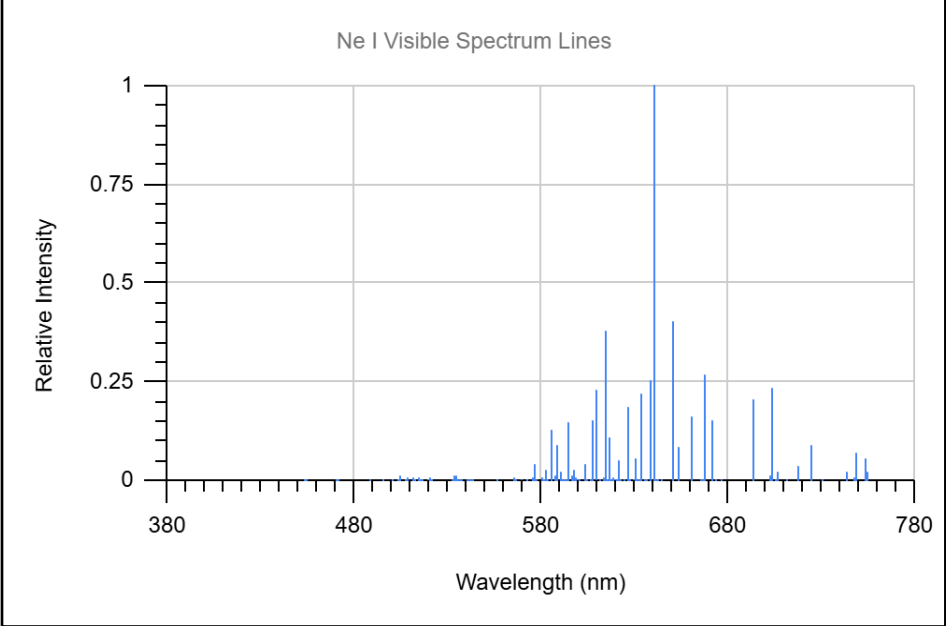
Electron Temperature: 3.62 T (eV) Electron Density: 4.89E+17 (cm⁻³)

λ (nm)	Rel Intensity	λ (nm)	Rel Intensity
393.85	0.08	420.01	0.14
399.86	0.11	451.49	0.16
400.36	0.16	463.41	0.31
409.74	1.00	464.06	0.55
410.34	0.50	486.72	0.08
419.57	0.08		

Neon - Neutral (Ne I)

(Return to Index)





Ne I Profile:

Peak Temperature: 12,500 K

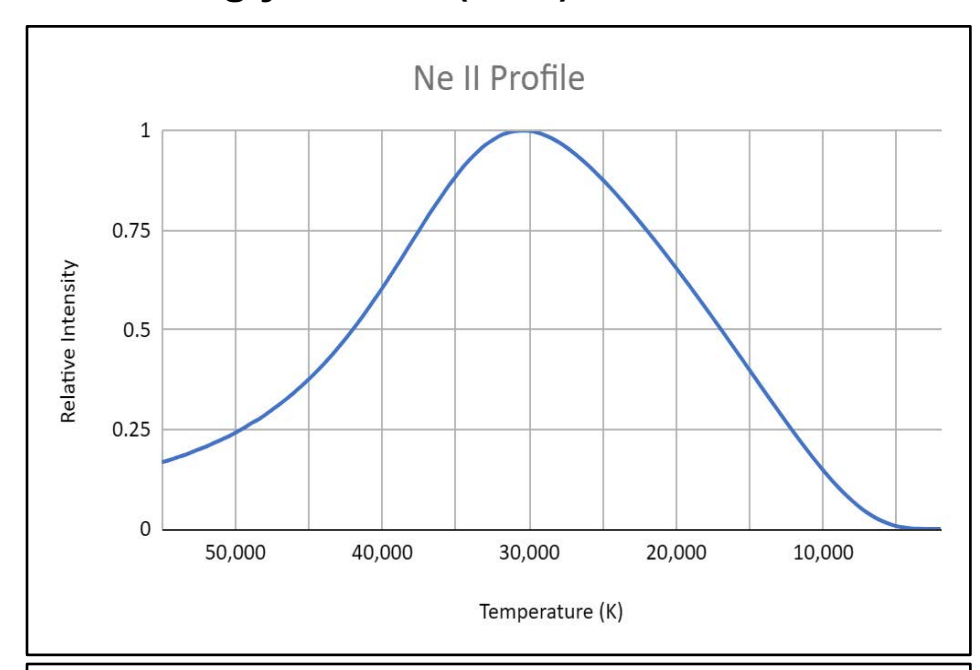
Ne I Visible Spectrum Lines:

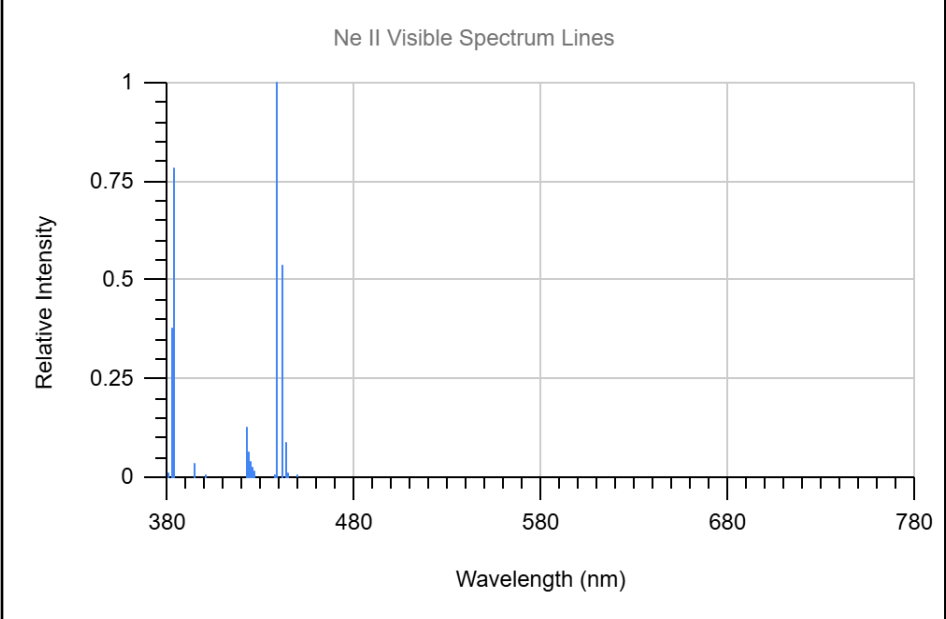
Electron Temperature: 1.08 T (eV) Electron Density: 6.03E+14 (cm⁻³)

λ (nm)	Rel Intensity	λ (nm)	Rel Intensity
585.25	0.13	640.22	1.00
588.19	0.09	650.65	0.40
594.48	0.15	653.29	0.08
607.43	0.15	659.90	0.16
609.62	0.23	667.83	0.27
614.31	0.38	671.70	0.15
616.36	0.11	692.95	0.21
621.73	0.05	703.24	0.24
626.65	0.19	724.52	0.09
630.48	0.05	748.89	0.07
633.44	0.22	753.58	0.06
638.30	0.25		

Neon - Singly Ionized (Ne II)

(Return to Index)





Ne II Profile:

Peak Temperature: 30,500 K

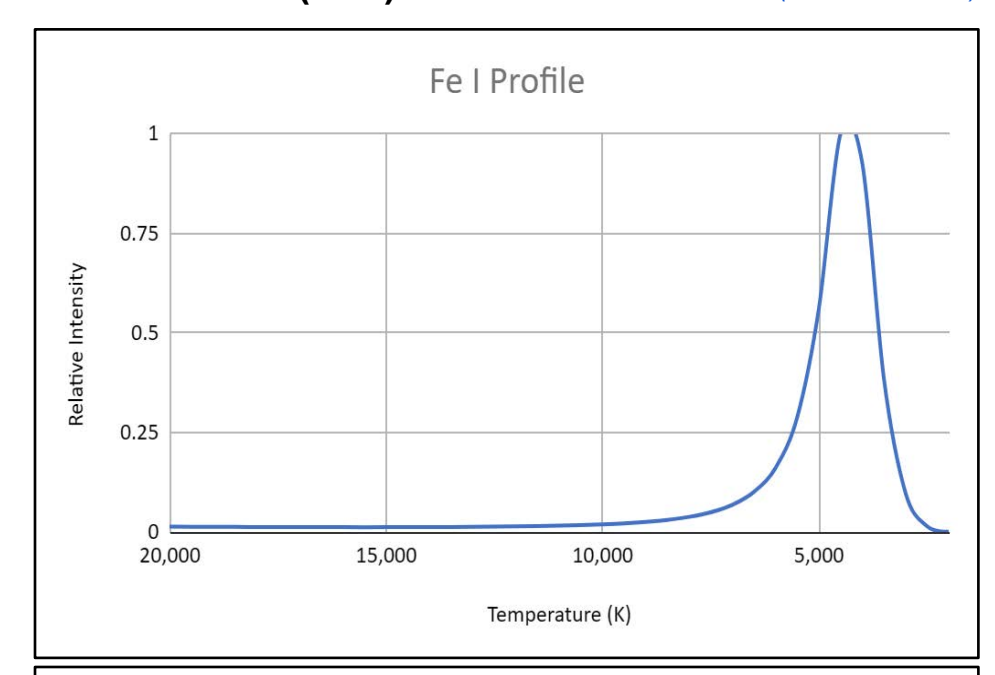
Ne II Visible Spectrum Lines:

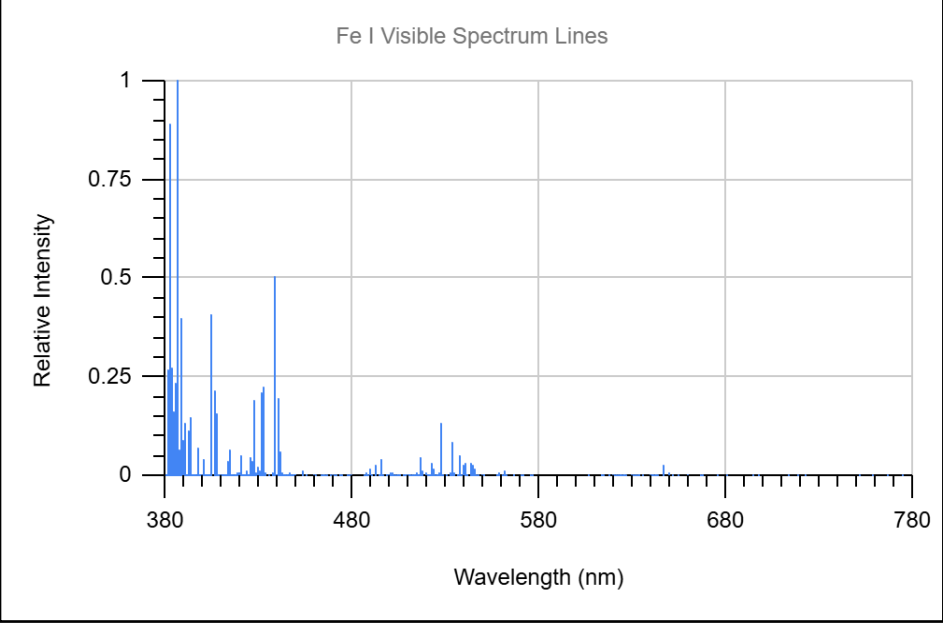
Electron Temperature: 2.63 T (eV) Electron Density: 8.34E+16 (cm⁻³)

λ (nm)	Rel Intensity	λ (nm)	Rel Intensity
381.84	0.38	437.95	1.00
382.98	0.78	438.51	0.72
421.94	0.13	441.31	0.54
423.15	0.06	442.85	0.09
437.94	0.07		

Iron - Neutral (Fe I)

(Return to Index)





Fe I Profile:

Peak Temperature: 4,500 K

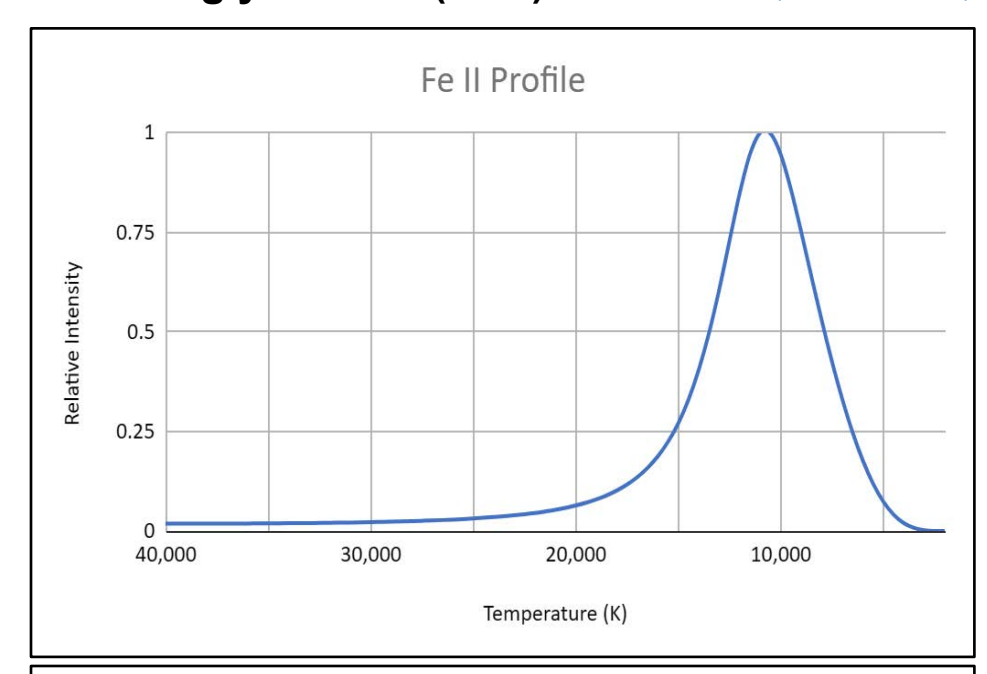
Fe I Visible Spectrum Lines:

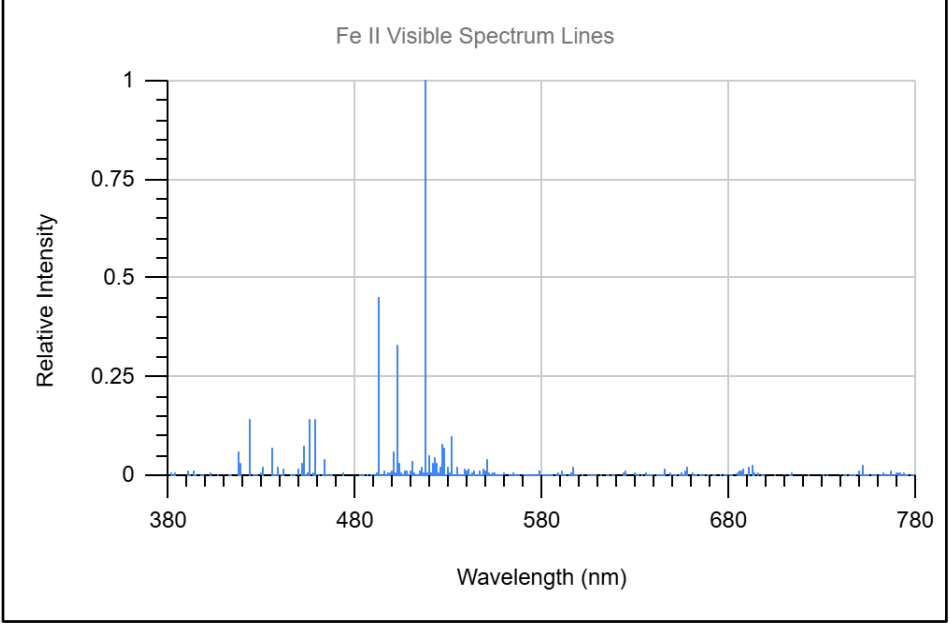
Electron Temperature: 0.39 T (eV) Electron Density: 2.13E+12 (cm⁻³)

λ (nm)	Rel Intensity	λ (nm)	Rel Intensity
381.58	0.268	392.03	0.076
382.04	0.892	392.29	0.111
382.44	0.212	392.79	0.132
382.59	0.552	393.03	0.149
382.78	0.155	396.93	0.072
383.42	0.274	404.58	0.409
384.04	0.161	406.36	0.214
384.10	0.110	407.17	0.158
385.00	0.067	414.39	0.063
385.64	0.235	420.20	0.051
385.99	1.000	427.18	0.193
386.55	0.053	430.79	0.209
387.25	0.064	432.58	0.227
387.80	0.071	438.35	0.503
387.86	0.180	440.47	0.198
388.63	0.397	441.51	0.060
389.57	0.090	526.95	0.131
389.97	0.131	532.80	0.086
390.29	0.051	537.15	0.053

Iron - Singly Ionized (Fe II)

(Return to Index)





Fe II Profile:

Peak Temperature: 11,000 K

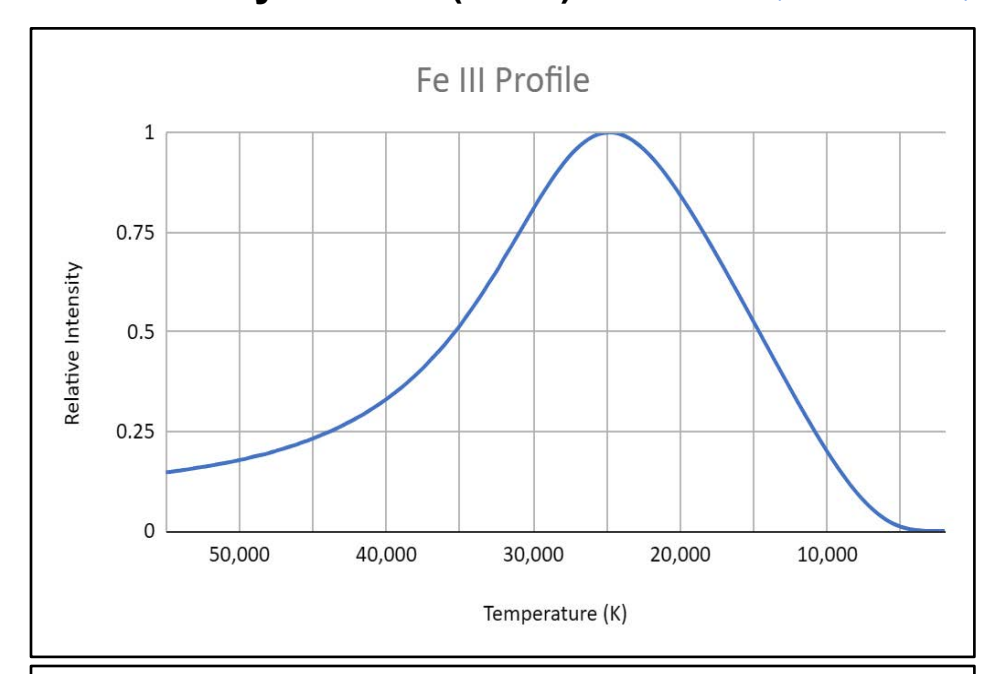
Fe II Visible Spectrum Lines:

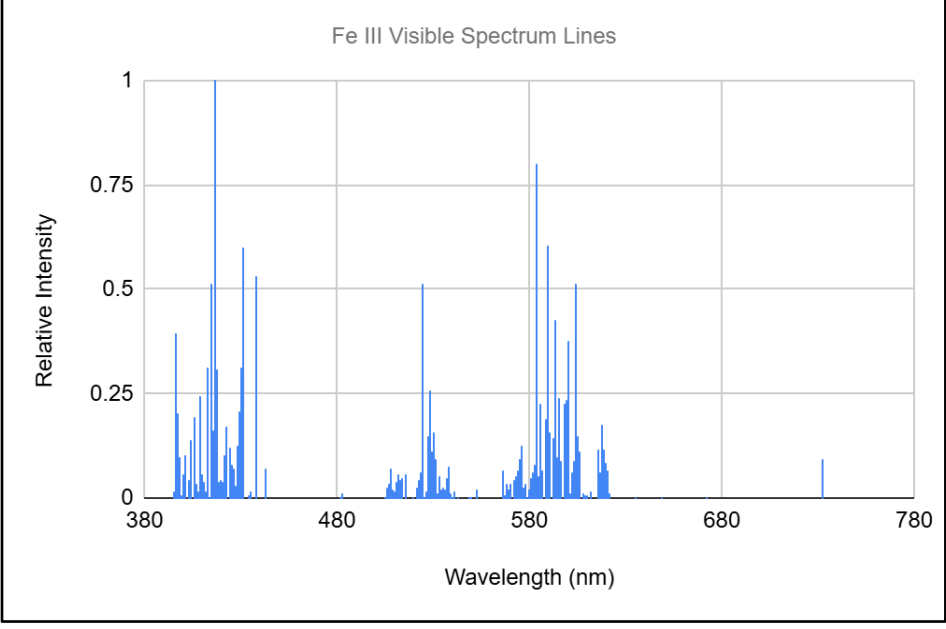
Electron Temperature: 0.95 T (eV) Electron Density: 2.98E+14 (cm⁻³)

λ (nm)	Rel Intensity	λ (nm)	Rel Intensity
417.35	0.061	510.07	0.035
417.89	0.033	514.95	0.022
423.32	0.141	516.90	1.000
430.32	0.020	519.76	0.049
435.18	0.068	521.69	0.030
438.54	0.020	522.75	0.044
450.83	0.022	523.46	0.034
451.53	0.032	524.80	0.021
452.26	0.077	526.03	0.079
454.95	0.140	527.60	0.070
455.59	0.042	529.17	0.021
458.38	0.141	531.66	0.097
462.93	0.042	533.96	0.021
492.39	0.451	550.62	0.043
500.20	0.061	596.17	0.024
500.42	0.023	657.14	0.020
501.84	0.332	690.57	0.022
503.06	0.020	692.20	0.027
503.57	0.030	751.32	0.026

Iron - Doubly Ionized (Fe III)







Fe III Profile:

Peak Temperature: 25,000 K

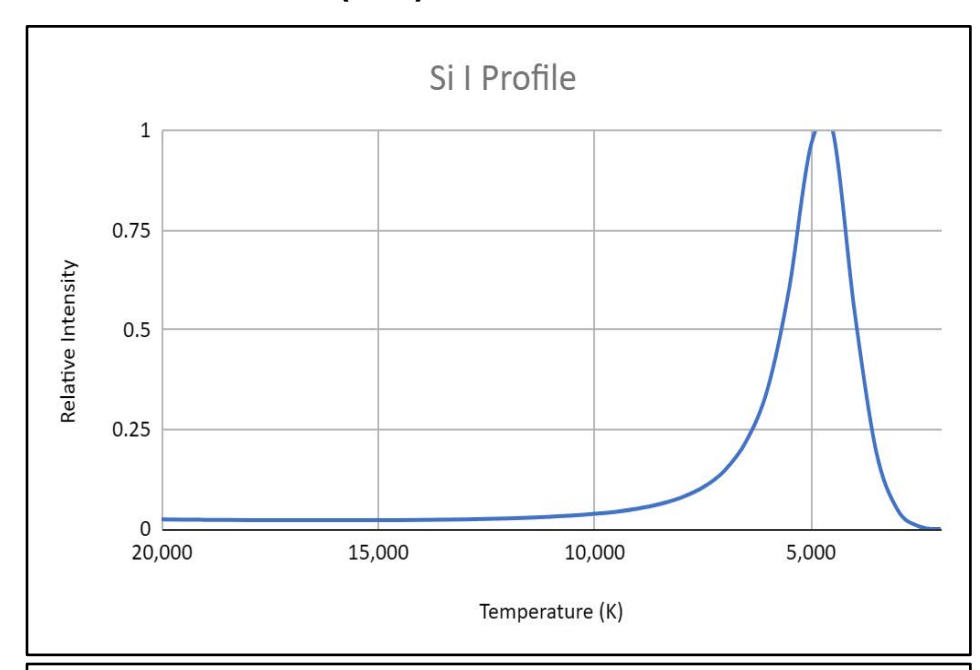
Fe III Visible Spectrum Lines:

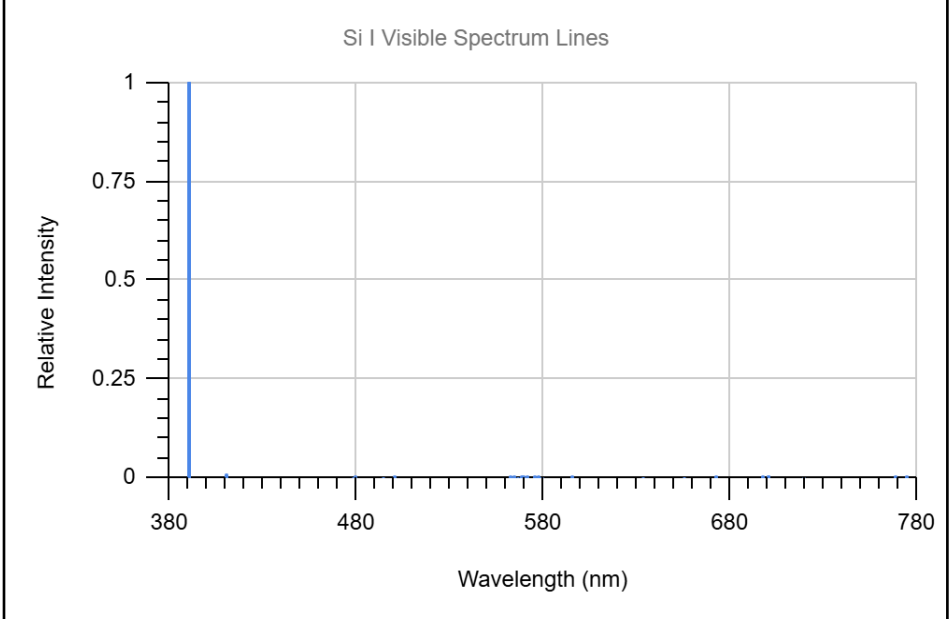
Electron Temperature: 2.16 T (eV) Electron Density: 2.78E+16 (cm⁻³)

λ (nm)	Rel Intensity	λ (nm)	Rel Intensity
395.43	0.394	437.22	0.219
396.87	0.202	437.23	0.300
405.31	0.193	437.25	0.403
408.10	0.246	437.28	0.531
412.09	0.187	524.33	0.515
412.20	0.311	527.65	0.203
412.28	0.280	528.23	0.259
413.78	0.515	583.39	0.800
413.93	0.402	585.46	0.228
415.50	0.163	587.63	0.187
416.47	1.000	589.19	0.603
416.49	0.218	592.97	0.426
416.68	0.308	595.36	0.241
417.43	0.281	597.93	0.227
422.23	0.172	598.91	0.235
428.62	0.207	599.95	0.375
429.69	0.314	603.26	0.515
430.48	0.443	603.66	0.207
431.04	0.598	616.98	0.175

Silicon- Neutral (Si I)

(Return to Index)





Si I Profile:

Peak Temperature: 4,500 K

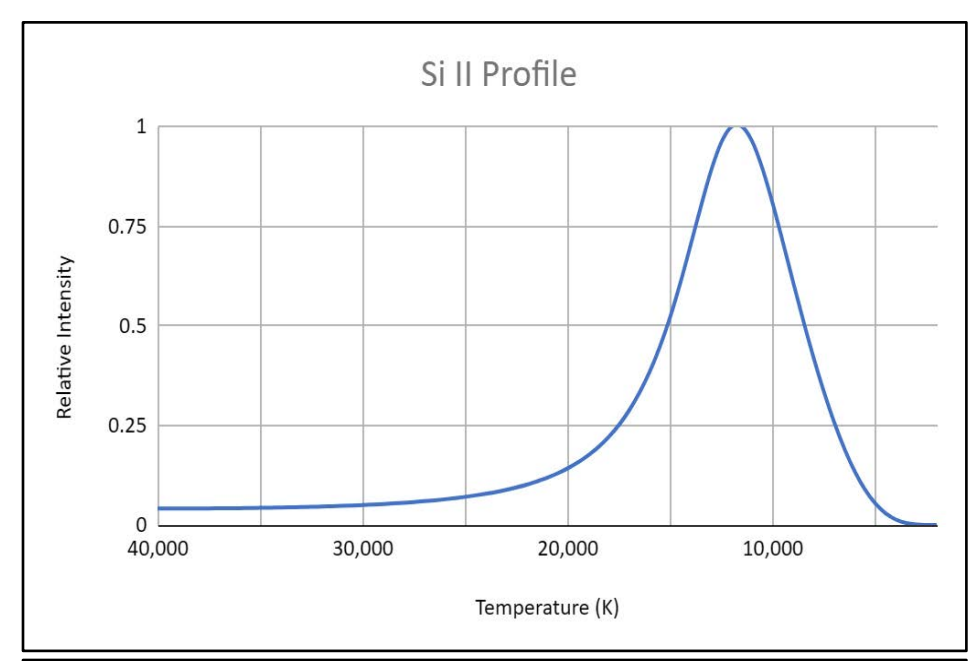
Si I Visible Spectrum Lines:

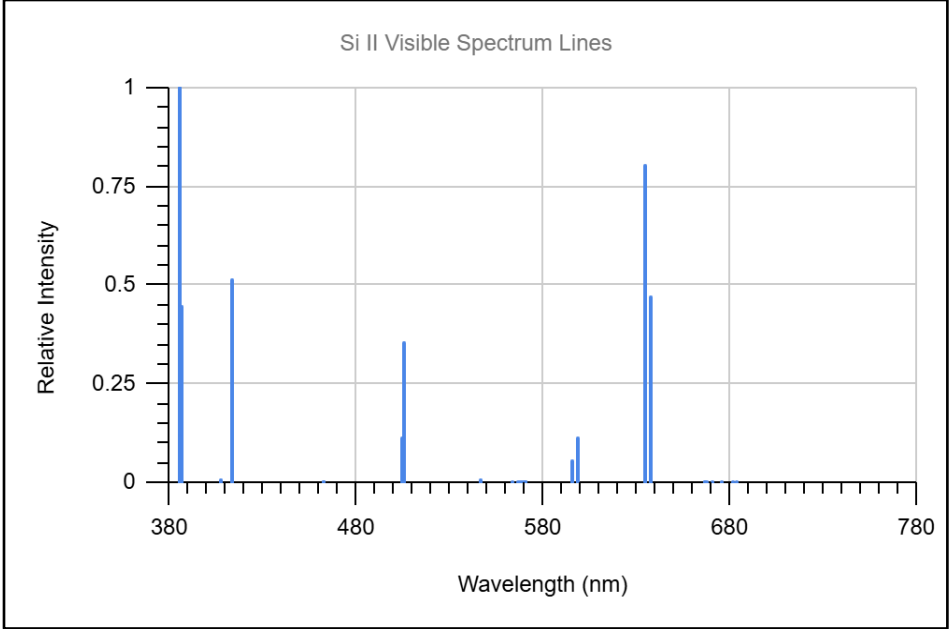
Electron Temperature: 0.39 T (eV) Electron Density: 2.13E+12 (cm⁻³)

λ (nm)	Rel Intensity	λ (nm)	Rel Intensity
390.55	1.00		

Silicon-Singly Ionized (Si II)

(Return to Index)





Si II Profile:

Peak Temperature: 12,000 K

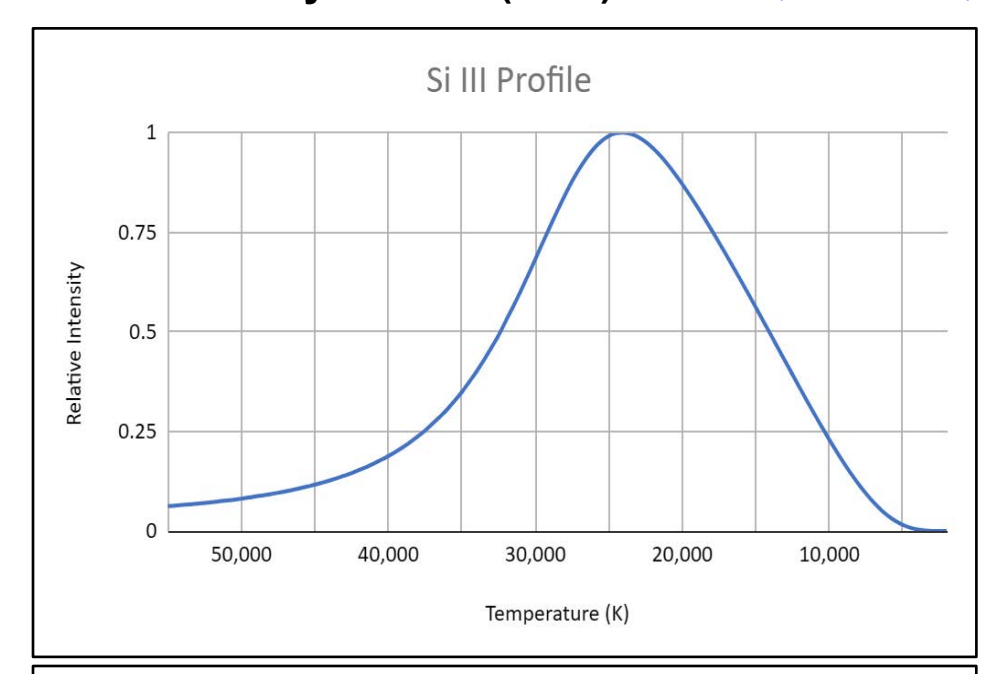
Si II Visible Spectrum Lines:

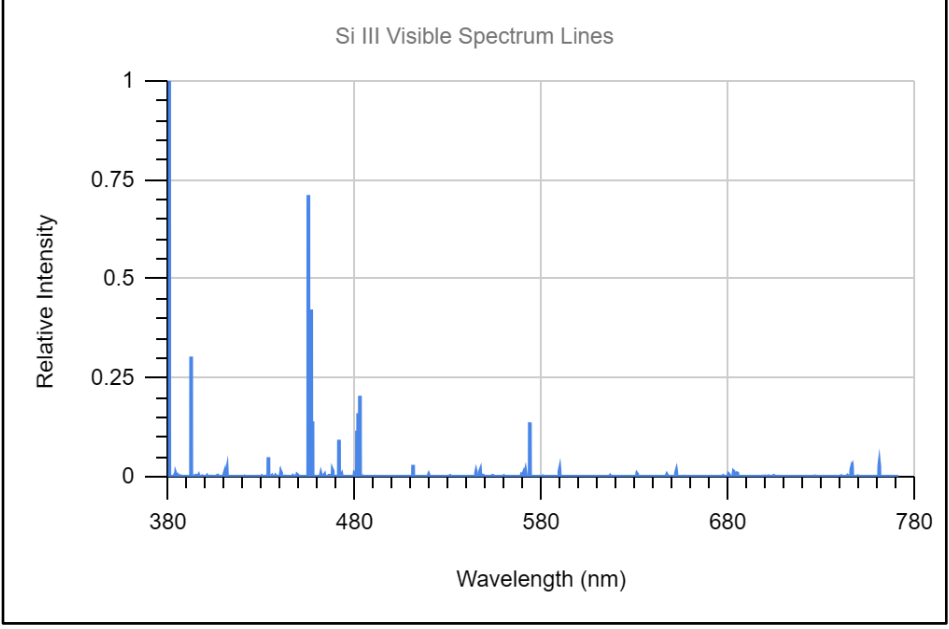
Electron Temperature: 1.04 T (eV) Electron Density: 4.81E+14 (cm⁻³)

λ (nm)	Rel Intensity	λ (nm)	Rel Intensity
385.37	0.12	505.60	0.36
385.60	1.00	595.76	0.06
386.26	0.45	597.89	0.11
412.81	0.33	634.71	0.81
413.09	0.52	637.14	0.47
504.10	0.12		

Silicon- Doubly Ionized (Si III)

(Return to Index)





Si III Profile:

Peak Temperature: 24,000 K

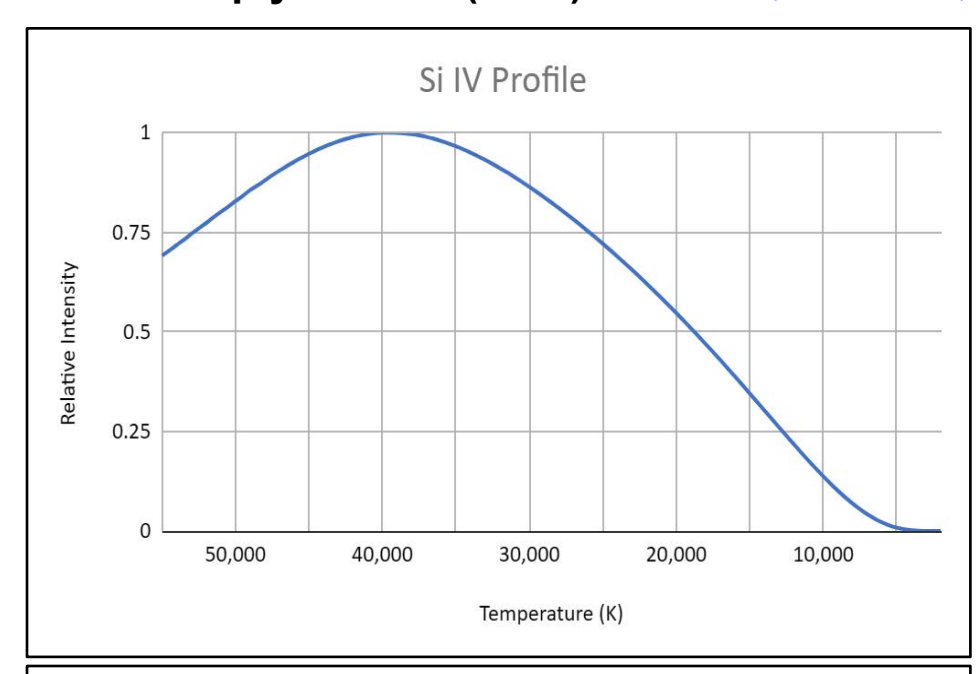
Si III Visible Spectrum Lines:

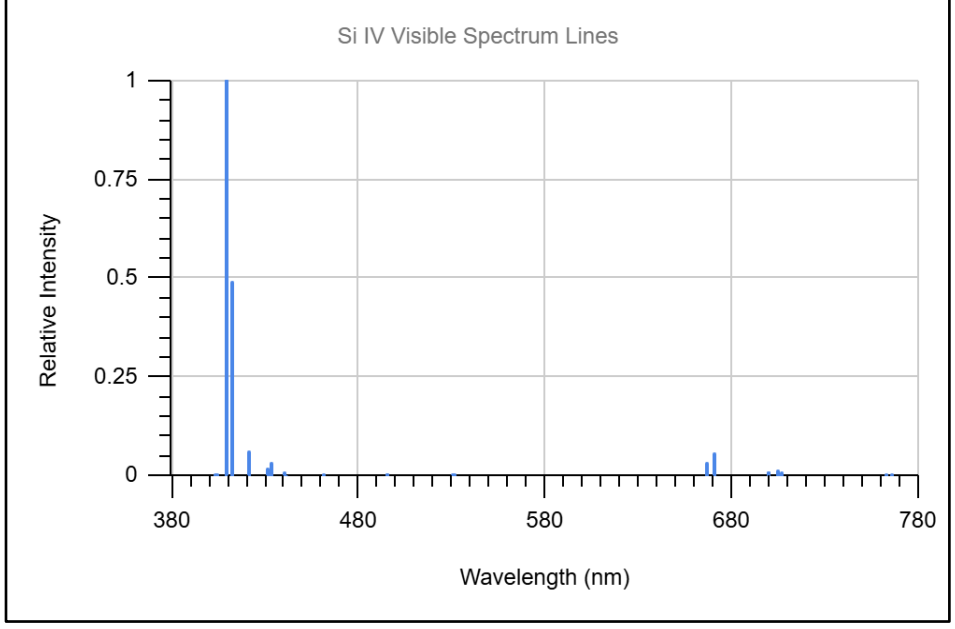
Electron Temperature: 2.07 T (eV) Electron Density: 2.22E+16 (cm⁻³)

λ (nm)	Rel Intensity	λ (nm)	Rel Intensity
455.26	1.00	482.90	0.14
380.65	0.87	481.97	0.11
456.78	0.60	481.33	0.08
392.45	0.21	471.67	0.07
457.48	0.20	433.85	0.07
573.97	0.19		

Silicon-Triply Ionized (Si IV)

(Return to Index)





Si IV Profile:

Peak Temperature: 39,500 K

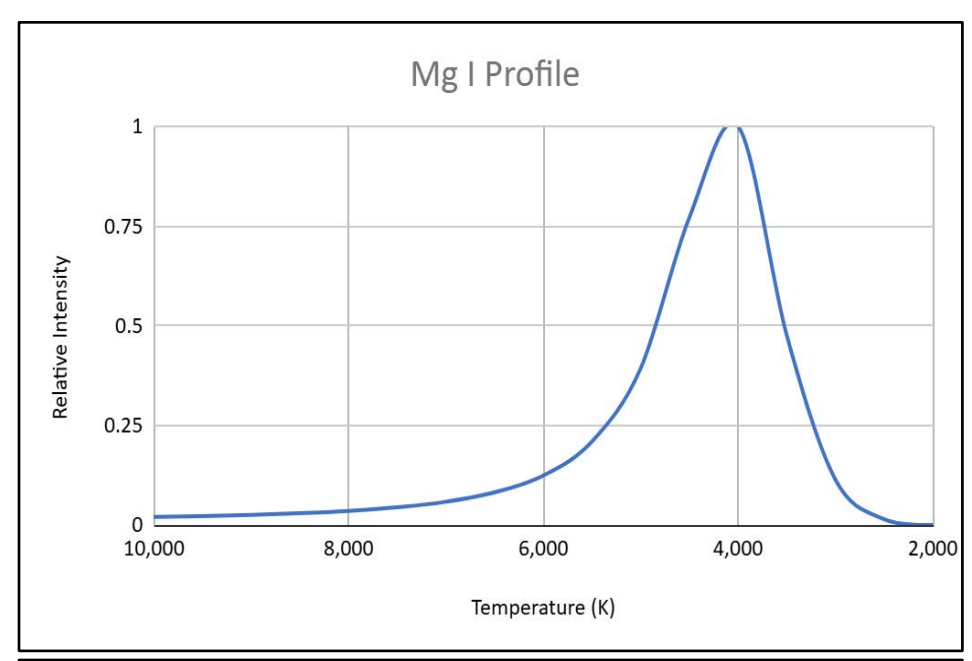
Si IV Visible Spectrum Lines:

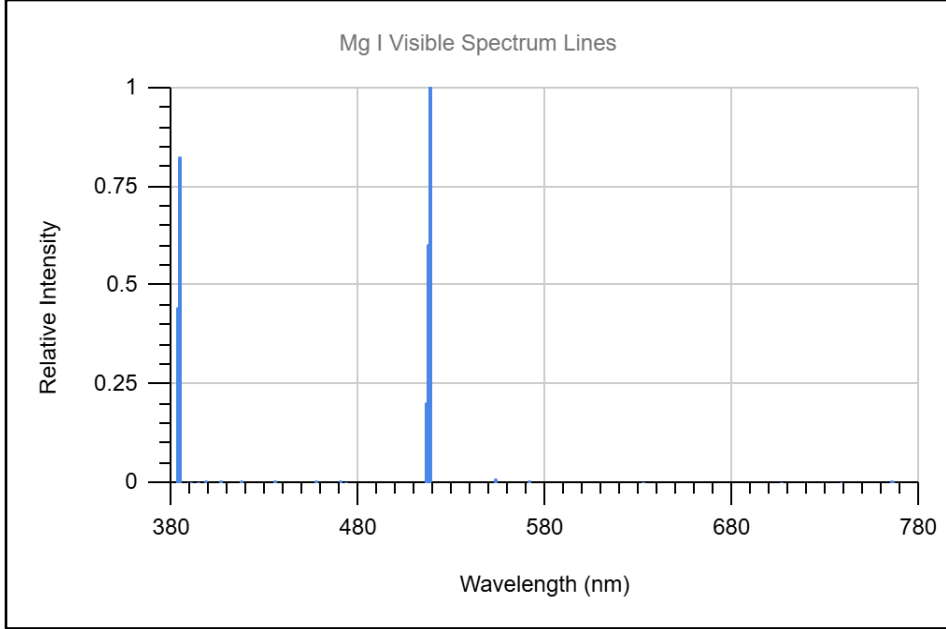
Electron Temperature: 3.40 T (eV) Electron Density: 3.48E+17 (cm⁻³)

λ (nm)	Rel Intensity	λ (nm)	Rel Intensity
408.89	1.00	421.24	0.06
411.61	0.49	670.12	0.06

Magnesium - Neutral (Mg I)

(Return to Index)





Mg I Profile:

Peak Temperature: 4,000 K

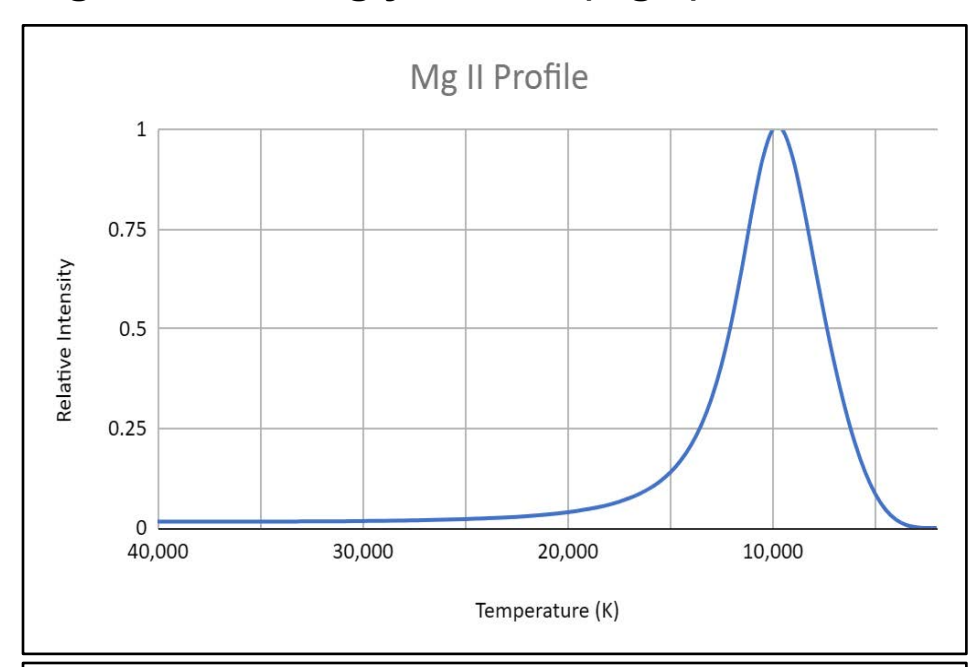
Mg I Visible Spectrum Lines:

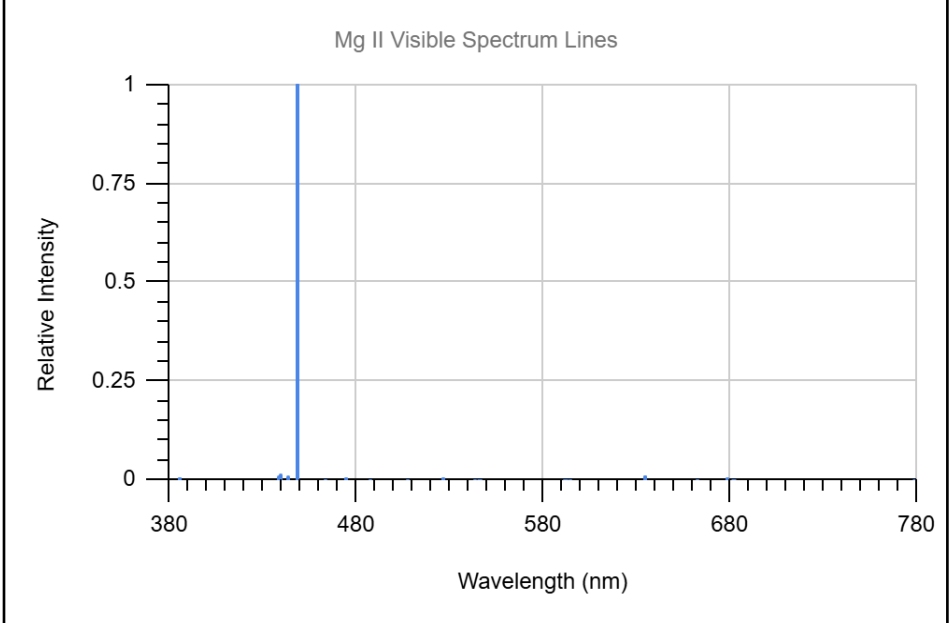
Electron Temperature: 0.35 T (eV) Electron Density: 1.11E+12 (cm⁻³)

λ (nm)	Rel Intensity	λ (nm)	Rel Intensity
382.94	0.20	383.83	0.15
383.23	0.15	516.73	0.20
383.23	0.44	517.27	0.60
383.83	0.82	518.36	1.00

Magnesium - Singly Ionized (Mg II)

(Return to Index)





Mg II Profile:

Peak Temperature: 10,000 K

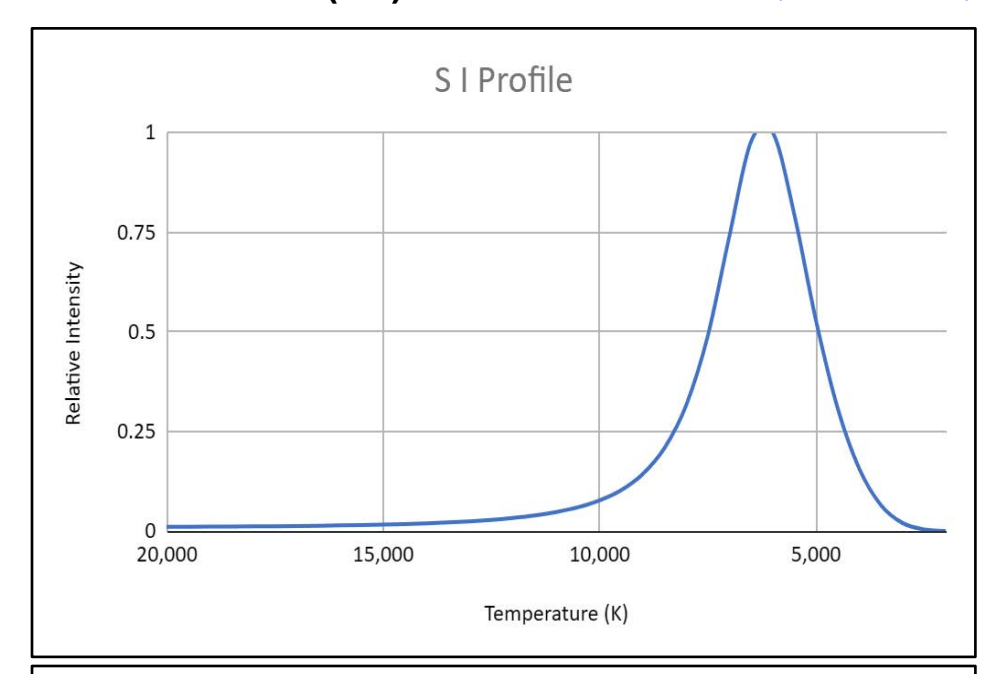
Mg II Visible Spectrum Lines:

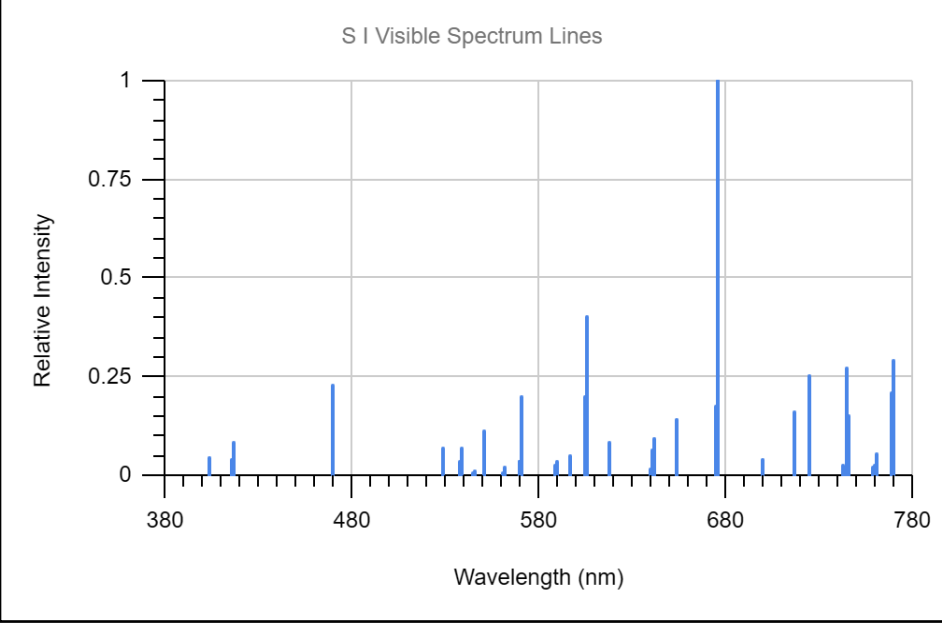
Electron Temperature: 0.86 T (eV) Electron Density: 1.76E+14 (cm⁻³)

λ (nm)	Rel Intensity	λ (nm)	Rel Intensity
448.11	1.00		
448.13	0.70		

Sulfur- Neutral (S I)

(Return to Index)





S I Profile:

Peak Temperature: 6,000 K

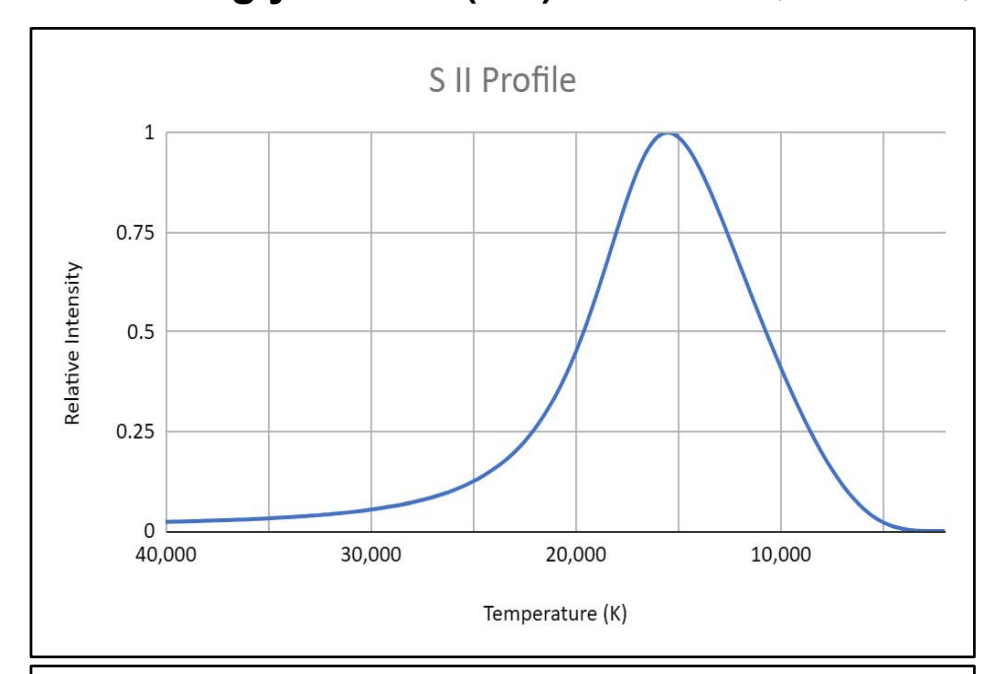
S I Visible Spectrum Lines:

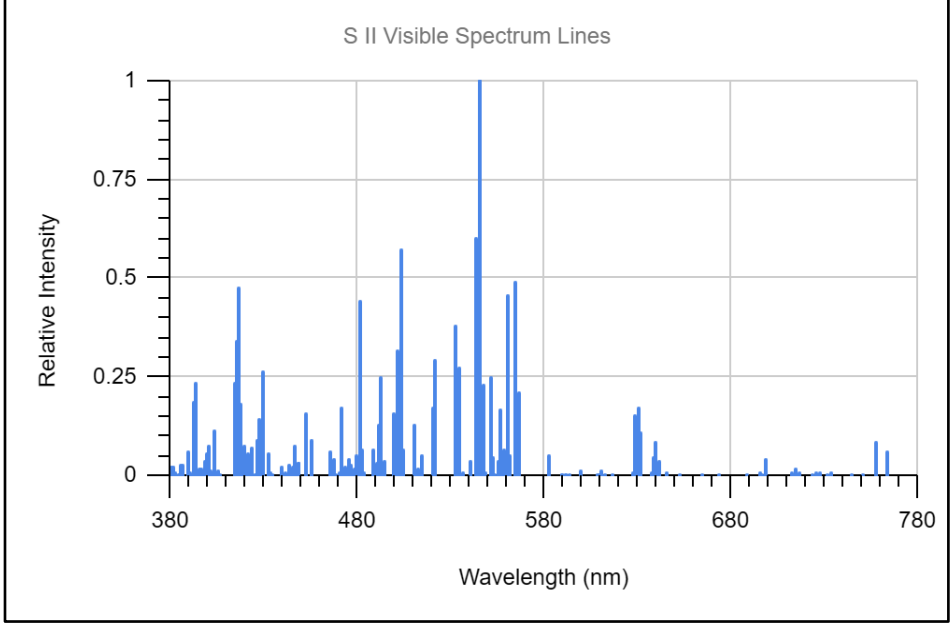
Electron Temperature: 0.52 T (eV) Electron Density: 1.04E+13 (cm⁻³)

λ (nm)	Rel Intensity	λ (nm)	Rel Intensity
403.40	0.05	653.64	0.07
415.77	0.09	653.86	0.14
469.41	0.23	674.37	0.17
469.54	0.15	674.89	0.50
469.62	0.07	675.72	1.00
527.90	0.07	716.14	0.16
538.10	0.07	716.66	0.06
550.15	0.06	716.78	0.09
550.70	0.12	724.31	0.13
570.02	0.10	724.37	0.05
570.61	0.20	724.48	0.25
596.12	0.05	744.33	0.27
604.19	0.08	744.77	0.06
604.19	0.07	744.90	0.10
604.61	0.20	745.02	0.15
605.27	0.40	760.08	0.06
617.58	0.08	767.96	0.12
640.81	0.07	768.61	0.21
641.55	0.09	769.67	0.29

Sulfur- Singly Ionized (S II)

(Return to Index)





S II Profile:

Peak Temperature: 15,500 K

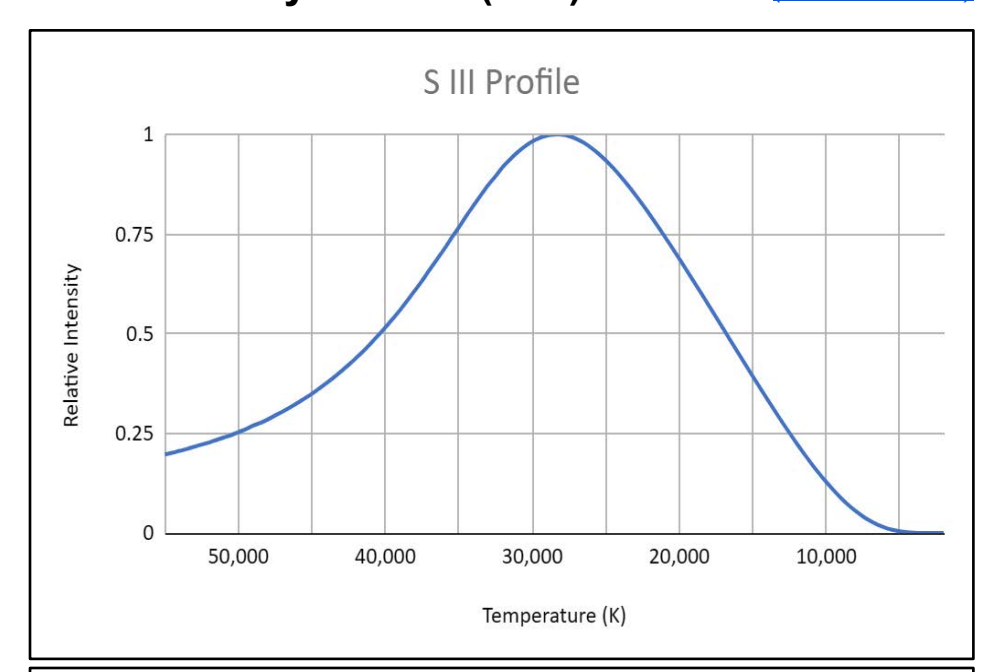
S II Visible Spectrum Lines:

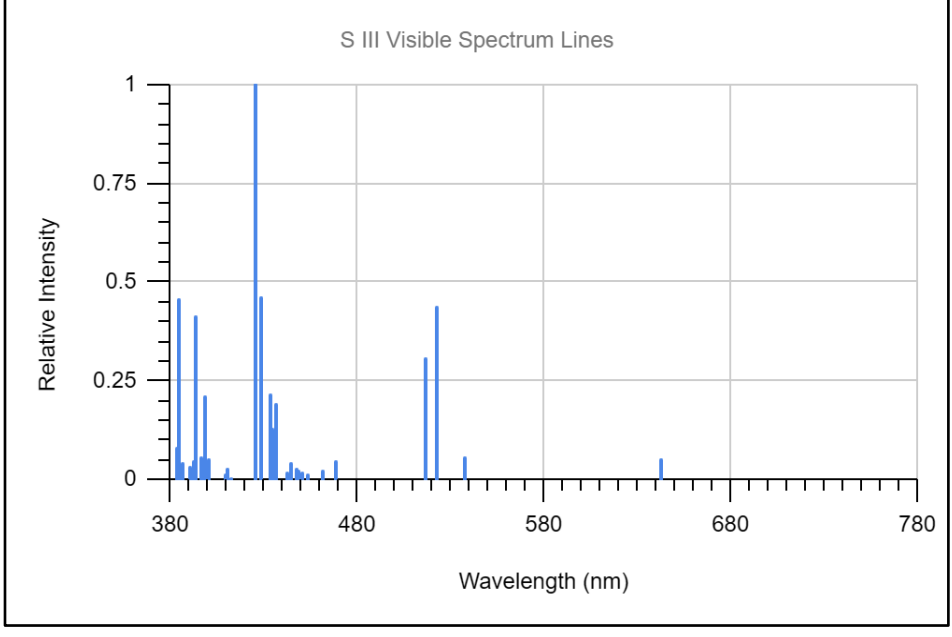
Electron Temperature: 1.34 T (eV) Electron Density: 1.98E+15 (cm⁻³)

λ (nm)	Rel Intensity	λ (nm)	Rel Intensity
392.34	0.18	510.33	0.13
393.33	0.24	520.10	0.17
414.23	0.15	521.26	0.29
414.51	0.23	532.07	0.38
415.31	0.34	534.57	0.27
416.27	0.48	542.87	0.26
417.40	0.13	543.28	0.60
417.43	0.18	545.39	1.00
426.78	0.14	547.36	0.23
429.44	0.26	550.97	0.25
452.49	0.16	556.50	0.16
471.63	0.17	560.62	0.45
481.56	0.44	564.00	0.49
492.41	0.18	564.03	0.32
492.53	0.25	564.70	0.30
499.20	0.15	566.00	0.21
500.96	0.23	566.48	0.13
501.40	0.32	628.70	0.15
503.24	0.57	630.55	0.17

Sulfur- Doubly Ionized (S III)







S III Profile:

Peak Temperature: 28,500 K

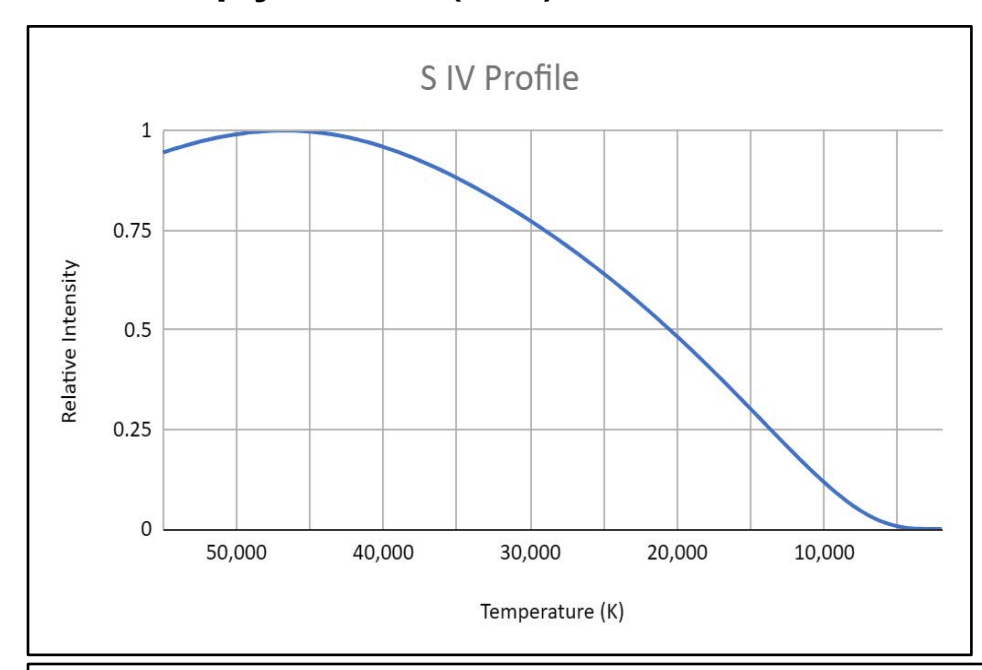
S III Visible Spectrum Lines:

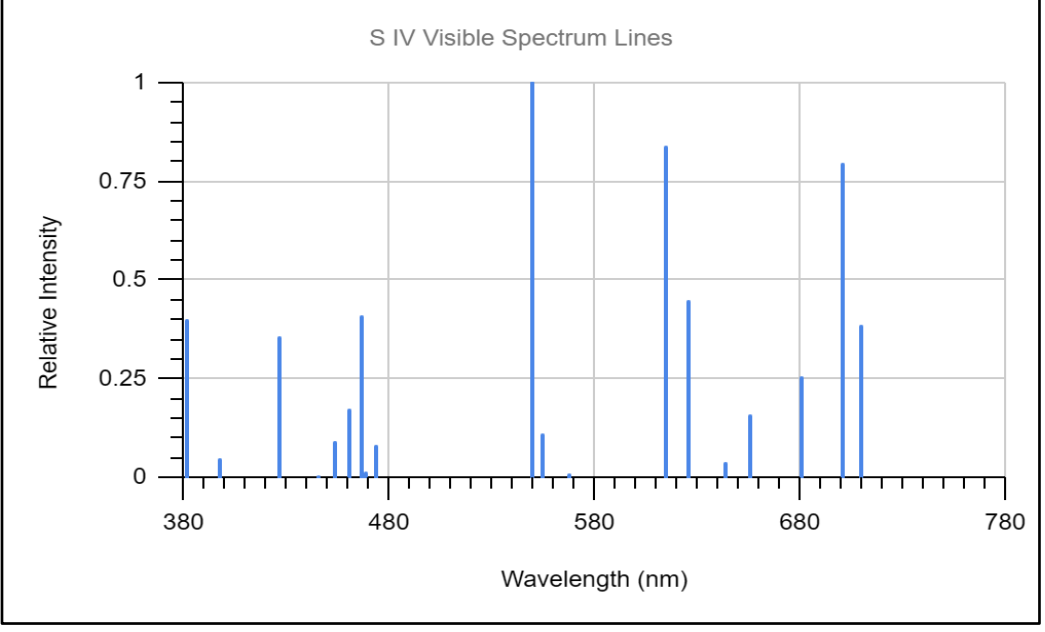
Electron Temperature: 2.46 T (eV) Electron Density: 5.73E+16 (cm⁻³)

λ (nm)	Rel Intensity	λ (nm)	Rel Intensity
425.35	1.00	436.47	0.12
428.49	0.46	398.59	0.11
383.83	0.46	435.45	0.08
521.93	0.44	383.18	0.08
392.86	0.42	536.96	0.06
516.01	0.31	396.15	0.05
433.27	0.21	399.79	0.05
398.37	0.21	641.89	0.05
436.15	0.19	467.76	0.05
383.77	0.15	392.03	0.05
434.02	0.13		

Sulfur-Triply Ionized (S IV)

(Return to Index)





S IV Profile:

Peak Temperature: 46,500 K

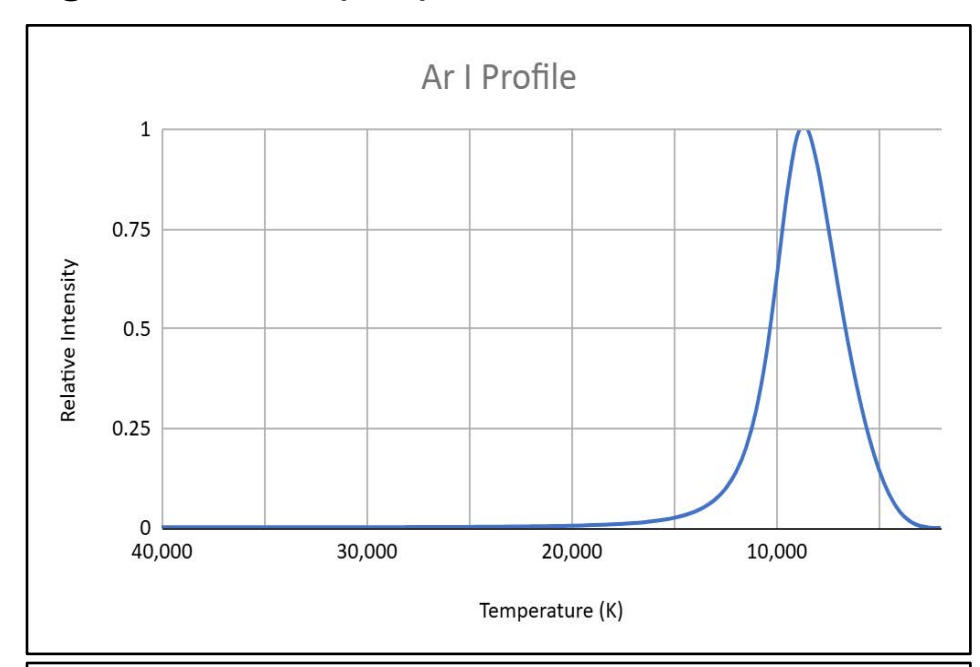
S IV Visible Spectrum Lines:

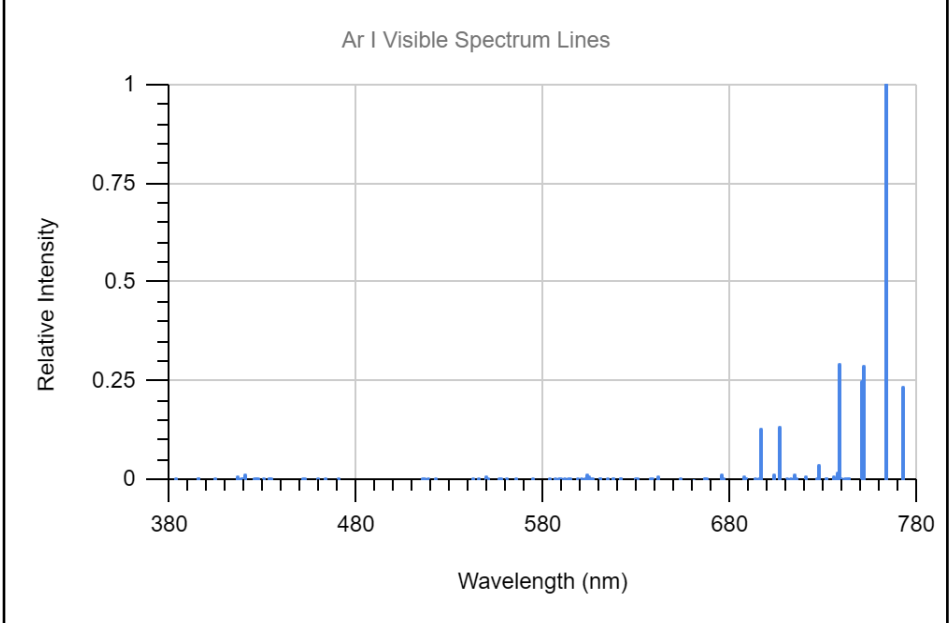
Electron Temperature: 4.01 T (eV) Electron Density: 8.58E+17 (cm⁻³)

λ (nm)	Rel Intensity	λ (nm)	Rel Intensity
381.50	0.40	554.11	0.11
426.05	0.35	614.07	0.84
453.03	0.09	625.31	0.45
459.80	0.17	655.20	0.16
465.92	0.41	655.21	0.08
473.08	0.08	680.39	0.25
548.83	0.56	700.33	0.79
549.78	1.00	708.96	0.38

Argon - Neutral (Ar I)

(Return to Index)





Ar I Profile:

Peak Temperature: 8,500 K

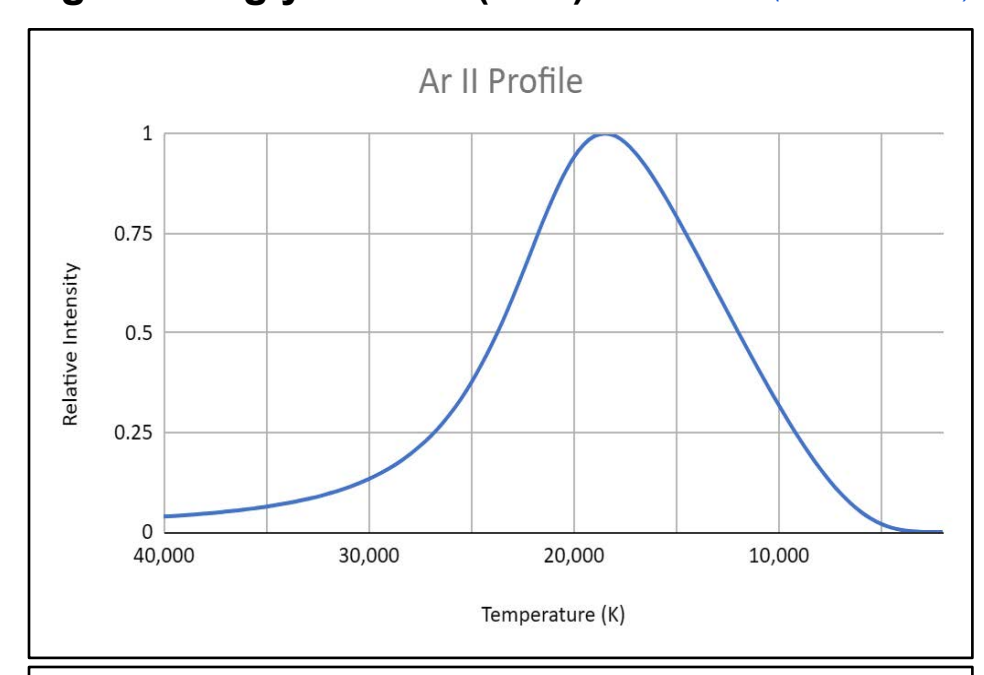
Ar I Visible Spectrum Lines:

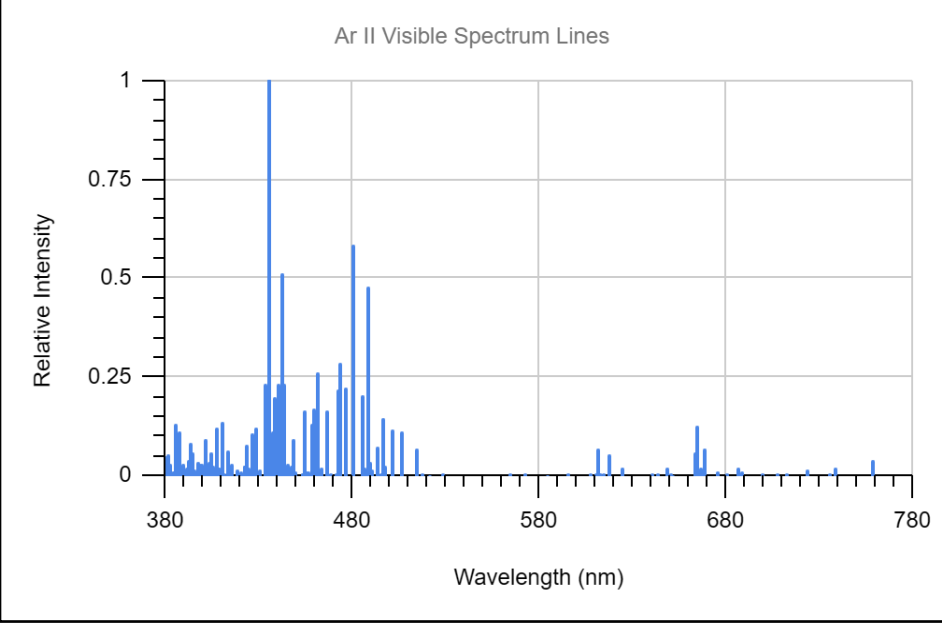
Electron Temperature: 0.73 T (eV) Electron Density: 7.16E+13 (cm⁻³)

λ (nm)	Rel Intensity	λ (nm)	Rel Intensity
696.54	0.13	751.47	0.29
706.72	0.13	763.51	1.00
738.40	0.29	772.38	0.13
750.39	0.25	772.42	0.23

Argon - Singly Ionized (Ar II)

(Return to Index)





Ar II Profile:

Peak Temperature: 18,500 K

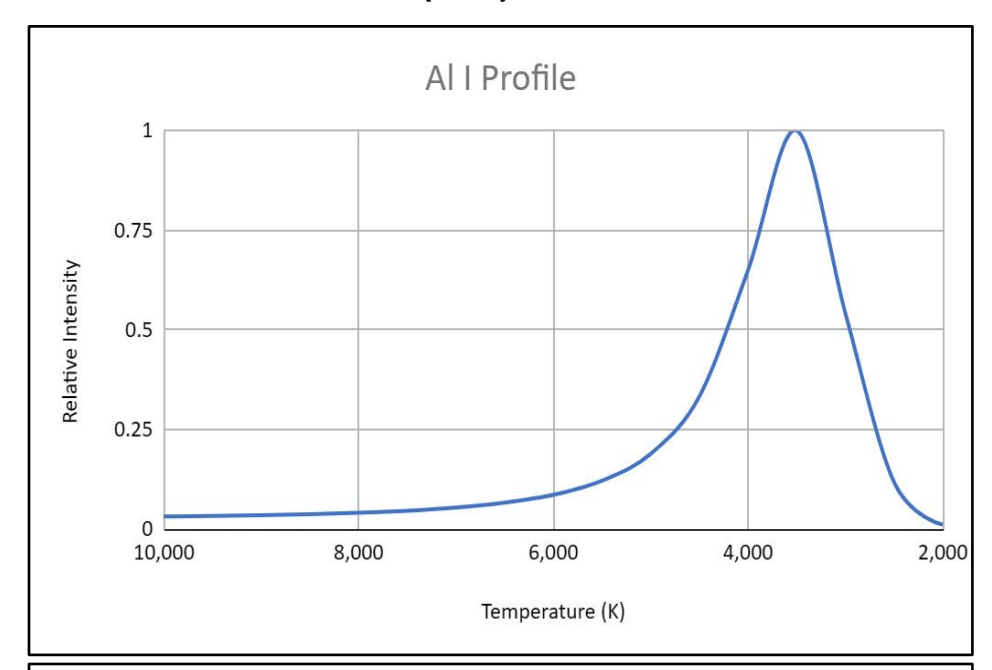
Ar II Visible Spectrum Lines:

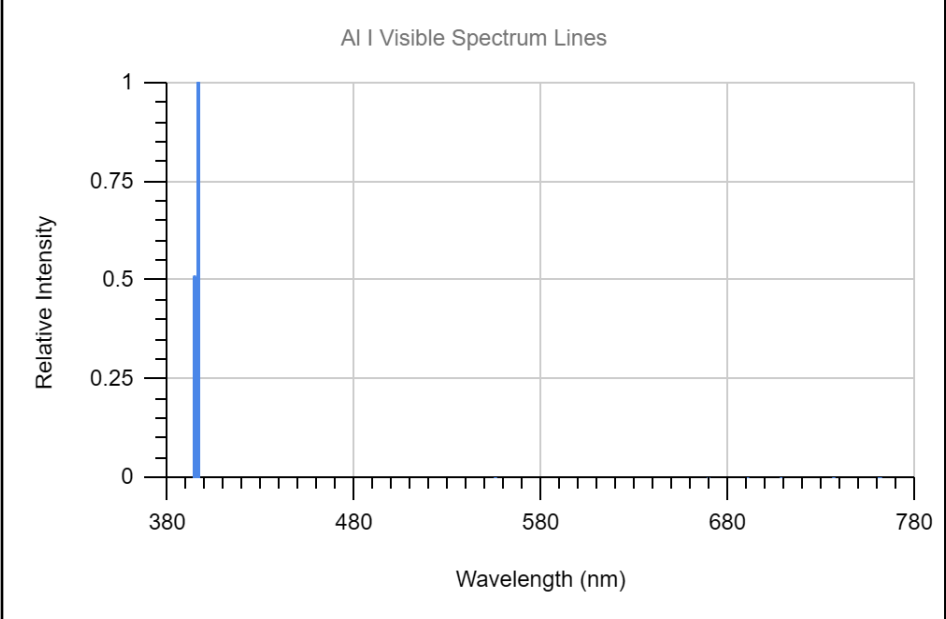
Electron Temperature: 1.60 T (eV) Electron Density: 5.26E+15 (cm⁻³)

λ (nm)	Rel Intensity	λ (nm)	Rel Intensity
385.06	0.13	443.10	0.08
386.85	0.11	448.18	0.09
392.86	0.08	454.51	0.16
401.39	0.09	457.93	0.13
407.20	0.12	458.99	0.17
410.38	0.09	460.96	0.26
410.39	0.13	465.79	0.16
422.82	0.08	472.69	0.22
426.65	0.10	473.59	0.28
427.75	0.12	476.49	0.22
433.12	0.23	480.60	0.58
434.81	1.00	484.78	0.20
437.08	0.09	487.99	0.47
437.13	0.11	493.32	0.07
437.97	0.20	496.51	0.14
440.01	0.08	500.93	0.11
440.10	0.23	506.20	0.11
442.60	0.51	664.37	0.13
443.02	0.23	668.43	0.07

Aluminum - Neutral (Al I)

(Return to Index)





Al I Profile:

Peak Temperature: 3,500 K

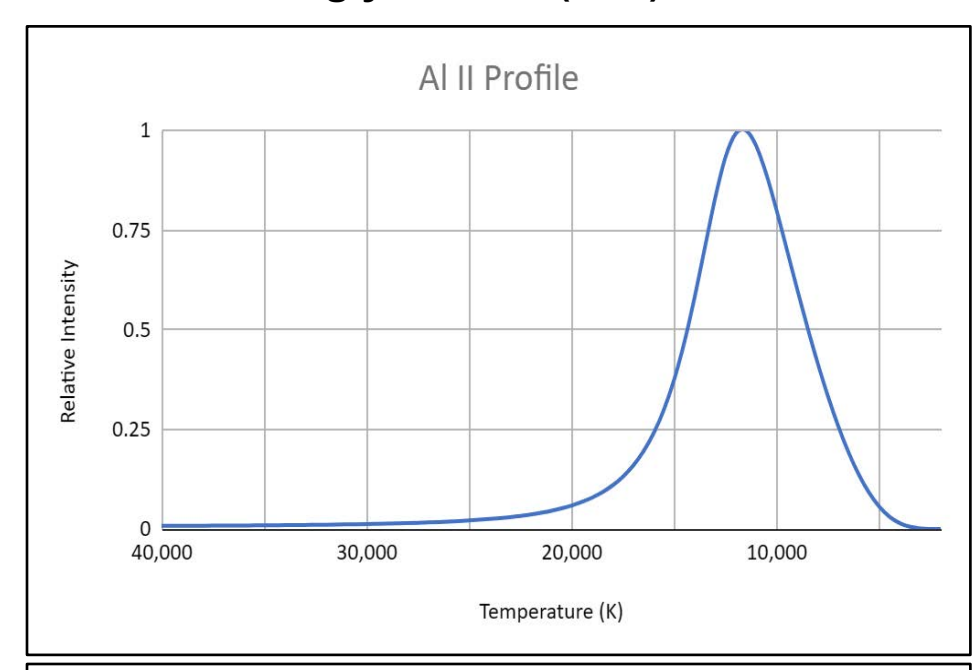
Al I Visible Spectrum Lines:

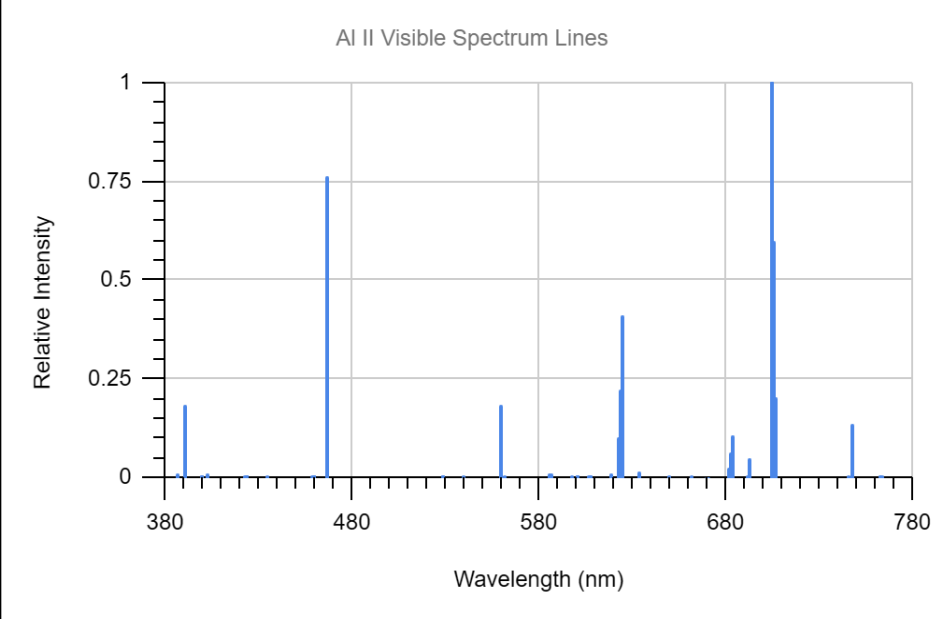
Electron Temperature: 0.30 T (eV) Electron Density: 5.31E+11 (cm⁻³)

λ (nm)	Rel Intensity	λ (nm)	Rel Intensity
394.40	0.51		
396.15	1.00		

Aluminum - Singly Ionized (Al II)

(Return to Index)





Al II Profile:

Peak Temperature: 11,500 K

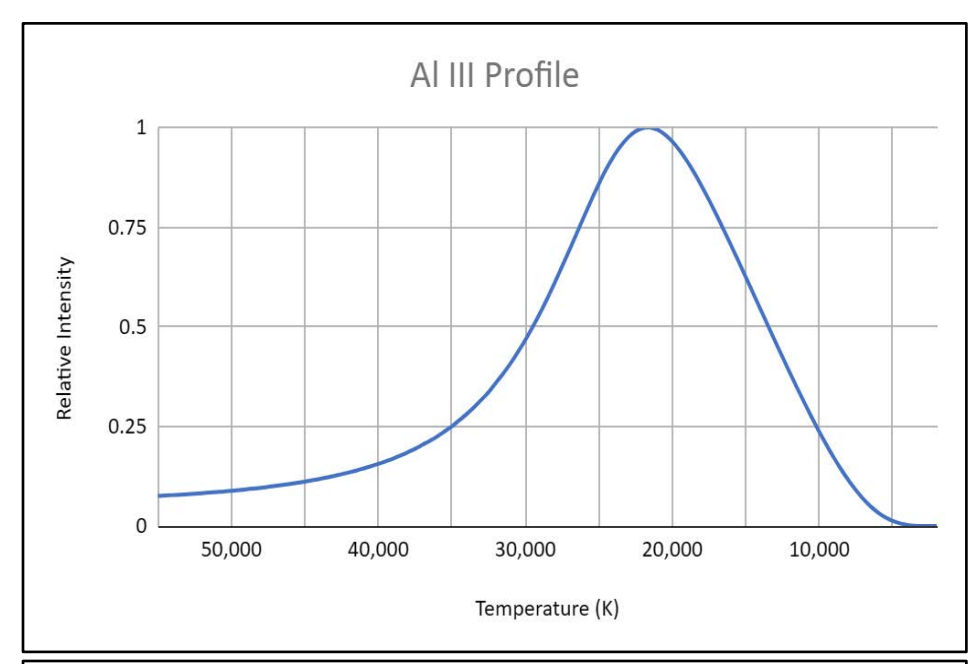
Al II Visible Spectrum Lines:

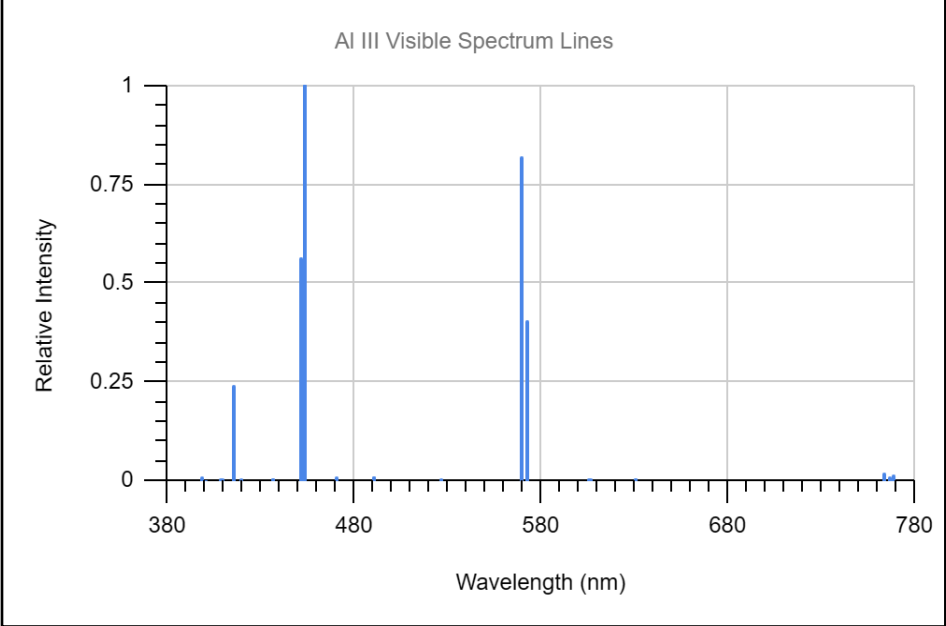
Electron Temperature: 0.99 T (eV) Electron Density: 3.80E+14 (cm⁻³)

λ (nm)	Rel Intensity	λ (nm)	Rel Intensity
390.07	0.18	683.71	0.10
466.30	0.76	692.03	0.05
559.33	0.18	704.21	1.00
622.62	0.10	705.67	0.60
623.18	0.22	706.37	0.20
624.34	0.41	747.14	0.13
682.34	0.06		

Aluminum - Doubly Ionized (Al III)

(Return to Index)





Al III Profile:

Peak Temperature: 21,500 K

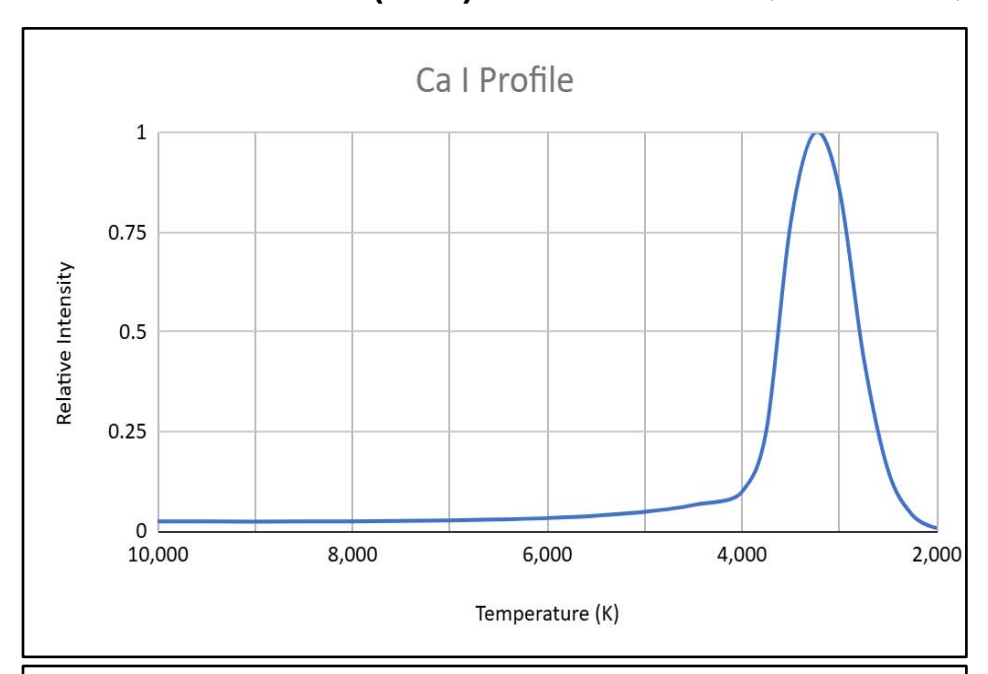
Al III Visible Spectrum Lines:

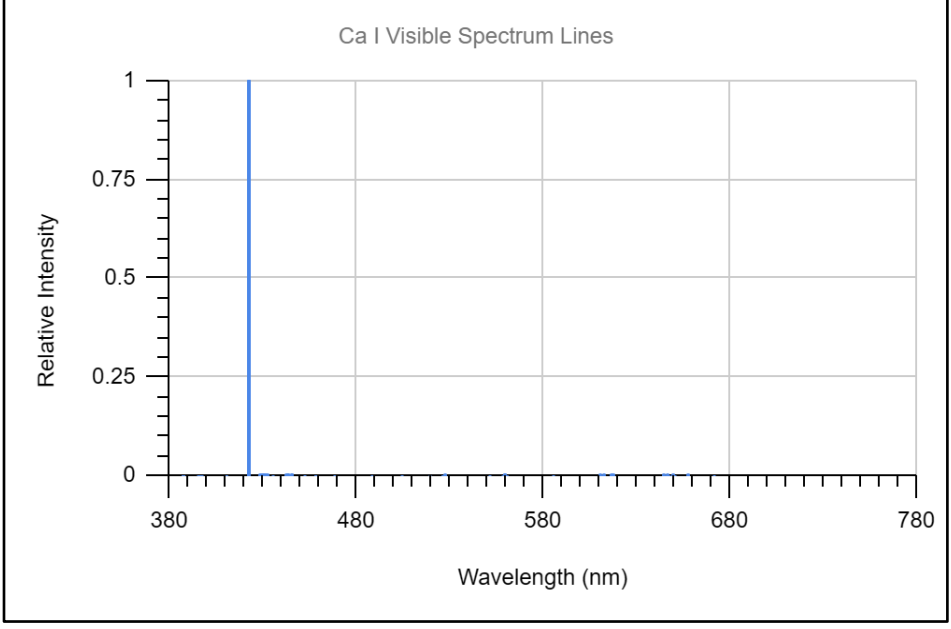
Electron Temperature: 1.85 T (eV) Electron Density: 1.21E+16 (cm⁻³)

λ (nm)	Rel Intensity	λ (nm)	Rel Intensity
414.99	0.24	452.92	1.00
415.02	0.17	569.66	0.82
451.26	0.56	572.27	0.40
452.89	0.11		

Calcium - Neutral (Ca I)

(Return to Index)





Ca I Profile:

Peak Temperature: 3,250 K

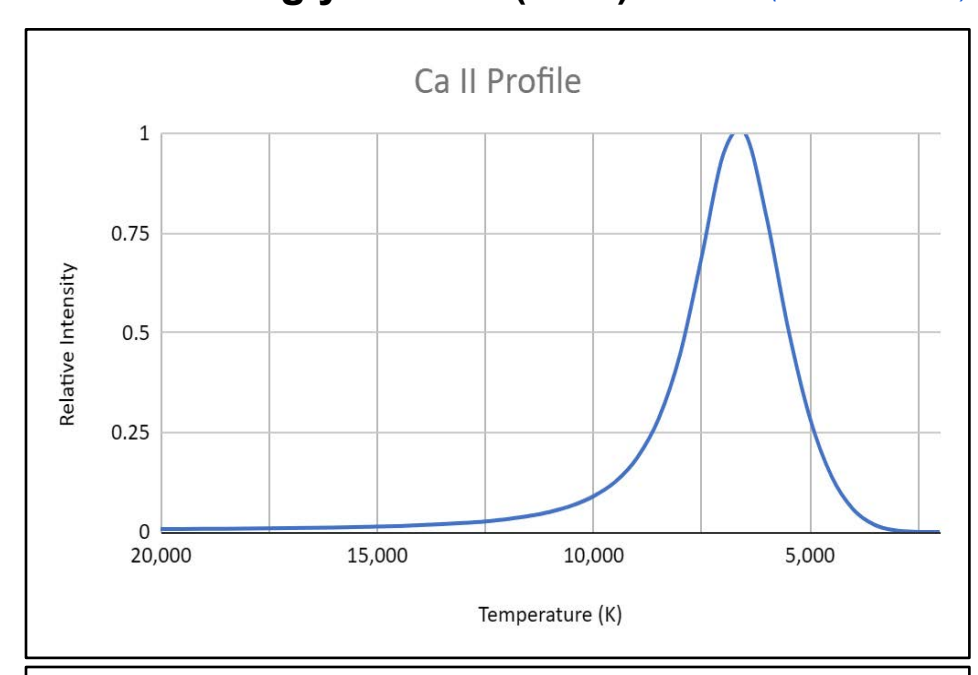
Ca I Visible Spectrum Lines:

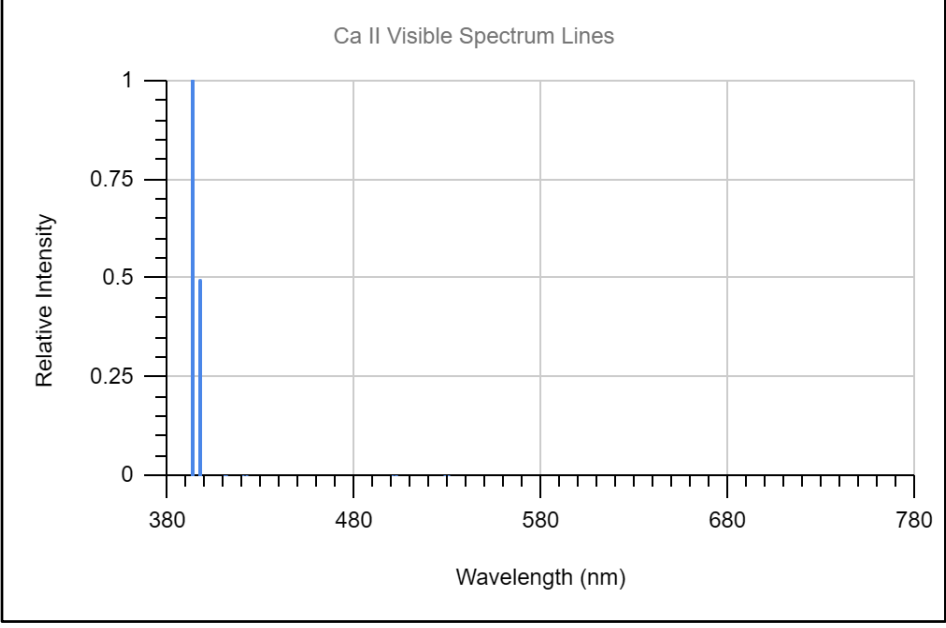
Electron Temperature: 0.28 T (eV) Electron Density: 3.53E+11 (cm⁻³)

λ (nm)	Rel Intensity	λ (nm)	Rel Intensity
422.67	1.00		

Calcium - Singly Ionized (Ca II)

(Return to Index)





Ca II Profile:

Peak Temperature: 6,500 K

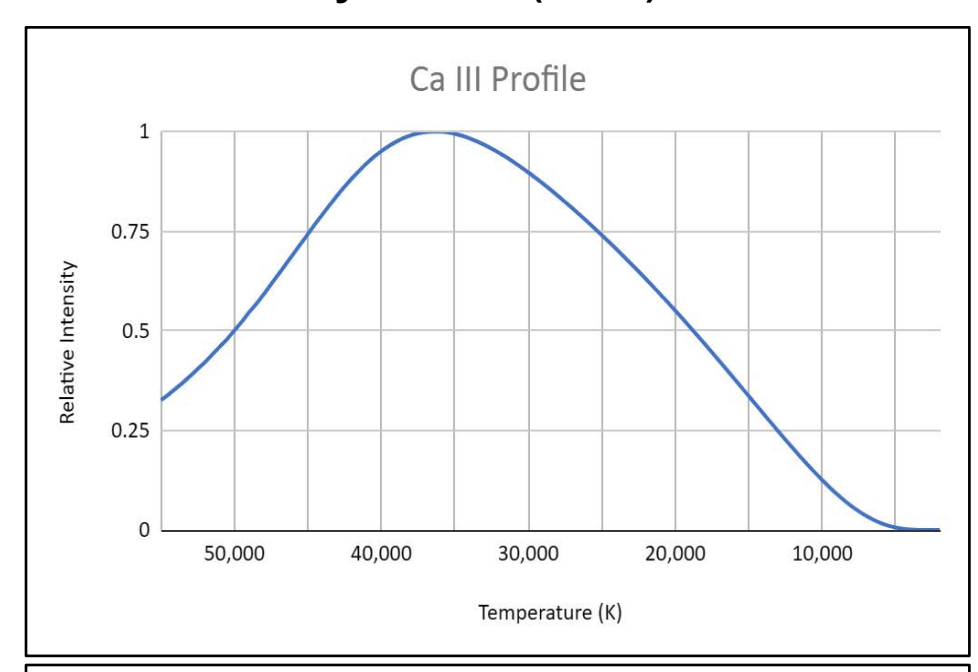
Ca II Visible Spectrum Lines:

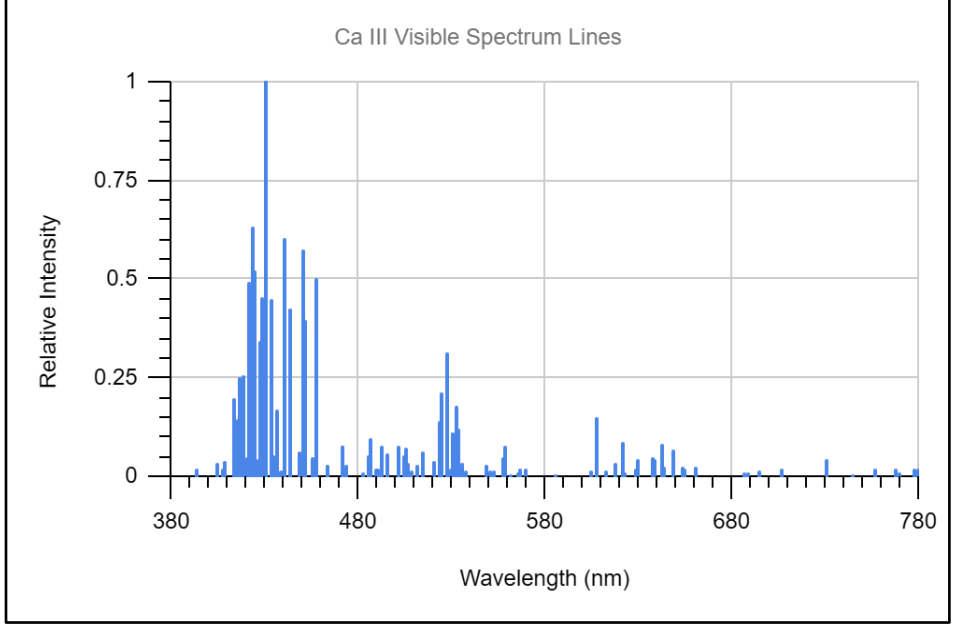
Electron Temperature: 0.56 T (eV) Electron Density: 1.63E+13 (cm⁻³)

λ (nm)	Rel Intensity	λ (nm)	Rel Intensity
393.37	1.00		
396.85	0.50		

Calcium - Doubly Ionized (Ca III)

(Return to Index)





Ca III Profile:

Peak Temperature: 36,500 K

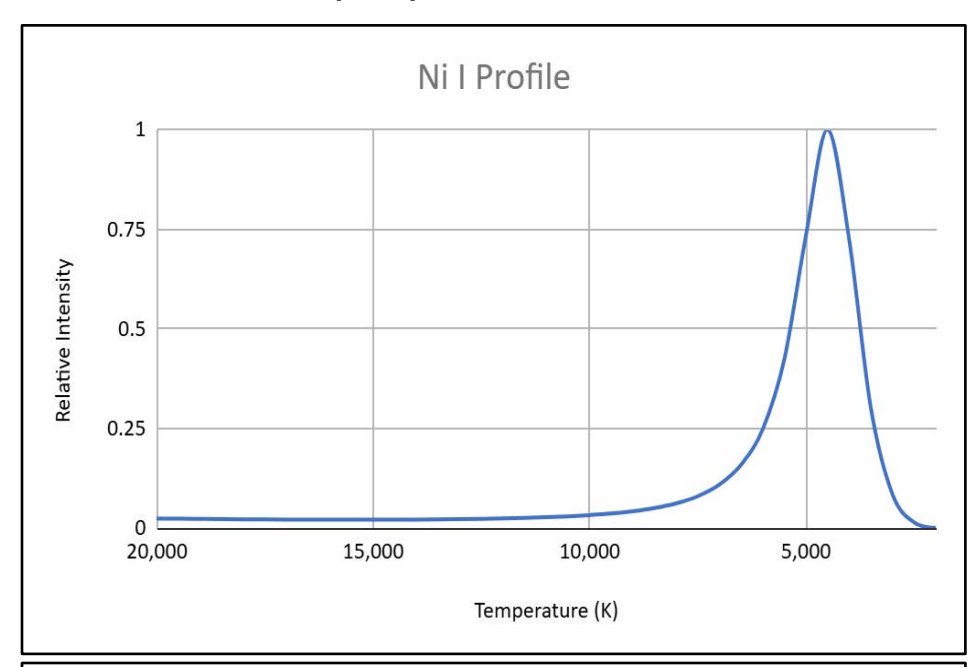
Ca III Visible Spectrum Lines:

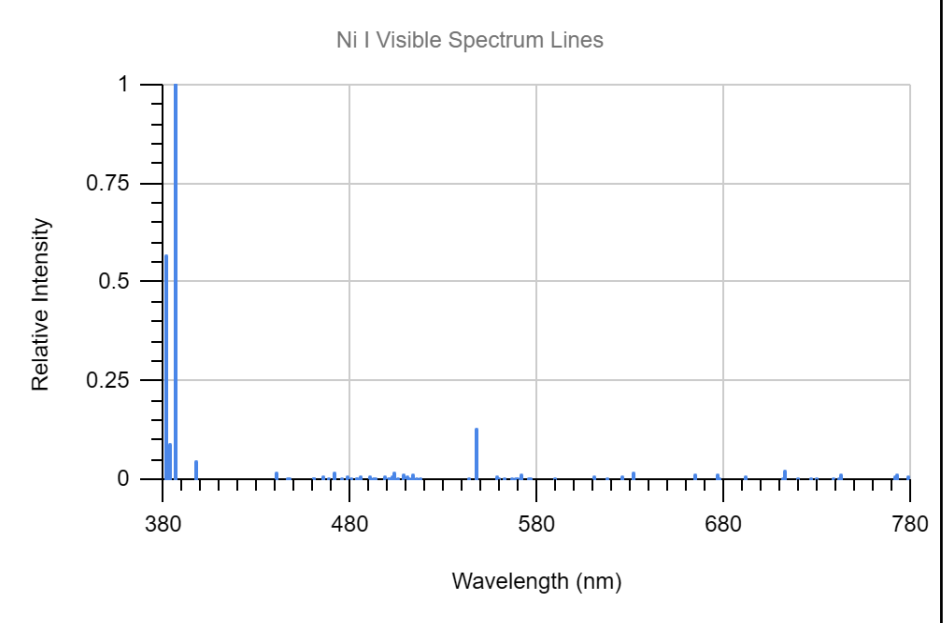
Electron Temperature: 3.15 T (eV) Electron Density: 2.25E+17 (cm⁻³)

λ (nm)	Rel Intensity	λ (nm)	Rel Intensity
413.62	0.19	433.36	0.45
415.36	0.14	435.84	0.17
416.43	0.25	439.96	0.60
417.57	0.11	440.63	0.44
418.42	0.25	443.13	0.42
420.72	0.49	449.99	0.57
421.31	0.12	451.66	0.39
422.82	0.35	457.21	0.50
423.37	0.63	471.63	0.08
424.07	0.52	485.92	0.09
427.19	0.34	523.18	0.14
427.82	0.10	524.74	0.21
427.97	0.35	527.20	0.31
428.44	0.45	530.13	0.11
429.01	0.24	532.13	0.18
430.10	0.25	532.81	0.12
430.15	0.12	607.00	0.15
430.28	1.00	621.40	0.08
432.92	0.35	642.45	0.08

Nickel - Neutral (Ni I)

(Return to Index)





Ni I Profile:

Peak Temperature: 4,500 K

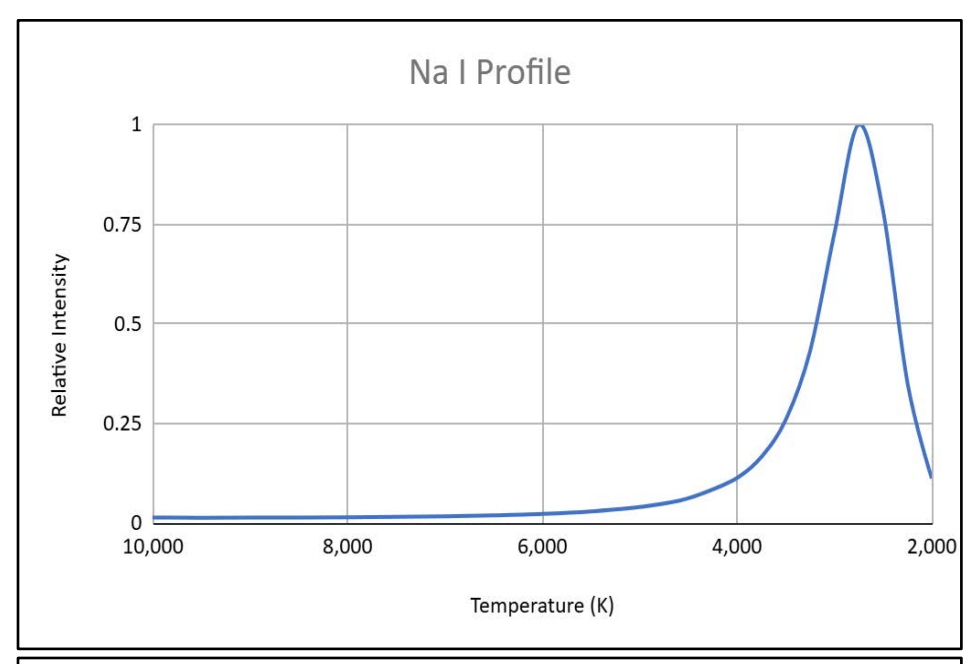
Ni I Visible Spectrum Lines:

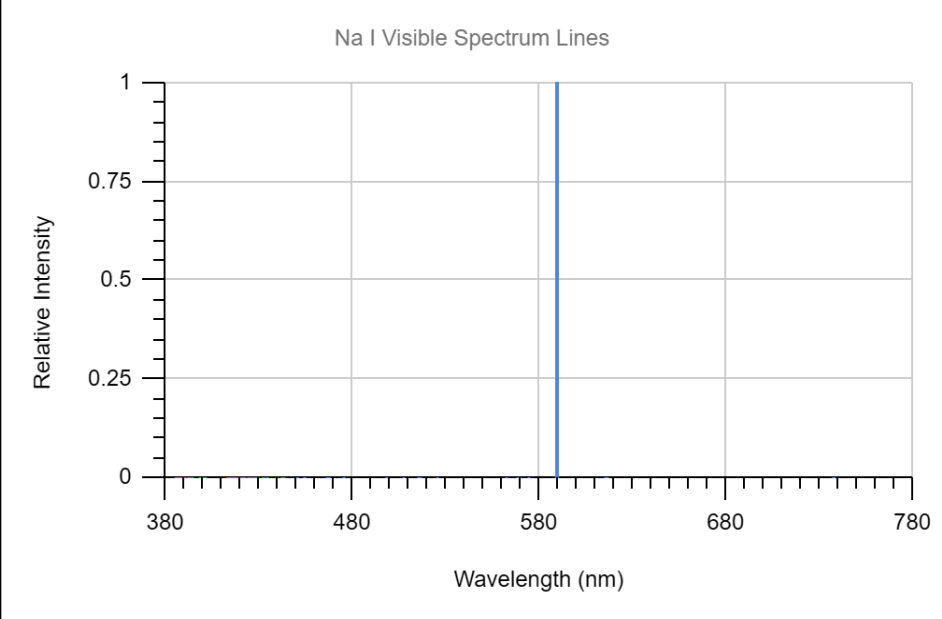
Electron Temperature: 0.39 T (eV) Electron Density: 2.13E+12 (cm⁻³)

λ (nm)	Rel Intensity	λ (nm)	Rel Intensity
380.71	0.57	397.36	0.05
383.17	0.09	547.69	0.13
385.83	1.00		

Sodium - Neutral (Na I)

(Return to Index)





Na I Profile:

Peak Temperature: 3,000 K

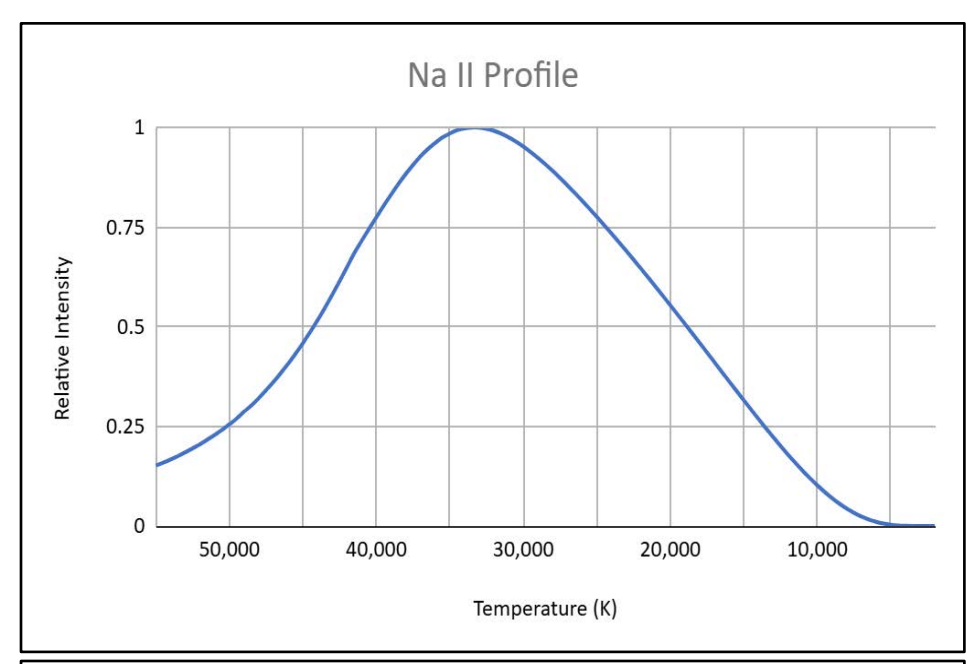
Na I Visible Spectrum Lines:

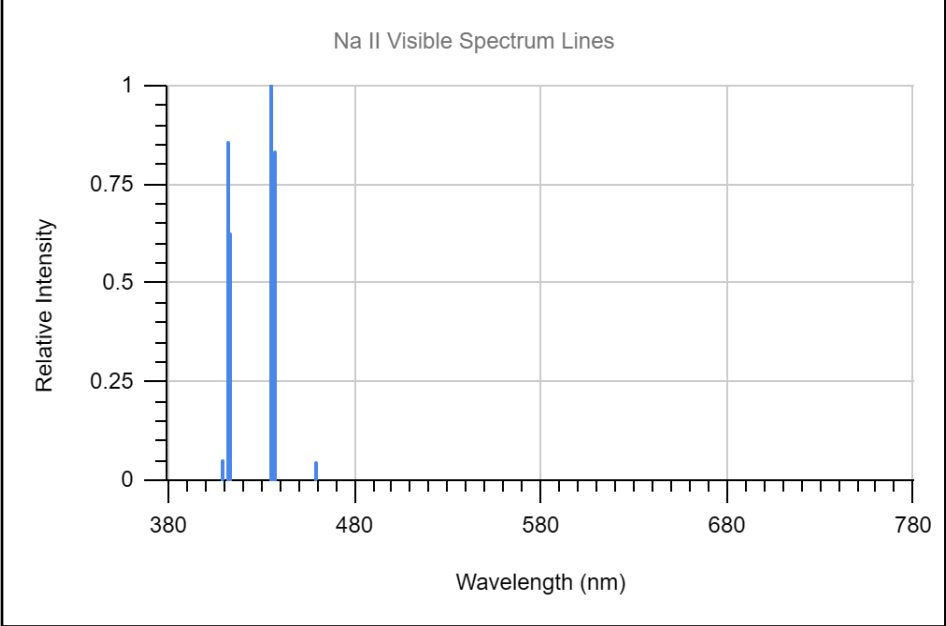
Electron Temperature: 0.26 T (eV) Electron Density: 2.27E+11 (cm⁻³)

λ (nm)	Rel Intensity	λ (nm)	Rel Intensity
589.00	1.00		
589.59	0.50		

Sodium - Singly Ionized (Na II)

(Return to Index)





Na II Profile:

Peak Temperature: 33,500 K

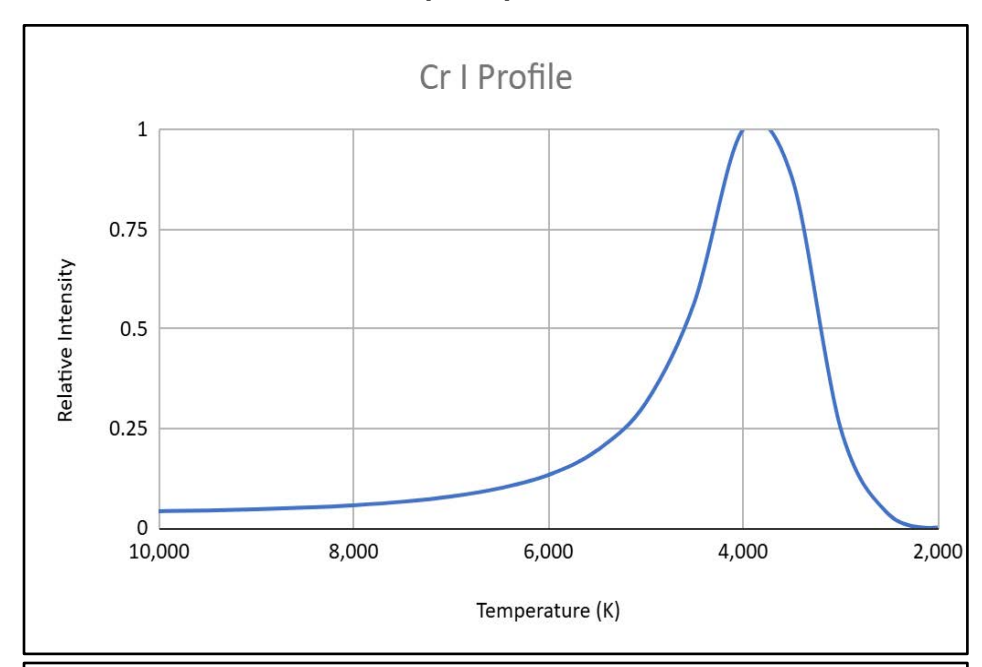
Na II Visible Spectrum Lines:

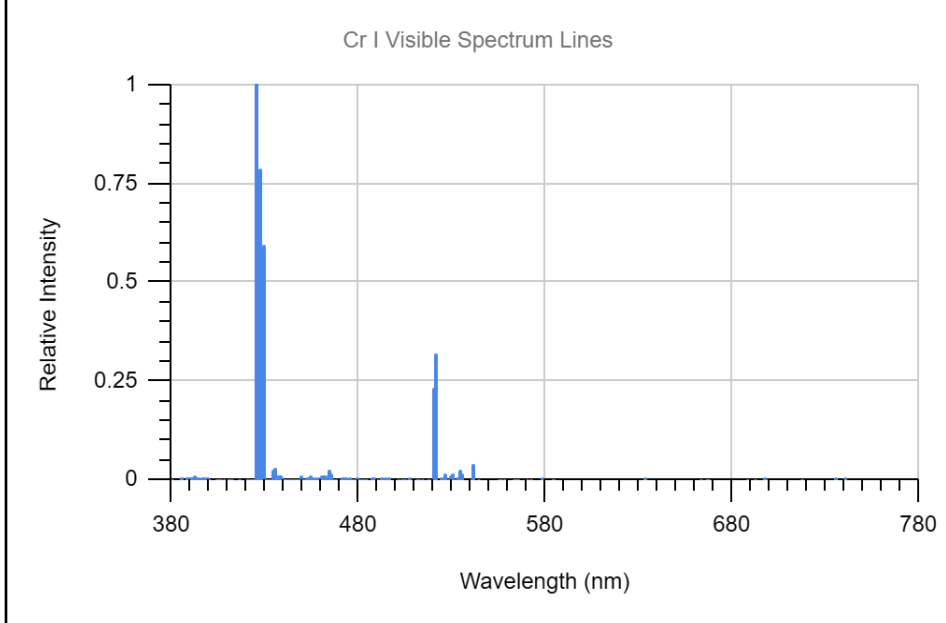
Electron Temperature: 2.89 T (eV) Electron Density: 1.40E+17 (cm⁻³)

λ (nm)	Rel Intensity	λ (nm)	Rel Intensity
408.76	0.05	434.41	1.00
411.37	0.86	436.86	0.83
412.31	0.62	459.09	0.05

Chromium - Neutral (Cr I)

(Return to Index)





Cr I Profile:

Peak Temperature: 4,000 K

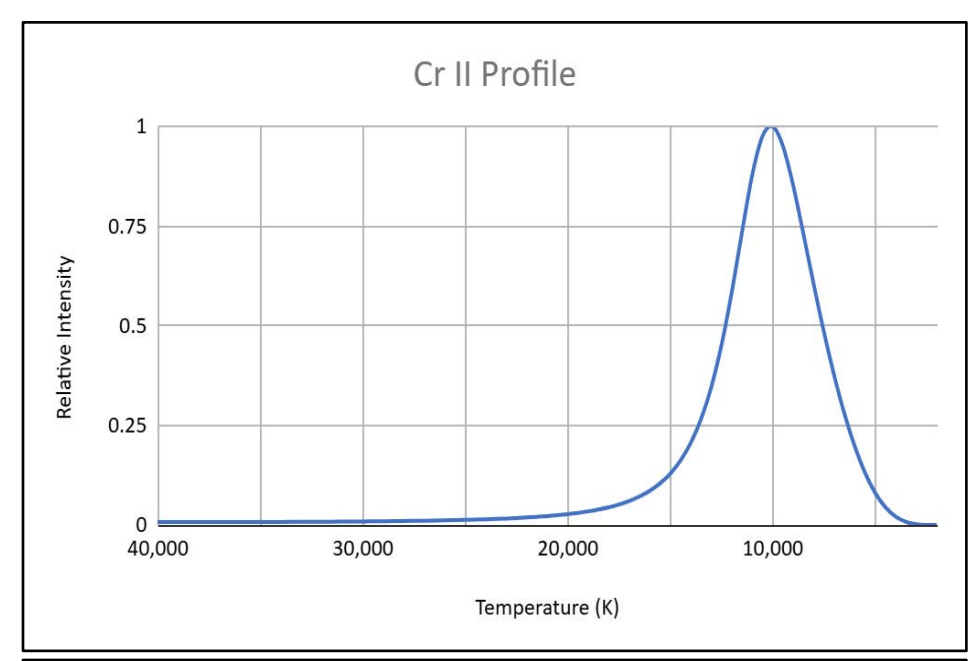
Cr I Visible Spectrum Lines:

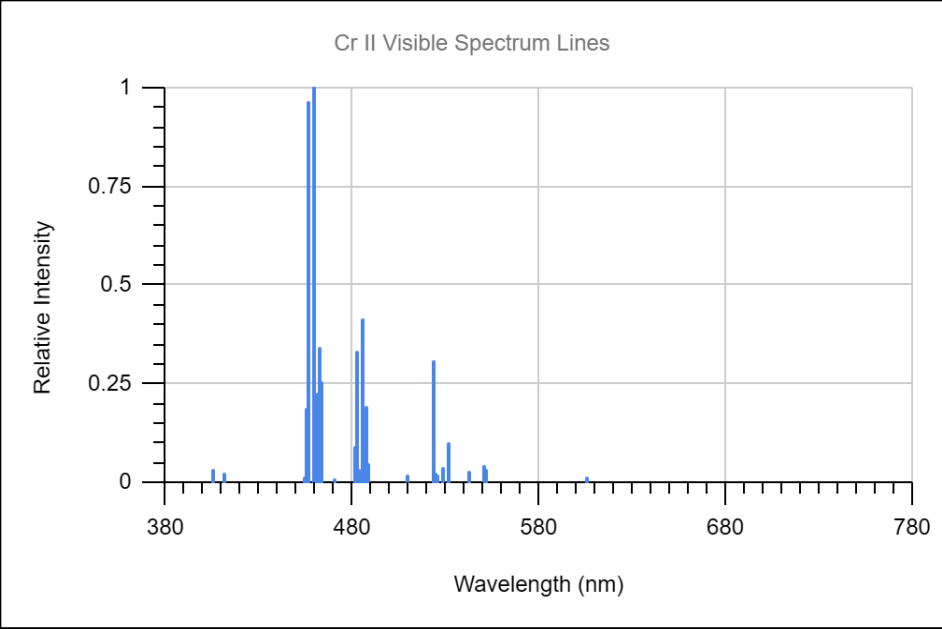
Electron Temperature: 0.35 T (eV) Electron Density: 1.11E+12 (cm⁻³)

λ (nm)	Rel Intensity	λ (nm)	Rel Intensity
425.43	1.00	520.45	0.14
427.48	0.79	520.60	0.23
428.97	0.59	520.84	0.32

Chromium - Singly Ionized (Cr II)

(Return to Index)





Cr II Profile:

Peak Temperature: 10,000 K

Cr II Visible Spectrum Lines:

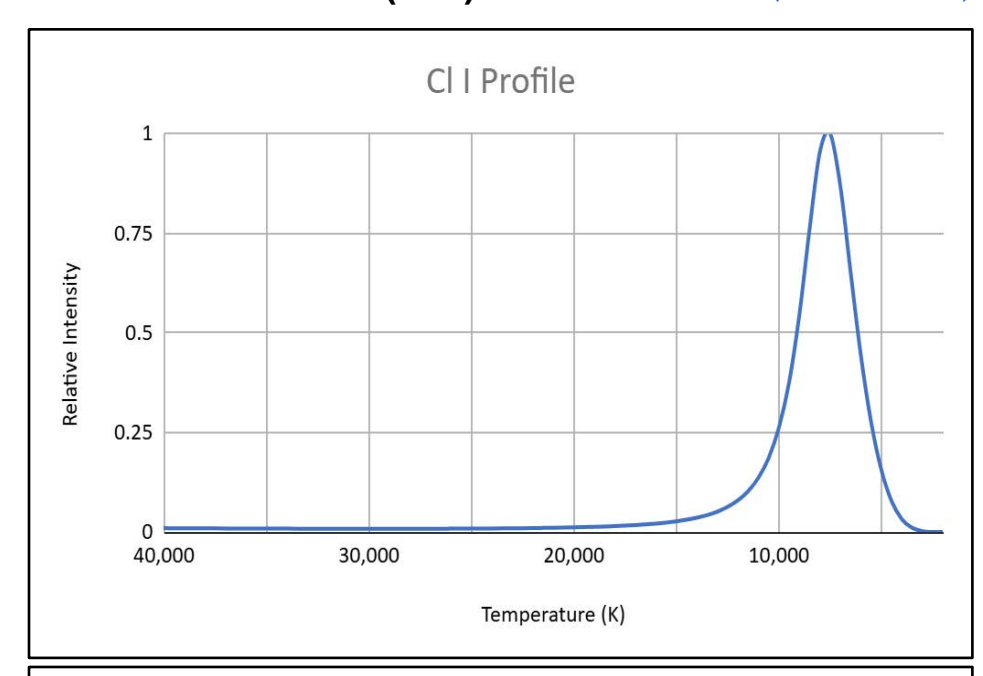
Electron Temperature: 0.86 T (eV)

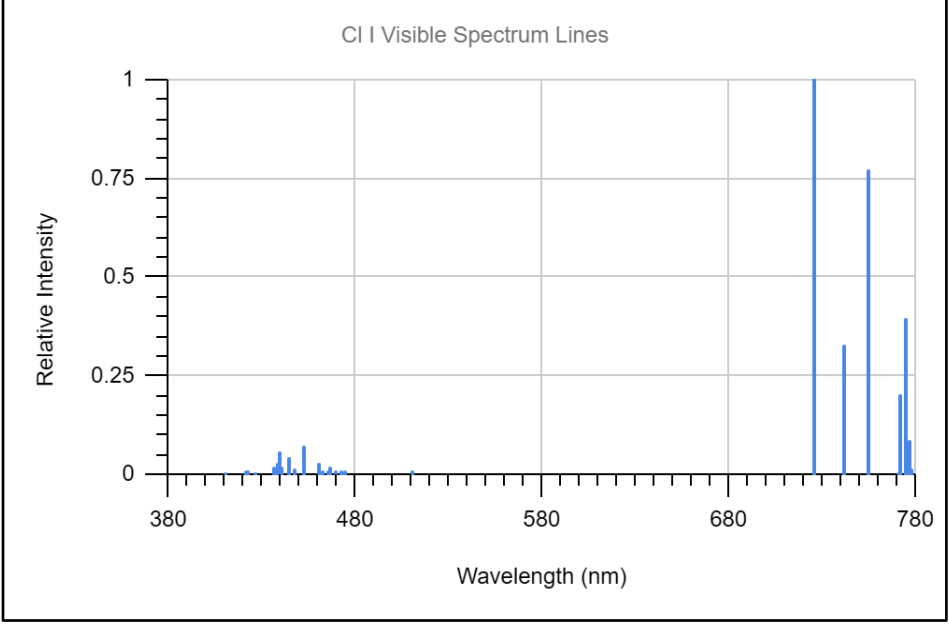
Electron Density: 1.7E+151.76E+14 (cm⁻³)

λ (nm)	Rel Intensity	λ (nm)	Rel Intensity
455.50	0.19	482.41	0.33
455.86	0.96	484.82	0.41
458.82	1.00	487.65	0.19
459.21	0.27	488.46	0.05
461.66	0.22	523.73	0.30
461.88	0.34	530.84	0.07
463.41	0.25	531.36	0.10
481.23	0.09		

Chlorine - Neutral (CI I)

(Return to Index)





CI I Profile:

Peak Temperature: 7,500 K

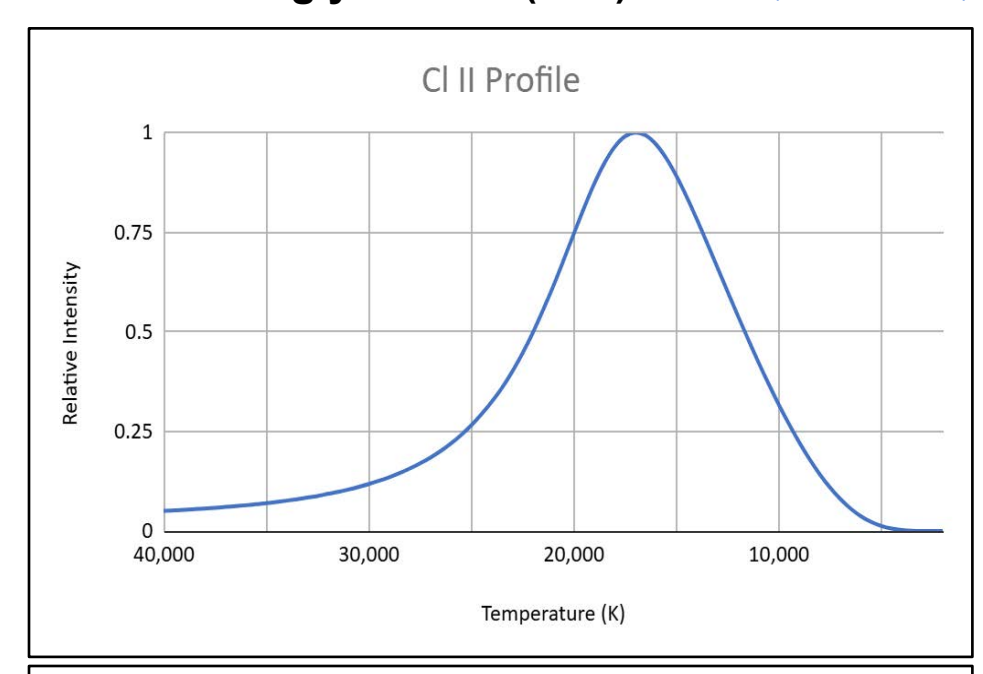
CI I Visible Spectrum Lines:

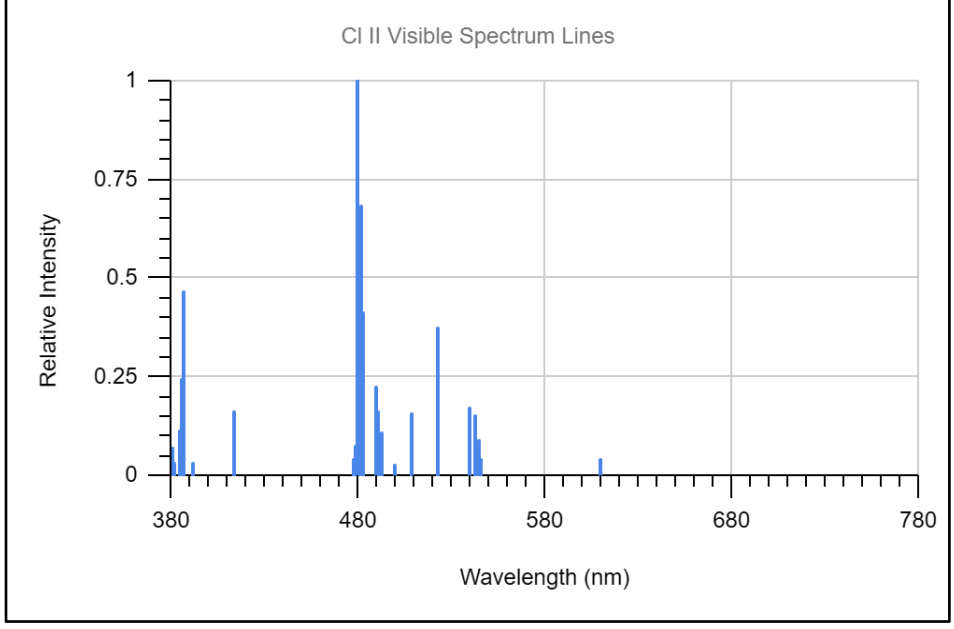
Electron Temperature: 0.65 T (eV) Electron Density: 3.58E+13 (cm⁻³)

λ (nm)	Rel Intensity	λ (nm)	Rel Intensity
438.98	0.06	754.71	0.77
452.62	0.07	771.76	0.20
725.66	1.00	774.50	0.39
741.41	0.32	776.92	0.08

Chlorine - Singly Ionized (CI II)

(Return to Index)





CI II Profile:

Peak Temperature: 17,000 K

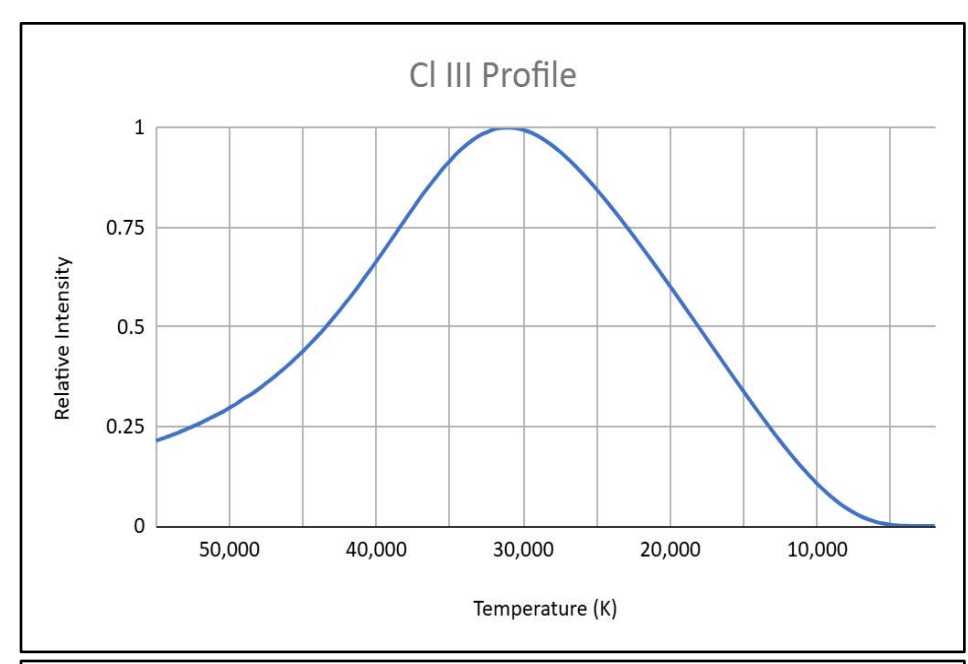
CI II Visible Spectrum Lines:

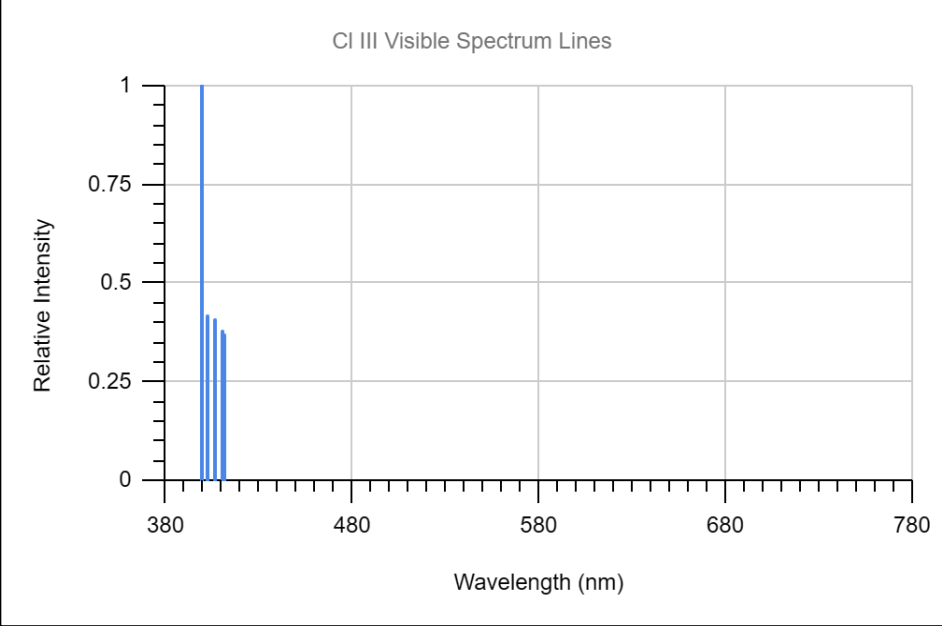
Electron Temperature: 1.47 T (eV) Electron Density:3.30E+15 (cm⁻³)

λ (nm)	Rel Intensity	λ (nm)	Rel Intensity
380.52	0.07	481.95	0.41
384.54	0.09	489.68	0.22
384.56	0.12	490.48	0.16
384.58	0.05	491.77	0.11
385.10	0.24	507.83	0.16
385.14	0.15	521.79	0.38
386.08	0.47	522.14	0.23
386.10	0.12	539.21	0.17
413.25	0.16	542.33	0.15
478.13	0.08	544.34	0.09
479.46	1.00	544.42	0.06
481.01	0.68		

Chlorine - Doubly Ionized (CI III)

(Return to Index)





CI III Profile:

Peak Temperature: 31,000 K

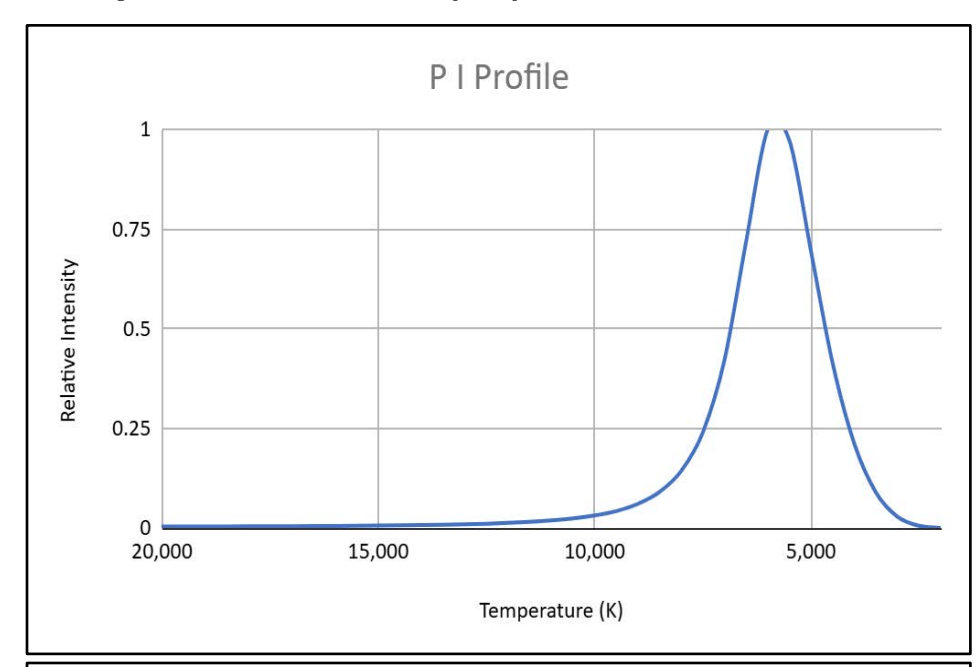
CI III Visible Spectrum Lines:

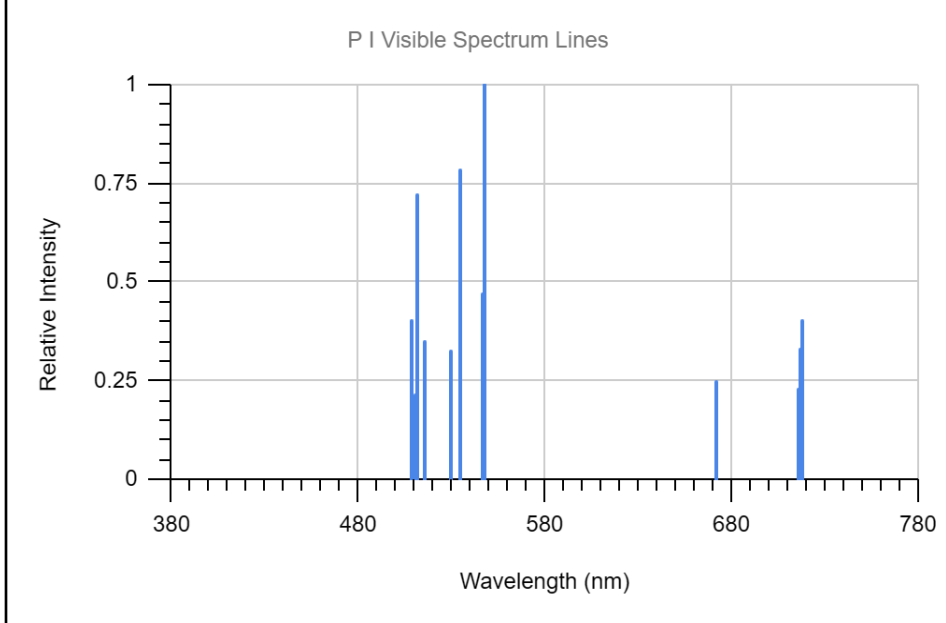
Electron Temperature: 2.67 T (eV) Electron Density: 9.12E+16 (cm⁻³)

λ (nm)	Rel Intensity	λ (nm)	Rel Intensity
399.14	1.00	410.41	0.38
401.84	0.42	410.68	0.37
405.89	0.41		

Phosphorus- Neutral (P I)







P I Profile:

Peak Temperature: 6,000 K

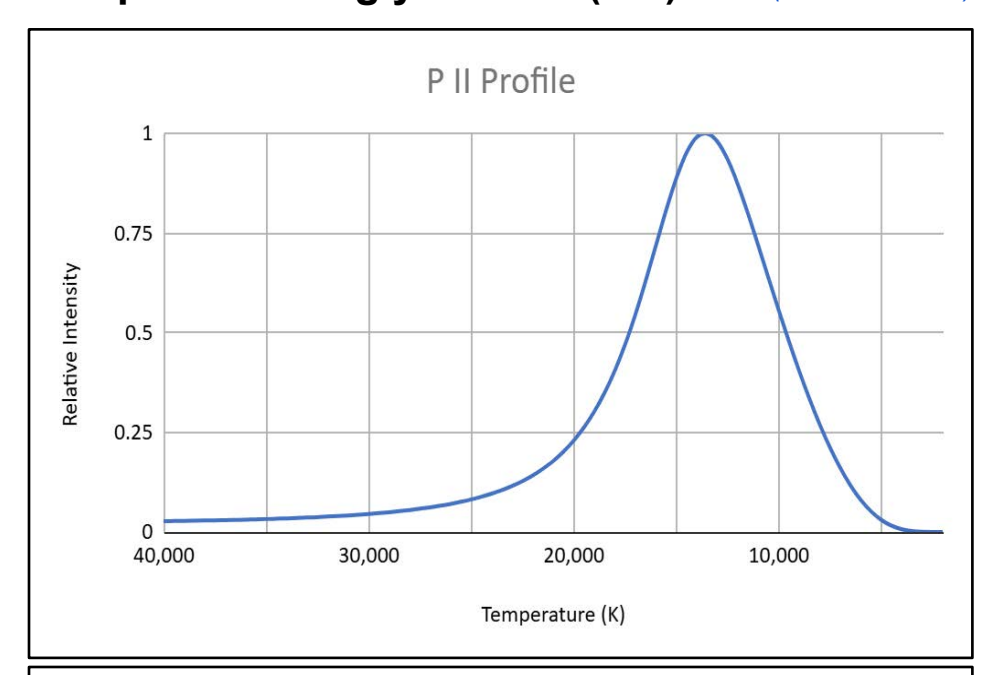
P I Visible Spectrum Lines:

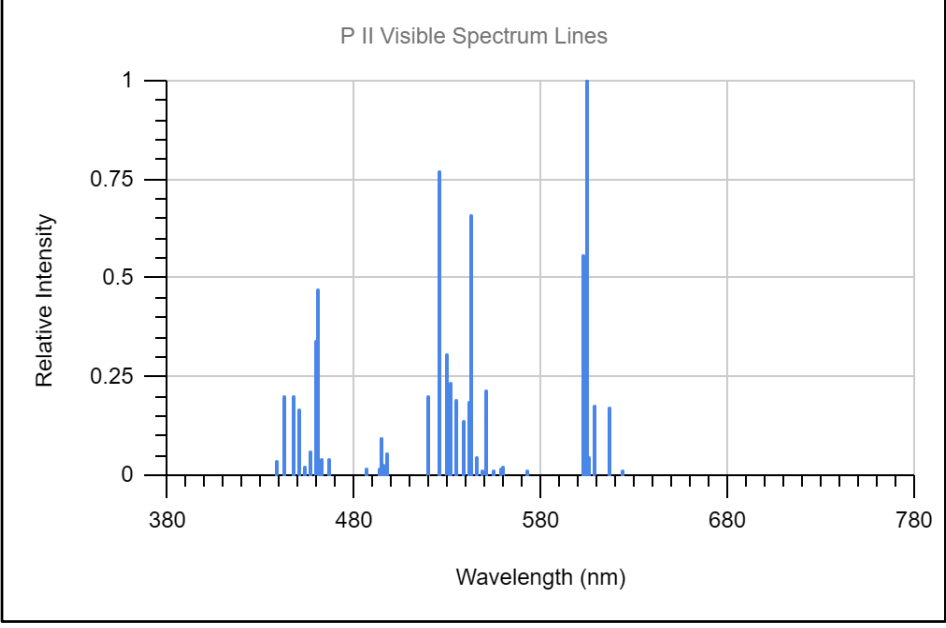
Electron Temperature: 0.52 T (eV) Electron Density: 1.04E+13 (cm⁻³)

λ (nm)	Rel Intensity	λ (nm)	Rel Intensity
507.94	0.40	545.83	0.47
509.82	0.22	547.77	1.00
510.10	0.07	671.74	0.25
510.96	0.72	715.84	0.23
515.48	0.35	716.55	0.33
529.35	0.32	717.67	0.40
534.59	0.79		

Phosphorus- Singly Ionized (P II)

(Return to Index)





P II Profile:

Peak Temperature: 13,500 K

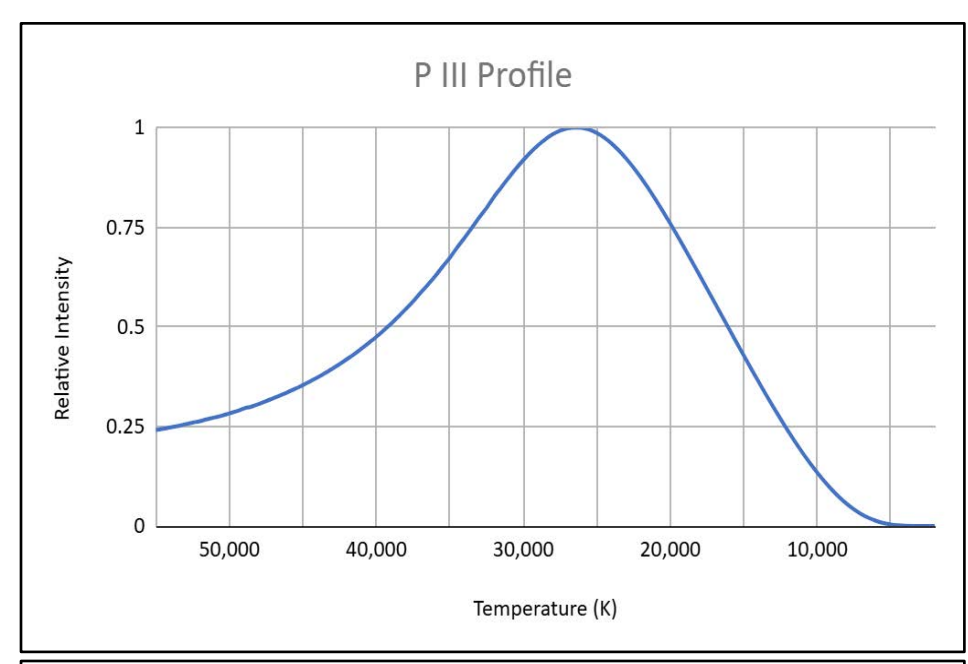
P II Visible Spectrum Lines:

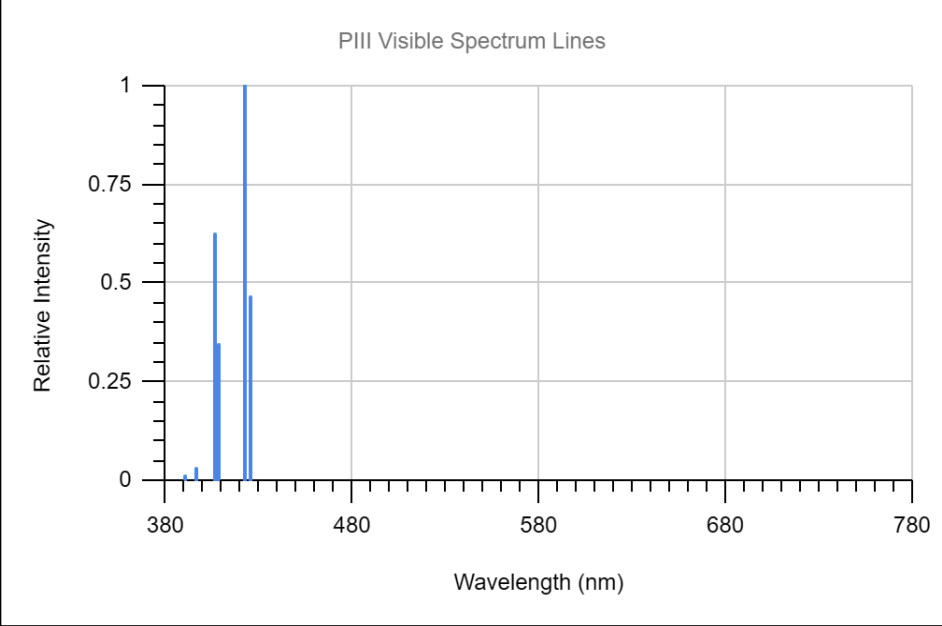
Electron Temperature: 1.17 T (eV) Electron Density: 9.23E+14 (cm⁻³)

λ (nm)	Rel Intensity	λ (nm)	Rel Intensity
442.07	0.20	534.47	0.19
447.53	0.20	538.69	0.14
449.92	0.17	540.97	0.19
455.81	0.06	542.59	0.66
458.80	0.34	545.07	0.05
458.98	0.23	549.97	0.22
460.21	0.47	602.42	0.56
494.35	0.09	603.40	0.25
496.97	0.05	604.31	1.00
519.14	0.20	605.55	0.05
525.35	0.77	608.78	0.18
529.61	0.31	616.56	0.17
531.61	0.23		

Phosphorus- Doubly Ionized (P III)

(Return to Index)





P III Profile:

Peak Temperature: 26,500 K

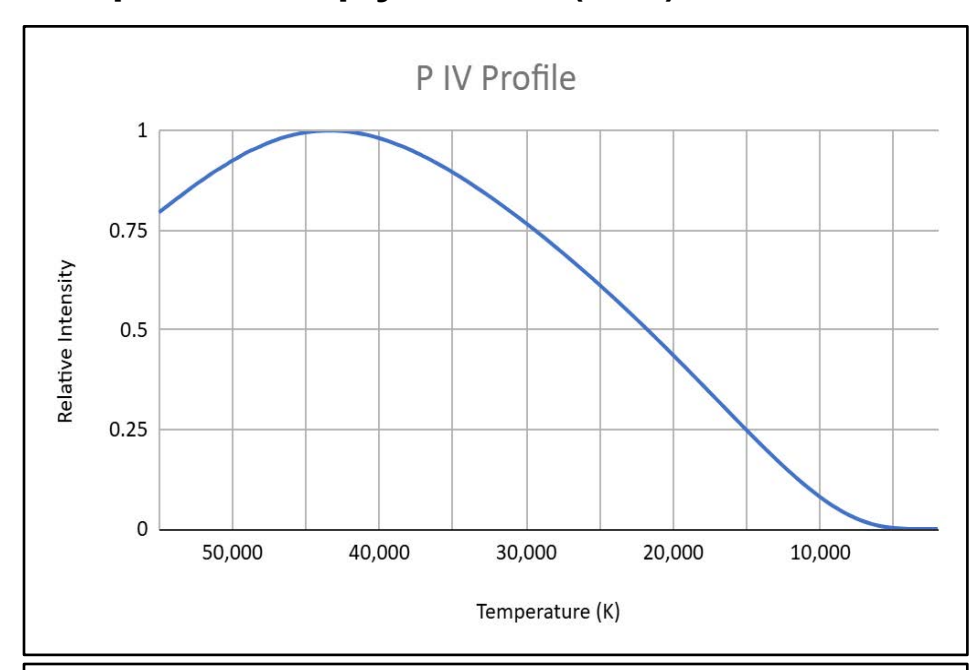
P III Visible Spectrum Lines:

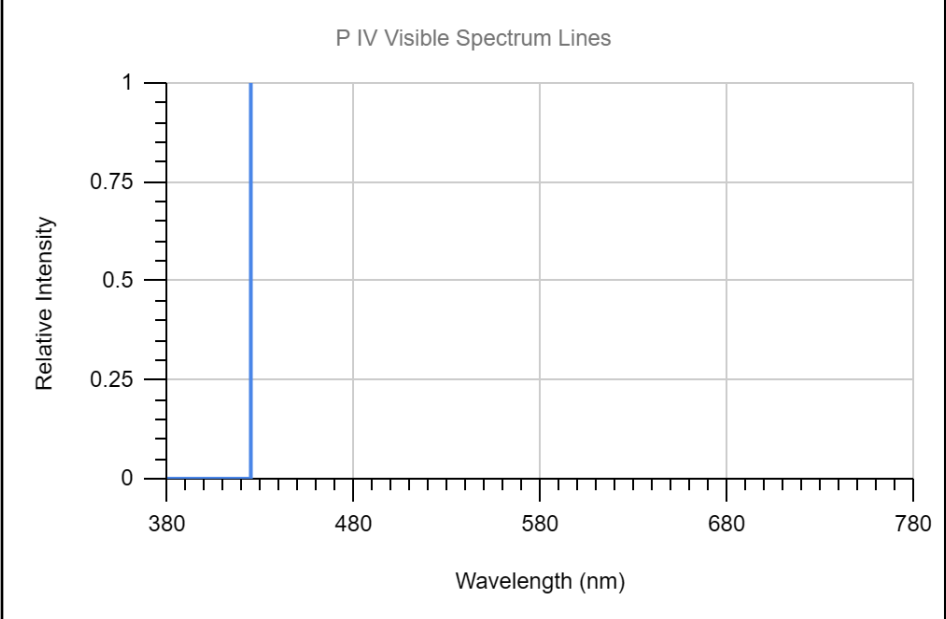
Electron Temperature: 2.28 T (eV) Electron Density: 3.83E+16 (cm⁻³)

λ (nm)	Rel Intensity	λ (nm)	Rel Intensity
405.74	0.07	422.22	1.00
405.93	0.62	424.67	0.47
408.01	0.34		

Phosphorus-Triply Ionized (P IV)

(Return to Index)





P IV Profile:

Peak Temperature: 43,500 K

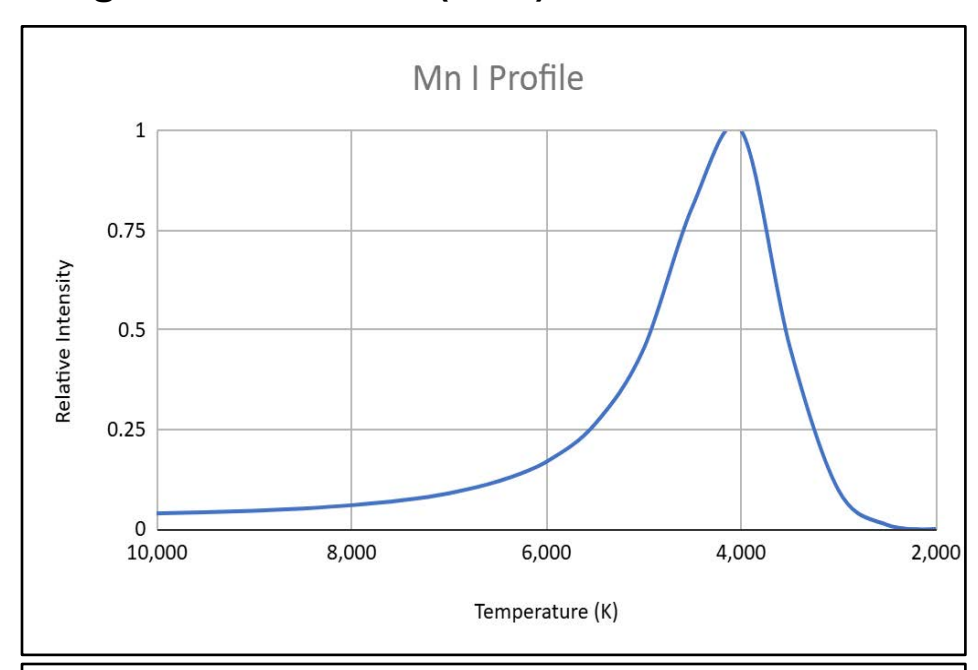
P IV Visible Spectrum Lines:

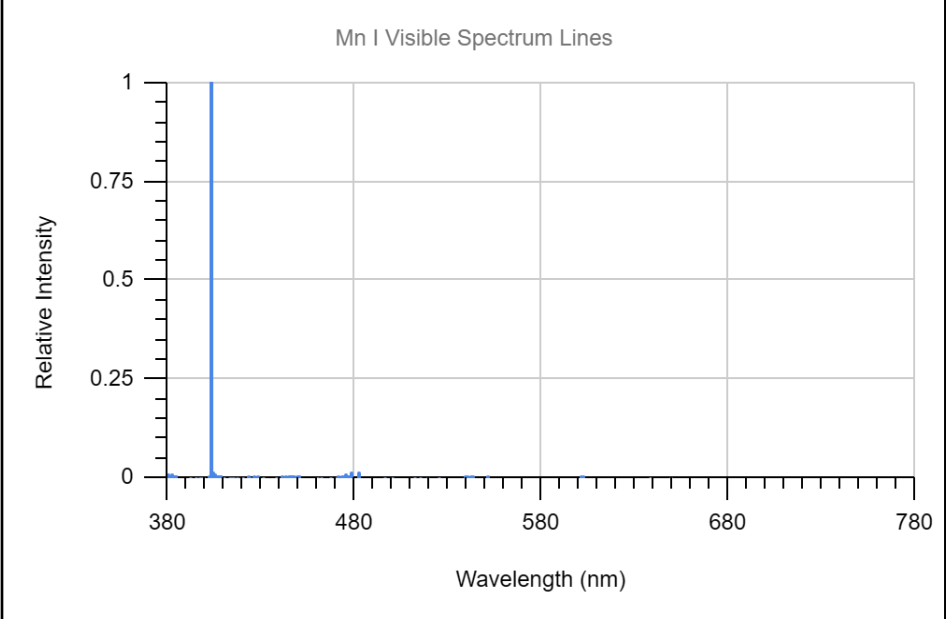
Electron Temperature: 3.75 T (eV) Electron Density: 5.93E+17 (cm⁻³)

λ (nm)	Rel Intensity	λ (nm)	Rel Intensity
424.97	1.00		

Manganese - Neutral (Mn I)

(Return to Index)





Mn I Profile:

Peak Temperature: 4,000 K

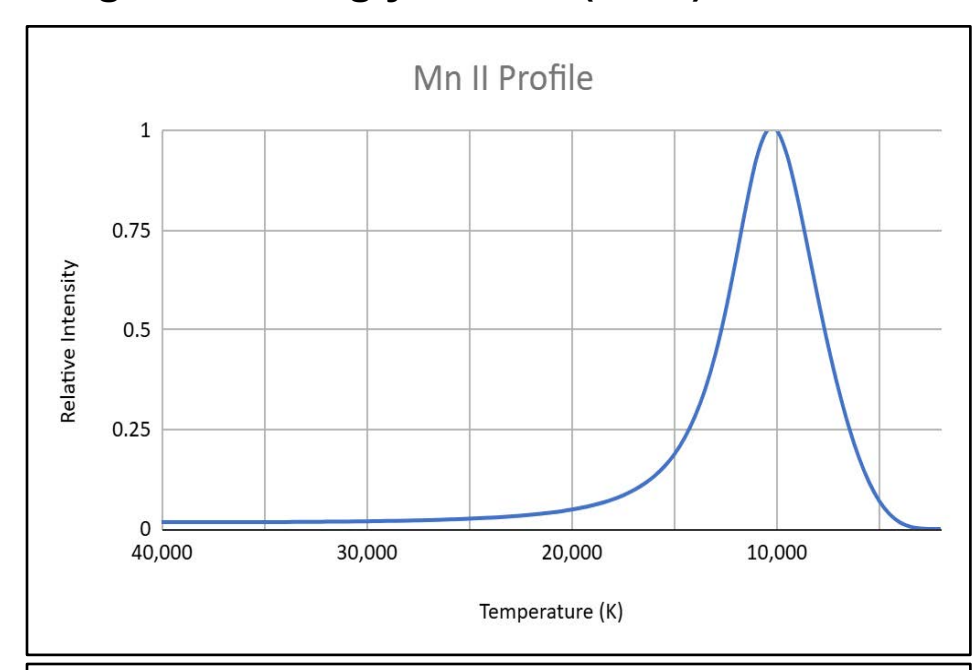
Mn I Visible Spectrum Lines:

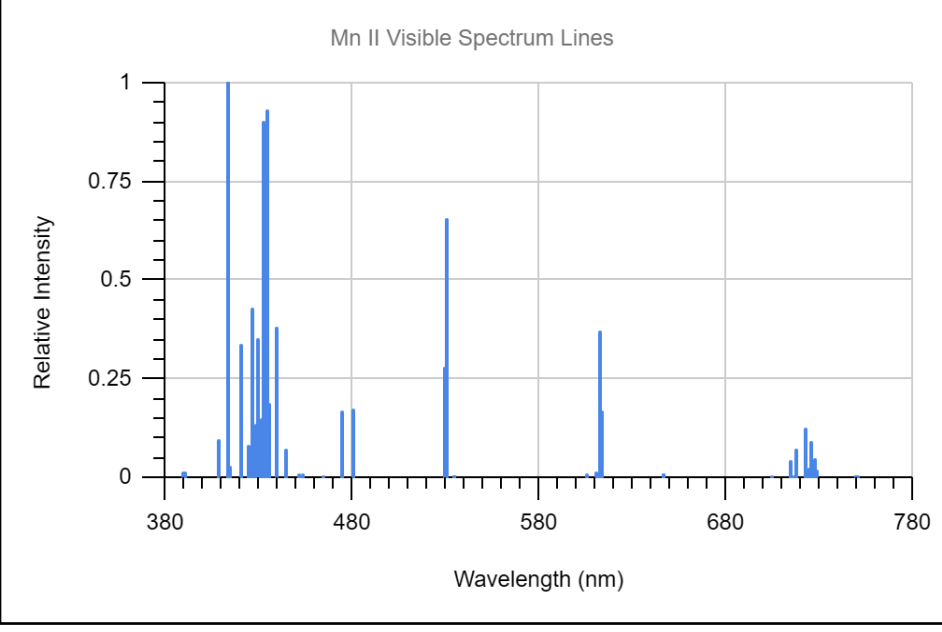
Electron Temperature: 0.35 T (eV) Electron Density: 1.11E+12 (cm⁻³)

λ (nm)	Rel Intensity	λ (nm)	Rel Intensity
403.08	1.00		
403.31	0.73		
403.45	0.47		

Manganese - Singly Ionized (Mn II)

(Return to Index)





Mn II Profile:

Peak Temperature: 10,000 K

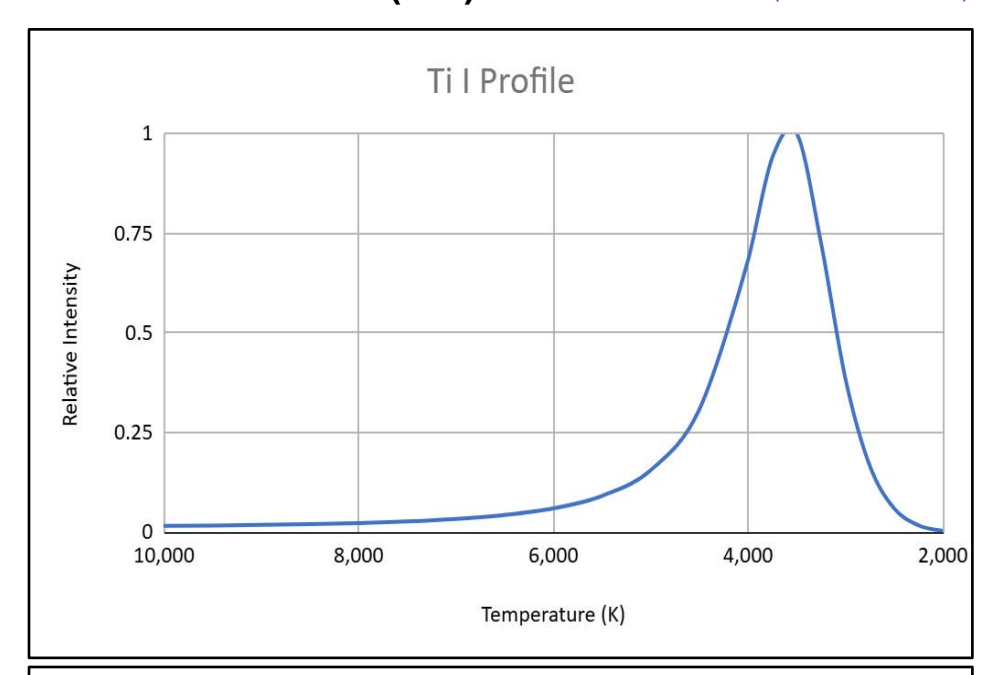
Mn II Visible Spectrum Lines:

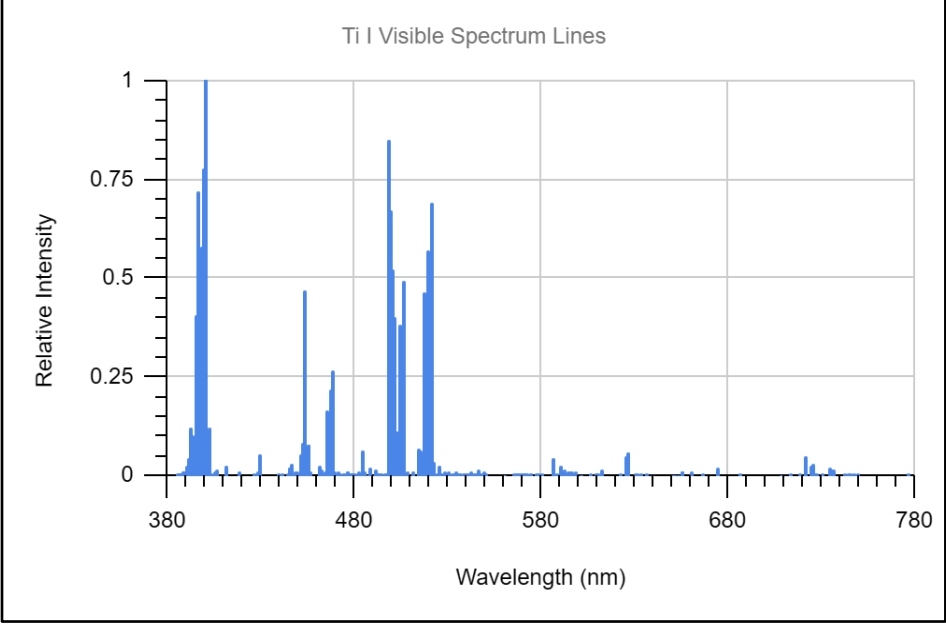
Electron Temperature: 0.86 T (eV) Electron Density: 7.7E+14(cm⁻³)

λ (nm)	Rel Intensity	λ (nm)	Rel Intensity
408.54	0.10	529.44	0.06
412.81	1.00	529.54	0.15
420.54	0.27	529.71	0.28
420.64	0.34	529.93	0.43
424.42	0.08	530.23	0.65
424.59	0.07	612.24	0.37
425.92	0.43	612.28	0.05
428.44	0.13	612.59	0.26
429.22	0.35	612.62	0.07
430.82	0.15	612.87	0.16
432.50	0.90	612.90	0.07
432.66	0.51	613.08	0.10
433.83	0.10	613.10	0.05
434.40	0.93	613.19	0.05
434.84	0.18	717.24	0.07
439.34	0.38	717.44	0.05
444.20	0.07	722.00	0.12
473.83	0.16	725.24	0.09
480.68	0.17	726.98	0.05

Titanium - Neutral (Ti I)

(Return to Index)





Ti I Profile:

Peak Temperature: 3,500 K

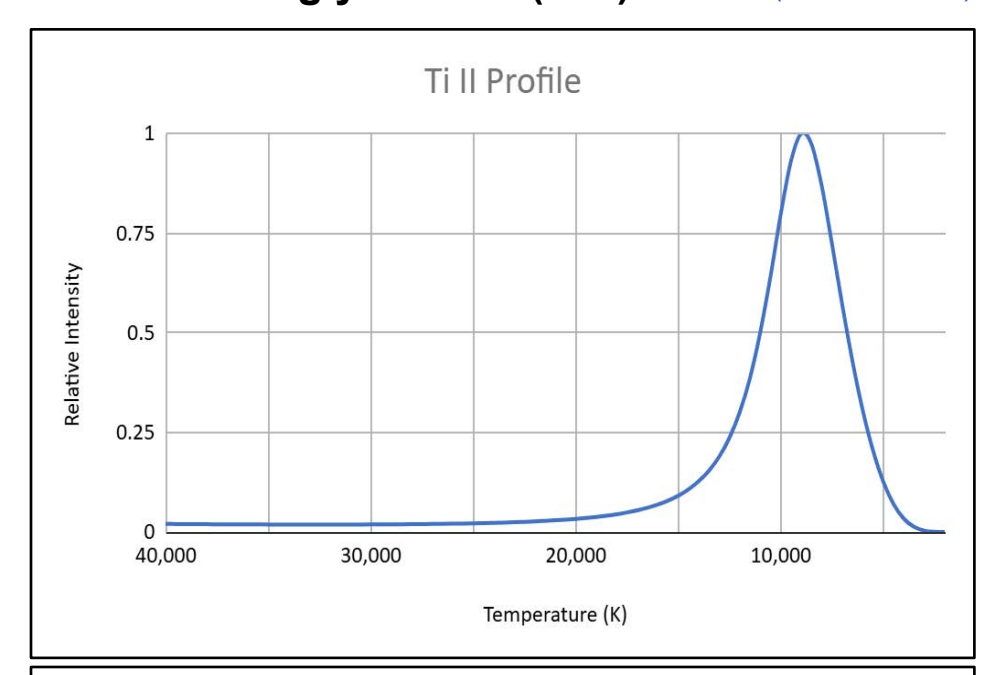
Ti I Visible Spectrum Lines:

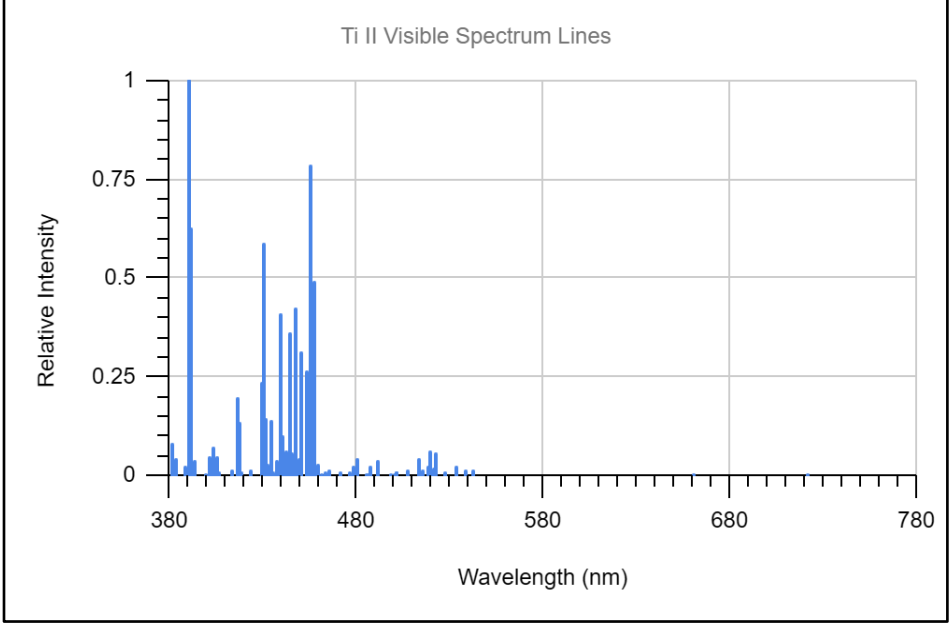
Electron Temperature: 0.30 T (eV) Electron Density: 5.31E+11 (cm⁻³)

λ (nm)	Rel Intensity	λ (nm)	Rel Intensity
392.45	0.12	465.65	0.16
392.99	0.10	466.76	0.21
394.78	0.11	468.19	0.27
394.87	0.40	498.17	0.85
395.63	0.40	499.11	0.67
395.82	0.72	499.95	0.52
396.29	0.08	500.72	0.39
396.43	0.08	501.42	0.27
398.18	0.58	501.43	0.40
398.98	0.78	501.62	0.07
399.86	1.00	502.00	0.11
400.89	0.10	502.29	0.11
402.46	0.12	502.48	0.08
451.80	0.08	504.00	0.38
452.28	0.07	506.47	0.49
453.32	0.46	514.75	0.07
453.48	0.31	517.37	0.46
454.88	0.08	519.30	0.57
455.25	0.08	521.04	0.69

Titanium - Singly Ionized (Ti II)

(Return to Index)





Ti II Profile:

Peak Temperature: 9,000 K

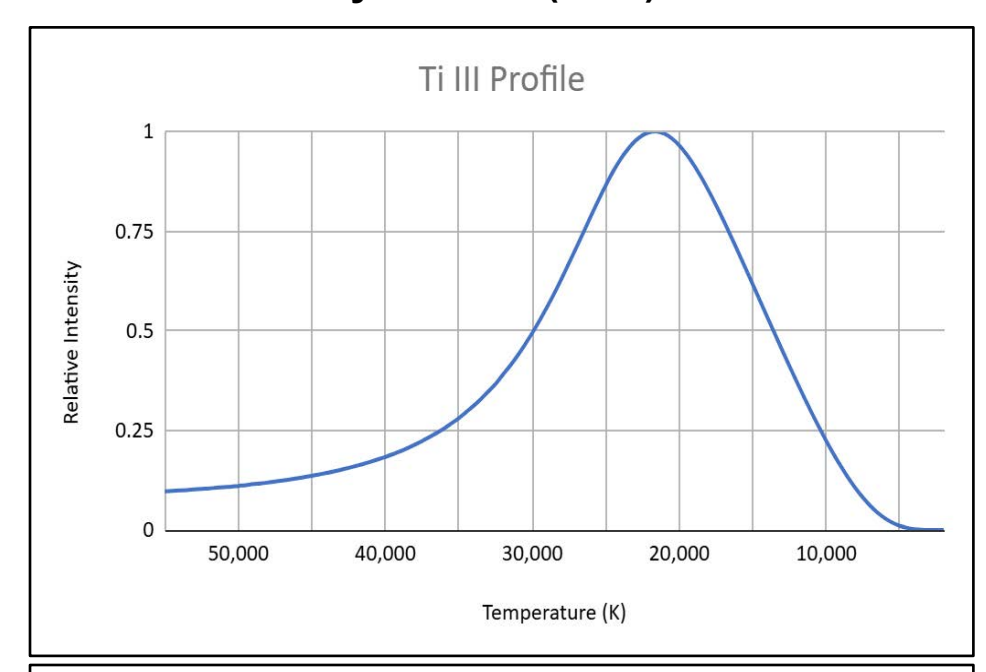
Ti II Visible Spectrum Lines:

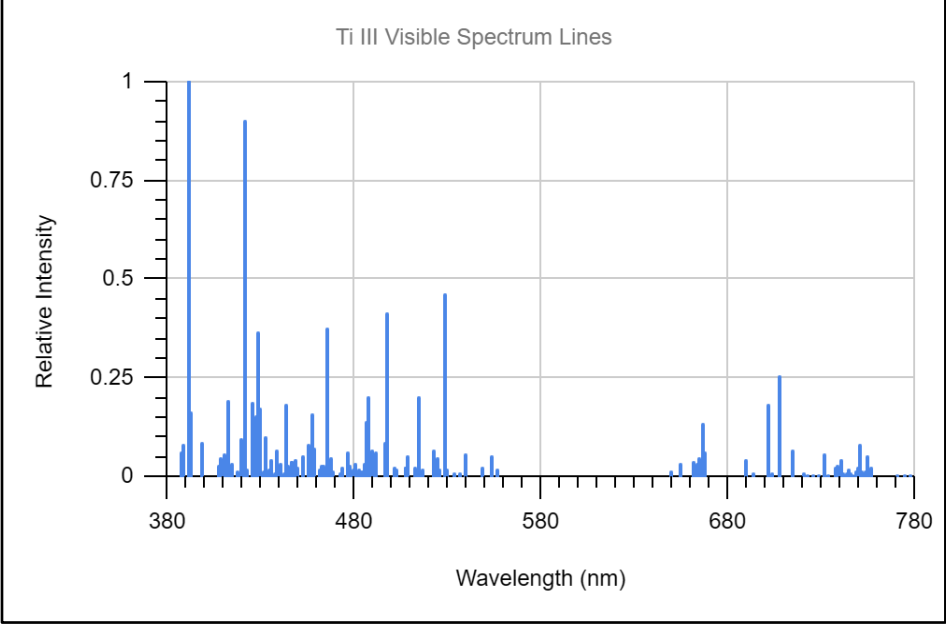
Electron Temperature: 0.78 T (eV) Electron Density: 9.28E+13 (cm⁻³)

λ (nm)	Rel Intensity	λ (nm)	Rel Intensity
381.46	0.08	433.79	0.14
390.05	1.00	439.50	0.41
391.35	0.62	439.98	0.10
401.24	0.05	441.77	0.06
402.83	0.07	444.38	0.36
405.38	0.05	445.05	0.06
416.36	0.19	446.85	0.42
417.19	0.13	450.13	0.31
429.02	0.23	453.40	0.27
429.41	0.14	454.96	0.79
430.00	0.59	456.38	0.18
430.19	0.12	457.20	0.49
430.79	0.14	518.87	0.06
431.29	0.13	522.65	0.05
431.50	0.13		

Titanium - Doubly Ionized (Ti III)

(Return to Index)





Ti III Profile:

Peak Temperature: 21,500 K

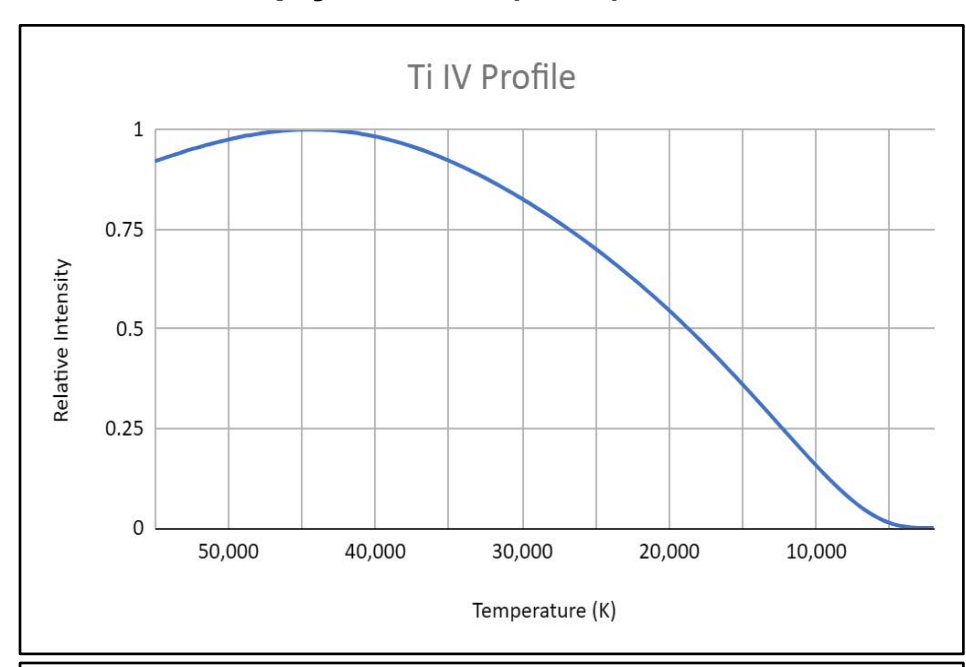
Ti III Visible Spectrum Lines:

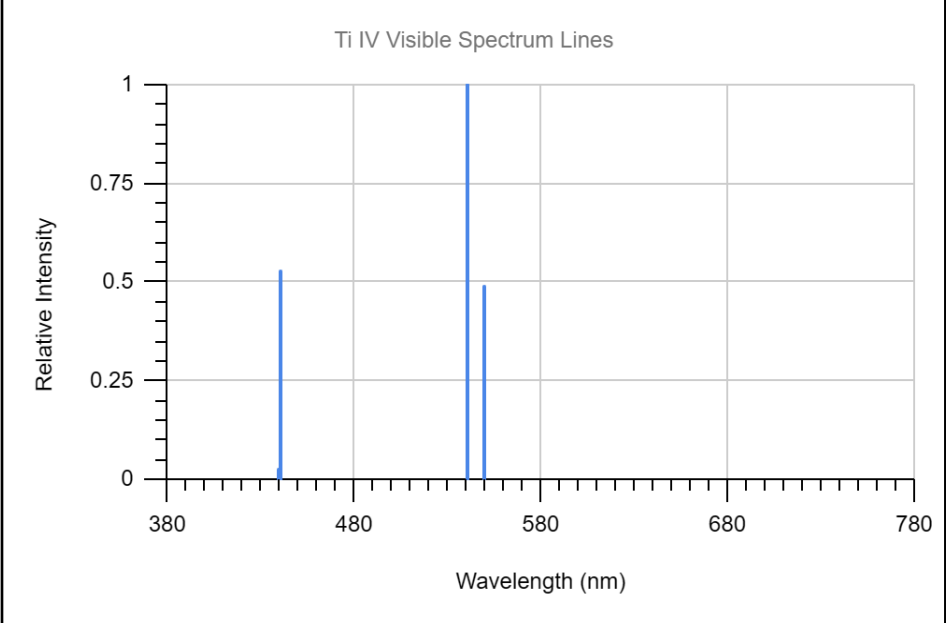
Electron Temperature: 1.85 T (eV) Electron Density: 1.21E+16 (cm⁻³)

λ (nm)	Rel Intensity	λ (nm)	Rel Intensity
388.12	0.08	455.55	0.08
391.55	1.00	457.65	0.16
392.49	0.16	457.85	0.07
398.64	0.08	464.95	0.13
411.91	0.19	465.29	0.38
419.11	0.09	485.81	0.14
421.33	0.21	487.40	0.20
421.55	0.90	489.28	0.07
424.76	0.12	496.14	0.09
424.85	0.14	497.12	0.41
425.01	0.19	514.73	0.20
425.90	0.10	522.63	0.06
426.98	0.15	527.81	0.46
428.56	0.36	666.80	0.13
428.87	0.12	701.54	0.18
429.67	0.17	707.26	0.25
431.96	0.10	714.18	0.07
437.89	0.06	750.69	0.07
443.39	0.18	750.77	0.08

Titanium - Triply Ionized (Ti IV)

(Return to Index)





Ti III Profile:

Peak Temperature: 44,500 K

Ti III Visible Spectrum Lines:

Electron Temperature: 3.83 T (eV) Electron Density: 6.73E+17 (cm⁻³)

λ (nm)	Rel Intensity	λ (nm)	Rel Intensity
439.73	0.53	539.89	1.00
440.34	0.37	549.25	0.49